Experimental and numerical study of springback of composite structures : considering mould/laminated part interaction.

Arnon Lerdwongpaisan

Université Fédérale
Toulouse Midi-Pyrénées

THÈSE

En vue de l'obtention du
DOCTORAT DE L'UNIVERSITÉ DE TOULOUSE

Délivré par l'Institut National des Sciences Appliquées de Toulouse

Présentée et soutenue par

Arnon LERDWONGPAISAN

Le 24 Avril 2023

Etude expérimentale et numérique du springback des structures composites : prise en compte de l'interaction moule/pièce stratifiée.

Ecole doctorale : **MEGEP - Mécanique, Energétique, Génie civil, Procédés**

Spécialité : **Génie mécanique, mécanique des matériaux**

Unité de recherche :
ICA - Institut Clément Ader

Thèse dirigée par
Bruno CASTANIÉ et Philippe OLIVIER

Jury
M. Zoheir ABOURA, Président
M. Toufik KANIT, Rapporteur
Mme Olga KLINKOVA, Rapporteure
Mme Anaïs BARASINSKI, Examinatrice
M. Bruno CASTANIÉ, Directeur de thèse
M. Philippe OLIVIER, Co-directeur de thèse

Acknowledgement

This Ph.D study was fully supported by The Royal Thai Government Scholarship Program and Burapha University. First of all, I would like to express my sincere gratitude to The Office of the Civil Service Commission (OCSC) in Thailand and Ambassade Royale de Thaïlande (OEA Paris) in France for supporting the funding and letting me be part of this incredible experience.

Words cannot express my gratitude to my thesis directors, Prof. Bruno CASTANIÉ and Prof. Philippe OLIVIER for providing guidance and feedback throughout this thesis. This thesis would not have been possible without their comments and recommendations. I definitely cannot forget to say big thanks to Dr. Laurent MEZIEX, my colleague at Burapha University who have helped me to get the opportunity to pursue my Ph.D in Toulouse. I would also like to thank to the members of the jury: Prof. Zoheir ABOURA, Prof. Toufik KANIT, Prof. Olga KLINKOVA and Dr. Anais BARASINSKI for accepting to evaluate my thesis manuscript.

I would like to thank to MEGEP doctoral school, INSA Toulouse and Institut Clément Ader (ICA) for providing the training programs, the procedures to complete my study and the equipment to carry out my research work.

I would also like say special thanks to the following people who have helped me for their contributions on this research or even the life in the laboratory: Nathalie ROCHER GLEIZES, Laurent CROUZEIX, Olivier CHERRIER, Abdallah BOUZID, Nicolas LAURIEN, Kamila KOZIURA, Myriam BOYER and Valérie MONNERIE-SEGALA.

Many thanks to all of my friends in France, even they are French, Thai or from other countries, inside and outside the laboratory, wherever you are, because of them, this is a very good memory.

Many thanks to my family, my father, my mother and my older sister for their very special and unconditional support from Thailand. And finally, to my wife Waranya LIMBUAN, for your kind love and encouragement during all these years.

Abstract

Composite laminates made of carbon fibre and thermosetting resin matrix have specific properties that are efficient for aeronautic structures which explains their large use today. However, during manufacturing, composite laminated parts undergo process-induced stresses and frequently exhibit some residual deformations at the end of cure commonly called “springback”. These deviations of geometry are a serious issue for parts in the assembly process and they can lead the part to be reworked or even scrapped. Therefore, the understanding and numerical modelling of springback sources is required to avoid coping with such problems and minimizing a very costly trial and error process.

The work conducted during this Ph.D is in the continuation of previous work on the characterization of thermomechanical behaviour of M21EV/IMA prepreg and the study (both experimental and numerical) of autoclave process-induced deformations and stresses. Our work focuses upon tool/part interaction and more especially on the effects of bagging products. Series of cross-ply (0/90) and angle-ply (45/-45) laminates were autoclave-cured on aluminum flat mould. Liquid release agent, ETFE release film and peel-ply were placed between the laminates' bottom face and the mould. The deflection of all laminates was measured at the end of cure and numerical simulations were performed by FEM (Abaqus) for comparison. These numerical simulations propose an original modelling enabling the behaviour of releasing film and peel-ply to be taken into consideration. It reveals that cross-ply (0/90) laminates are sensitive to the presence of the Peel-ply layer while angle-ply laminates are less.

The thermal behaviour of ETFE release film and peel-ply was investigated by thermomechanical analysis (TMA). The results showed that thermal behaviour of ETFE release film expanding followed the cure cycle temperature path as expected while the contraction of peel-ply textile structure was observed differently between weft and warp directions. The coefficients of thermal expansion (or contraction) were characterised and implemented into FEA numerical modelling. The results from simulations are in good agreement with the experiment and showed that the effect of release agents between tool/part interfaces cannot be ignored for process induced deformation in composite parts.

The last part of this thesis focuses on the modification of metallic mould shape to compensate the out-of-plane distortion of a laminated plate. At the beginning of this work, attention was paid to the simulation of mould compensation for angle-ply (45/-45) laminates which exhibited considerably larger warpage than cross-ply (0/90) ones. The first stage of simulation consisted in designing both female and male compensated moulds by mirroring the cured shape of (45/-45) laminates with the aim of producing flat laminates at the end of curing. In a second stage FEA simulations performed on the curing of (45/-45) laminates showed that it was possible to get almost flat laminates (even if they are not symmetrical) owing to compensated female moulds that were designed.

KEYWORDS: Composite materials, tool/part interaction, autoclave curing, FEA numerical simulation, mould compensation.

Résumé

Les stratifiés composites constitués de fibres de carbone et d'une matrice de résine thermodurcissable ont des propriétés spécifiques adéquates pour les structures aéronautiques ce qui explique leur large emploi aujourd'hui. Cependant, lors de leur fabrication, ces pièces stratifiées composites subissent des contraintes induites par le procédé et présentent fréquemment des déformations résiduelles en fin de cuisson communément appelées « springback ». Ces écarts de géométrie sont un problème sérieux lors du processus d'assemblage et peuvent conduire la pièce à devoir être réusinée ou même mise au rebut. Par conséquent, la compréhension et la modélisation numérique du springback sont nécessaires pour minimiser un processus d'essais et d'erreurs très coûteux.

Les travaux menés au cours de cette thèse s'inscrivent dans la continuité de travaux antérieurs sur la caractérisation du comportement thermomécanique du préimprégné M21EV/IMA et l'étude (à la fois expérimentale et numérique) des déformations et contraintes induites par le procédé de cuisson à l'autoclave. Ces travaux portent sur l'interaction outil/pièce et plus particulièrement sur les effets des produits environnementaux. Une série de stratifiés à 0°/90° et à 45°/-45° ont été polymérisés à l'autoclave sur un moule plat en aluminium. L'influence d'un agent démoulant, d'un séparateur ETFE non perforé et d'un tissu d'arrachage a été étudié selon différentes configurations à l'interface du stratifié et du moule. La déformation de tous les stratifiés fabriqués a été mesurée après la cuisson et des simulations numériques ont été effectuées par éléments finis (Abaqus) à des fins de comparaison. Ces simulations numériques proposent une modélisation originale permettant de prendre en compte le comportement du séparateur ETFE non perforé et du tissu d'arrachage. Il révèle que les stratifiés à 0°/90° sont sensibles à la présence d'une couche de tissu d'arrachage, tandis que les 45°/-45° le sont moins.

Les comportements thermiques du séparateur ETFE non perforé et du tissu d'arrachage ont été étudiés par analyse thermomécanique (TMA). Les résultats ont montré que le comportement thermique du séparateur ETFE non perforé suivait le cycle de durcissement comme prévu, tandis que la contraction de la structure textile du tissu d'arrachage était différente entre les directions de trame et de chaîne. Les coefficients de dilatation (ou de contraction) thermiques ont été caractérisés et implémentés dans la modélisation numérique FEA. Les résultats de la simulation sont en bon accord avec l'expérience et ont montré que l'effet des agents de démoulage entre l'interface outil/pièce ne peut être ignoré pour la déformation induite par le processus dans la pièce composite.

La dernière partie de cette thèse porte sur la modification de la forme des moules métalliques (aluminium) pour compenser la distorsion hors plan des stratifiés. La première étape de ce travail a porté sur la conception de moules mâles et femelles compensés. Ils ont été conçus en réalisant une image miroir des formes des stratifiés (45°/-45°) choisis pour leur déformation nettement supérieure à celle des (0°/90°). La seconde étape dédiée à la simulation de la cuisson des (45°/-45°) sur les moules compensés a montré que l'on pouvait produire des stratifiés quasiment plats en dépit de leur drapage non symétrique.

MOTS-CLÉS : Matériaux composites, interaction outil/pièce, cuisson autoclave, simulation numérique FEA, compensation de moule.

Index

List of tables

List of figures

Chapter 1

General introduction

This chapter presents an introduction to the subject and content on the development of this thesis. This starts from the discussion in general application of composite materials and then the issues of composite manufacturing to the deformation problem are criticized.

1.1 Application of composite in aerospace

Because of their exceptional stiffness to weight and strength to weight ratios, carbon fibres reinforced plate composites are widely used in several industrial sectors for high performance aircraft parts. It is largely the case in aerospace industry where composite materials represent more than 50% of the mass of modern long-range aircraft. Composite materials combine the stiffness and strength of reinforced fibres such as carbon fibres bonded together using a light polymeric material (thermoset or thermoplastic) which gives the part in its final shape.

The use of modern composite materials in aircraft started about 40 years ago but they were not the main consideration for big structures until the development of knowledge has increased. Composite became more important for wings and fuselages because it can reduce the weight percentage of structure [1]. Figure 1.1 shows the distribution of materials in Boeing 787 and Airbus A350 [2]. It can be seen that the distribution of carbon composite materials is about 50 % or more. Moreover, the lightweight of composite materials increased the primary use in Airbus transport aircraft because it has the potential to reduce the fuel consumption. Composite structures designed of high performances applications can either be monolithic laminated parts or sandwich structure as illustrated in Figure 1.2 [3]. The Figure 1.2 shows that monolithic laminated are made of several plies or thin layers of fibres (Unidirectional or textiles) exhibiting various orientations while sandwich structures are made of two skins of monolithic laminates separated by a core material (honeycomb, foam,…) and bonded together on top and bottom surfaces of a core with additional adhesives. The properties of laminate composite generally depend on fibre direction, fibre location and number of layer. The aim of sandwich structure is to reduce the weight while increasing the bending stiffness and the buckling strength. The bending stiffness of sandwich structure can be enhanced by increasing the core thickness or modifying a core material with very low additional weight.

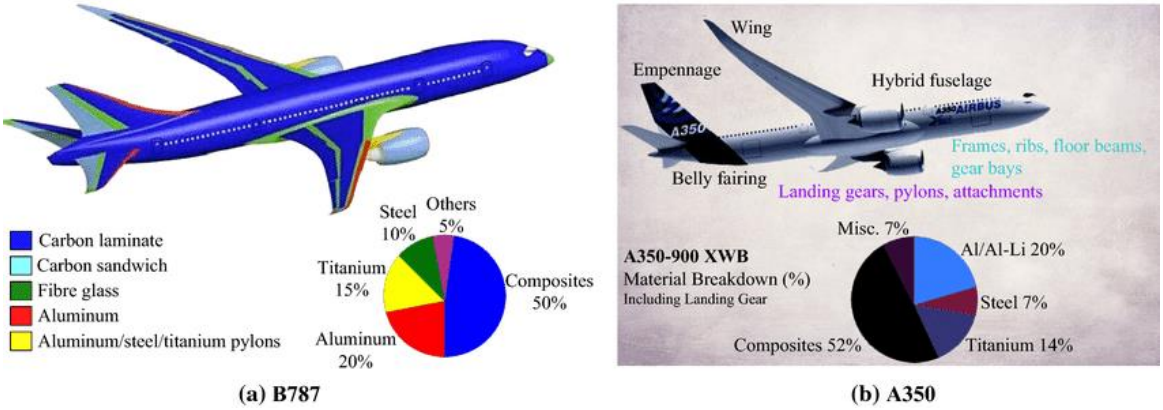

Figure 1.1 The distribution of materials in Boeing 787 and Airbus A350. [2]

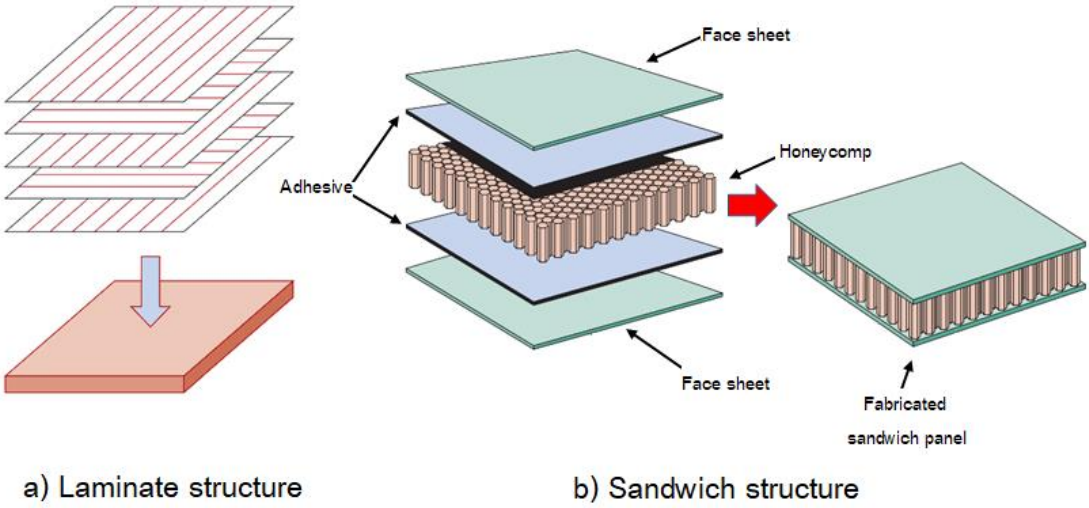

Figure 1.2 Laminate and sandwich structure. [3]

1.2 Structure and manufacturing of laminate composite

1.2.1 Laminate part and fibres orientation

Reinforcements are available under various commercial forms (see Figure 1.3): unidirectional continuous fibres, woven textile product and discontinuous aligned or random fibres directions [4]. There are three types of fibre reinforcement widely used in industry including glass fibres, carbon fibres and Kevlar fibres. Depending on the use of the composite part and the in-service conditions that it must withstand, the designer will choose to use one of these reinforcement forms and types and will arrange fibres orientation to force to mechanical stress. The ability of composite part to cope with in-service mechanical stress is linked to fibres orientations [5]. The highest strength and stiffness will be obtained in the fibre direction of an unidirectional laminate but it is unlikely that a composite part undergoes stress in a single direction. This is why in most of composite part, the stacking sequence (fibre orientation to part thickness) is designed to make the part to comply with stress directions. One simple and widespread rotation is to use quasi-isotropic laminates with reinforcements oriented in 0°, 90° and ±45° directions.

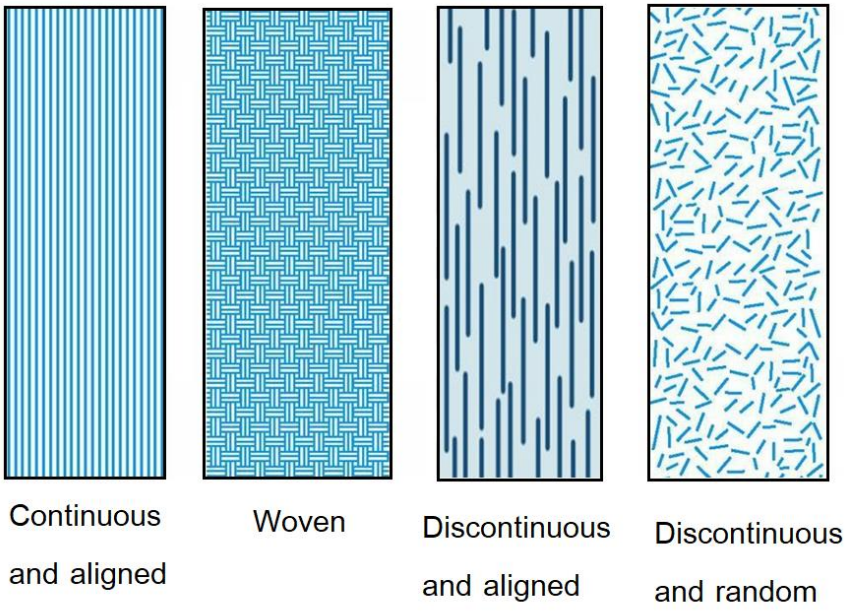

Figure 1.3 Schematic representation of the fibre orientations. [4]

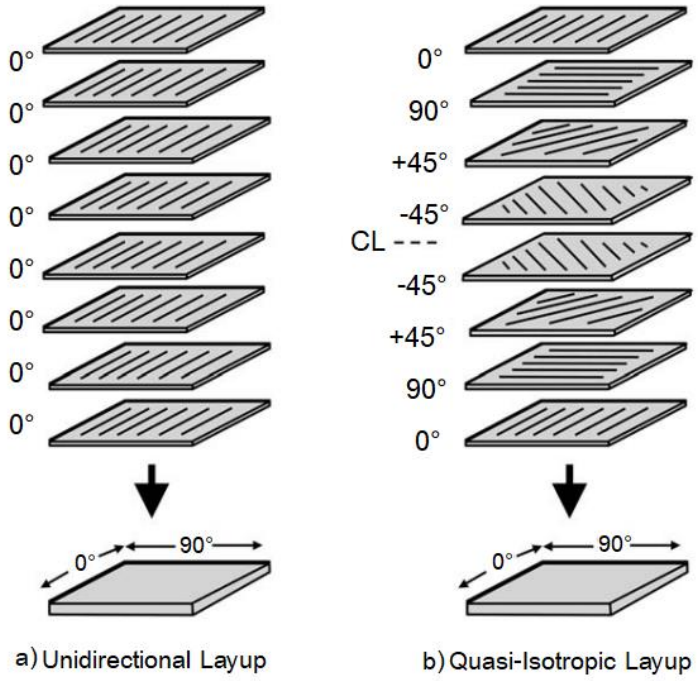

Figure 1.4 Stacking of laminate plies. [6]

The stacking sequence of laminate can be described by an orientation code of each ply. The building block of laminate can be symmetric or asymmetric stacked (layups) in different fibre directions on each ply with respect to the midplane. For example, an orientation code for Figure 1.4(b) is [0º/90º/+45º/-45º/-45º/+45º/90º/0º] or $[0º/90º/+45º/-45º]_s$, where the subscript “s” stands for “symmetric” [6]. Another example is presented in Figure 1.5 and there

are several ply type examples with symmetrical and asymmetrical layups were used in the study of Basim Mohamme Fadhil [7] and shown in Table 1.1.

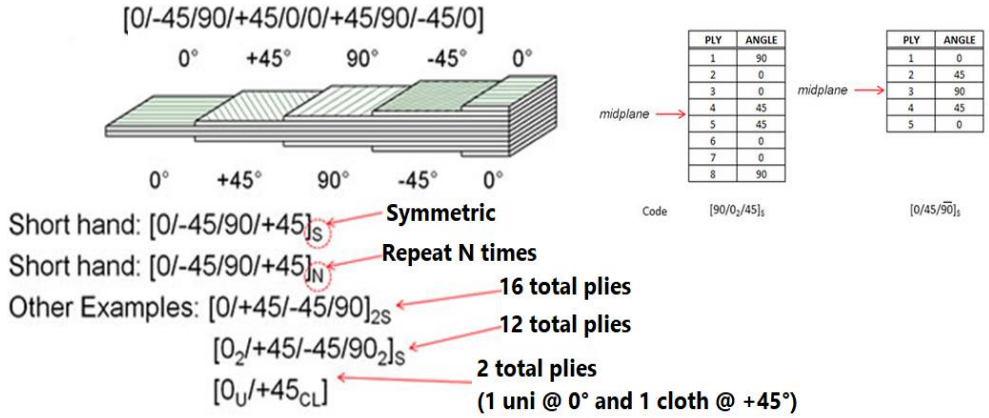

Figure 1.5 Examples of stacking sequence code. [7]

Table 1.1 Examples of ply types. [7]

Case	Ply types	Stacking sequence
1	Multi-Symmetric	[-45º/45º/0º/90º/90º/0º/45º/-45º]
2	Cross-ply Symmetric	[0º/90º/0º/90º/90º/0º/90º/0º]
3	Angle-Ply Symmetric	[45º/-45º/45º/-45º/-45º/45º/-45º/45º]
4	Multi-Symmetric	[30º/-30º/0º/90º/90º/0º/-30º/30º]

1.2.2 A few words about manufacturing methods

There are various methods and processes to manufacture composite parts. A good overview of manufacturing process can be found in [8]. Manufacturing processes and their applications and limitations will not be described in this manuscript. However, we are going to introduce prepreg materials, vacuum bagging and autoclave curing since these are the methods used on the Ph.D work. Prepregs are normally used as a raw material to manufacture aerospace parts. Composite prepreg is a ready-made material in the form of roll or tape which consists of fibres in woven or unidirectional form impregnated with partially precured epoxy resin matrix (B-stage) [9, 10]. Prior to plies cutting, since most of thermoset matrices such as epoxies used in structural composites can react at ambient temperature, they are required to store in a freezer at -18 °C. Figure 1.6 shows the unidirectional prepreg used in this Ph.D work. To fabricate a composite part, prepreg layer has to be cut to the desired shape and direction and laid up on a tool or mould by hand or machine. In this latter

case we speak about automated tape placement. A robotic head makes the deposition of a narrow prepreg tape (typically 6.35 mm width) directly into the part mould. The stacking sequence can be designed as discussed previously.

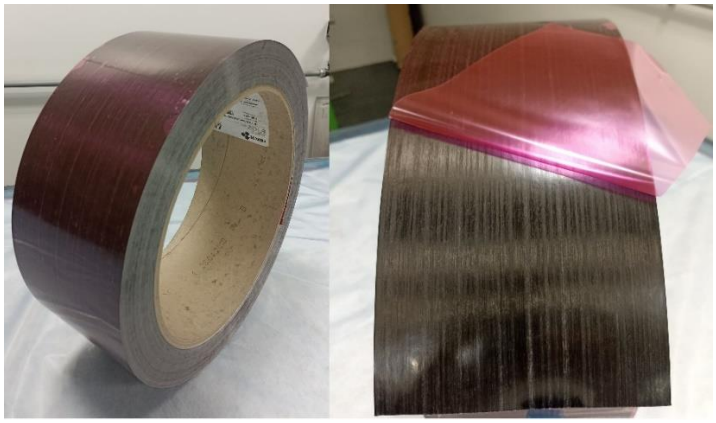

Figure 1.6 The Unidirectional prepreg used in this Ph.D work.

As regards moulds they can be made of several materials. In the case of manufacturing parts for which a high dimensional stability is required, moulds are produced with low coefficient of thermal expansion metal such as Invar or even carbon epoxy. Otherwise, moulds are made of steel or aluminium. In this study as it is planned to put in the evidence of the tool-part interaction without working in the frame of industries partnership, it was decided to use aluminium 2024 moulds. In the configuration – carbon/epoxy laminates cured on aluminium moulds, the highest mismatch between laminate and mould coefficient of thermal expansion will be obtained. Prepreg plies cutting as well as ply collection are usually performed in a clean room with controlled relative humidity and temperature, this was the case in this work. In order to reduce the chance of air-trapped voids between plies to develop during the cure cycle, plies are pre-compacted under vacuum by for 20 minutes. The effects of such pre-compaction have been studied in the thesis of Léonard Serrano [11]. At the end of ply collection, which starts directly on the mould surface coated or covered by release agents, vacuum bagging products are placed on the stack of prepreg plies as shown in Figure 1.7. Vacuum port depending on the mould design can either be located on the vacuum bag (as shown by Figure 1.7) or plugged on the mould. Mould with prepreg plies and bagging products are placed into an oven or an autoclave for the curing of the thermoset matrix. An example of cure cycle with temperature, pressure and vacuum paths is given in Figure 1.8 [12]. Cure cycle brings the composite to its final solid state (vitrified material). Changes in the matrix during the curing are usually followed owing the degree of cure (α) and the glass transition temperature (T_g). Generally, it is aimed to get the higher possible value for α ($0 < \alpha < 1$) and T_g (°C). Once the laminated part is demoulded, its dimensions and

geometry are controlled and compared to the one of the CAD part. All differences between the CAD part and the real one manufactured stand for the problems of dimensional/geometrical stability. This is exactly studied in this thesis.

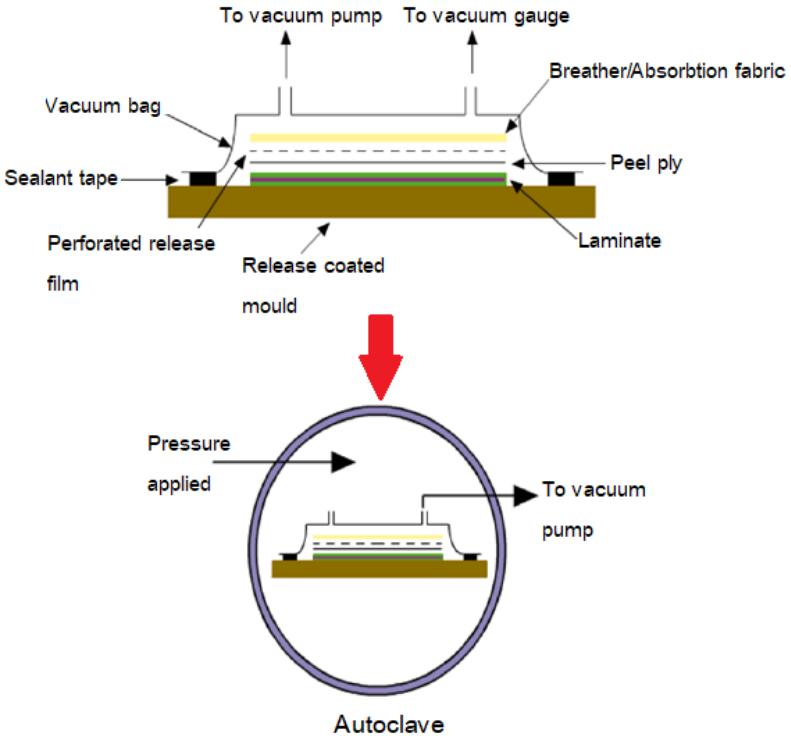

Figure 1.7 The assembly of vacuum bag.

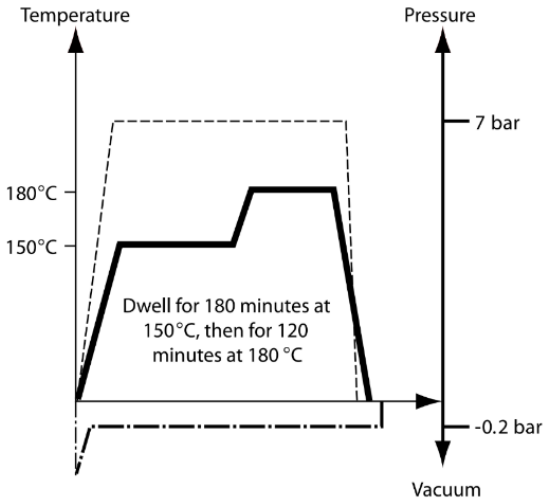

Figure 1.8 Cure cycle with temperature, pressure and vacuum paths. [12]

1.3 Shape distortion in composite manufacturing

Continuous fibres and a thermoset matrix are the main compositions of high performance composites which requires processing at elevated curing temperature. During manufacturing, residual stresses are formed due to several parameters [13, 14]. The first consideration at a micromechanical scale should focus on the mismatch in coefficients of thermal expansion between the fibres and the matrix followed at the mesoscale by the mismatch in coefficients of thermal expansion between part and mould. Consecutive plies and at the macromechanical scale (i.e. at the scale of the manufactured part) between the part and its mould. Effectively under the effects of atmospheric pressure, the part is in a vacuum bag and those of the autoclave pressure while cured, the composite part is pressed against the mould surface and stressed by this later to follow its own thermal expansion. This occurs in split of the release agents (liquid or film) placed between the mould surface and the laminate bottom surface. Moreover, the crosslinking reaction of the polymeric matrix is the cause of chemical shrinkage from the whole cure cycle and cool down stage [15]. These phenomena will generate stress locked in composite part after demoulding and finally the deformation take places. Some examples of typical part warpages are presented in Figure 1.9 [16, 17, 18]. Figure 1.9 shows what is called warpage, out of plane deflection, spring-in, spring-forward and so on. This will enable the reader to clearly understand the bibliographical results presented in chapter 2 because most of authors are focusing their analysis upon these after curing deformation.

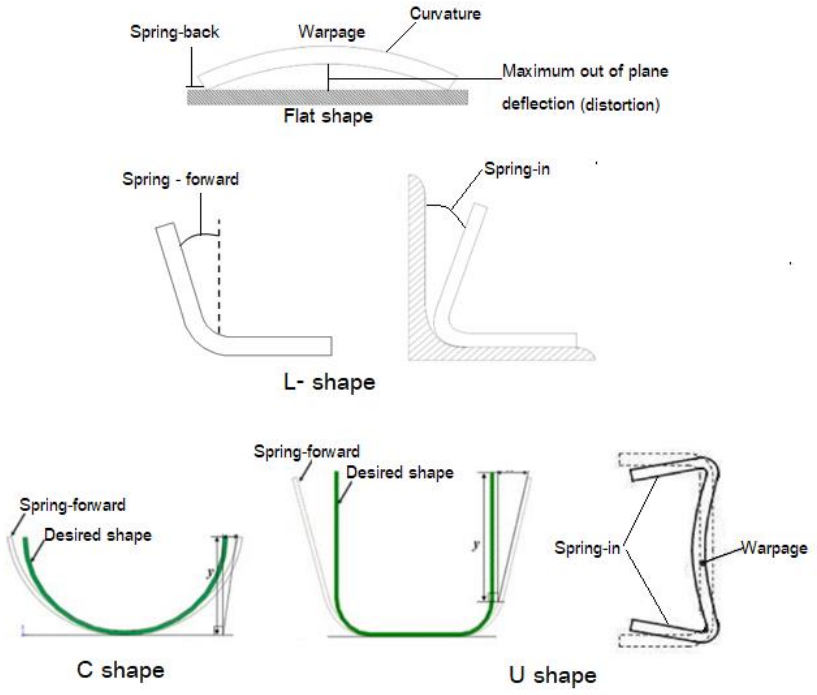

Figure 1.9 The typical part warpages of composite part. [16, 17, 18]

The parameters influencing the deformation of laminate parts after manufacturing can be classified into intrinsic and extrinsic sources as presented in Figure 1.10, intrinsic is related to the characteristic of the part itself while extrinsic is related to the manufacturing process. The details of literature review on these parameters will be discussed in Chapter 2.

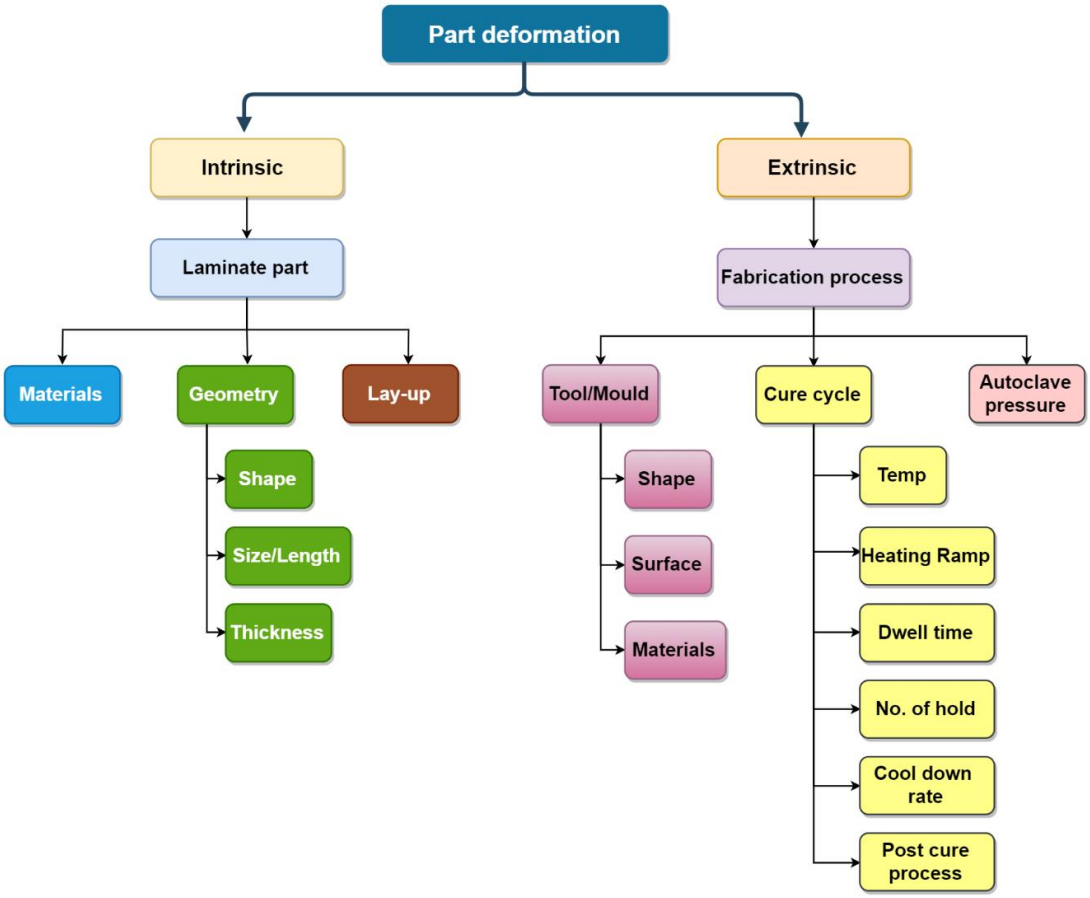

Figure 1.10 The parameter influence on part deformation.

1.4 Content of the thesis

Following the discussion in section 1.3, we can draw the content of the thesis to fulfil research gap and make a comparison with vague results on the distortion of laminate part. However, the work conducted during this Ph.D is in the continuation of recently finished previous work on the characterization of thermomechanical behaviour of M21EV/IMA prepreg and the study (both experimental and numerical) of process-induced deformations and stresses. In L. Moretti Ph.D thesis work [19], the numerical simulation of process-induced stresses, strains and deformations was made under Abaqus® with a specific law of behaviour of the carbon-epoxy material during its curing. Modelling effect were made to simulate the manufacturing of self-stiffened panels co-cured or co-bonded. Consequently, the thesis did not have more time to focus upon the interaction between the cured part and the mould. This explains why it has been decided for the current Ph.D thesis to study

mould/part interaction and to set up a modelling relying on previous development in order to predict the deformed shapes of laminated parts once cured. A special interest is given to the influence of ply layup with varying tool surface conditions on the warpage of thin and flat laminate autoclave cured. The objectives of the thesis can be summarized as follow:

1) To collect a data base on deformation of composite specimens in different fibre directions and tool surface conditions.

2) To investigate the effect of tool/part interaction by measuring and simulating the deformed shapes of laminated parts after their curing.

3) To predict the warpage using FEA simulation.

4) To propose an experimentally proven FEA simulation and a method to modify the metallic mould shape to compensate or reduce part deformation.

Chapter 2

State of the art of process induced distortion in composite manufacturing

This chapter is a literature review focused upon process induced distortion for laminate composite manufacturing. First, the physical phenomena related to deformation behaviour are presented including physics of resin polymerization and thermomechanical phenomena. Then, the effect of composite laminate part in terms of part geometry and layup and the effect of fabrication process in term of effect of mould and cure cycle are considered. Finally, a few examples of modelling for predicting the part deformation are discussed.

2.1 Physical phenomena during manufacturing of laminate

Physical phenomena of composite laminate parts have been investigated by many researchers. During manufacturing of laminate, the phenomena can be varying due to several parameters because the thermoset resin undergoes the curing cycle at elevated temperature. Consequently, this section will discuss in more details physical phenomena, starting with the physics of resin polymerization, followed by the thermomechanical phenomena.

2.1.1 A few reminders upon thermoset matrices reaction and phases changes

Since we have worked as many researchers in the field of composites manufacturing with industrial products, it was decided not to go deeply into the chemistry of crosslinking reaction but to follow the reaction through measurable parameters such as the degree of cure (α) and the glass transition temperature (T_g). Both can be experimentally determined by differential scanning calorimetry [20, 21, 22]. Thermoset matrices such as the one used in carbon/epoxy prepreg are cured at elevated temperatures. During the curing, resin matrices undergo two phase changes named gelation and vitrification. The prepolymer (or resin) is reacting with the curing-agent (or hardener) as illustrated in Figure 2.1 [23]. In liquid composite moulding processes such as resin transfer moulding, the matrix is initially liquid. Here with prepregs, the matrix is precured and viscous at room temperature when being cut and performed ply collection and therefore prior to curing. Nevertheless, whatever the initial shape of thermoset resin prior to its curing (liquid or prepreg), the system is undergoing two phases changes while cured: gelation and vitrification [20, 24]. An illustrated of these phenomena is schematic in Figure 2.1. The curing reaction of thermoset matrices can be followed and monitored owing the following parameters: degree of cure (α), glass transition temperature (T_g), resin viscosity (η), resin shear modulus (G) and the average molecular mass between crosslinking point ($\overline{Mc}$). The illustration of the changes in α, T_g, η, and G during cure cycle are given in Figure 2.2 and Figure 2.3 [25, 26, 27]. Figure 2.2 a) and b) describe the changes in degree of cure for resin matrix as a function of time and temperature. More degree of cure can be obtained following the increase of temperature at the same time period (Figure 2.2 a)) while longer time period is required to reach higher cure degree for low curing temperature (Figure 2.2 b)). Figure 2.2 b) also reminds that the temperature is the first consideration parameter to achieve higher degree of cure rather than the time period. Figure 2.3 a) shows the relation between degree of cure (α) and glass transition temperature (T_g), the development of T_g follows the evolution of fractional degree of conversions. Figure 2.3

b) shows the relation of resin viscosity (η) with the heating rate, fast heating rate clearly increase the viscosity for shorter time compared to slower heating rate. Figure 2.3 c) presents an example of the relation between resin shear modulus and resin viscosity at the heating rate of 3°C/min, the path of shear resin modulus value fairly well follows the evolution of resin viscosity: this observation is also visible for other heating rates appeared in the reference [27].

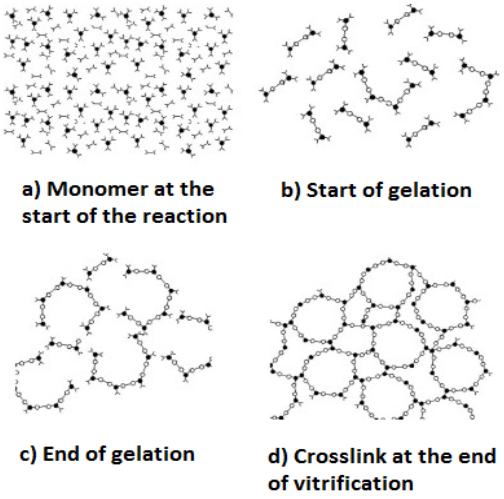

Figure 2.1 Reaction of resin. [23]

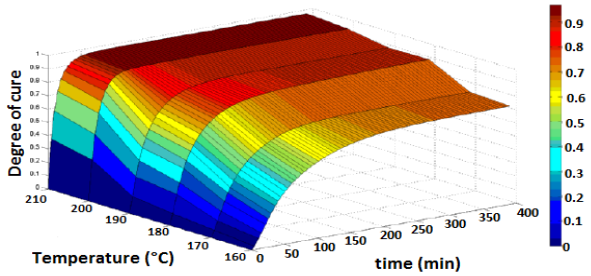

a) Degree of cure at the functions of time and temperature.

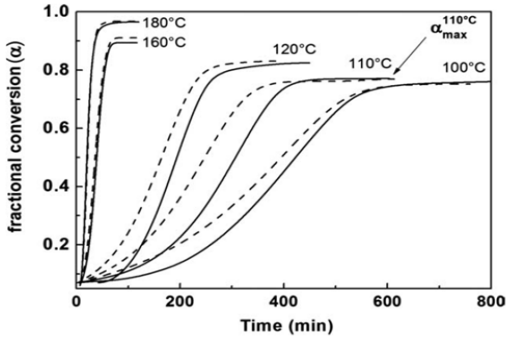

b) Evolution of degree of cure as a function of curing time at various isothermal temperature.

Figure 2.2 The relation between degree of cure and temperature. [25, 26, 27]

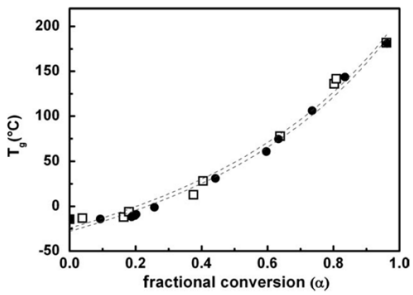

a) Glass transition temperature dependence on the fraction degree of conversions.

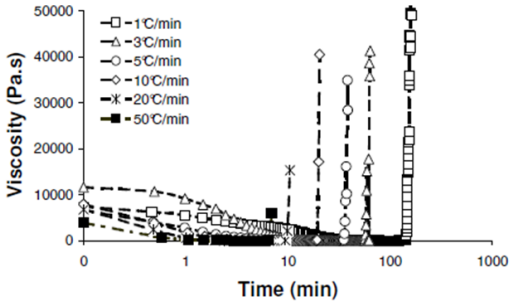

b) Changes in the resin viscosity as a function of heating rate.

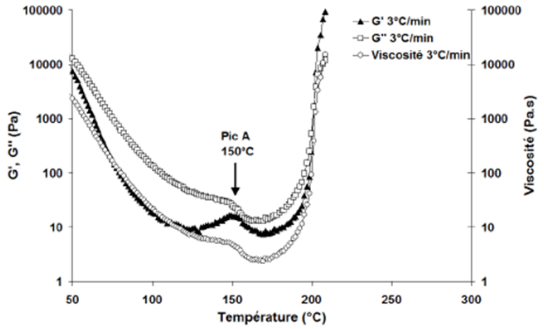

c) Resin shear modulus dependence on the temperature.

Figure 2.3 The illustration of the changes in Tg, η, and G during cure cycle. [25, 26, 27]

2.1.2 Thermoset matrices volume changes during curing.

There is another phenomenon that occurs during cure which is called “the volumetric change”, it can be shortly described in Figure 2.4 [23]. The resin is heated up from point a to b (T_0 to T_c) which the volume is increased due to thermal expansion. Point b to c represent the dwell (holding temperature), chemical shrinkage causes decrease in volume. Point c to d represent cool down stage, thermal shrinkage causes decrease in volume.

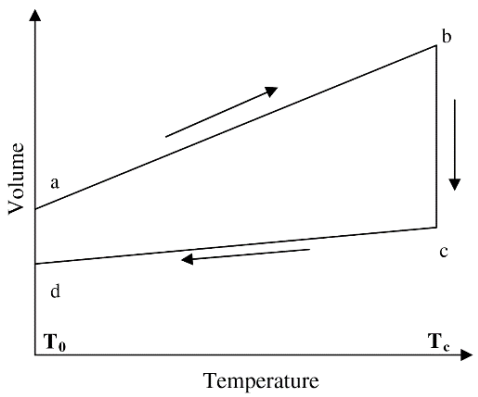

Figure 2.4 Schematic of volume change of epoxy resin during cure. [23]

Since the beginning of the 90's, some researchers have focused their research work upon thermoset matrices shrinkage [28, 29, 30, 31, 32, 33, 34, 35]. Resin chemical shrinkage for epoxy systems not generating any by-product during their reaction is due to the changes in the resin states and crosslinking reaction. A few examples of founding in resin shrinkage are presented in Figure 2.5 [28, 29, 30, 31, 15]. It is all in the same trend that the curing temperature not only induce the expansion of the resin but also the resin shrinkage. However, the resin shrinkage is more relative to the curing time which mean that the phase transformation (liquid → gel → solid) has more impact on resin shrinkage from crosslinking reaction. The literature also mentioned that the formulation of the resin and different batches (age of resin) of resin also have an influence on resin shrinkage since the contraction behaviour was differently observed in Figure 2.5 a) and b).

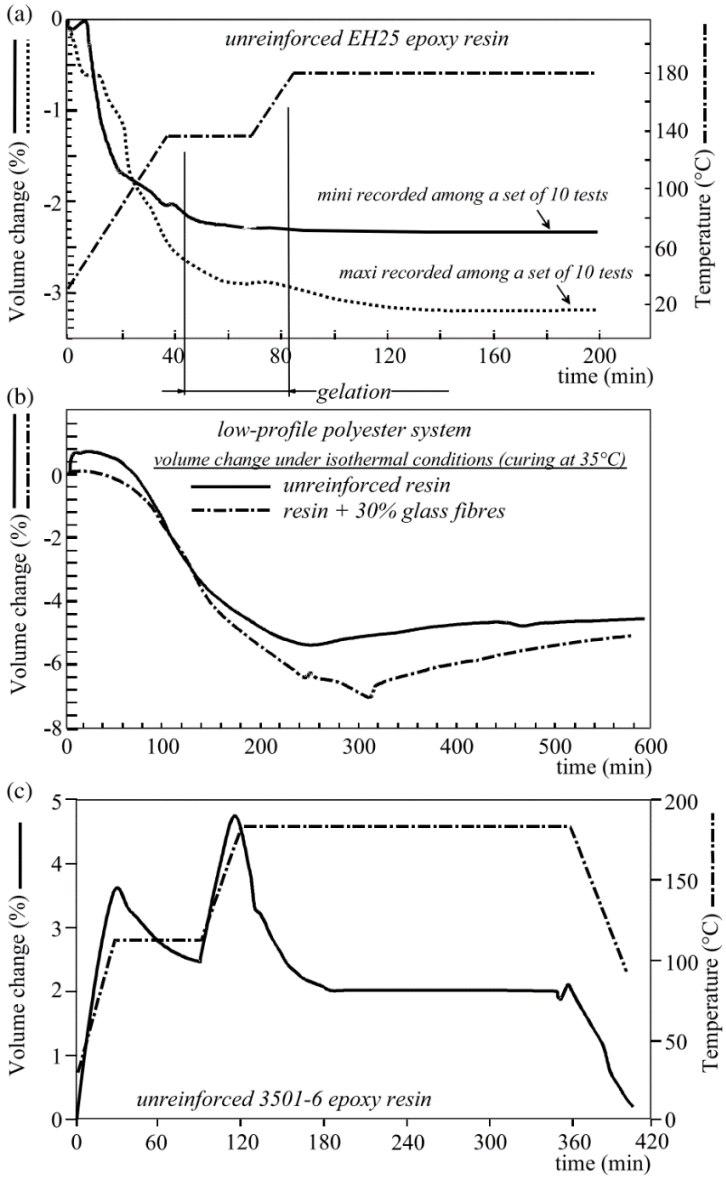

Figure 2.5 Shrinkage in resin during MRCC. [28, 29, 30, 31, 15]

Msallem et al. [36] studied on the changes in sample thickness during cure. Figure 2.6 a) shows the variation of sample thickness throughout the cure cycle, the expansion behaviour follows heating ramp at the beginning but the contraction was observed during isothermal dwell due to the chemical shrinkage. Figure 2.6 b) also shows that the chemical shrinkage of the resin increases linearly with the degree of cure.

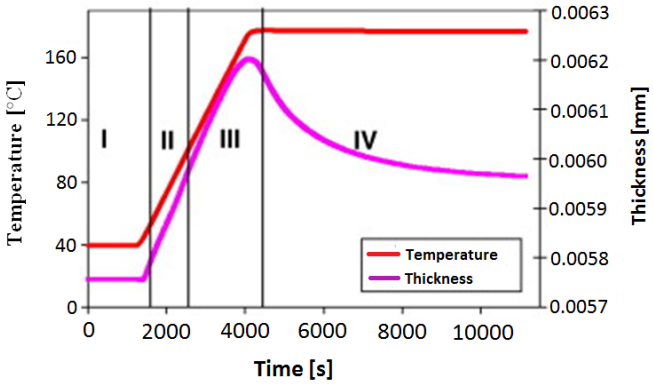

a) Sample thickness variation and the surface temperature during the cure cycle.

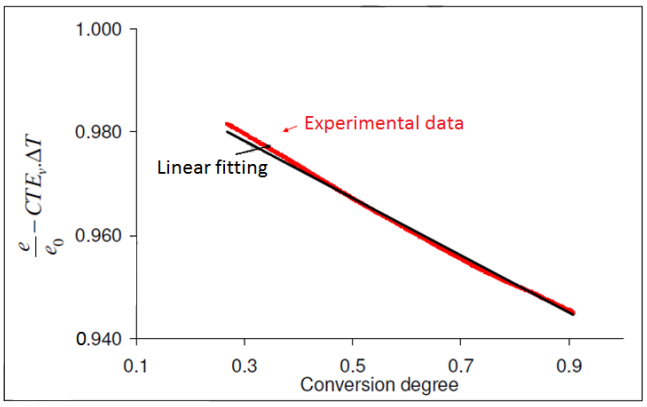

b) Sample thickness variation, due to chemical shrinkage, as a function of the conversion degree.

Figure 2.6 Sample thickness variation due to temperature and chemical shrinkage. [36]

Phase changes can also be followed on Time-Temperature-Transformation (TTT) diagram. This type of diagram was first proposed by Enns and Gillham [37]. There is also another example TTT diagram which was proposed in the thesis of C. PARIS [27] in 2011. He measured the viscosity of the M21 resin under isothermal and dynamic tests. The construction of TTT diagrams for both isothermal and dynamic tests is illustrated in Figure 2.7 a) and b) respectively. In these diagrams, gelation and vitrification phase changes are plotted together with degree of cure (α) curves. They were able to clearly spot a mapping of the resin transformations from one state to one another (liquid-gel-glassy states) during its

crosslinking and facilitated the definition of the optimal cure cycle. When referring to Figure 2.1, Figure 2.2, Figure 2.3 and Figure 2.7, the reader clearly understands that before reaching the gel point (end of gelification inside the matrix), a fraction of the matrix remains liquid so a zero stress state can reasonably considered. An another fact to underline is that between the beginning and the end of its curing, the thermoset polymer undergoes some volume changes mainly stemming from phase changes.

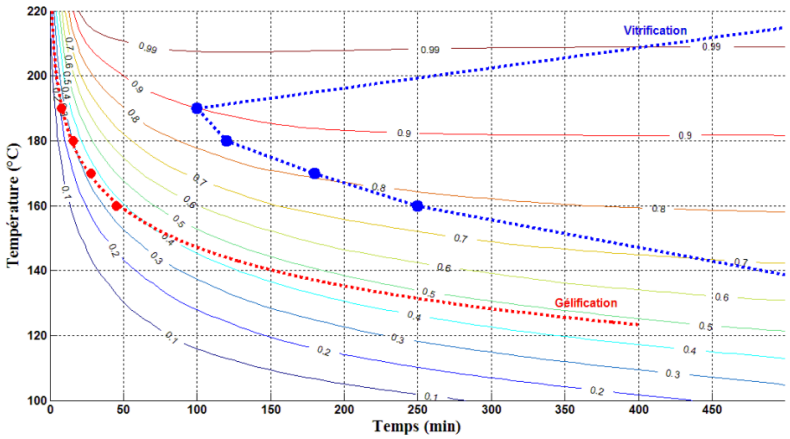

a) Isothermal TTT diagram of the unreinforced M21 resin.

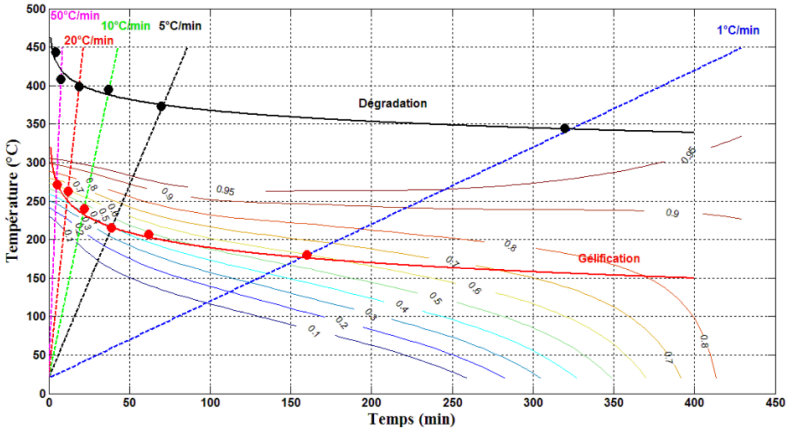

b) Dynamic TTT diagram of the unreinforced M21 resin.

Figure 2.7 TTT diagram of unreinforced M21 resin. [27]

P. Olivier work performed on unsymmetrical $[0_1/90_1]$ laminated strips made of T2H/EH25 carbon/epoxy prepreg in 1998 enabled to show owing to measurement of process-induced displacement by thermomechanical analysis that a non-neglectable fraction of process induced stresses occur under isothermal condition and are totally due to matrix chemical shrinkage. Figure 2.8 shows the changes in the curvature of these $[0_1/90_1]$ laminated strips monitored by DMA and shows the TMA configuration used during these tests. It can be seen that $[0_1/90_1]$ laminated strips start to exhibit a curvature development under isothermal condition. When referring to the phase transitions recorded for this

carbon/epoxy system, it can be imagined that none stress appears before the end of gelation [14]. The other information is that for this carbon/epoxy system at maximum 8% of the out-of-plane deflection or spring-in is from chemical origin. Secondly, some may wonder which kind of behaviour should be used to simulate process-induced stress development: thermostatic?, CHIELD? or thermoviscoelastic? They are invited to pay careful attention to Figure 2.8 which can be seen that the curvature development curve is purely linear with respect to temperature.

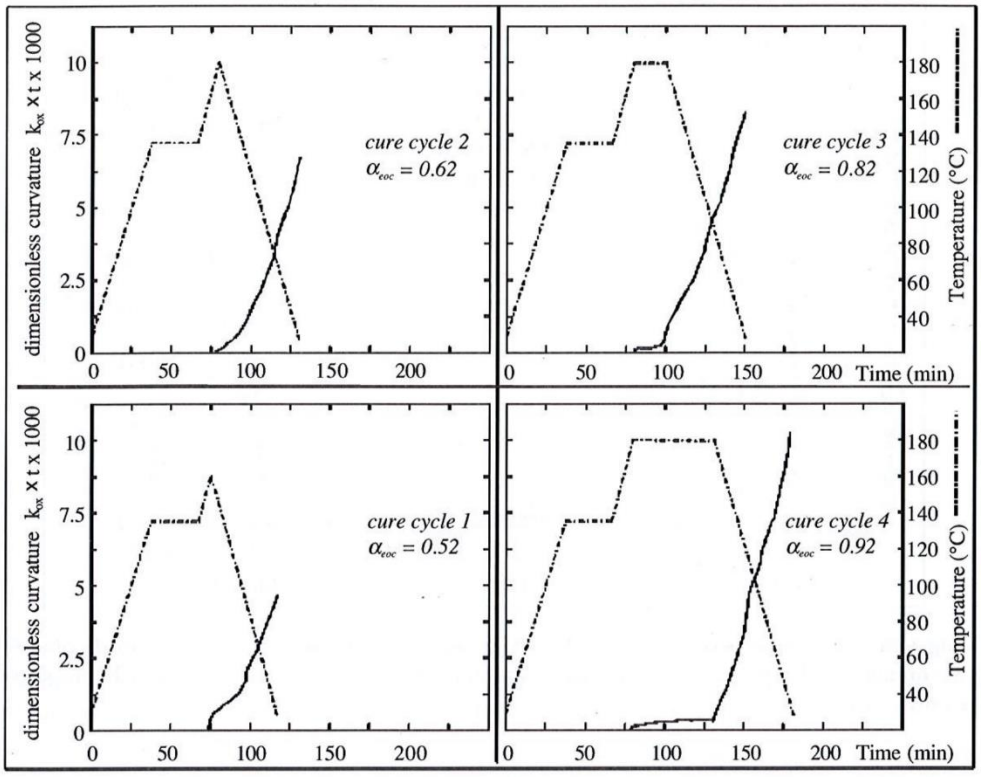

Figure 2.8 The changes in the curvature of [0_1/90_1] laminated strips during various cure cycles. [14]

2.2 Intrinsic origins of laminated parts distortion

Figure 1.10 diagram has purposed an identification and a classification of process-induced deformations. This part of the second chapter will present to the reader the stat of the art about these deformations by following Figure 1.10 classification. The idea is to examine all the parameters influencing and all the factors generating process-induced deformations in the case of autoclave cured path.

2.2.1 Effect of stacking sequence or layup

The effect of stacking sequence to part deformation has been investigated because differences in fibre direction between each layer of ply will cause warpage. Thus, the

deformation from the stacking take places due to different in-plane stress is generated within the plies [38], this is by reason of the difference in the coefficients of thermal expansion at the ply level. However, part shape and size should be identical in order to compare the effect of stacking sequence efficiently.

Starting from flat laminate, Nasir et al [39, 40] studied the effect of stacking layup on spring-back deformation for IMA/M21E flat laminate composite with four plies thickness and symmetrical layup, the dimension all part samples was 300 X 300 mm^2, and they were autoclave-cured on carbon steel tool. There were four conditions of stacking sequences, including [0º/90º]s, [0º/45º]s, [45º/0º]s and [45º/-45º]s. The results of maximum spring-back warpage are shown in Figure 2.9 and compared to unidirectional laminate $[0]_4$ from another study performed by same authors [41]. The unidirectional layup ($[0]_4$) exhibited lowest out-of-plane deflection but the interesting point is that the angle-ply laminate ([45º/-45º]s) provided closer magnitude of deformation to unidirectional laminate and also extremely lower than the others even if it has lower longitudinal and transversal stiffness compared to cross-ply laminate ([0º/90º]s), see Table 2.1. This conclusion was justified by the effect of quasi-isotropic nature of angle-ply laminate that might reduce the warpage. The study also showed that the effect of ply in contact with mould and alternating ply between [0º/45º]s and [45º/0º]s has no influence on part distortion. The work discussed earlier is the case of flat laminate with a square in-plane shape. However, the research work of Sun et al [42] indicated that having more 0º plies placed along part length can reduce the distortion of flat part when the width is relatively small compared to the length. This is the comparison of unsymmetrical flat laminates between $[0_6/90_6]$ and $[0_9/90_3]$ which indicated that $[0_9/90_3]$ gave lower distortion for the same thickness of 12 plies.

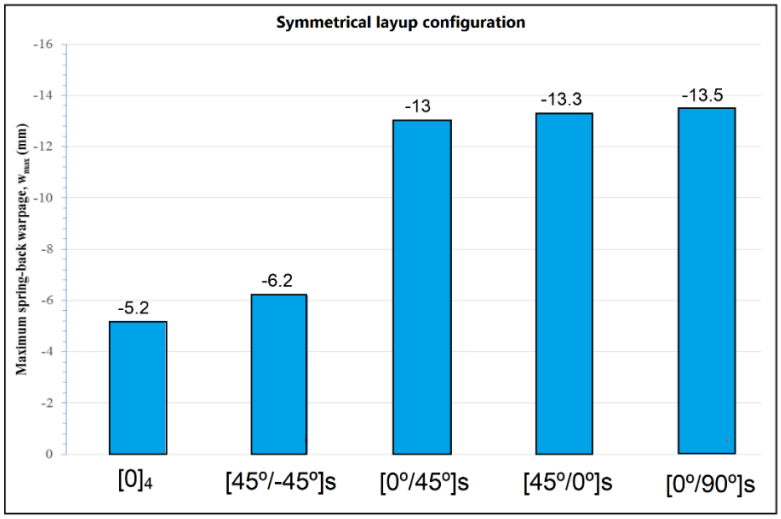

Figure 2.9 Maximum warpage of the samples. [39, 40, 41]

Table 2.1 Stiffness of the laminate from Nasir et al. [39, 40, 41]

Layup	Longitudinal stiffness	Transversal stiffness
$[0]_4$	154 GPa	8.5 GPa
[45º/-45º]s	12.2 GPa	12.2 GPa
[0º/45º]s	83.1 GPa	10.3 GPa
[45º/0º]s	83.1 GPa	10.3 GPa
[0º/90º]s	81.3 GPa	81.3 GPa

Apart from initial flat laminate, the curve initial shaped laminates in the form of L and U (or C shape) (see Figure 1.9) were extensively studied in the past researches. Early started in 2002, Fernlund et al. [43] compared the effect of different part layups of L shape laminates for unidirectional (UD, $[0]_{12}$), cross-ply (CP, $[0/90]_{6s}$) and quasi-isotropic (QI, $[0/+45/-45/90]_{2s}$). QI exhibited a little higher spring-in than UD and CP laminates but it was difficult to make value judgments because their thicknesses were not identical and the difference in spring-in values was only about 0.15°. However, similar trend was found in the same year from Albert and Ferlund [44]. In fact, QI obviously had average more spring-in than UD in all cases for L and U shape parts. Their conclusion was that the QI contains greater through-thickness contraction due to Poisson's effect which generates anisotropy mechanism vary in the ply level. This was also mentioned by Radford and Rennick [45]. Erik et al. [46] investigated in more details deformation of L and U shape parts in terms of spring-in of flang angle and web warpage for the following layups UD32 ($[0]_{32}$), CP32 ($[0/90]_{8s}$) and QI32 ([[45/-45/90/0]s]2s). The schematic of flang spring-in and web warpage are presented in Figure 2.10. Spring-in angle of the UD32 was lower than CP32 and QI32 for both L and U specimens, this might ensure the transversely isotropic of UD layup is able to reduce in-plane and through thickness strain and results in less spring-in. The web-warpage of UD32 was also lower than CP32 and QI32 when it was fabricated on low CTE tool made of Invar but the result was in contrast to what fabricated on high CTE tool made of aluminium. The explanation for this change put forward by Ersoy et al. [47] that stress transfer between identical orientation plies in contact is higher than different ply orientation in contact and tend to increase stress magnitude in the specimen and increase web warpage.

In 2013, Kappel et al. [48] investigated more variety of part layups for L shape laminates and found that having more 0 plies aligned in the circumferential direction can decrease the spring-in for symmetrical QI laminates ([45,-45,90,0]s vs [45,-45,0,90,0]s vs [45,-45,02,90,03]s), this is due to larger bending stiffness dominates the spring-in. Moreover, alternative ply layups including $[0]_4$, $[90]_4$, [0/90]s and [45/-45]s were also examined. The maximum spring-in distortion was observed from [45/-45]s followed by [0/90]s and $[0]_4$,

similar trend was also achieved by Erik et al. [49], this can confirm that the number of 0 ply can increase bending stiffness and then dominate the spring-in distortion. The results can be considered in agreement with many research works for angle laminate discussed above. However, it was surprising that the $[90]_4$ configuration provided dramatically less spring-in compared to the others. It should be noted that the part stiffness of $[90]_4$ is very low because of resin dominate the bending stiffness, so, it can be easily deformed.

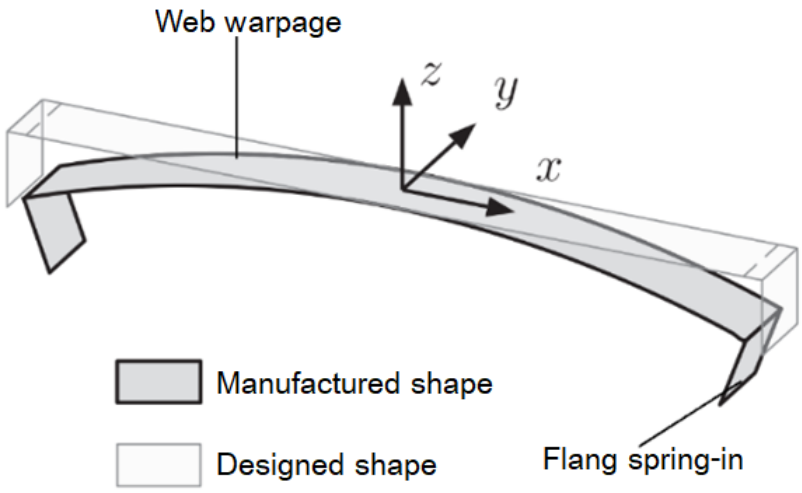

Figure 2.10 Flang spring-in and web warpage at room temperature measured after curing. [46]

In 2017, Bellini et al. [50] performed the experiment for L shape specimens made of unidirectional AS4/8552 prepreg. The picture of fabrication and the full factorial plan are shown in Figure 2.11. The stacking sequence consisted of various unidirectional layups including [0]n, [30]n, [45]n, [60]n, [90]n, a cross-ply ([0/90]s), and a quasi-isotropic ([45/-45/90/0]s). Other details of fabrication were identical except mould corner radius and part thickness, as specified in reference [50]. Spring-in results were measured by CMM (Coordinate-Measuring Machine) and effect of changes in radius, layup and number of plies upon spring-in are plotted in Figure 2.12. Increment of layup angle form 0˚ to 90˚ can markedly reduce spring-in for unidirectional layups. Similar results were also obtained by Johnton et al. [51] for layups between $[0]_{24}$ and $[90]_{24}$, and by Kappel et al. [48] as discussed earlier. The conclusion of outcome was not provided in the literature, while cross-ply [0/90]s and quasi-isotropic [45/-45/90/0]s still exhibited greater spring-in than [0] layup. In contrast, Lalit et al. [52] found that laminates with layups such as [0]n, [45]n and [0/45]s exhibited insignificant differences in their spring-in measured at room temperature after curing. In 2018, Bellini et al. [53] repeated the experiment with U shape specimens, similar trend was obtained as in Figure 2.12. The conclusion was mentioned to the highest bending stiffness along the circumference direction (according to the length of the specimens) of [0] laminate

that might enhance the springback of fibre. When looking at Figure 2.12, it can be seen that the springback level is dependence in the layup and is higher when the layup generates differences in CTE between plies. Effectively the highest springback is obtained with [0/90] laminate which are no symmetrical. So, the symmetry of the layup has equally a great influence upon the springback.

Factor	# levels	Level value
Mould corner radius [mm]	3	4, 8, 16
Number of plies	3	4, 8, 16
Stacking sequence	7	[0], [30], [45], [60], [90], $[0/90]_s$, $[45/-45/90/0]_s$

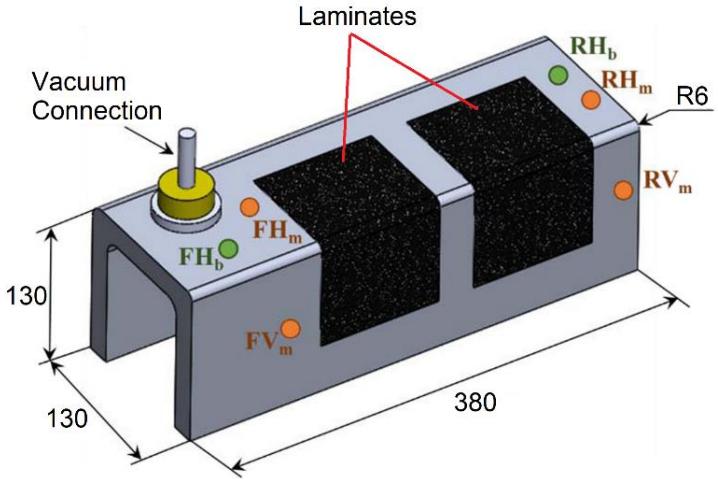

Figure 2.11 Mould for cure of L-shape laminate and the full factorial plan from Bellini et al. [50]

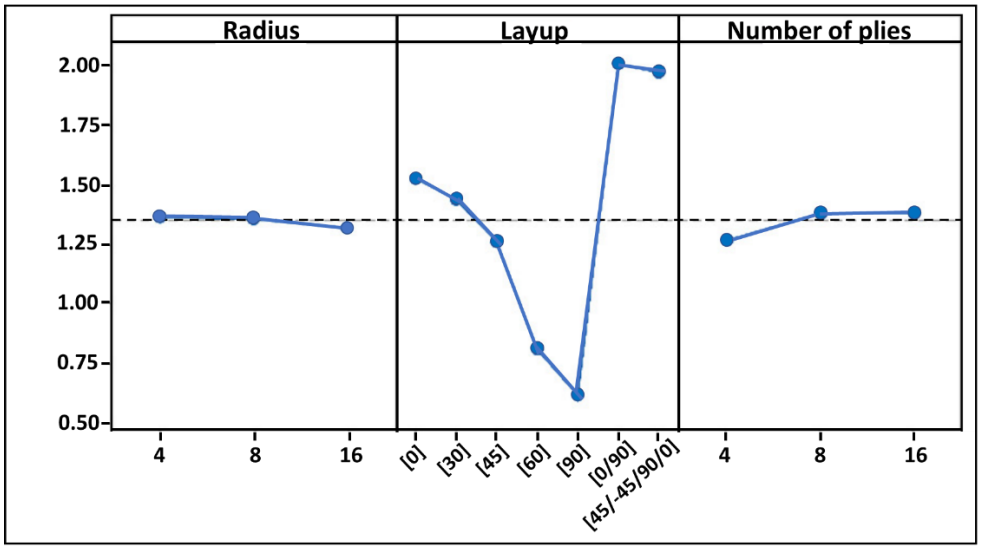

Figure 2.12 Main effects plot for spring-in from Bellini et al. [50]

Pooneh et al. [54] investigated the effect from stacking sequence for flat, L-shape, and U-shape samples in term of symmetric versus asymmetric and balanced versus unbalanced layups. The samples were made of IM7/997-2 UD, more information upon this material properties can be found in literature. The set of experiment performed in [54] is illustrated in Table 2.2, other details of fabrication can be seen in the reference. The warpage of initially flat samples cured on aluminium mould and measured by CMM scanner are plotted in Figure 2.13. Focusing on 16 plies layup, it can be seen that asymmetric samples (panels 1 and 4) provided markedly greater warpage than symmetric samples (panels 2 and 3). When considering symmetrical samples (panels 2 and 3 - Figure 2.13), it can be seen that the distortion seems unsensitive to the fact that the stacking sequence was balanced or not. Lalit et al. [52] obtained similar results. Their conclusion was that there was no significant difference of the layup sequence for symmetrical layup between [90/0/90/0]s and [0/90/0/90]s. If we now pay attention to panels 1 and 4 (Table 2.2 and Figure 2.13) which have not a symmetrical stacking sequence, we see that the fact that panel 1 layup in balanced produced a higher warpage than the one exhibited by the unbalanced panel 4. When looking at panels 5 and 6 which are thinner than panels 1 to 4 with only 8 plies instead of 16, it can be seen (Figure 2.13) that their warpage is larger than the one exhibited by the thicker laminates with the same plies orientations when comparing panel 2 with panel 5 and panel 1 with panel 6. This shows the effect of the bending stiffness upon room temperature warpage of initial flat laminates measured after curing. Effectively in terms of bending the second moment of area of 16 plies laminates is 8 times higher than 8 plies laminates one. Spring deformation was also investigated in [54] for L-shaped samples as shown in Figure 2.14, greatest and lowest spring-in were observed for symmetric balanced and asymmetric unbalanced stacking sequence respectively. Reference [54] also studied U-shaped laminates (Table 2.2). Obtained results show that a symmetric balanced laminate exhibited a larger spring-in angle than an asymmetric balanced one, this is the same trend with L shaped laminates. Unfortunately, Pooneh et al. did not provided any reasonable conclusion for all outcomes of this study.

Table 2.2 Manufacturing configuration from Pooneh et al. [54]

No	Geometry Prior to curing	No. of plies	Stacking sequence	Laminate type	Tooling material
1	Flat (430x430 mm^2)	16	$[0/45/90/-45]_4$	Asymmetric, balanced	Aluminium
2	Flat (430x430 mm^2)	16	$[0/45/90/-45]_{2s}$	Symmetric, balanced	Aluminium
3	Flat (430x430 mm^2)	16	$[0/45/90/45]_{2s}$	Symmetric, unbalanced	Aluminium
4	Flat (430x430 mm^2)	16	$[0/45/90/45]_4$	Asymmetric, unbalanced	Aluminium
5	Flat (430x430 mm^2)	8	$[0/45/90/-45]_s$	Symmetric, balanced	Aluminium
6	Flat (430x430 mm^2)	8	$[0/45/90/-45]_2$	Asymmetric, balanced	Aluminium
7	Flat (430x430 mm^2)	16	$[0/45/90/-45]_4$	Asymmetric, balanced	Steel
8	Flat (430x430 mm^2)	16	$[0/45/90/-45]_4$	Asymmetric, balanced	Carbon fibre-epoxy composite
9	L-shape	16	$[0/45/90/-45]_4$	Asymmetric, balanced	Aluminium
10	L-shape	16	$[0/45/90/-45]_{2s}$	Symmetric, balanced	Aluminium
11	L-shape	16	$[0/45/90/45]_4$	Asymmetric, unbalanced	Aluminium
12	L-shape	16	$[0/45/90/45]_{2s}$	Symmetric, unbalanced	Aluminium
13	U-shape	16	$[0/45/90/-45]_4$	Asymmetric, balanced	Aluminium
14	U-shape	16	$[0/45/90/-45]_{2s}$	Symmetric, balanced	Aluminium

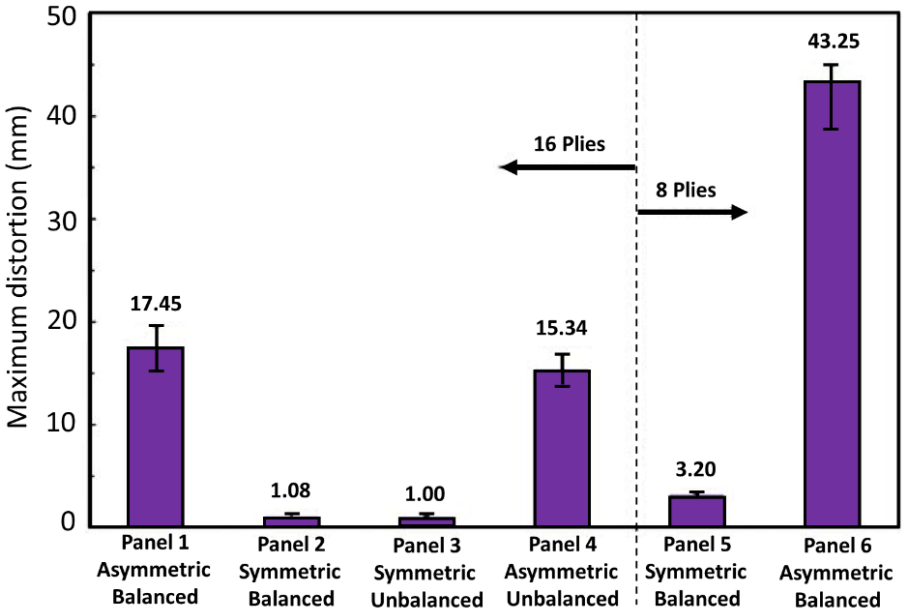

Figure 2.13 The distortion of flat samples cured on aluminium mould from Pooneh et al. [54]

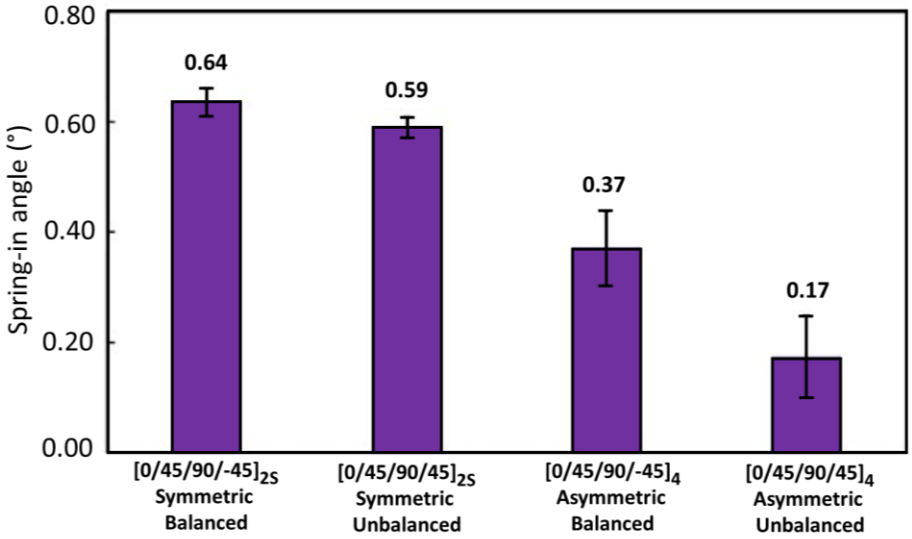

Figure 2.14 Effect of stacking sequence on spring-in angle of the L-shape from Pooneh et al. [54]

2.2.2 Effect of part shape

The part shape is the first parameter to determine the characteristic of part deformation. Several research works received funding support and case study from manufacturers to conduct the experiment based on the actual geometry to clarify the problem which is the most effective way. However, in most cases, the researchers pay the effort to study on the geometry close to the original one to simplify the fabrication parameters for instance the manufacturing of mould shape.

The effect of geometry locking was studied in the research of Fernlund et al [55]. They fabricated the sample boxes structure with one side open called the T-45 rib shown in Figure 2.15, five samples were manufactured with eight layers of AS4/977-3 woven carbon/epoxy prepreg (code $[0^o/45^o_3]s$) on a convex aluminium tool. Then, the spring-in deformation was measured along the length of all samples. Afterwards, all samples were cut to be 5 sections and spring-in were again measured. The results of spring-in deformation before and after sectioning are illustrated in Figure 2.16. Consider the results before sectioning, the largest spring-in distortion appeared in the middle, at both ends gave lowest deformation due to geometry locking. On the other hand, the deformation after sectioning looked stable because of unlocking in part geometry even though they provided higher spring-in value compared to full box structure. Goran also studied the effect of geometry locking by comparison between L and U shape part [43]. At the same conditions of material, the lay-up sequence, tool surface, and cure cycle, U shape specimen gave higher spring-in than L shape specimen which agrees with another work from Carolyne [44], Erik [46] and the experiment from Pooneh et al. that compared L and U shape samples [54].

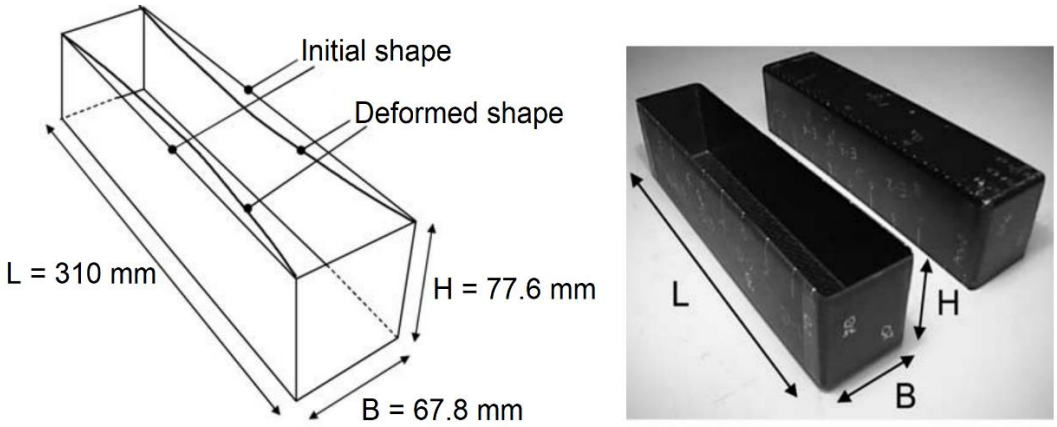

Figure 2.15 The T-45 rib sample. [55]

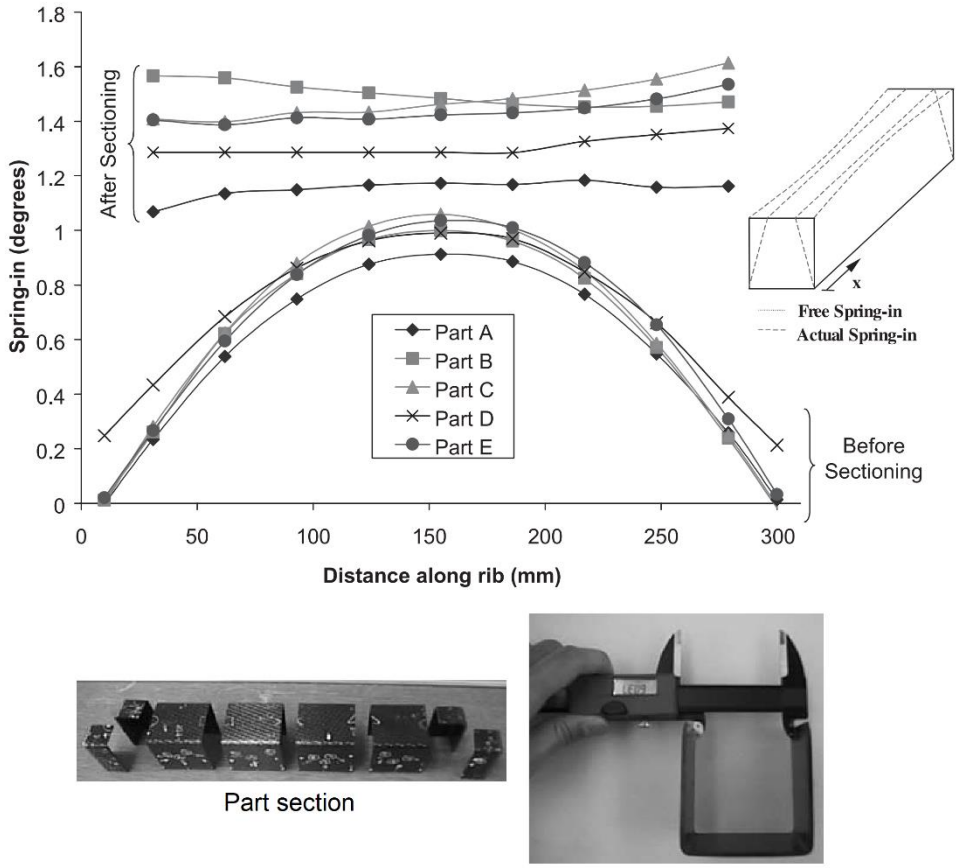

Figure 2.16 Spring-in deformation results. [55]

Moreover, Fernlund and his team also studied the effect of geometry locking on actual part [55], the Boeing 777 Aft Strut Trailing Edge Fairing (Figure 2.17) which is similar to a box structure. Its structure consisted of Nomex honeycomb core and carbon/epoxy skins (Hexcel F593 style 3K-70-PW fabric prepreg), fabricated on a concave tool with adhesive film (Cytec Fibreite Metalbond 1515) between core and skins. The maximum spring-in was

at the wide end in section1 and decreased along the length to the tip in section4, this is because of the section 4 has higher stiffness due to geometry locking.

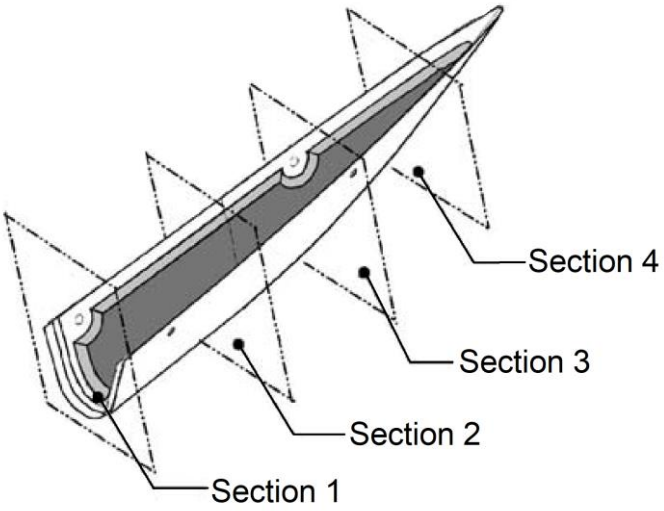

Figure 2.17 The Boeing 777 Aft Strut Trailing Edge Fairing. [55]

2.2.3 Effect of part dimension

The effect of part dimension is referring to the size and thickness. As shown in several studies carried out either on unidirectional or on unsymmetrical initial flat laminates, the laminate area for instant the laminate surface in contact with the tooling as an effect on the deformed shape after curing if the laminate is not free standing during the cure cycle. Their effect is strongly linked as we will see later with the processing conditions such as pressure level, mould material and release agent. In this section, the reader will be provided with the subject dealing with the effect of laminated part surface and laminated part cross-section (in the case of semi-closed shapes or boxes).

Let look first at laminate size. By size we consider the area of the laminate in contact with the mould surface. For initially flat laminate, in one of their very first work, A. Poursatip [56] and his research team showed how the laminate length and surface for UD plates influences the out-of-plane deflection after curing (see Figure 2.18). Similarly, K. E. Tarsha-Kurdy and P. Olivier [57, 58] have shown for $[0_2/90_2]$ laminates how the reduced curvature measured after curing was depending on laminate surface (see Figure 2.19) which indicated the presence of interfacial forces between the mould and the laminate bottom surface.

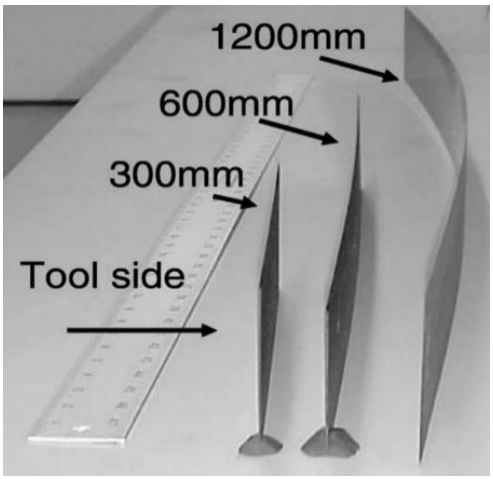

Figure 2.18 The out-of-plane deformation shape for UD laminates with various lengths. [56]

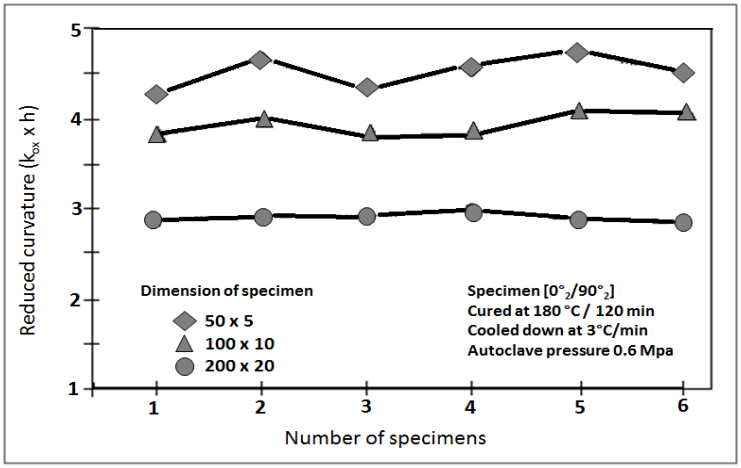

a) Reduced curvature (k_{ox} x h) of [0°$_2$/90°$_2$] cured with ETFE film between mould and specimen

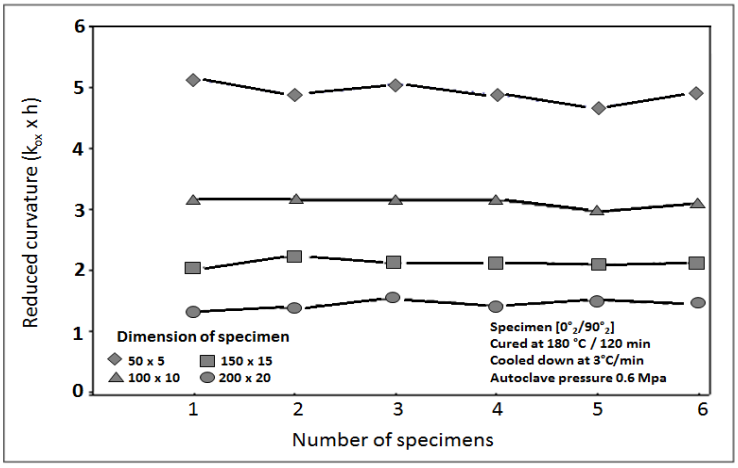

b) Reduced curvature (k_{ox} x h) of [0°$_2$/90°$_2$] cured with silicone sheet between mould and specimen

Figure 2.19 Reduced curvature (k_{ox} x h) results of [0°$_2$ / 90°$_2$] after curing. [57, 58]

Mezeix et al. [41] also studied the effect of laminate dimension but for initial flat specimen. The specimens were laid up by UD prepreg IMA/M21E and cured on carbon steel tool. The differences in sizes and thicknesses of flat samples were prepared as in Table 2.3, five samples for each configuration were manufactured, so totally 45 samples were measured. The definition of the warpage is shown in Figure 2.20 and the average values are placed in the Table 2.3. The results are markedly verified that at the same sample size, increment of thickness will dramatically reduce the warpage due to an increase of bending stiffness as mentioned from Pooneh et al. [54] and Tushar et al. [59]. In other words, increasing laminate size enlarges the warpage at the same thickness. In conclusion, small size and large thickness will result the lowest warpage. This conclusion is in agreement with those of Carolyne [44], Stefaniak [60, 61], Radford [45], Zakaria et al. [62] [63] and Graham et al [56]. The study of E. Kappel [46] also reported the same result for the experiment of sample UD16, UD32, UD48, and UD 64, the lowest warpage was observed from UD64. Cleary showing once again as if it was necessary the effect of bending stiffness. Contradictory, Bellini et al. [50] mentioned that thickness in term of number of plies has no effect on spring-in, they found a little different spring-in between 4, 8, and 16 plies for L-shape specimen (see Figure 2.12). Lalit et al. [52] also found no difference spring-in between $[0]_4$, $[0]_6$, and $[0]_{10}$; and between $[45]_4$, $[45]_6$, and $[45]_{10}$ layups. The result from Lalit et al. is according to E. Kappel et al. [48] that “spring-in of unidirectional laminates is independent from the part thickness”. One more interesting conclusion was reached by Satish and Smith [64] who mentioned that spring-in is independent of thickness for thick parts with more than eight plies.

In reality, it is complicated to avoid the effect of part shape and dimension on part distortion after curing because the aircraft parts have their own requirement design on the geometry and weight limit. The modification of part shape, size and thickness is usually not allowed to reduce or eliminate those deformation. Various part researches have studied those effects but it is only for a comprehension strategy. From our point of view, it is more logical to put emphasis on the effect of stacking sequence and curing environment.

Table 2.3 Experimental schedule for warpage investigation (mm). [41]

Thickness	Sample size		
	300X300 mm^2	400X400 mm^2	500X500 mm^2
4 plies	5.2	9.19	23.3
8 plies	1.45	2.37	4.5
16 plies	0.32	0.6	1.47

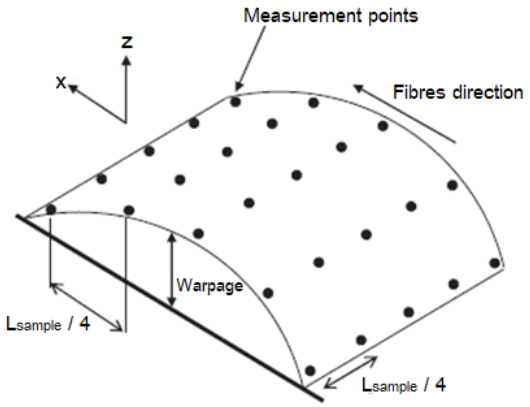

Figure 2.20 Warpage definition of Mezeix et al. [41]

2.2.4 Miscellaneous

The effect from thickness might be counterbalanced by the effect of temperature in term of thermal mismatch as mentioned in research work from Woo-Kyun Jung et al [65]. They studied the samples of composite beams that consisted of 8 plies carbon fibre with different numbers (thickness) of glass plies. The conditions in their experiment were unidirectional layup between carbon 8 plies and glass 4, 8, 12, 16 and 20 plies. Basically, 8 plies carbon with 4 plies glass should give maximum springback due to the thinnest condition but 8 plies carbon with 8 plies glass exhibited highest springback instead, this is because of largest thermal mismatch between these two materials was enhanced for equal number of plies between two different materials. In contrast, 4 plies glass samples can reduce the effect of thermal mismatch whereas in the other 3 conditions, thicker glass plies could dominate the thermal mismatch.

2.3 Extrinsic origins of laminated parts distortion

Higher performance composite parts reinforced with carbon fibres generally induce high cost in terms of material, curing facility and moulds which results in expensive parts. Scraping such parts because of dimensional stability problems is a fact that all industries would like to avoid. This is why the deformation of composite parts after their curing has become several tens of years a real challenge for aerospace industries [60, 61, 66]. In the current section, the reader will be provided with a state of the art about the effects of moulds (material and shape), the effect of release agent and lately those of cure cycles.

2.3.1 Effect of mould

In composite manufacturing, mould is one of the most important tool to form the final shape of laminated parts. Several factors related to mould characteristics were examined in

many research works. There are many types of mould which depend on the considered manufacturing process. This section will describe the effect of mould in terms of tool/part interaction to the behaviour and the deformation of laminated part. The effect of mould in several factors including material and coefficient of thermal expansion, shape, surface and release agent will be discussed.

2.3.1.1 Effect of mould material and coefficient of thermal expansion

The mismatch of coefficient of thermal expansion between the part and mould generates the residual stress during manufacturing. In principle, the composite part is laid up and formed with applied pressure and vacuum on the metallic tool which has much higher coefficient of thermal expansion than itself and the part is stretched during processing [47]. Figure 2.21 shows a simple mechanism, the surface of the part that is attached to the mould will undergo higher tension causing unbalance of in-plane and through thickness stresses [67]. At the early stages of curing, the resin modulus is low and easy to be formed by the expansion of the mould. The highest stretching takes place on the bottom ply adjacent to the mould surface. After the curing is completed, a bending moment can be generated due to this condition which finally generate a warpage. However, The CTE's for the tool may be slightly different between longitudinal and transverse directions but it can be neglected and considered to be constant [60, 61].

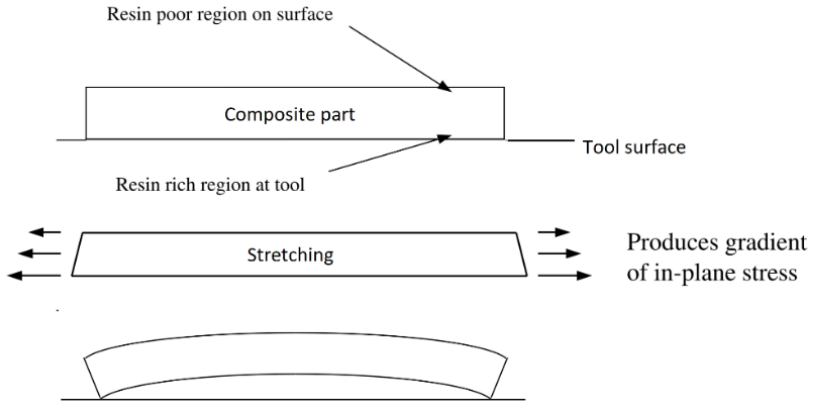

Figure 2.21 Distortion due to shear interaction at tool surface. [67]

R. de Oliveira et al [68] investigated the effect of the mould thermal expansion on the development of internal stresses during cure. They studied unidirectional ($[0]_4$, 250X150X1.2 mm) and cross-ply ($[0_2/90]$s, 250X150X1.8 mm) laminates cured on four different flat moulds. The moulds were divided into 2 groups between metallic based (aluminium and steel) and carbon based (carbon composite and carbon foam), the coefficient of thermal expansion for each material is shown in Table 2.4. For other conditions of the experiment, applied vacuum compaction for each two layers stacking, applied release agent, inserted optical fibre

between two layers in the middle of the samples to measure strain, packed in vacuum bag and cured in autoclave with a first dwell at 77 ˚C and a second dwell at 120 ˚C and applied pressure of 5 bars. The results of this experiment illustrated in Figure 2.22, the samples those were cured on aluminium and steel moulds exhibited higher strain than the one cure on carbon-based mould and this for unidirectional laminate (Figure 2.22 a) and in the 0 direction of cross-ply laminates (Figure 2.22 b). In other words, higher shrinkage was observed in the transverse direction of cross-ply laminate cured on aluminium mould due to higher thermal expansion of the mould.

Table 2.4 The coefficient of thermal expansion for four material moulds. [68]

Materials	**Coefficient of thermal expansion (K^{-1})**	
	Longitudinal	**Transversal**
Steel plate	12 X 10^{-6}	
Aluminium plate	23 X 10^{-6}	
Carbon fibre-epoxy quasi-isotropic composite rectangular plate	1.9 X 10^{-6}	0.9 X 10^{-6}
Grafoam FPA35 carbon foam	2.3 X 10^{-6}	

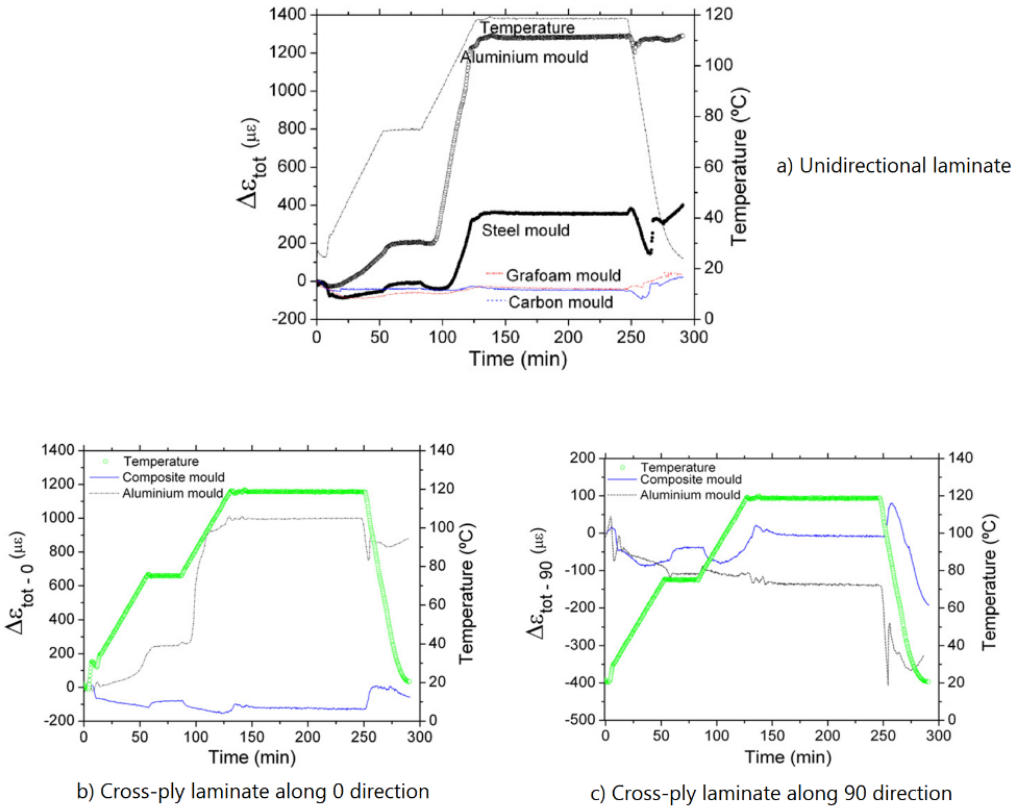

Figure 2.22 Strains during cure for the different moulds. [68]

Carolyne and Goran [44] also obtained similar results about the effect of mould materials with a 6061-T6 aluminium and a A36 steel moulds, they found that aluminium mould always provided a greater spring-in than steel mould. In this case, it is also in agreement with the literature from Pooneh et al. [54], but the distortion of the flat composite part is slightly dissimilar only 7 % between aluminium, steel, and composite tools until their conclusion becomes no significant effect of tooling material on distortion. These authors left this conclusion without providing the reader with additional explanation.

However, the effect of difference in CTEs of metallic tooling materials was also studied by Kappel et al [48]. They compared the results of spring-in of AS4/8552 L-shape specimens with unidirectional, angle-ply ([45,-45]s) and cross-ply ([0,90]s) laminates laid up on an aluminium (CTE = 24 ppm/K) or on an invar (Ni36, CTE 0.50-2 ppm/K) mould. Surprisingly, these authors [48] found out that thin laminate L-shape parts (with 4 plies at 0°) exhibited very close spring-in value whatever the mould material was (aluminium or Invar). In contrast, eight-plies specimens obviously showed lower spring-in value for the specimens cured on invar mould. The results for UD specimens were unclear for this study since lower CTE of invar should induce lower spring-in. Accordingly, aluminium mould also provided higher spring-in than invar mould for angle-ply and cross-ply laminates. In 2016, the same authors [46] carried out another study about the effect of mould material upon the spring-in of large series of L and C-shape laminates made of AS4/8552 carbon/epoxy prepreg (see Table 2.5). In this study, all manufacturing parameters such as cure cycle, bagging products and mould surface were identical. The specimen shape configuration is illustrated in Figure 2.23 and the results of warpage and spring-in are illustrated in Figure 2.24. It is clearly seen and confirmed that lower warpage and spring-in could be obtained from the Invar tool for every sample configuration, in agreement with Satish and Smith [64]. However, although the Invar tool has high performance in composite manufacturing due to their low CTEs compared to the CFRP laminate but its cost is exceeding for cost saving efficiency and the machining is more difficult compared to aluminium. Thus, low cost tool for instance aluminium or steel might be a better choice but additional ways need to be examined to reduce part distortion.

Table 2.5 Configurations of E. Kappel ‘s study with the number of specimens manufactured. [46]

Layup		UD				QI				CP			
Tool material		Alu		Inv		Alu		Inv		Alu		Inv	
Specimen shape		C	L	C	L	C	L	C	L	C	L	C	L
Plies	Thickness [mm]												
16	2.05	✓³	✓²	✓³	✓²								
32	4.10	✓³	✓²	✓³	✓²	✓³	✓²	✓³	✓²	✓³	✓²	✓³	✓²
48	6.14	✓³	✓²	✓³	✓²								
64	8.19	✓³	✓²	✓³	✓²								

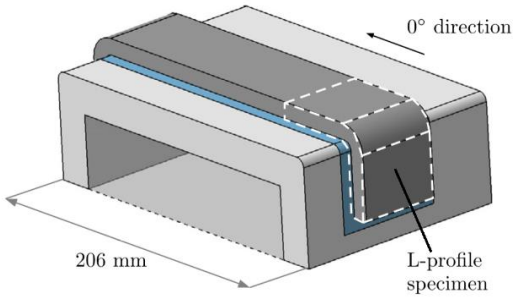

Figure 2.23 Specimen shape (L and C-shape specimens) for E. Kappel ‘s study. [46]

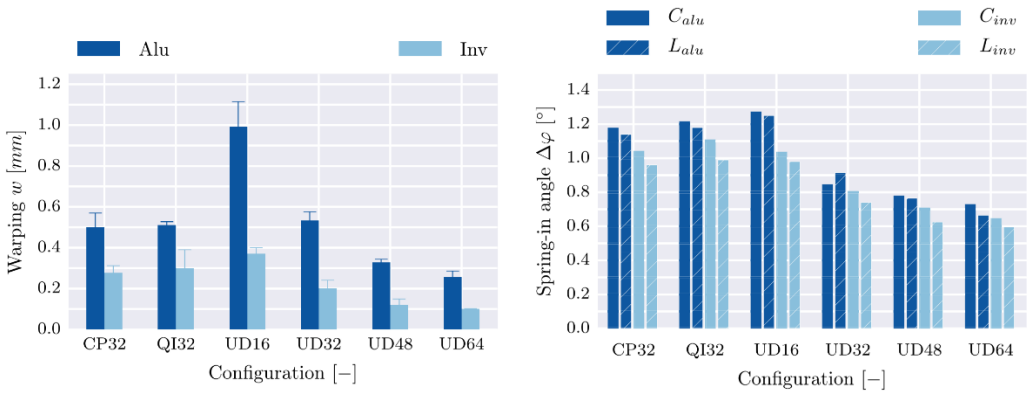

Figure 2.24 Warpage and spring-in distortions from E. Kappel ‘s study. [46]

In other words, composite tools are probably another choice for manufacturers due to less mismatch in the CTEs of composite parts and reasonable cost investment. The design of composite tools was discussed in the literature by Yong Lu et al. [69] with the schematic shown in Figure 2.25. The configuration of composite tools consisted of tool face plate and hollow support structure for hot gas flow for a temperature distribution. The support structure and face plate were bonded by the flexible and heat resistance adhesive. In principle, composite parts will be placed to the face plate during cure and CTEs of the face plate directly affect part distortion. The aluminium and composite tools were employed in the

experiment to fabricate C and V specimens, the ply sequence of face plate was designed to be similar to the composite part but the thickness was larger to enhance the stiffness of the tool. Unfortunately, the effect of tool material was not discussed at the end because both tools were cured according to different curing profiles.

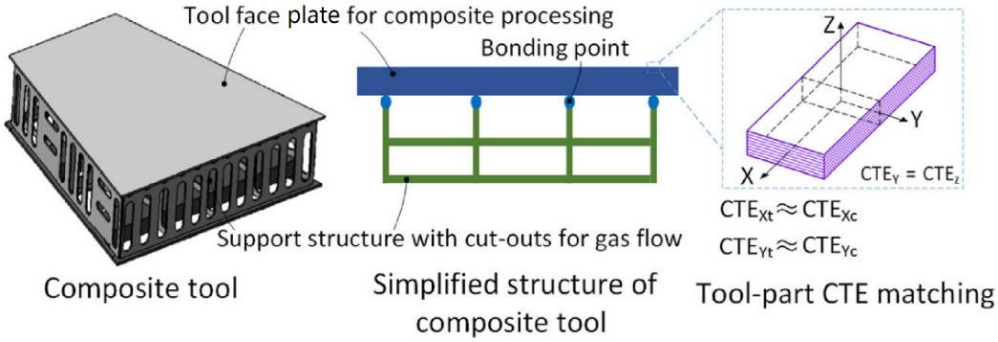

Figure 2.25 The schematic of composite tool, simplified structure, and tool-part CTE matching process. [69]

2.3.1.2 Effect of mould shape

The shape and complexity of the mould are generally defined by the part. This part of chapter 2 will discuss the effect of mould shape in terms of mould angle and radius for manufacturing composite parts exhibiting some radius and angles. There were some investigations on the effects of mould geometry upon the deformation of composite parts. Huang and Yang [70] studied on the warp angle deformation of sample plates ($[0_8]$, 100 x 50 mm^2) manufactured on aluminium moulds with various angles and radii at the same cure cycle. The configurations of aluminium tools are presented in in Figure 2.26. The difference in radius was investigated only on 90˚ mould. The results are given in Figure 2.27 where it can be seen that increasing the mould angle definitely induces a decrease in the warp angle of composite parts. This is in agreement with Zakaria et al. [62] research work, meanwhile the mould radius shows a low effect on the warp angle distortion. This is in agreement with Kappel et al. [49] results. Haung and Yang [70] explained the influence of the mould angle upon the warp angle distortion by the differences in fibre volume fraction in radius area. Increasing mould angle would result in lowering the differences in fibre volume fraction between laminate's flat and radius areas. These conclusions are rather in agreement with those reached by Lalit et al. [52] who investigated the effects of tool angle and radius with various types of layup and tool materials. Their results [52] indicated that spring-in could be decreased by increasing tool angle in every configuration of layups and tool materials, and that mould radius had a limited effect upon spring-in for almost all cases of male tool with different layups. In 2013, Kappel et al. [48] examined the effect of changing in mould radii among 4, 6, 8, and 12 mm. The experiment was set with different types of layup of prepreg AS4/8552 consisting unidirectional, quasi-isotropic, bi-axial, and cross-ply specimens cured

on aluminium and invar moulds with identical cure cycles. The obtained experimental results revealed that spring-in was independent from mould radius, in agreement with Bellini et al. [50] that investigated the effect of varying mould radii 4, 8, and 16 mm for L shape specimens and 5 and 10 mm for U shape specimens. This finding was also validated by Sonnenfeld et al. [71] for the experiment of Z-shape specimen with 8 mm and 22 mm radius not inducing any differences in spring-in.

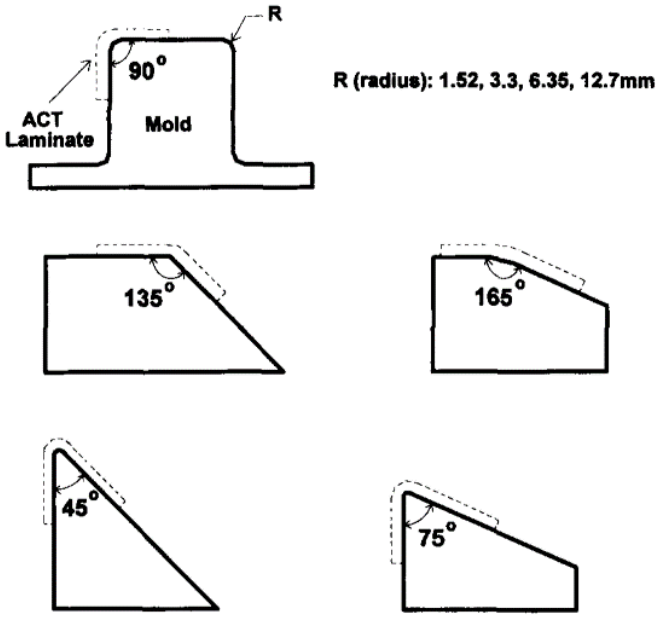

Figure 2.26 Aluminium moulds with various angles and radii. [70]

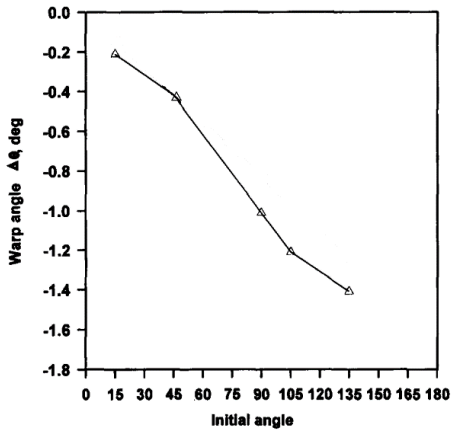

Mold angle (°)	Initial angle[a] (°)	Warp angle (°)
45	135	-1.41
75	105	-1.21
90	90	-1.01
135	45	-0.42
165	15	-0.21

[a]Initial angle = 180°-mold angle.

Mold radius (mm)	Warp angle (°)
1.52	-1.06
3.3	-1.05
6.35	-1.01
12.7	-0.92

Figure 2.27 Experimental results from Huang and Yang. [70]

Another interesting study from Nasir et al. [72] investigated the effect of tool angle on the warpage of angle L specimens. Tool was made of steel with different angles of 30˚, 45˚, and 90˚. IMA/M21E prepreg was chosen to fabricate four plies specimens with unidirectional layup 500 x 500 mm^2. The definition and the results of warpage are illustrated in Figure 2.28 and compared with the result of flat sample (180˚) from another study [41]. It could be observed that the warpage was extremely decreased with increasing tool angle from 30˚ to

90˚ while 180˚ exhibited higher warpage than 90˚ but it was considered to be an error from the measurement method or it might be incomparable between flat and L shapes. They concluded that only tool angle less than 90˚ has an impact on the warp angle while tool angles from 90˚ to 180˚ have less influence on part deformation.

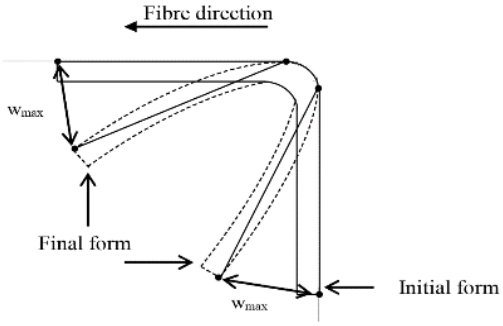

Tool corner angle	Mean warpage
30 º	-36.88 mm
45 º	-33.07 mm
90 º	-19.6 mm
180 º	-23.3 mm

Figure 2.28 The definition of warpage and the results from Nasir et al. [72]

In addition, some authors have shown that the mould angle also has an influence on the fibre bridging problem in the radius area due to resin flow. As discussed in a review paper from Ismet et al. [73], resin flow plays an important role on the fibre volume fraction (vf %). In principle, the part is forced to conform to mould shape by vacuum compaction and pressure applied during manufacturing. In general, the efficiency of applied pressure is low at the corner and lets the resin percolate down which results in corner thickening. This phenomenon encourages low fibre volume fraction at the corner, it inevitably induces more shrinkage in the through the thickness direction and eventually more spring-in. Figure 2.29 shows the schematic of corner thickening of the composite part fabricated on female mould. In this context, if the mould angle is smaller, it will dramatically enhance this phenomenon. In addition, the experimental results of Mujahid et al. [74] also recommended to fabricate L shape part on convex mould rather than concave mould. In this research work [74], Mujahid et al. have settled a modelling of resin flow during the curing of an L-shape part moulded on a concave mould schematically showing what could be the resin flow. Unfortunately, this schematic modelling has not been verified and this can be suspected of lack of consistency.

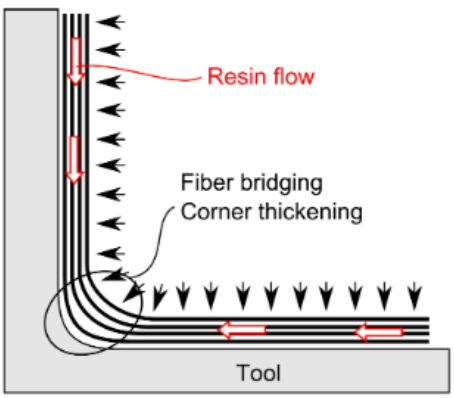

Figure 2.29 Corner thickening due to the resin flow. [73]

In 2018, C. Bellini and L. Sorrentino [53] conduced the experiments of U shape laminates made of AS4/8552 prepreg (dimension shown in Figure 2.30 a)) which were fabricated on aluminium male mould by using a full factorial DOE (Design of experiment). The configurations of experiment are illustrated in Figure 2.30 b). The tool radius was divided into two levels between 5 and 10 mm. The results from ANOVA show that tool radius had a slight influence on the spring-in and this is in accordance with the discussion above. However, they investigated the effect of tool radius from the male mould; on the other hand, too small tool radius directly increased spring-in of the part fabricated on female mould due to matrix bridging from resin rich layer that appeared in the experiment of Lalit et al. [52]. Nevertheless, these authors are claiming that there are some fibre volume fraction (vf %) effects in radius areas do not perform any vf % measurement and do not provide any micrography of the material that can support this statement.

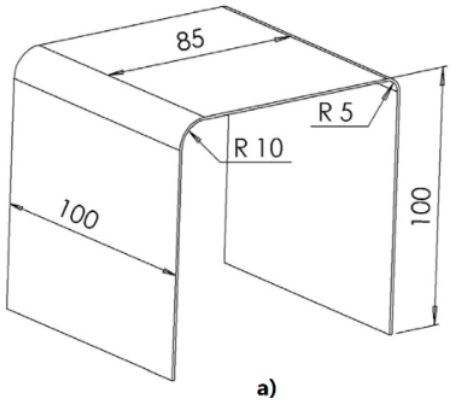

a)

Factor	# levels	Level value
Mould corner radius [mm]	2	5, 10
Number of plies	3	4, 8, 16
Stacking sequence	7	[0], [30], [45], [60], [90], $[0/90]_s$, $[45/-45/90/0]_s$

b)

Figure 2.30 The experiments of Costanzo and Luca. [53]

2.3.1.3 Effect of mould surface and release agent

From a manufacturing point of view, these are 2 main categories of releasing agents: liquid releasing agent and polymer sheet releasing agent such as PTFE-based films. Releasing agent plays a vital role between part and mould in composite manufacturing. It acts like a barrier to avoid stick-up between part and mould surface and alleviate the difficulty of part removal [75]. Moreover, the surface preparation and surface roughness of metallic mould have high impact on the friction coefficient between part and mould [76]. Generally, a release agent is applied to the tool surface in the form of wax, polymer-based liquid or polymer film sheet which can be done by spray, brush or wipe. However, there are various

key points to select the type of release agent, for example, fast evaporation rate, low degradation to the mould surface, absence of effect to surface of final part, easier cleaning, long shelf life, and no hazard to human skin [77]. This section compiles the effect of mould release agent to the deformation of laminated parts from the literature.

The effect of tool surface and release agent was one of various parameters studied by Albert and Fernlund in 2002 [44]. Tools were made of 6061-T6 aluminium and A36 steel with milled surface condition. They investigated the difference in configuration of tool surface between the coating of liquid release agent layers and the use of fluorinated ethylene propylene (FEP) sheets, those affected to spring-in of C and L shape angle and the warpage of flat section. In summary, the condition of tool surface could be divided into two categories, (1) applied only liquid release agent, (2) applied liquid release agent with FEP. The results of their experiments are given in Figure 2.31. These results evidently show greater spring-in and warpage for parts fabricated without FEP sheet, particularly for thin and long part which a big difference was observed.

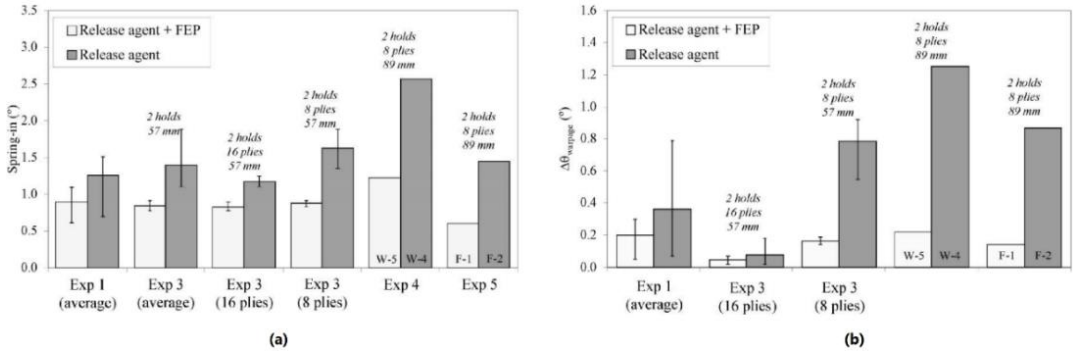

Figure 2.31 Effect of tool surface on spring-in and warpage from the experiment of Albert and Fernlund. [44]

However, the conclusion discussed above does not conform to some of the results from the same group of authors [43] published in the same year and gathered in Table 2.6. Different configurations of tool surfaces were defined and compared. Batch B, C, D, and D* provided similar spring-in values for different tool surface conditions compared within their own group except batch E and E* gave the same trend to Albert and Fernlund. It might be because the sample length in this study was smaller. To clarify the tool surface condition in Table 2.6, the multishield (x) means the number of layers that liquid release agent was applied on the mould surface. However, the method of part/tool removal when no release agent or FEP was not used was not provided in the literature.

Table 2.6 Experimental results from Fernlund et al. in 2002. [43]

Part number	Material	Shape	Lay-up	Tool surface (no of layers)	Holds in cure cycle	Measured spring-in[a] (°)
A-1	AS4/8552	L	$[0]_{12}$	Multishield (1)	1	1.06 ± 0.01
A-2	AS4/8552	L	$[0, +45, -45, 90]_{2S}$	Multishield (1)	1	1.22 ± 0.01
A-3	AS4/8552	L	$[0, 90]_{6S}$	Multishield (1)	1	1.09 ± 0.01
B-1	AS4/8552	C	$[0, +45, -45, 90]_{2S}$	FEP (1) and Multishield (1)	1	1.41 ± 0.01
B-2	AS4/8552	C	$[0, +45, -45, 90]_{2S}$	Multishield (1)	1	1.47 ± 0.05
B-3	AS4/8552	C	$[0, +45, -45, 90]_{2S}$	Multishield (3)	1	1.45 ± 0.09
C-1	T800H/3900-2	C	$[0, +45, -45, 90]_{2S}$	FEP (1) and Multishield (1)	1	0.80 ± 0.03
C-2	T800H/3900-2	C	$[0, +45, -45, 90]_{2S}$	Multishield (1)	1	0.85 ± 0.05
C-3	T800H/3900-2	C	$[0, +45, -45, 90]_{2S}$	Multishield (3)	1	0.72 ± 0.06
D-1	T800H/3900-2	C	$[0, +45, -45, 90]_{2S}$	Multishield (3)	1	1.05 ± 0.18
D-2	T800H/3900-2	C	$[0, +45, -45, 90]_{2S}$	No release agent or FEP	1	0.85 ± 0.10
D*-1	T800H/3900-2	C	$[0, +45, -45, 90]_{2S}$	Multishield (3)	1	1.19 ± 0.20
D*-2	T800H/3900-2	C	$[0, +45, -45, 90]_{2S}$	No release agent or FEP	1	0.75 ± 0.16
E-1	T800H/3900-2	C	$[0, +45, -45, 90]_{2S}$	Multishield (3)	2	1.07 ± 0.09
E-2	T800H/3900-2	C	$[0, +45, -45, 90]_{2S}$	No release agent or FEP	2	1.71 ± 0.10
E*-1	T800H/3900-2	C	$[0, +45, -45, 90]_{2S}$	Multishield (3)	2	1.24 ± 0.07
E*-2	T800H/3900-2	C	$[0, +45, -45, 90]_{2S}$	No release agent or FEP	2	1.71 ± 0.10

In 2004, Twigg et al. [56] from the same research group as authors of references [43, 44] examined the effect of tool surface conditions for the use of two sheets of FEP and Freekote 700 NC liquid release agent with various conditions. The unidirectional flat specimens ($[0]_n$) consisted of the difference in length (300 mm, 600mm, 1200mm), thickness (4, 8, 16 plies) and pressure applied (103, 586 kPa). All specimens were fabricated on aluminium mould. The results are plotted to compare between those two surface conditions appeared in Figure 2.32. In Figure 2.32, the x-axis shows the configuration of the specimen starting by number of plies followed by part length (mm) and pressure (kPa). We can see that FEP and Freekote 700 NC release agent gave similar warpage in almost all cases except in condition of 4 and 8 plies thickness with 1200 mm in length and 103 kPa pressure that FEP exhibited dramatically larger warpage than Freekote. In this case, no general tendency could be observed.

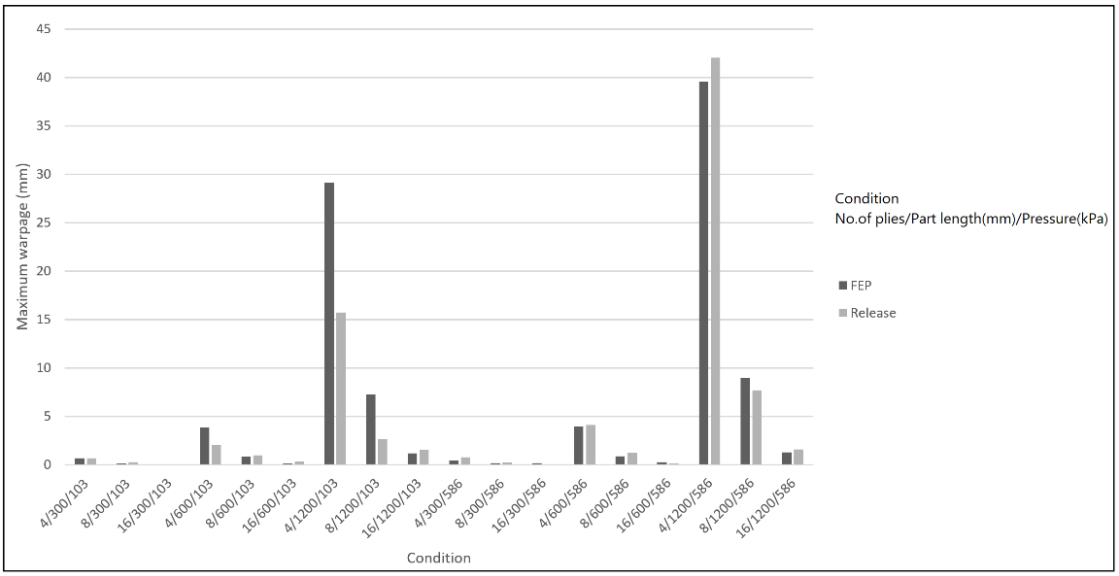

Figure 2.32 Effect of tool surface from Twigg et al. [56]

In 2012, Stefaniak et al. [60] studied the effect of different surface roughness of flat steel tool on the out-of-plane deformation of initially (prior to curing) unidirectional flat samples with different prepreg systems. The prepreg systems used were 997-2/IMS, M21p/T800, M21/T800, and AS4/8552. The tool surface exhibited three different roughnesses. Laminates were cured with or without release, see reference [60] for more details. The deflection of the samples is illustrated in Figure 2.33. As seen in Figure 2.33 in absence of releasing film, increasing the mould surface roughness results in increasing the maximum out-of-plane deflection which is in accordance to what concluded seven years earlier by Kappel et al. [61]. Ronald et al. [78] also mentioned that low surface roughness can decrease shear stress between tool/part interfaces. When considering now samples cured using a release film, the deflection of AS4/8552 and M21/T800 markedly increased while the deflection of M21p/T800 is not predictable but for 977-2/IMS considerably decreased. In summary, the use of release film could reduce the warpage for some prepreg systems but in contrast the warpage of some prepreg systems was enhanced. It was concluded that the amounts of shear stress might be transferred from release film for some prepreg system. However, this inference needs further investigation.

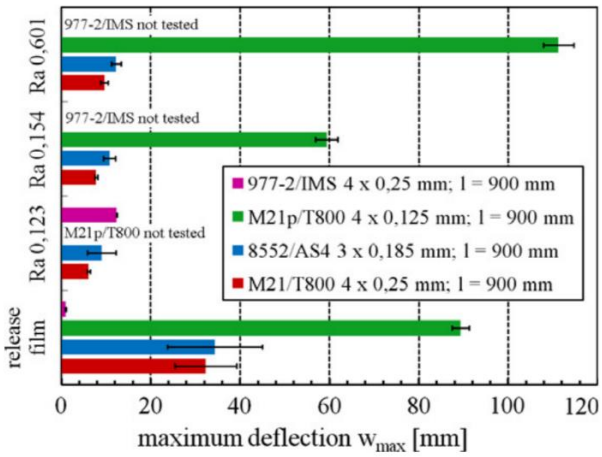

Figure 2.33 Maximum specimen deflections on different surface conditions. [60]

Most researchers usually played with release agents in the form of liquid or polymer film sheet. However, K.E. Tarsha Kurdi and P. Oliver [57] have studied on the effect of thick rubber release agent silicone sheet compared with ETFE release film for the out-of-plane curvature of non-symmetric laminate strip ([0°$_2$/90°$_2$]). Figure 2.34 compares the ETFE and silicone release agent for the evolution of curvature as a function of the initial flat dimension of specimens. Except in the case of small specimens (50 x 5 mm), the curvatures are clearly influenced by type of release agents, silicone sheet providing lower deformation. This influence is more obvious when the surface of specimens in contact with the release agent is larger (see the diagram of 200 x 20 mm size). This might be able to imagine that the thick silicone sheet can reduce the shear stress transfer from mould to laminate.

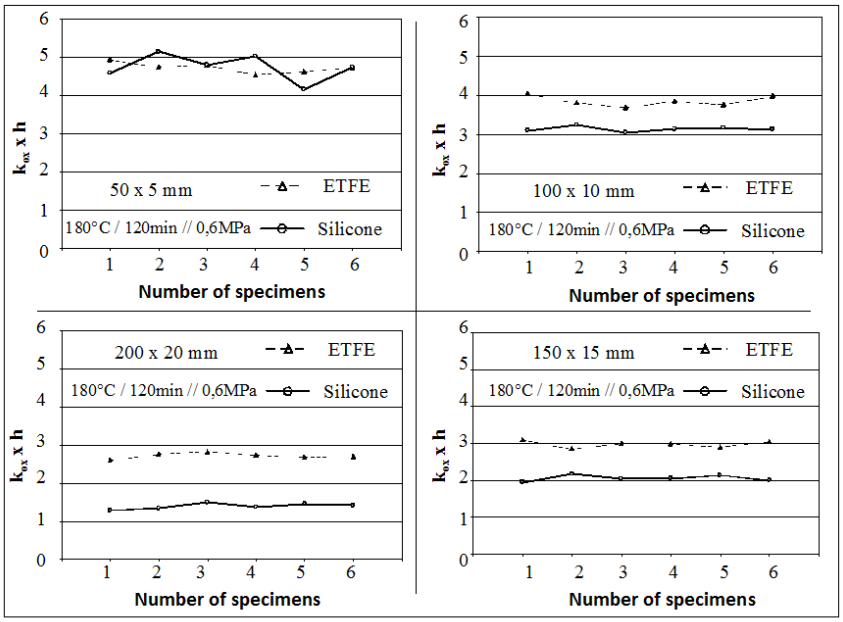

Figure 2.34 Effect of ETFE and silicone release agents on out-of-plane curvature of non-symmetric laminate strip ([0°2/90°2]) with different initial flat dimensions. [57]

2.3.2 Effect of cure cycle

We are now going to examine literature papers dealing with the effects of cure cycle (temperature, time, pressure and vacuum) upon process-induced stresses cured deformation of laminates. It is very important to keep in mind that it is during the cure cycle that the thermosetting matrix is passing from its initial state of partially cured material (called “B-stage” for prepreg) to its final stage of vitreous solid exhibiting high mechanical characteristics. Their changes in thermosetting matrix state can be followed owing to several parameters such as degree of cure (α), glass transition temperature (T_g), viscosity (η), matrix elastic modulus (E_m) and average molecular mass between crosslinking ($\bar{M}c$). Because they can easily be accessed owing to DSC scans, α and T_g are parameters largely studied to follow matrix curing. Any change in α and/or T_g values is synonymous of changes in matrix elastic modulus and CTE and makes purely incomparable results (we mean here process-induced stress and deformations) obtained on laminates not exhibiting identical α and T_g values. In addition, since we are speaking here of composite laminates, the effects of pressure (in the case of hot press or autoclave-cure laminates) must be considered. Effectively modifying the pressure value or the pressure path will undoubtedly result in fibres volume fraction (vf%). Everyone knows that the moduli of unidirectional ply strongly depend on vf%. So, this means that modifying the pressure will result in changes in laminate part moduli and CTE and therefore in its process-induced deformation as it has been shown in 2002 by K.E. Tarsha-Kurdi and Ph. Olivier [58, 79]. Figure 2.35 extracted from their work shows how autoclave pressure influences the residual curvature (k_{ox} x e, curvature x laminate thickness) of unsymmetrical [0°$_2$/90°$_2$] laminated strips made of T2H132300-EH25 carbon/epoxy prepreg. Furthermore, this figure clearly illustrates the effects of interfacial forces between the laminate and the mold since the reader will see that the reduced curvature depends on the laminated strip length (50, 100 or 200 mm)

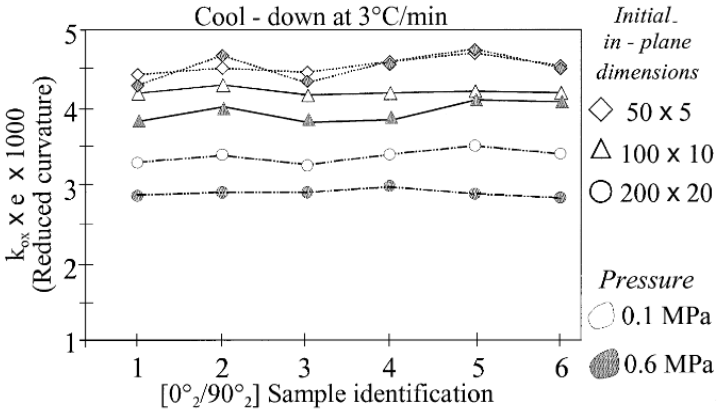

Figure 2.35 Effects of autoclave pressure upon the reduced curvature (k_{ox} x e) of [0°$_2$/90°$_2$] laminate strips. [58, 79]

Figure 2.36 shows the composition of one and two holds cure cycles which can be found in the literature. This section will discuss the effect of cure cycle composition which consists of the ramps rate, holding time and temperature, number of hold and cool down rate. Their effect on the deformation is summarized from the experiment from various literatures

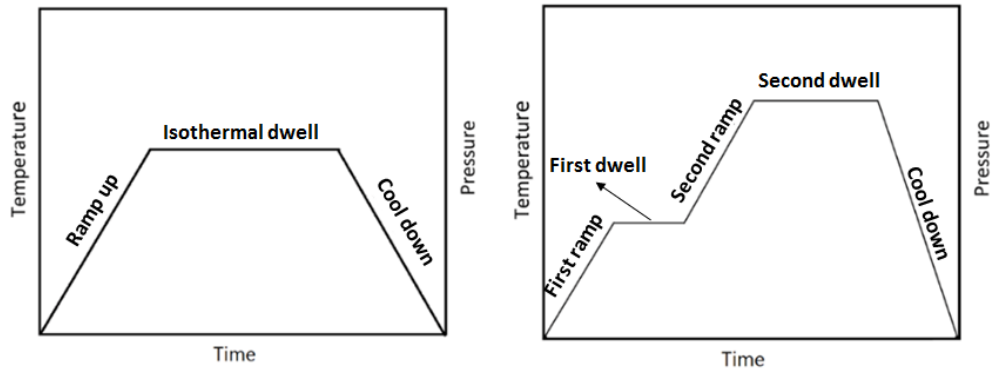

Figure 2.36 Composition of cure cycle.

Svanberg and Holmberg [80] performed experiments on glass-fibre epoxy composites brackets L-shape fabricated by Resin Transfer Moulding (RTM) with different in-mould temperature control, to investigate spring-in deformation. In detail, Aradite LY5052/Hardener HY5052 with the mixing ratio 100:38 by weight was used as matrix and a harness satin glass weave (Hexcel 7781-127) was used as reinforcement. The stiff female mould (Figure 2.37) was made of steel with two sides top and bottom parts, the water channels were designed for temperature control during cure. The varying cure schedules are shown in Table 2.7, cooling time was approximately 45 minutes, while fast and slow cooling could be managed by flushing and without flushing cold water into the water channels respectively. Moreover, post cure and second post cure were operated for all samples after de-moulding in an oven at 120 ˚C for 4 hours and 150 ˚C for 2 hours respectively and cooled down naturally to room temperature, other details can be seen in the reference.

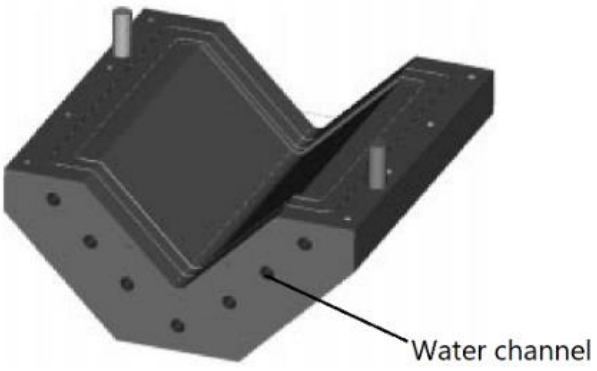

Figure 2.37 Female mould half from Svanberg and Holmberg. [80]

Table 2.7 Cure schedules for Svanberg and Holmberg's experiment. [80]

Num. of Spec.[a]	Cure schedule	Cooling
2	40°C/24 h	Fast
2	60°C/20 h	Fast
3	80°C/15 h	Fast
3	80°C/15 h	Slow **(12 h)**
2	100°C/12 h	Fast

The results of Svanberg and Holmberg experiments are gathered in Table 2.8. Considering the fast cooling rate, the spring-in slightly increased when in-mould cure temperature increased, while post-cure was an efficient way for only in-mould cure 40 ˚C which spring-in could be reduced. Considering the effect of cooling rate between fast and slow cooling from the samples in-mould cured at 80 ˚C, the hypothesis of this study indicated that there was no significant difference between fast and slow cooling rate. It is of prime important to understand that Svanberg and Holmberg conclusion about the variation effects of changing curing routes upon L-shape laminates spring-in must be considered only as technical results since these authors completely ignore the changes in α and T_g and therefore matrix stiffness induced changes in curing route. These results are not bringing any scientific reliable facts.

Table 2.8 Measured spring-in results after in-mould cure and after post cure from Svanberg and Holmberg. [80]

Specimen	Cure schedule	Cooling	Measured spring-in (˚)	
			After in-mould cure	After post cure
1	40˚C/24h	Fast	0.53	0.30
9	40˚C/24h	Fast	0.64	0.33
2	60˚C/20h	Fast	0.74	0.74
8	60˚C/20h	Fast	0.81	0.81
3	80˚C/15h	Fast	0.99	1.16
6	80˚C/15h	Fast	1.00	1.19
7	80˚C/15h	Fast	1.02	1.26
4	100˚C/12h	Fast	1.74	2.12
10	100˚C/12h	Fast	1.35	1.74
5	80˚C/15h	Slow	1.25	1.41
11	80˚C/15h	Slow	0.98	1.18
12	80˚C/15h	Slow	0.99	1.17

The effect of number of holds (isothermal dwells) in cure cycle was studied by Albert and Fernlund [44] in 2002, the details were briefly explained in section 2.3.1.3, more details of their experimental program are presented in the literature. Figure 2.38 shows the cure cycles of their study and Figure 2.39 shows the effect of number of holds on the distortions of the samples through the measurement of both spring-in angle and warpage of the flat section for L and C shaped laminates. At the uniform conditions, greater spring-in and warpage were clearly observed for the samples cured from two holds cycle, contradictory result was obtained from Niraj et al. [81].

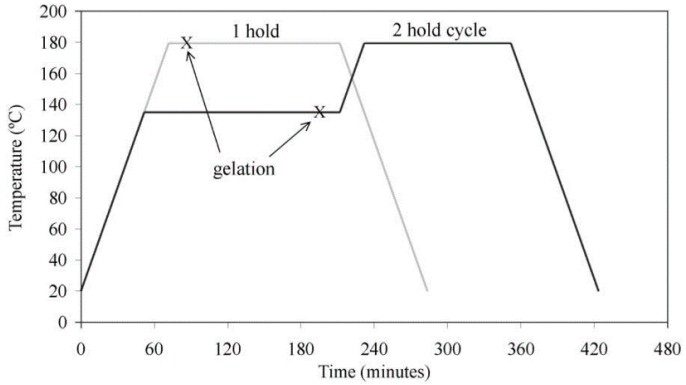

Figure 2.38 Cure cycle of Albert and Fernlund's experiment. [44]

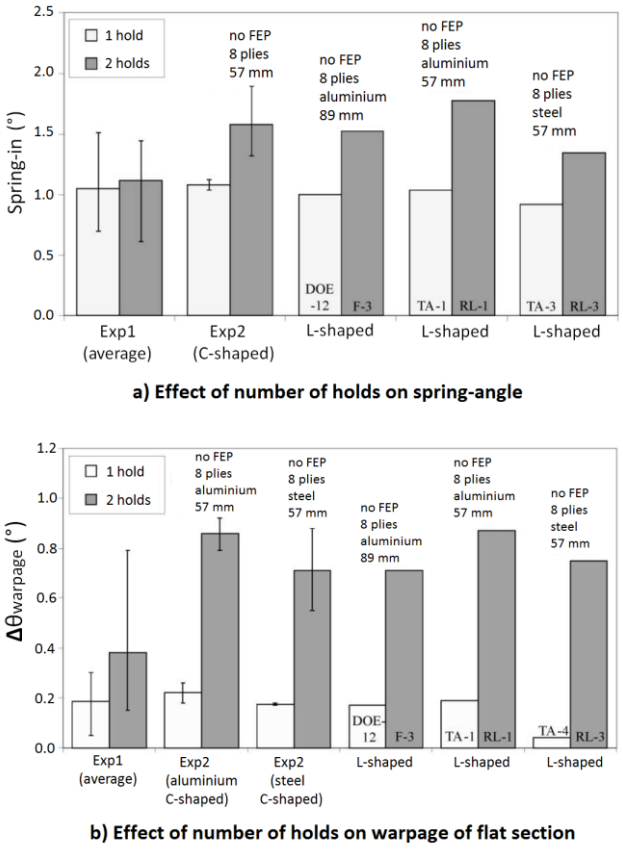

Figure 2.39 Effect of cure cycle on the distortion from Albert and Fernlund. [44]

In 2007, W. K. Jung et al. investigated the effect of curing on the spring-back deformation of a hybrid composite beam made of carbon/epoxy and glass/epoxy prepregs (Figure 2.40) cured by hot press (see details in reference [65]). The parameters related to curing conditions consisted of cure cycle temperature path, cooling rate and cure sequence. The configurations of their experiment are given in Table 2.9 while cure cycles of this study are shown in Figure 2.41. In Table 2.9, “one step” means eight plies carbon and eight plies glass were stacked and cured together, “carbon first” means eight plies carbon were stacked and cured first then stacked eight plies glass and cured again together, “glass first” is similar to “carbon first” but was done in opposite way. As shown in Table 2.9, the 8 carbon/epoxy plies and the 8 glass/epoxy plies were cured together or separately according to reference cure cycle (Figure 2.41 a)). W.K. Jung and co-authors used also three other cure cycles for curing together (i.e. in one shoot) the 16 plies (8 of carbon plus 8 of glass fibres/epoxy) of their unidirectional laminates (see Figure 2.41 b, c and d). Here, in this work [65], it is obvious when looking at Figure 2.41 that the different cure cycles result in large changes in epoxy matrix α and T_g. So, it is more than touchy to setup any conclusion with a real physical meaning since the materials at the end of cure do not exhibit the same characteristics. As a consequence result obtained by W.K. Jung et al. upon the effect of curing path disagreement with those obtained by Albert and Fernlund [44] and the reader can understand why strictly no control matrix physical properties! Their results are shown in Figure 2.42 and Figure 2.43. It can be seen in Figure 2.42 that the effect of the cooling rate that was classified of quick (Q) or slow (S) is not clear from one cure cycle to the other. Moreover, cure cycle as it has already been underlined cannot be compared between each other since they bring the matrix to different physical state characterized by α and T_g. In such conditions, it is strictly forbidden to bring any conclusion on the effect of cooling rate.

Table 2.9 The configurations of experiment for curing conditions from Woo-Kyun Jung et al. [65]

Cure cycle/cooling rate	Lay-up	Thickness	Cure sequence
Cycle-ref-Q/S	[0]4	Carbon 8 plies+glass 8 plies	One step Carbon first Glass first
Cycle-1-Q/S	[0]4	Carbon 8 plies+glass 8 plies	
Cycle-2-Q/S	[0]4	Carbon 8 plies+glass 8 plies	
Cycle-3-Q/S	[0]4	Carbon 8 plies+glass 8 plies	

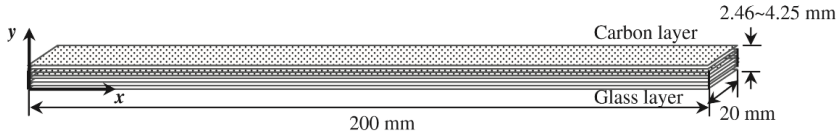

Figure 2.40 Lay-up of prepregs from Woo-Kyun Jung et al. [65]

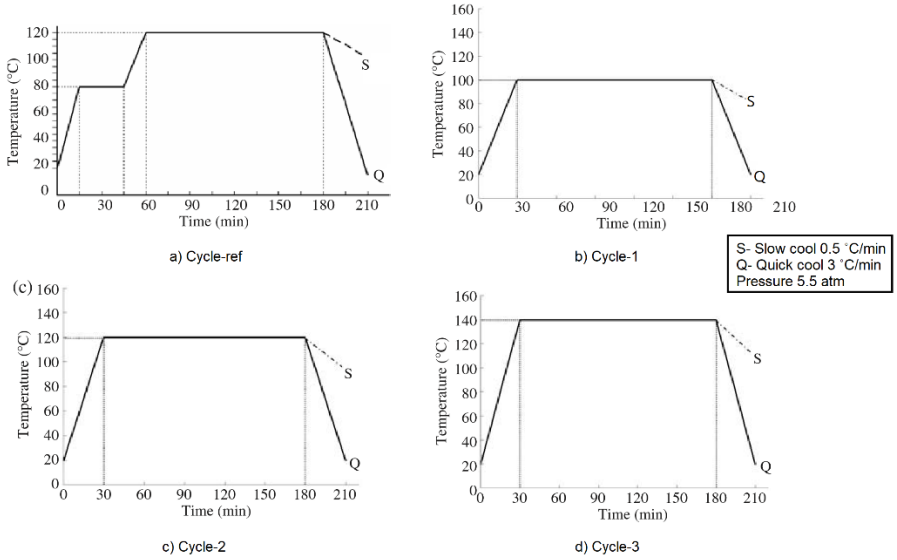

Figure 2.41 Cure cycles for experiment of Woo-Kyun Jung et al. [65]

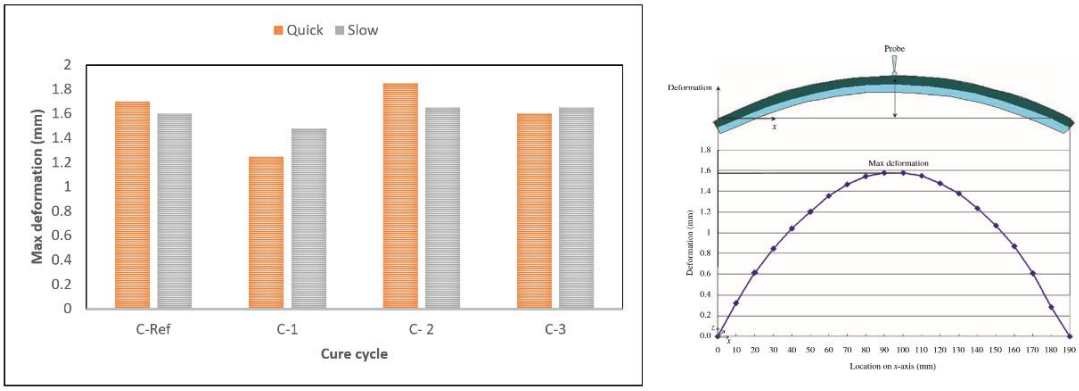

Figure 2.42 Effect of cure cycle and cooling rate from Woo-Kyun Jung et al. [65]

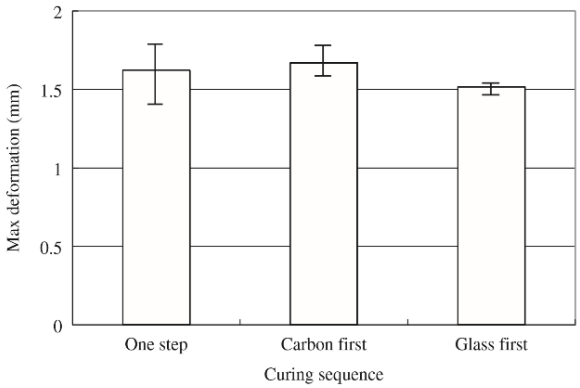

Figure 2.43 Effect of cure sequence from Woo-Kyun Jung et al. [65]

Five years earlier than the work of W.K. Jung et al., K.E. Tarsha-Kurdi and Ph. Olivier [58] have studied for a fixed temperature path the only effect of cooling rate and this with industrial reachable margins i.e. according to the cooling capacities on an industrial autoclave. The conditions used by K.E. Tarsha-Kurdi and Ph. Olivier have nothing to do with those used by O. Sicot et al. [82] with cooling rate unreachable in the case of structural composite parts autoclave cured. Since the samples were cooled down at rate of -80 °C/min using a cold bath (F) (see Figure 2.44). Result obtained by K.E. Tarsha-Kurdi and by O. Sicot are respectively plotted on Figure 2.45 and Figure 2.46. In the case of K.E. Tarsha Kurdi work, the changes in process-induced stress during cooling at 0.5 or at 5 °C/min were predicted using a thermoviscoelastic modelling of composite behaviour. In the case of O. Sicot work, since the work was performed on unidirectional and on symmetrical laminate (see Figure 2.46), the process induced strains were measured by incremental drilling method.

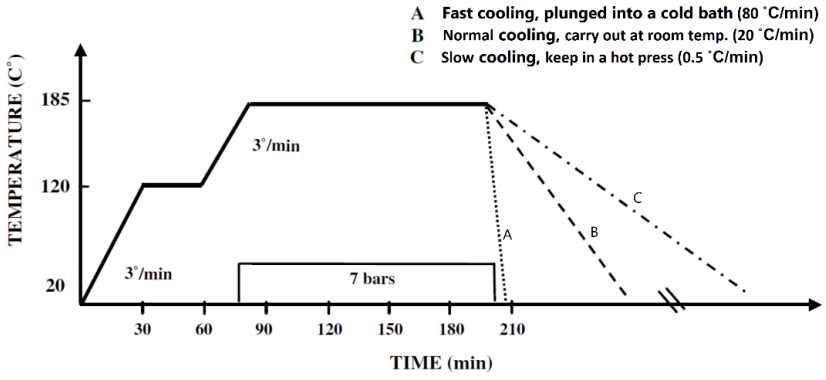

Figure 2.44 Cure cycle of Sicot et al. [82]

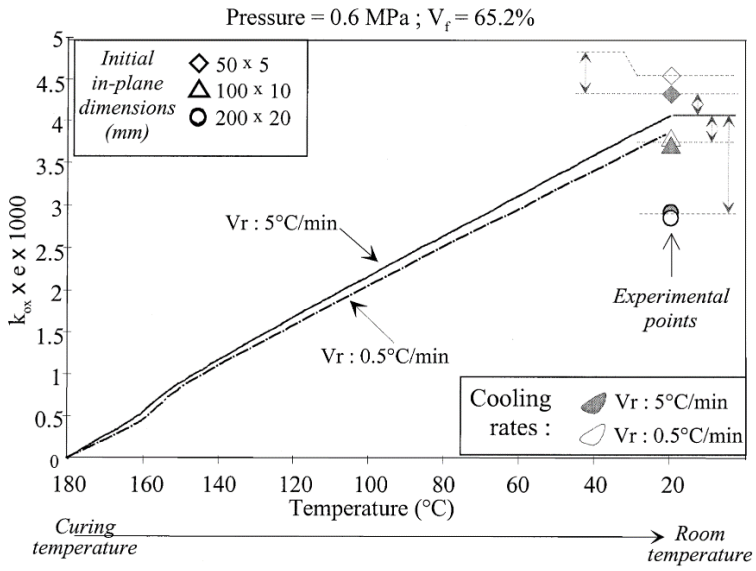

Figure 2.45 Result obtained by K.E. Tarsha-Kurdi for the effect of cooling rate. [58]

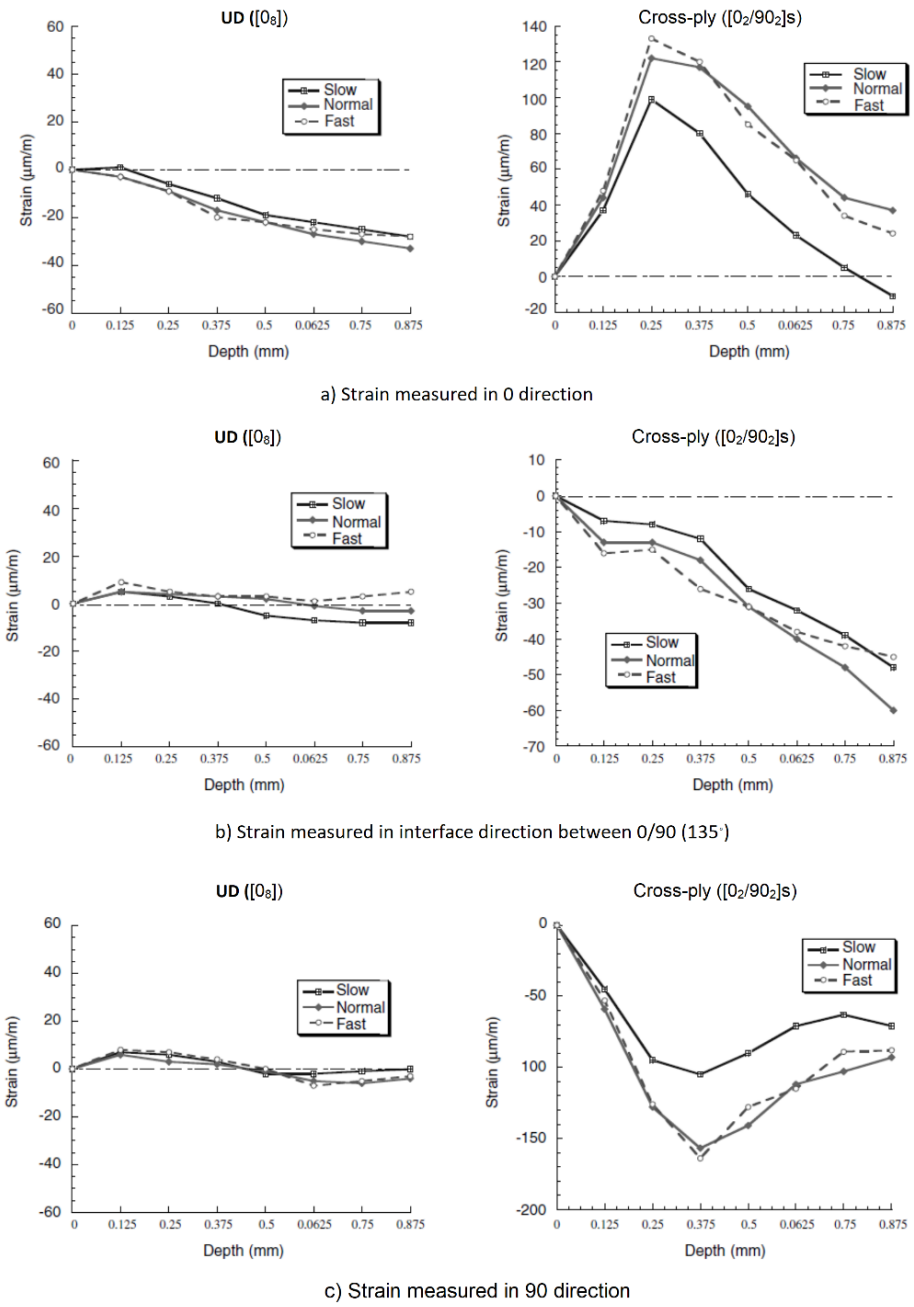

Figure 2.46 Experimental results from Sicot et al. [82]

White and Hahn [83] investigated the effect of curing in many parameters, including cure temperature, cool-down rate, Dwell time, post cure, and step in cure cycle. Their objective was to optimize the curing profile to reduce the residual stress. Their experiments used the IM6/3100 material which is a carbon/BMI polymer system. Curing schedule of this material was recommended as in Figure 2.47. They studied $[0_4/90_4]$ and $[90]_8$ samples with initial in-plane dimension of 25.4 x 152 mm. The out of plane deformation or curvature of the samples was measured at room temperature after curing. The arrangement of experiment is summarized in Table 2.10.

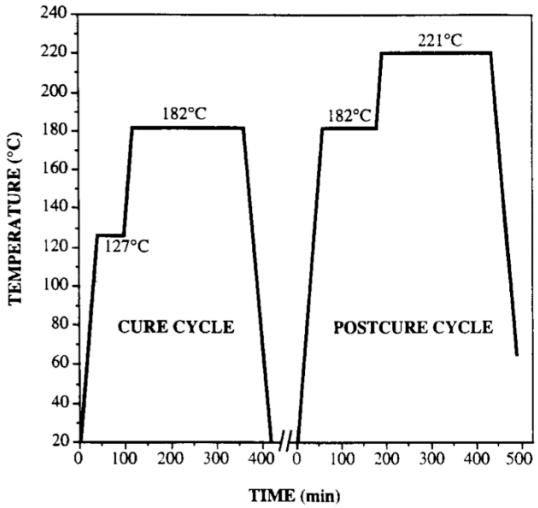

Figure 2.47 Manufacturer's recommended cure (MRC) cycle and posture cycle for IM6/3100 graphite/BMI composite material. [83]

Table 2.10 The arrangement of experiment from White and Hahn. [83]

Variable	Design	MRC	Remark
Cure temperature (˚C)	171 165 160 149	182	Dwell time 4 hours
Dwell time (min)	240 (@160 ˚C) 480 (@160 ˚C) 720 (@160 ˚C) 240 (@165 ˚C) 420 (@165 ˚C)	240	
Cool-down rate (˚C/min)	0.56	5.6	

The outcome of this study will be presented one by one. The effect of cure temperature is illustrated in Figure 2.48. A lower cure temperature results in a decrease of the curvature deformation, in agreement with Svanberg and Holmberg [80]. The effect of isothermal dwell duration (Figure 2.49) is that longer dwell duration induce high curvature measured at room temperature after curing for $[0_4/90_4]$ specimen. Figure 2.50 shows the effect of cool-down rate for non-post cured and post cured samples. It can be seen that slow cool-down rate could reduce the curvature for non-postcured sample, but it contrarily has no effect on post cured sample, while post cure process was mentioned to give an increase in curvature for all samples.

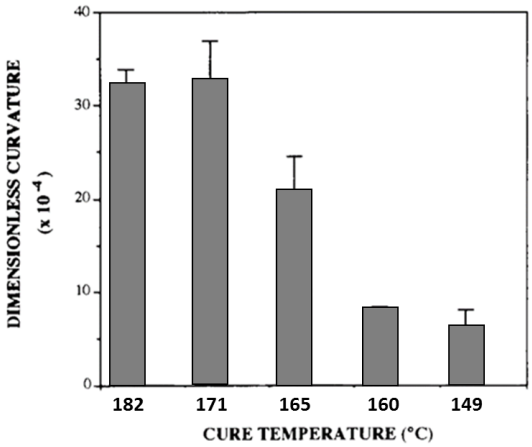

Figure 2.48 Effect of cure temperature on dimensionless curvature from White and Hahn. [83]

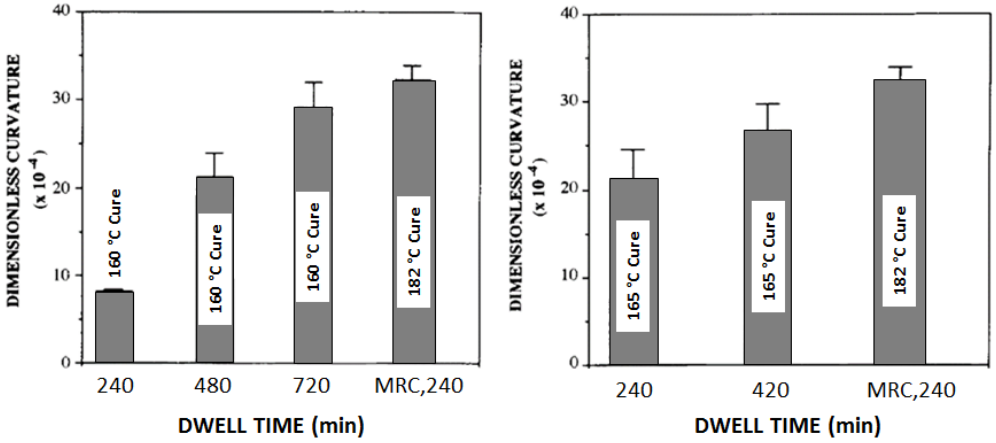

Figure 2.49 Effect of dwell duration on dimensionless curvature from White and Hahn. [83]

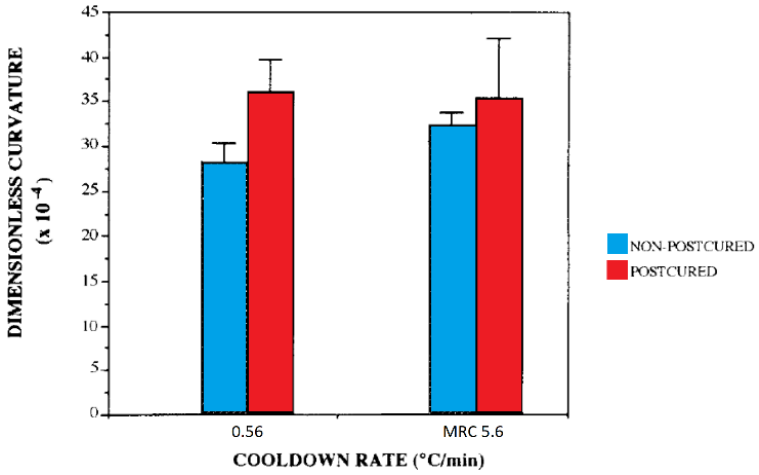

Figure 2.50 Effect of cool-down rate on dimensionless curvature from White and Hahn. [83]

In addition, the modified three steps cure cycle from White and Hahn is presented in Figure 2.51 with two different second isothermal dwell temperatures of either 149 or 160 ˚C. The results obtained were compared to those resulting from MRC in Figure 2.52. The reduction in curvature deformation was observed from a three steps cure cycle compared to MRC. Finally, the conclusion was presumed that the residual stresses of laminates can be reduced by curing at lower temperature for a longer period of time. Effectively this conclusion could have easily been expected since curing at a lower temperature provides a lower temperature difference between room and curing temperatures and thus lower process-induced stress from a thermomechanical origin. However, the modification of three steps cure cycle should be kept in mind to minimize the process-induced stress because the degree of cure was mentioned to achieve (nearly one) after the final isothermal dwell at 182 ˚C.

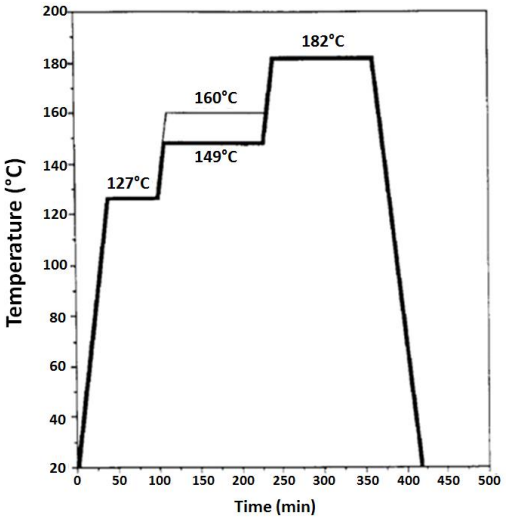

Figure 2.51 Three step cure cycle from White and Hahn. [83]

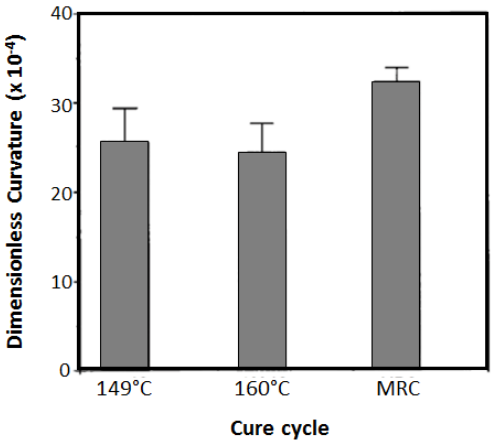

Figure 2.52 Results of three step cure cycle to curvature deformation from White and Hahn. [83]

Hak-Sung Kim et al. [84] studied process-induced strains using the optical fibres with FBG sensor embedded between the plies of flat laminates ($[0_5/90_5]s$). They compared the changes in longitudinal (according 0° direction) strains occurring during conventional and modified cure cycles (Figure 2.53). In detail, a modified cure cycle was interrupted by immediate cooling down at region 2; thus, it could be divided into two steps. It can be observed that the first negative strain was generated during the first heating ramp (region 1 of conventional cure cycle and region 1 to 2 of modified cure cycle) due to (according to these authors) thermal contraction of the liquid resin. The strain became positive due to thermal expansion at the holding period (regions 2 and 3 of conventional cure cycle and regions 3 and 4 of modified cure cycle). Negative strain took place again at the cool down stage (region 4 of conventional cure cycle and region 5 of modified cure cycle). Finally, laminates cured according to a modified cure cycle exhibited a negative strain lower than the one of the laminates cured according to conventional cure cycle. It seems that thermal strain can be relieved by cooling interruption made in the middle of the isothermal dwell but rapid cooling during the curing might be complicated in practical and very energy consuming.

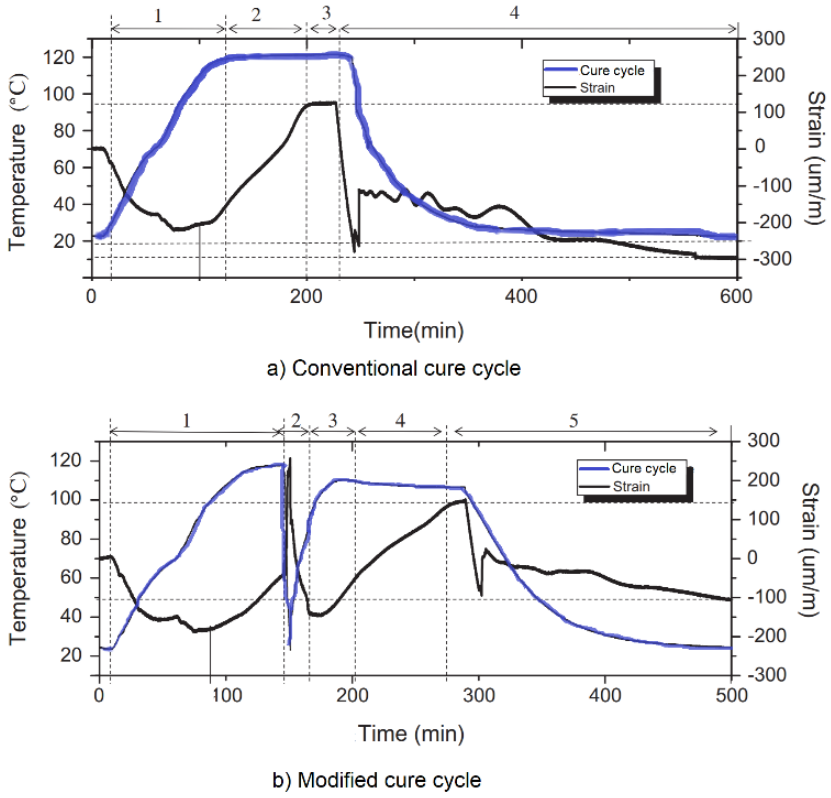

Figure 2.53 Cure cycle from Hak-Sung Kim et al. [84]

In 2017, Yong lu et al. [69] proposed a modified cure cycle to reduce composite deformation. In this work a specific attention was paid to thermosetting matrix chemical shrinkage (see Figure 2.54) and they focused their research effect on the early stage of cure cycles. It was considered that from the beginning of cure until the matrix gelation that none

process-induced stress was able to develop exactly has assumed demonstrated by Ph. Olivier in [15]. Thus, the authors [69] played with the first heating ramp rate to reach more or less quickly the gelation and then get the lock of process-induced stresses more or less early in the cure cycle. Slowly the heating rate enable to reduce the level of chemical shrinkage (Figure 2.54).

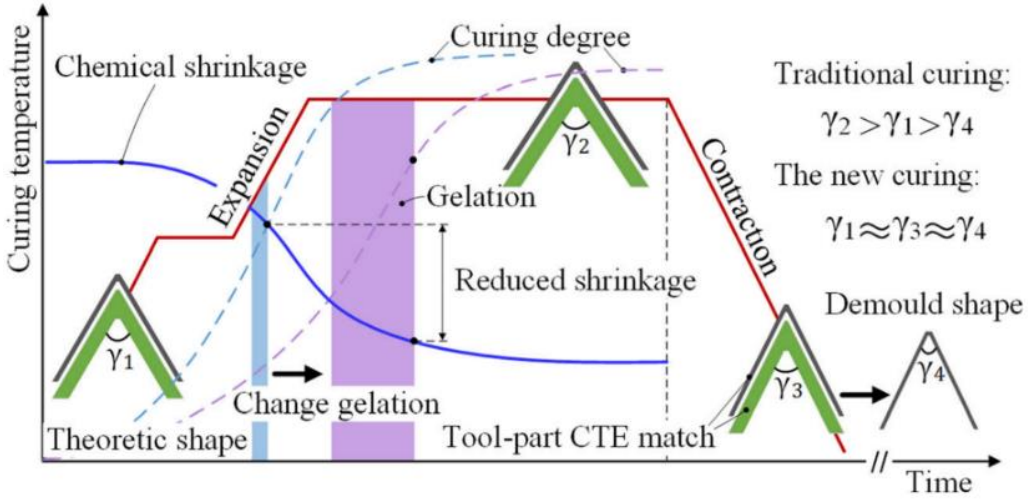

Figure 2.54 The schematic of chemical shrinkage reduction. [69]

The authors in [69] fabricated composite tools made of DGEBA epoxy resin reinforced by T300 carbon fibre (see detail in the reference [69]) to fabricate the C and V-shape samples according different curing conditions. The traditional and new curing profiles are illustrated in Figure 2.55 and the configurations of experiment are presented in Table 2.11. The definition of deformation in this study was divided into warpage and spring-back deformations as seen in Figure 2.56. The warpage deformation showed broader shape angle which was indicated by positive value while spring-back deformation showed smaller angle which was indicated by negative value. The outcomes of this experiment appear in Figure 2.57. It is evident that new cure cycle was successful to reduce the deformation due to the reason above and it is in accordance with White and Hahn conclusions [83]. However, it should be noted that the modified step of cure cycle should provide lower temperature than the original one, otherwise, the number of holds may enhance the residual stress as mentioned by Albert and Fernlund [44].

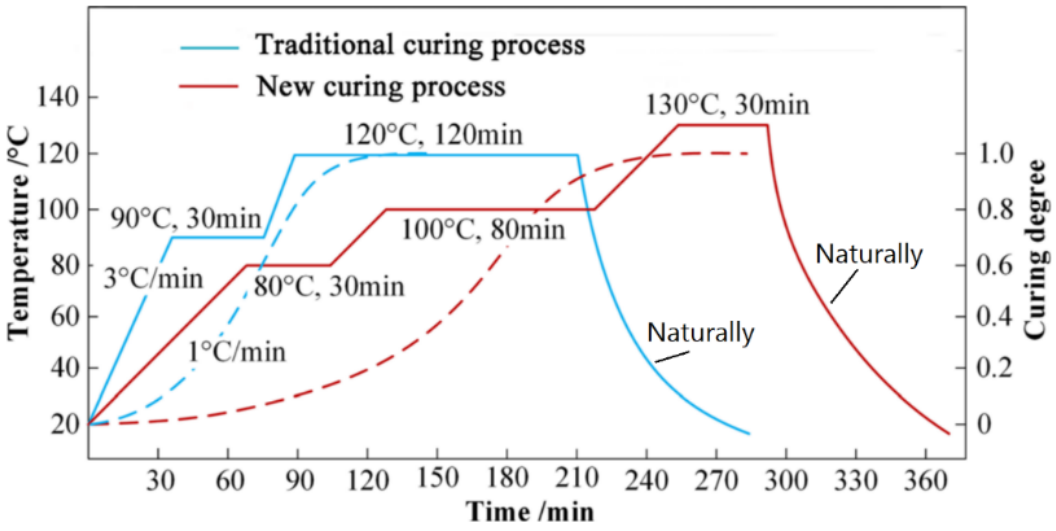

Figure 2.55 The tradition and new curing process from Yong lu et al. [69]

Table 2.11 The configuration of experiment from Yong lu et al. [69]

Ply sequence (Part)	Ply sequence (tool)	Traditional curing		New curing	
		C shape	V shape	C shape	V shape
$[0]_{18}$	$[0]_{18}$	T1-C	T1-V	N1-C	N1-V
$[90]_{18}$	$[90]_{18}$	T2-C	T2-V	N2-C	N2-V
$[0/90/+45/0/-45/0/+45/90/0]_s$	$[0/90/+45/0/-45/0/+45/90/0]_s$	T3-C	T3-V	N3-C	N3-V

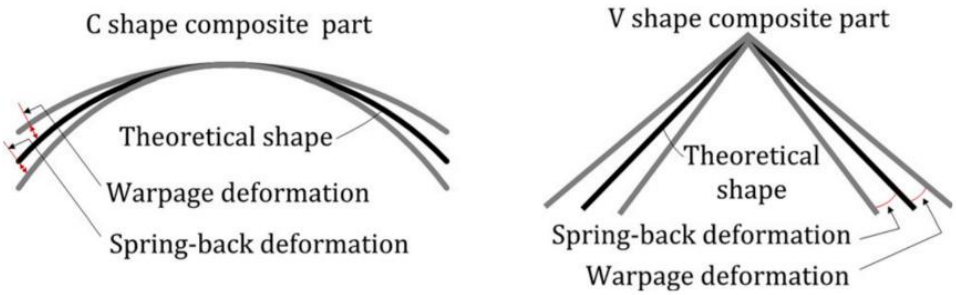

Figure 2.56 The warpage and spring-back deformations from Yong lu et al. [69]

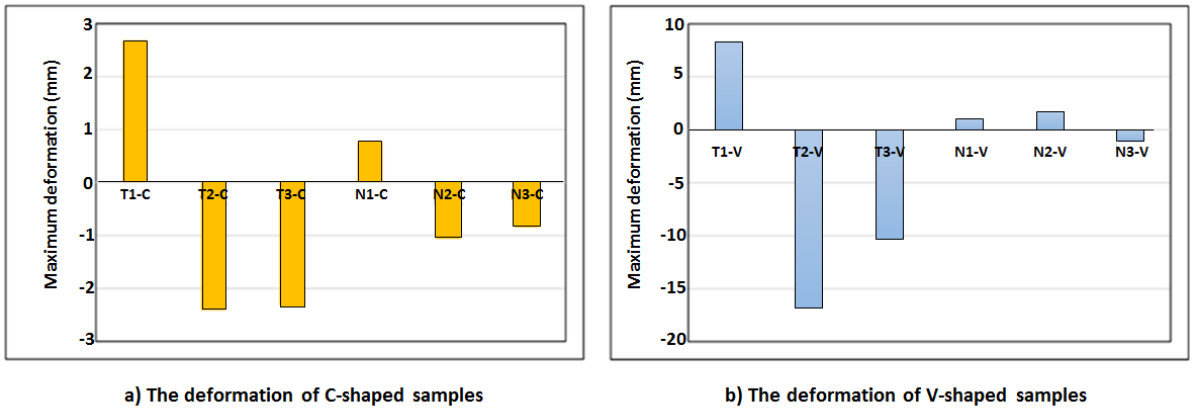

a) The deformation of C-shaped samples

b) The deformation of V-shaped samples

Figure 2.57 The deformation of samples from Yong lu et al. [69]

The effect of heating rate was also examined by Oleksandr et al. [85]. They fabricated bi-lamina specimen ($[0/90_4]$) from thermosetting prepreg CYCOM 5320-1 with the in-plane size of 158 x 25.4 mm and thickness 0.9 mm. The specimens were fixed at one end and free at another end to see the deformation during cure (see detail in reference). Two similar cure cycles with different heating profile were applied to cure the specimens in an oven. Both cure cycles are presented in Figure 2.58, fast and slow heating rates were defined by single ramp and multiple ramps with the same heating stage at 2 ˚C/min, respectively. The deformation at end of specimens is presented in Figure 2.59, both cure cycles gave about the same deflection in cool down stage while multi-ramp cycle could decrease the deflection before cool-down which resulted in lower deflection at the final.

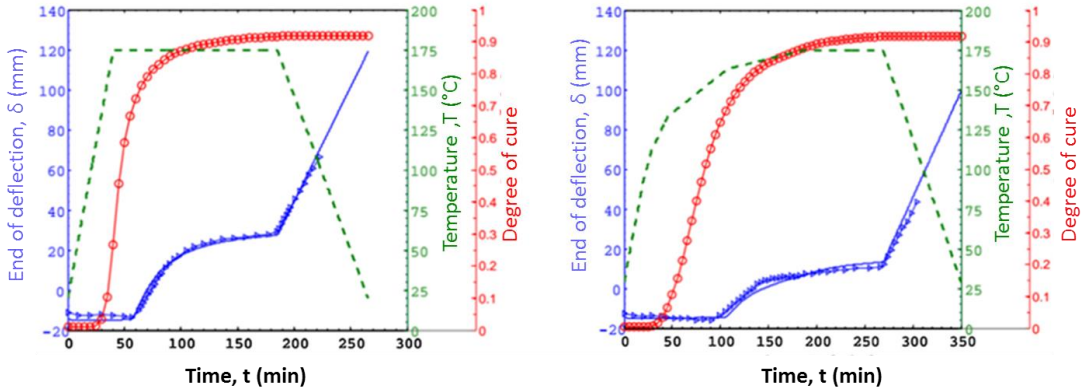

a) Single ramp cure cycle

b) Multi ramp cure cycle

Figure 2.58 Cure cycle from Oleksandr et al. [85]

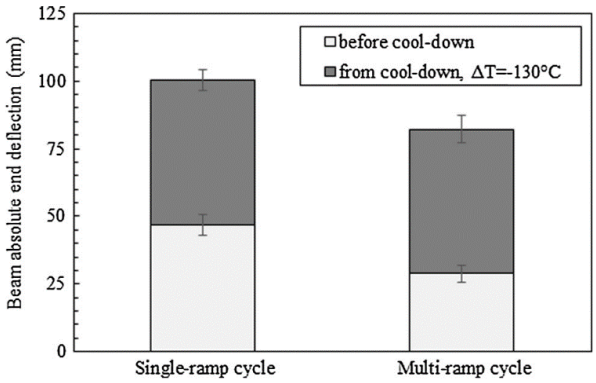

Figure 2.59 The deformation of specimen from Oleksandr et al. [85]

Moreover, Oleksandr et al. [85] also investigated the effect of heating rate in different three cure cycles (detail in Figure 2.60) upon the deformation of bi-lamina specimens. The idea was to modify the second heat ramp of Manufacturing Recommended Cure Cycle (MRCC). The results of experiment (Figure 2.61) indicated that MRCC with slowest heating rate provided lowest curvature due to no deflection was generated before cool down, in agreement with all discussions above. In addition, these authors said that a fast heating rate could significantly reduce the resin viscosity at the first stage of curing due to high heat generation [86]. This may induce inappropriate resin flow and cause corner thickening or thinning for curved part as discussed in section 2.3.1.2.

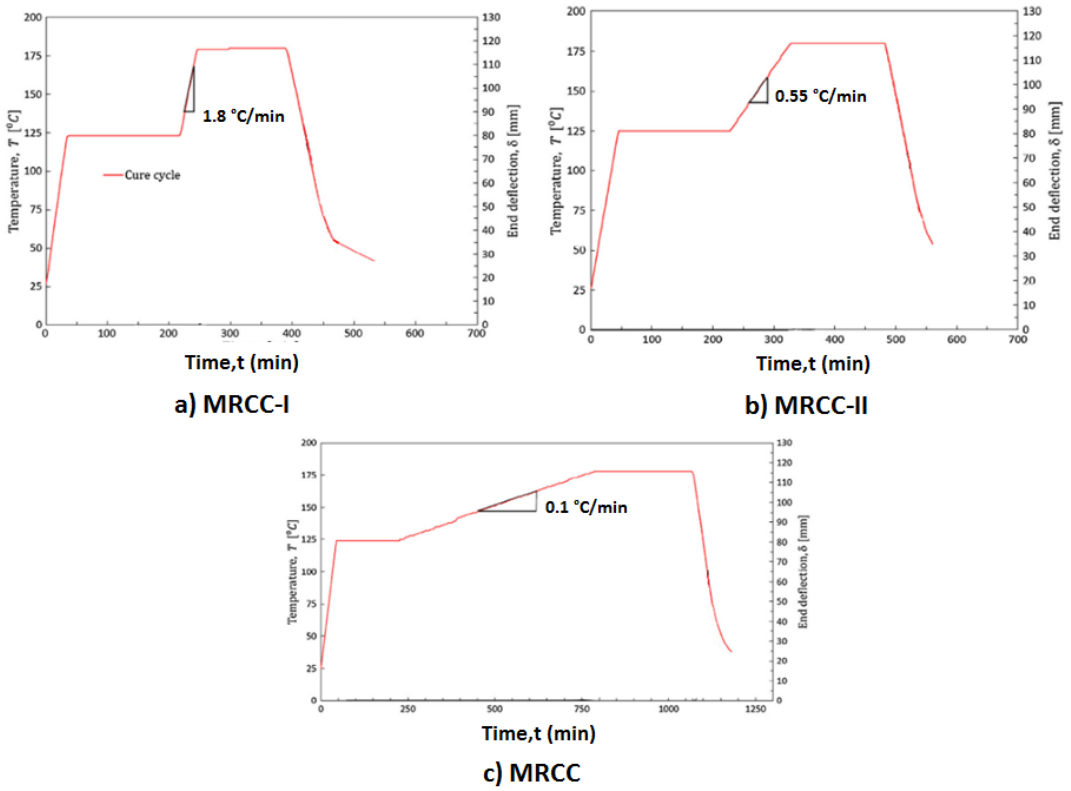

Figure 2.60 Cure cycles with different heating rate from Oleksandr et al. [85]

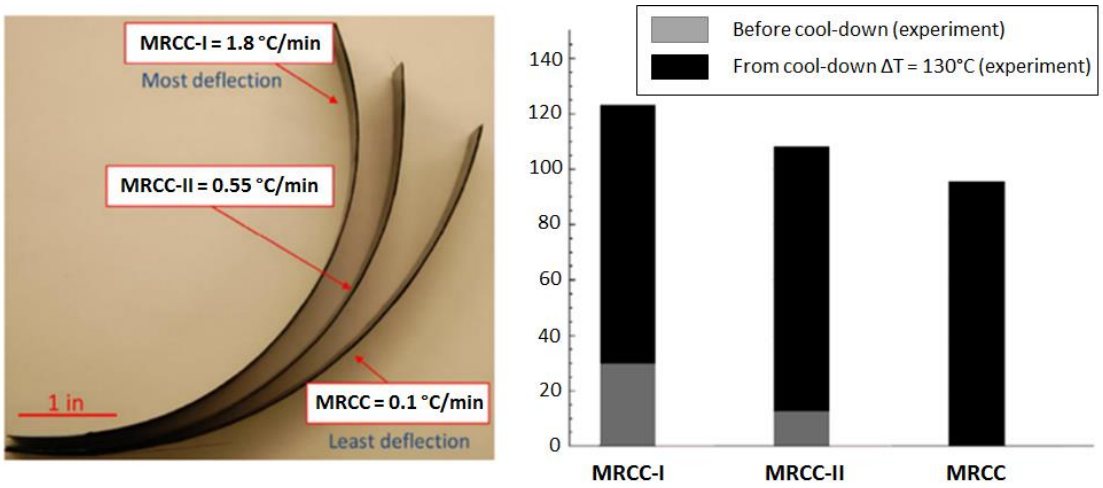

Figure 2.61 The deformation of different heating rate from Oleksandr et al. [85]

2.4 Modelling of composite deformation

2.4.1 History of analytical analysis

Analytical and numerical methods are helpful in terms of reduction in cost and time consuming for the experiment. However, an analytical approach can provide an exact solution but it is unable to solve complex problems. Then numerical approaches are needed although it can only provide an estimated solution. When analytical solutions of the mathematically defined problem are possible but are time-consuming, the error of approximation we obtain with a numerical solution is acceptable. This section will present a few examples of modelling that have been performed by various researchers in terms of prediction of composite distortion due to the manufacturing process.

Process-induced stress in structural composite material have been studied since the middle of to 1970. This means that the very first attempts to settle modelling for predicting residual curing stresses were published around 1975 with for example the work of C.C. Chamis in 1974 [87] or the research of H.T. Hahn in 1975 [88], without forgetting the results published by Weitsman in 1979 [89]. In this very first work showing the way to predict process-induced (or residual) stress, material behaviour was considered as thermoelastic of thermoviscoelastic [89]. From that time, numerous researchers have proposed more or less refined modelling of the prepreg ply behaviour during a cure cycle. The highest degree of refinement was reached with work S.R. White et al. [90, 91] in which the behaviour is considered as thermoviscoelastic depending on the matrix degree of cure and thus described (for the moduli) by continuous functions. All these evolutions in the way of calculating process-induced stresses using classical lamination theory with various material behaviours are synthesized by equations 2-1 to 2-5.

- Thermoelastic [92].3-143-14

$$\{\sigma\}_{x,y}^{k} = \left[\overline{Q}\right]^{k} \cdot \{\varepsilon\}_{x,y}^{k} - \Delta T \cdot \{\overline{\alpha}\}_{x,y}^{k} \tag{2-1}$$

- Thermoelastic including temperature dependent properties [93].

$$\{\sigma\}_{x,y}^{k} = \left(\left[\overline{Q}\right]^{k} \cdot \{\varepsilon\}_{x,y}^{k} - (T_g - T_c) \cdot \{\overline{\alpha}\}_{x,y}^{k}\right)_{T_c>T>T_g} + \left(\left[\overline{Q}\right]^{k} \cdot \{\varepsilon\}_{x,y}^{k} - (Ta - Tg) \cdot \{\overline{\alpha}\}_{x,y}^{k}\right)_{T_a<T<Tg} \tag{2-2}$$

- Thermoviscoelastic [89, 94, 95].

$$\left[\sigma_{(t,T)}\right]_{x,y}^{k} = \int_0^t \left[\overline{Q}(\xi - \xi')\right]^{k} \cdot \frac{\partial}{\partial \tau}\left(\int_{T(0)}^{T(\tau)} \left[\alpha(T)\right]_{x,y}^{k} \cdot dT\right) d\tau \tag{2-3}$$

With $\xi = \xi(t) = \int_0^t \frac{dt'}{a_T[T(t')]}$ and $\xi' = \xi(\tau) = \int_0^\tau \frac{dt'}{a_T[T(t')]}$ (2-4)

- Thermoviscoelastic with properties of the UD ply as a function of the degree of cure (α) of the crosslinking reaction [90, 91, 96].

$$\sigma_i(t) = \int_0^t Q_{ij}(\alpha, \xi - \xi') \cdot \frac{\partial}{\partial \tau}\left[\varepsilon_j(\tau) - \tilde{\varepsilon}_j(\tau)\right] d\tau \tag{2-5}$$

However, all this work was merely transferred from analytical to numerical tools and in this latter case, material behaviour numerically simulated is frequently less complex than what was done by the end of the year 1990 within the frame of analytic calculations of residual stresses. An exception must be made with the work of Zhang et al. [97] who developed an extremely refined model in 2016.

2.4.2 Modelling the behaviour of the unidirectional ply during a cure cycle

Thermoviscoelastic models depending also on matrix degree of cure (α) are very complex to build since this requires numerous experiments. This is why several authors have decided to use simplified modelling which does not require any numerical integration. The most simplified material behaviour used in numerical simulation of process-induced stresses for modelling the material behaviour during a cure cycle is the CHILE model (Cure Hardening Instantaneous Linear Elastic). In the CHILE model, the material elastic modulus increases linearly with the matrix degree of cure. The resin is considered to be isotropic and has a linear elastic response. The principle of the CHILE model was initially developed by Bogetti and Gillespie in 1992 [98]. The original CHILE model is presented in Figure 2.62 a). The resin is in viscous state when the degree of cure is below the gel point and the resin modulus is relatively low and considered to be constant. The resin modulus linearly increases with the

progress of reaction during vitrification. Finally, the model was developed by Johnson et al. [51] with the consideration of temperature dependence for constant resin elastic modulus development (Figure 2.62 b)). Figure 2.63 shows how CHILE and CHILE modified models predict the changes in a matrix elastic models according to temperature in which Figure 2.63 b) shows modified version of Khoun [99] that describes more states of elastic modulus behavior of an epoxy/carbon composite. More recently, L. Moretti et al. [19, 100] have proposed a new modification of modified CHILE model enabling a better description of the changes in matrix (or UD ply transverse modulus) as a function of temperature during a cure cycle. In this case, the very first stages of the cure cycle are considered while it was not the case with past modelling such as Khoun modified CHILE model. The details of L. Moretti's modified CHILE model will be briefly explained in chapter3 and/or the reader can see a full detail in [19, 100]. This is the behaviour considered for the unidirectional ply transverse (E_t) and in-plane shear moduli (G_{lt}) in this current work and programed for being used in ABAQUS.

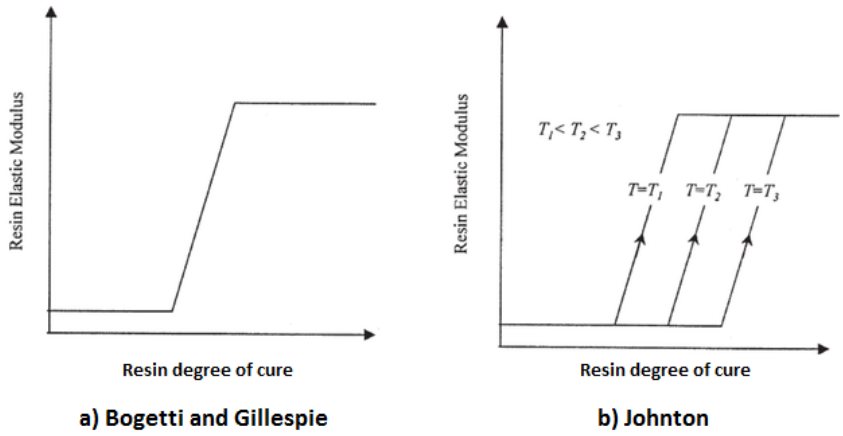

Figure 2.62 CHILE model from Bogetti and Gillespie and Johnston. [51, 98]

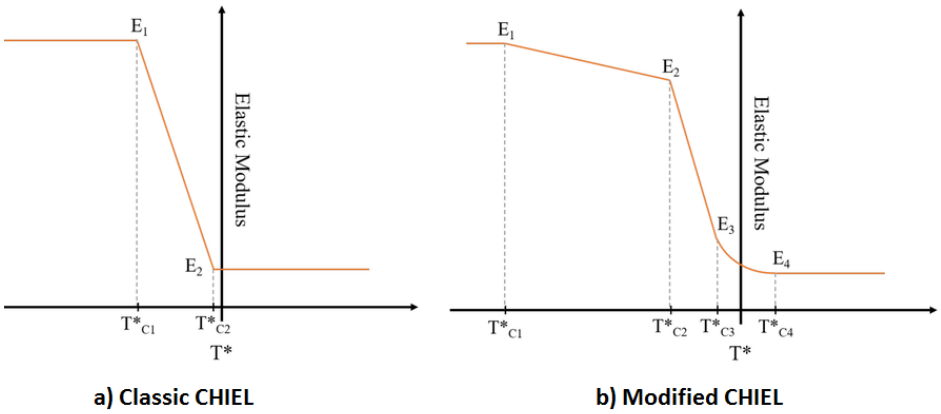

Figure 2.63 Classic and modified CHILE models. [99]

2.4.3 Analytical modelling applied to non-initially flat laminated parts

Some authors have carried-on using analytical calculation schemes for predicting the post cure deformation of non-initially flat laminated parts such as L-shape parts. In 1995, Radford [101] developed the model for laminate shape change to predict the warp value of curved composite plate in terms of the differences between in-plane and through-thickness thermal contraction and chemical shrinkage. This model investigated the physical behaviour of anisotropic laminate in different directions. In principal, cross-ply and quasi-isotropic laminates have relatively small shrinkage in the in-plane direction due to the dominance of fibre property while through-thickness direction has no reinforcing fibre; large amounts of shrinkage take place in this direction and force the laminate to deform after fabrication. Equation 2-6 was presented in order to predict the degree of warpage in term of the temperature change, the laminate cure shrinkage and the initial include angle as follows:

$$\Delta\theta = \theta\left[\left[\frac{(\alpha_I - \alpha_T)\Delta T}{1+\alpha_T\Delta T} + \left(\frac{\emptyset_I - \emptyset_T}{1+\emptyset_T}\right)\right]\right] \quad (2\text{-}6)$$

Where

$\theta =$ initial component included angle

$\Delta\theta =$ change in component included angle

$\Delta T =$ change in temperature

$\emptyset_I =$ in-plane fabrication expansion

$\emptyset_T =$ through-thickness fabrication expansion

$\alpha_I =$ in-plane composite coefficient of thermal expansion

$\alpha_T =$ through-thickness composite coefficient of thermal expansion

This model was used by Haung and Yang [70] to predict the warp angle compared to the experimental results as a function of different mould angles (male mould) while other factors were constant. The trend of predicted results conformed to the experiment although they were about 14% lower. Then the mould angle as well as the difference between in-plane and through-thickness thermal expansion and chemical shrinkage have an influence on the warpage.

In addition, laminate distortion can be induced by the thermal load due to anisotropy of thermal expansion coefficient when the temperature changes in both symmetric and asymmetric or balanced and unbalanced laminates. O'Neill et al. [102] proposed a modelling of curvature change of the curved section angle area of an L-shapes part depending on the thermal effect (equation 2-7). Schematic distortion of the curved section is shown in Figure 2.64.

$$\Delta\theta_{\text{thermal}} = \int_{T_f}^{T_0} \theta_0 \{\alpha_z(T) - \alpha_x(T)\} dT \quad (2\text{-}7)$$

Where

$\Delta\theta = \theta_1 - \theta_0$

θ_0 = the angle of the arc sector of the curve laminate

α_z = the CTEs in the through thickness direction

α_x = the CTEs in the principal direction

T_f = the curing temperature

T_0 = the room temperature

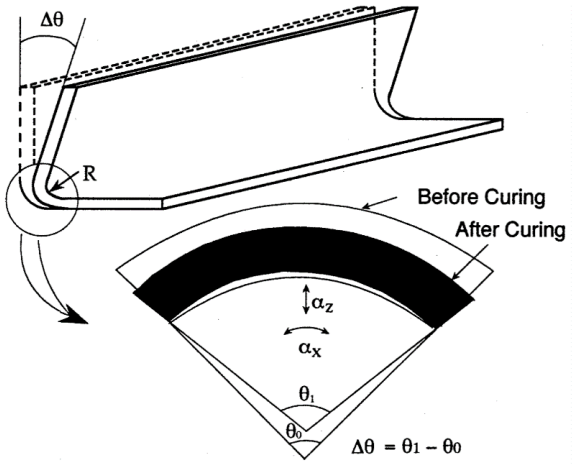

Figure 2.64 Thermal Distortion of Curved Section of Anisotropic Material Structure. [102]

However, the model from O'Neill has to be focused on the change in CTE for temperature variation which depends on temperature. Yoon and Kim [66] proposed an analytical model to calculate the change in CTE's for general laminates as (equation 2-8).

$$\begin{Bmatrix} \alpha_x^0(T) \\ \alpha_y^0(T) \\ \alpha_{xy}^0(T) \end{Bmatrix} = [A'(T)] \int [\bar{Q}(T)]_k \begin{Bmatrix} \alpha_x(T) \\ \alpha_y(T) \\ \alpha_{xy}(T) \end{Bmatrix}_k dz + [B'(T)] \int [\bar{Q}(T)]_k \begin{Bmatrix} \alpha_x(T) \\ \alpha_y(T) \\ \alpha_{xy}(T) \end{Bmatrix}_k z dz \quad (2\text{-}8)$$

Where

$$\begin{Bmatrix} \alpha_x \\ \alpha_y \\ \alpha_{xy} \end{Bmatrix}_k = [T_\varepsilon]_k^{-1} \begin{Bmatrix} \alpha_1(T) \\ \alpha_2(T) \\ 0 \end{Bmatrix} \quad (2\text{-}9)$$

$\{\alpha^0\}$ = the CTE at laminate's mid-plane

[A'] = the extension part of the inverse matrix of a combined extension, coupling and bending stiffness matrix

[B'] = the coupling part of the inverse matrix of a combined extension, coupling and bending stiffness matrix

$[\bar{Q}]$ = the transformed reduced stiffness matrix

α_1 = the CTE in the fibre direction of UD ply

α_2 = the CTE in the transverse direction of UD ply

$[T_\varepsilon]_k^{-1}$ = transformation matrix (k denotes the k_{th} ply of the considered laminate)

Effect of chemical shrinkage was reported to be another source of deformation due to the mismatch of chemical shrinkage between the in-plane and the out-of-plane directions. The curvature change can be expressed in equation 2-10 which was modified from equation 2-7. The in-plain chemical shrinkage strain can also be obtained from the modification of equation 2-8 as showed in equation 2-11.

$$\Delta\theta_{thermal} = \theta_0 \left(\varepsilon_z^{0C} - \varepsilon_x^{0C}\right) \tag{2-10}$$

Where

ε_z^{0C} = the chemical shrinkage strains in the through thickness direction during cure

ε_x^{0C} = the chemical shrinkage strains in-plain direction during cure

$$\begin{Bmatrix} \varepsilon_x^{0C} \\ \varepsilon_y^{0C} \\ \gamma_{xy}^{0C} \end{Bmatrix} = [A'] \int [\bar{Q}]_k \begin{Bmatrix} \varepsilon_x^{C} \\ \varepsilon_y^{C} \\ \gamma_{xy}^{C} \end{Bmatrix}_k dz + [B'] \int [\bar{Q}]_k \begin{Bmatrix} \varepsilon_x^{C} \\ \varepsilon_y^{C} \\ \gamma_{xy}^{C} \end{Bmatrix}_k z dz \tag{2-11}$$

Where

$$\begin{Bmatrix} \varepsilon_x^{C} \\ \varepsilon_y^{C} \\ \gamma_{xy}^{C} \end{Bmatrix}_k = [T_\varepsilon]_k^{-1} \begin{Bmatrix} \varepsilon_1^{C} \\ \varepsilon_2^{C} \\ 0 \end{Bmatrix}_k \tag{2-12}$$

ε_1^C = the chemical shrinkage strain in the fibre direction

ε_2^C = the chemical shrinkage strain in the transverse direction

The model of Yoon and Kim [66] was verified by some experiments for L-shaped specimens with various stacking sequences (see Table 2.12). All specimens were cured by autoclave and measured the angle changes at room temperature (25°C). The predicted values are also shown in Table 2.12. The predicted and measured data are compared in Figure 2.65 and it can be seen that thermal and chemical shrinkage are the main cause of angle distortion since the combination of these shrinkages provides the angle changes close to the results measured from experiment even if it is underestimated but the model gives a similar trend.

Table 2.12 Comparison of predicted distortion angles with experimental data from the work of Yoon and Kim. [66]

Stacking Sequences	Predicted			Measured
	$\Delta\theta_{thermal}$	$\Delta\theta_{chemical}$	$\Delta\theta_{total}$	$\Delta\theta$ (std)
$[0]_{8T}$	0.5101	0.6766	1.1867	1.2953 (0.167)
$[\pm15]_{2S}$	0.5348	0.7202	1.2583	1.7561 (0.169)
$[\pm30]_{2S}$	0.5941	0.8646	1.4183	1.7701 (0.173)
$[\pm45]_{2S}$	0.4938	0.6567	1.1505	1.2491 (0.143)
$[\pm60]_{2S}$	0.2178	0.1922	0.4100	0.8961 (0.145)

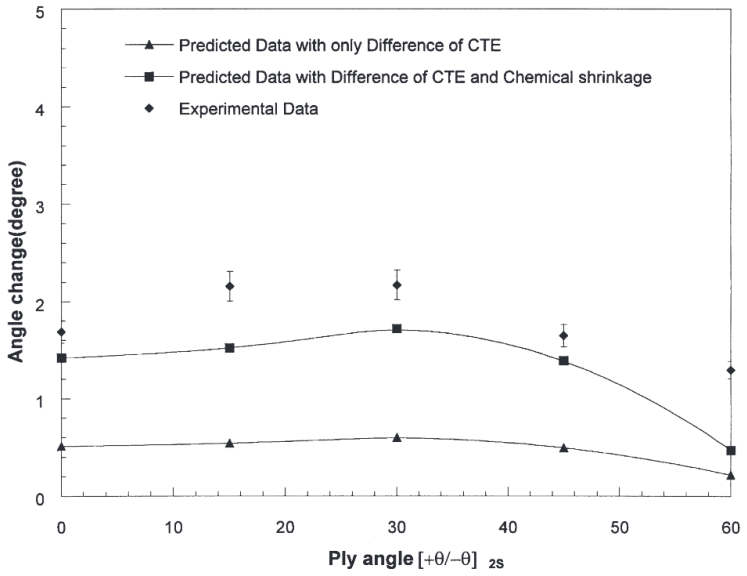

Figure 2.65 Comparison of predicted distortion angles with experimental data from the work of Yoon and Kim. [66]

2.4.4 Analytical modelling considering tool/part interaction

In 2004, the analytical model of tool-part interaction related to tool-part interfacial shear stress was proposed by Twigg et al. [56], sliding friction was the main consideration for the warpage during cure. The assumptions of their model can be summarized as follows:

- The tool-part interfacial shear stress is constant along the length of the part.
- Through-thickness stress gradient in the part is induced by the interfacial shear stress.
- Sliding friction occurs only at two interfaces consisting of the interface between tool surface and the first ply adjacent to the tool and another one for the interface between interply of the first ply and second ply.

- The sliding friction coefficient of the tool-part interface is greater than the one at the interply.
- The bending moment is only induced by the residual stress in the first ply, no through thickness stress gradient in the upper plies.
- The effect of degree of cure on modulus and interface friction is ignored
- The model is valid for unidirectional laminate in which the modulus and thermal of each ply is uniform.

Figure 2.66 shows the assumption for loading scenarios for the analytical model. The force equilibrium equation for ply 1 can be express in equation 2-13, $\tau_{Interface}$ represents the interfacial shear stress between tool surface and bottom of ply1, $\tau_{Interply}$ represents the interfacial shear stress between plies.

$$(\sigma_1 + d\sigma_1 - \sigma_1)bt_{Ply} + (\tau_{Interface} - \tau_{Interply})bdx = 0 \quad (2\text{-}13)$$

Assume $\tau_{Interface} - \tau_{Interply} = \tau_{Net}$ which is constant along the length of the laminate and rearranging.

$$d\sigma_1 = \frac{-\tau_{Net}}{t_{Ply}}\, dx \quad (2\text{-}14)$$

$$\int_0^{\sigma} d\sigma_1 = \int_L^x \frac{-\tau_{Net}}{t_{Ply}}\, dx \quad (2\text{-}15)$$

$$\sigma_1 = \frac{\tau_{Net}\,(L-x)}{t_{Ply}} \quad (2\text{-}16)$$

From equation 2-16, the stress in the rest of the laminate is:

$$\sigma = \frac{\tau_{Interply}\,(L-x)}{t_{Lam} - t_{Ply}} \quad (2\text{-}17)$$

From equation 2-17, it can be considered that the thickness of laminate is much greater than the thickness of ply and $\tau_{Interface}$ was assumed to be greater than $\tau_{Interply}$, the stress subjected to the rest of laminate is small compared to the first ply. Moreover, equation 2-16 can conclude that stress in the first ply is increased when part length is increased.

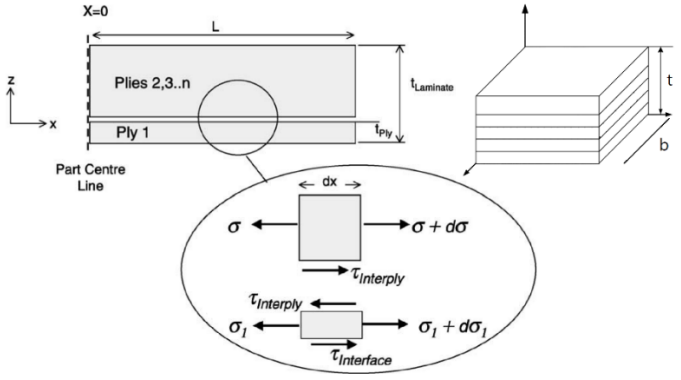

Figure 2.66 The assumption for loading scenario for the analytical model. [56]

The stress is locked in the ply after curing is completed, bending moment can be generated due to the residual stress in the first ply from equation 2-18, the graphic is illustrated in Figure 2.67, c is the distance from the ply centroid to the neural axis of the laminate which is approximated as in equation 2-19. Substituting equation 2-16 and 2-19 into equation 2-18, equation 2-20 was proposed.

$$M = \sigma \cdot t_{Ply} \cdot b \cdot c \tag{2-18}$$

$$c = \frac{t_{Lam}}{2} \tag{2-19}$$

$$M = \tau_{Net} \cdot (L - x) \cdot \frac{t_{Lam}}{2} \cdot b \tag{2-20}$$

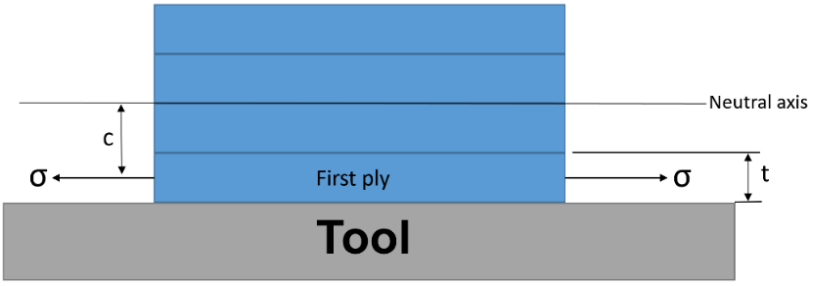

Figure 2.67 The graphic of component of equation. [56]

The relationship between the moment and curvature is

$$k = \frac{d^2z}{dx^2} = \frac{M}{E_{Part} \cdot I} = \frac{\tau_{Net} \cdot t_{Lam} \cdot b}{2E_{Part} \cdot I} \cdot (L - x) \tag{2-21}$$

Where E_{Part} is the Young's modulus and I is the moment of inertia. Integrating equation 2-21 twice and input the boundary condition from equation 2-22 and 2-23, the equation for the warpage of part as a function of x can be expressed in equation 2-24.

$$\frac{dz}{dx} = 0 \qquad at \ x = 0 \tag{2-22}$$

$$z = 0 \quad at \ x = 0 \tag{2-23}$$

$$z = \frac{\tau_{Net} \cdot t_{Lam} \cdot b}{2E_{Part} \cdot I} \left(\frac{Lx^2}{2} - \frac{x^3}{6} \right) \tag{2-24}$$

Substituting for I from equation 2-25 into equation 2-24, the equation for maximum part warpage can be expressed in equation 2-26.

$$I = \frac{t_{Lam}^3 \cdot b}{12} \tag{2-25}$$

$$W_{max} = \frac{2 \cdot \tau_{Net} \cdot L^3}{E_{Part} \cdot t_{Lam}^2} \tag{2-26}$$

Equation 2.26 was used to predict the warpage against the experiment discussed in the literature, see Table 2.13 for the configuration of experiment and results. Focusing on the effect of the part length, models of warpage prediction compared the length among L^2, L^3, and L^4 are shown in Figure 2.68; it can be observed that the L^3 curve provided good agreement with the experimental result. In the same way, the thickness effect was modeled among 1/t, $1/t^2$, and $1/t^3$ against the experimental data as shown in Figure 2.69, which $1/t^2$ showed the best agreement, this is in agreement to what examine by Mezeix et al. [41] and later was employed to predict the spring-in of L shape from Airbus A350 rib [103].

Table 2.13 Measured maximum warpage from Twigg et al. [56]

Number of plies	Part length (mm)	Pressure (kPa)	Interface condition[a]	Maximum warpage (mm)
4	300	103	FEP	0.70
8	300	103	FEP	0.13
16	300	103	FEP	0.04
4	600	103	FEP	3.84
8	600	103	FEP	0.81
16	600	103	FEP	0.12
4	1200	103	FEP	29.10
8	1200	103	FEP	7.26
16	1200	103	FEP	1.18
4	300	586	FEP	0.43
8	300	586	FEP	0.15
16	300	586	FEP	0.16
4	600	586	FEP	3.94
8	600	586	FEP	0.86
16	600	586	FEP	0.28
4	1200	586	FEP	39.57
8	1200	586	FEP	8.97
16	1200	586	FEP	1.31
4	300	103	Release	0.67
8	300	103	Release	0.26
16	300	103	Release	0.07
4	600	103	Release	2.03
8	600	103	Release	0.97
16	600	103	Release	0.31
4	1200	103	Release	15.72
8	1200	103	Release	2.67
16	1200	103	Release	1.56
4	300	586	Release	0.78
8	300	586	Release	0.25
16	300	586	Release	0.08
4	600	586	Release	4.09
8	600	586	Release	1.23
16	600	586	Release	0.11
4	1200	586	Release	42.04
8	1200	586	Release	7.71
16	1200	586	Release	1.58

[a] FEP = 2 Plies of FEP, Release = Release agent.

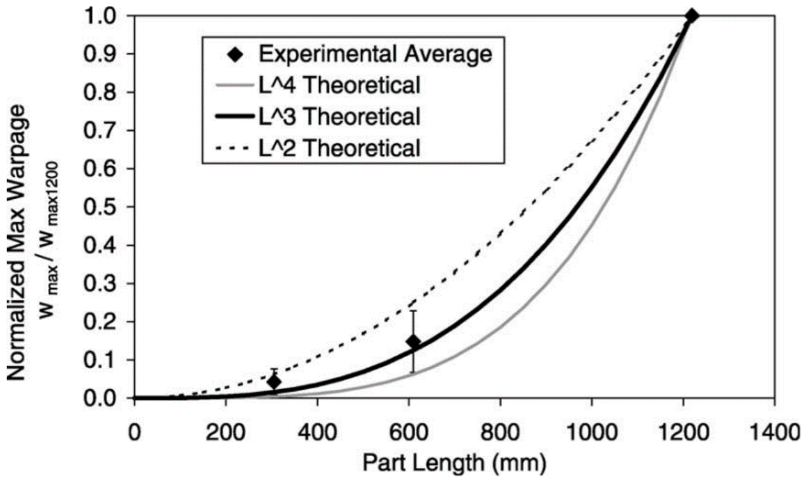

Figure 2.68 Normalized maximum warpage averaged for all experimental conditions contrasted with various theoretical warpage–length relationships. [56]

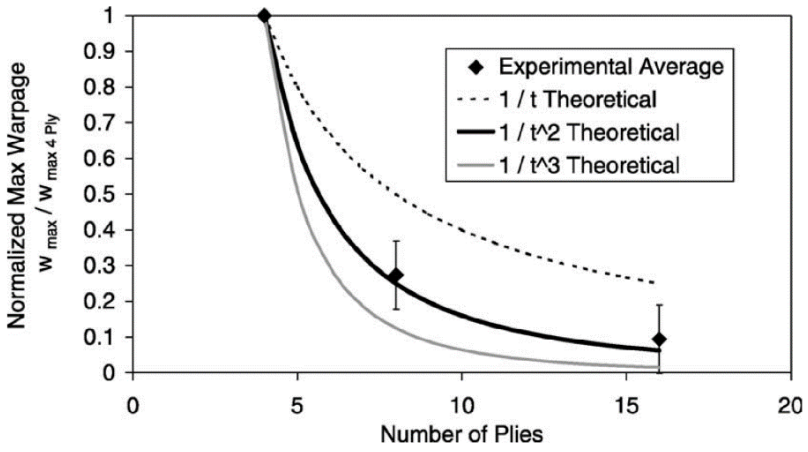

Figure 2.69 Normalized maximum warpage averaged for all specimen conditions contrasted with various theoretical warpage–thickness relationships. [56]

However, the relation of tool thermal expansion and laminate length can be amplified from equation 2-16 to find the critical part length (L_c) which is no longer strain mismatch between the tool and first ply when the part length is longer than critical value. Applying Hook's Law to the stress term at x = 0 give:

$$\varepsilon = \frac{\tau_{Net} \cdot L}{E_{Part} \cdot t_{Ply}} \tag{2-27}$$

The critical condition is :

$$(CTE_{Tool} - CTE_{Part})\Delta T = \frac{\tau_{Net} \cdot L_c}{E_{Part} \cdot t_{Ply}} \tag{2-28}$$

Then,

$$L_c = \frac{(CTE_{Tool} - CTE_{Part}) \cdot \Delta T \cdot E_{Part} \cdot t_{Ply}}{\tau_{Net}} \tag{2-29}$$

And the maximum stress can be calculated from:

$$\sigma_{Max} = (CTE_{Tool} - CTE_{Part})\Delta T \cdot E_{Part} \quad (2\text{-}30)$$

These equations explained that different tool materials can generate different magnitudes of warpage due to different coefficients of thermal expansion because a greater bending moment is induced and results in greater curvature. From equation 2-24, the maximum warpage for part length less than and greater than critical part length can be expressed as follow:

$$W_{max} = \frac{1}{3} \cdot C \cdot L^3 \qquad L < L_c \quad (2\text{-}31)$$

$$W_{max} = C \cdot \left(\frac{1}{2} \cdot L_c \cdot L^2 - \frac{1}{6} \cdot L_c^3\right) \qquad L > L_c \quad (2\text{-}32)$$

2.4.5 Finite element modelling

In 2001, Fernlund et al. [43] employed a COMPRO prediction Finite Element commercial software which was developed by the Composites Group at The University of British Columbia [104, 51, 105] for the modelling of autoclave processing of complex composite structure. This software is able to predict part deformation considering all relevant effects, including autoclave conditions, tool characteristics and material behaviour. COMPRO Finite Element commercial software was used to predict the effect of tool/part interaction. These interactions are modelled in COMPRO Finite Element software owing to a shear layer located between mould and part. This shear layer interface is modeled owing to a single layer of finite elements as presented in Figure 2.70. This shear layer has transversely isotropic elastic properties. The composite part is allowed to slide on the tool, parallel to the tool surface, but not allowed to move in its thickness direction. This was to make the shear layer stiff through the thickness and compliant in-plane. A tool surface with a release agent was modeled by a soft shear layer between part and tool surface, it was assumed that no any shear stresses are transferred between the tool and the part during cure; while a tool surface with no release agent was modeled with a hardening shear layer that gains stiffness during cure which is developed with the degree of cure, it was assumed that a thin resin film is created between the tool surface and the part after curing is accomplished, this is like the part is bonded to the tool after gelation. After the cure cycle was completed, the shear layer was removed in order to remove the part from the tool.

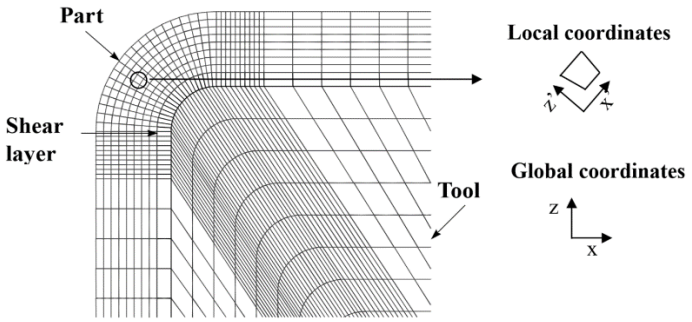

Figure 2.70 Finite element mesh showing corner geometry of part, shear layer, tool, local and global coordinates. [43]

Fernlund et al. [43] performed the modelling of L and C specimens in the experimental program from Table 2.6, only half of C specimen was modelled due to the symmetric condition. The finite element model is illustrated in Figure 2.71 which only part of the tool was included. A convective heat was applied on the external surface of the composite part in the location B1, B3, and B5 and the side of the tool on B4 and B6; heat was not allowed to transfer on the inside boundary of the tool (B2). In addition, no resin flow condition was allowed, autoclave pressure was applied to the surface of composite part (B1), the tool boundaries (B4 and B6) were set to slide along their axis, no pressure or displacement was defined on B2 boundary. The final shape of the parts after the tool was removed is indicated in Figure 2.72 and spring-in was observed. The comparison of measured and predicted spring-in for L and C shape parts is shown in Figure 2.73, it can be aggregated that COMPRO performed quite well in predicting since the most trends were similar to the experiment.

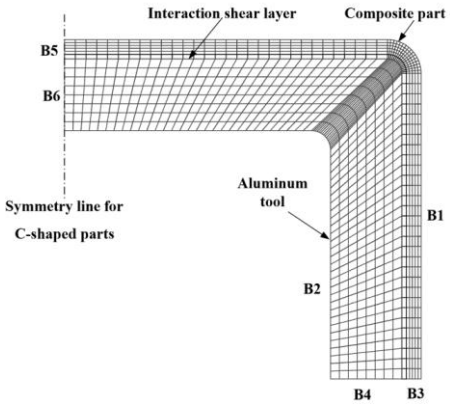

Figure 2.71 A Finite element mesh for L and C specimens. [43]

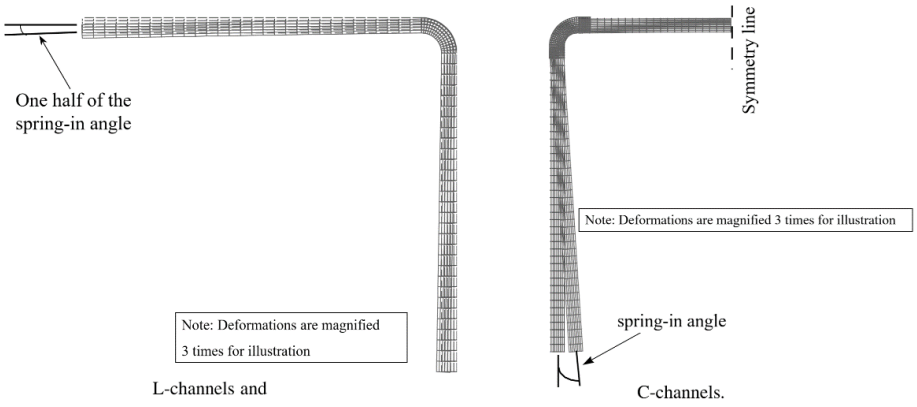

Figure 2.72 Initial and deformed shape of FE models. [43]

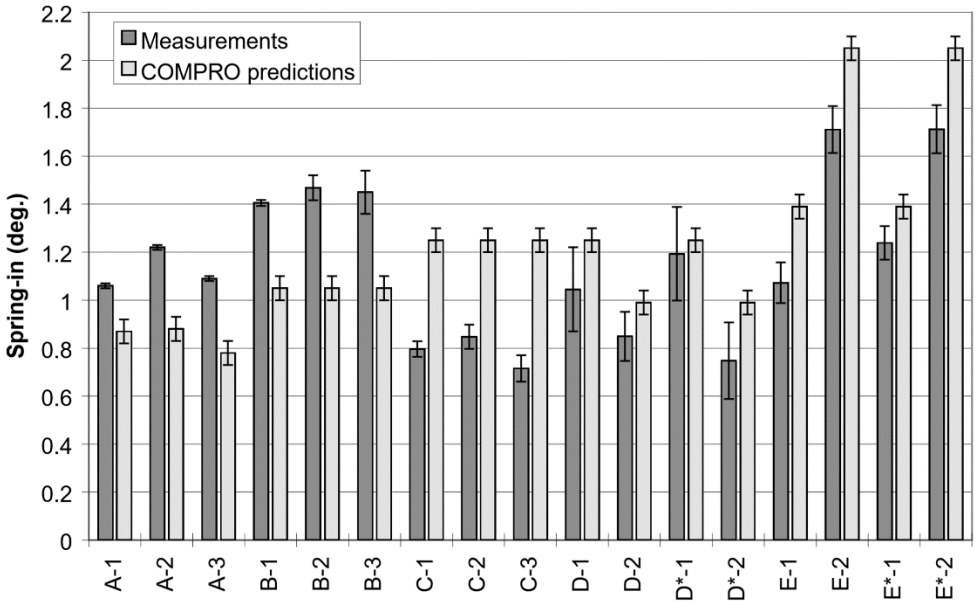

Figure 2.73 Comparison of measured and predicted spring-in for L and C shape parts. [43]

In 2003, Fernlund et al. [55] applied two-dimensional (2D) process models and three-dimensional (3D) structural models to predict the deformation of complex part. Their investigations started with a simple shape part called “the T-45 rib” as discussed in section 2.2.2. A 2D plane strain FE model of a rib cross-section was created in COMPRO. Only half of the section was modeled due to symmetrical condition. The model is shown in Figure 2.74. There were many details of parameter applied to the model which are not discussed here, finally, 1.6˚ free flange spring-in was predicted with 15% higher than 1.4˚ from experimental value, this might be because of the properties of Hexcel Style 3K-70-PW F593 were used by these authors in the model instead of those of AS4/977-3 composite due to unavailability.

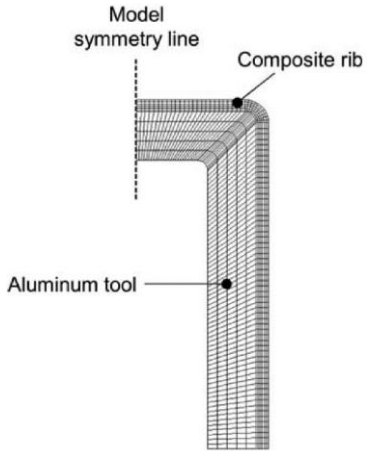

Figure 2.74 FE model of half of a rib section including the aluminium process tool. [55]

Moreover, the 2D/3D technique for the ribs was validated in ANSYS finite Element software by using 3D shell model as presented in Figure 2.75. Flanges of the rib were modeled as freely sprung-in and the structure is stress free. The vertical edges of the rib were not matched up. The 3D rib was modeled as an elastic fully cured composite. The predicted results were compared with experiment results (see Figure 2.76). They exhibited a good agreement trend conforming to Figure 2.16.

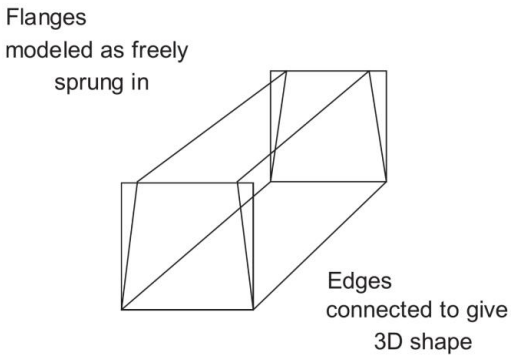

Figure 2.75 Schematic of 3D shell model. [55]

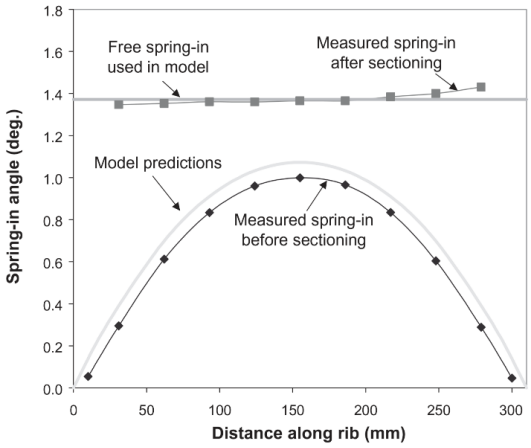

Figure 2.76 Comparison of spring-in results between model and experiment. [55]

The methodology for 2D/3D technique was also employed to predict the deformation of more complex geometry for the 777 Aft Strut Trailing Edge Fairling, the details of its structure were discussed in section 2.2.2. The part was divided into four sections perpendicular to its length (see Figure 2.77) because the deformation was observed from manufacturing experience. The 2D models were created and run for each section which mesh, boundary condition, material properties as well as cure cycle were assigned to the models; only half of the part was modelled due to symmetrical shape (see Figure 2.77). All four models were run and spring-in was observed as seen in Figure 2.78. Then, a full 3D model of the part was created as a shell element and stripped corresponding to 2D sections as shown in Figure 2.79, the moments were applied to the stripped model to make the deformation corresponding to the 2D process model and after the loads were applied between the separated cross-sections. The results of the models are indicated in Figure 2.80, 2D predictions showed good agreement with measurement results among section 2, 3, and 4 but extremely poor in section 1 while 2D/3D technique showed good agreement with experiment in all sections except some ranges in section 1 of the wide end that the honeycomb core was slightly thicker for the experiment and made spring-in decrease.

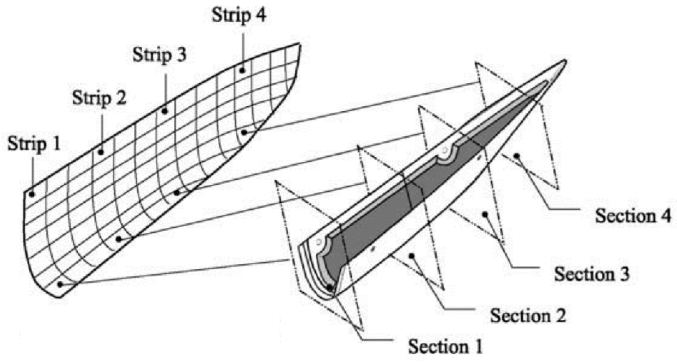

Figure 2.77 The model of The 777 Aft Strut Trailing Edge Fairling. [55]

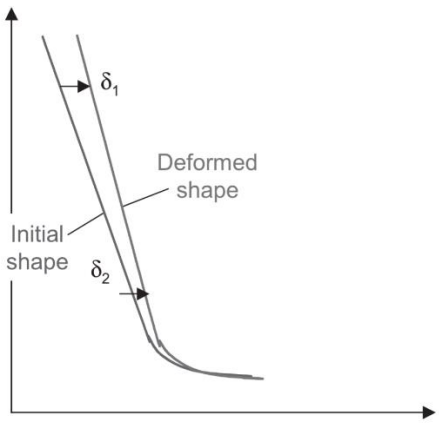

Figure 2.78 Spring-in from the model of the 777 Aft Strut Trailing Edge Fairling. [55]

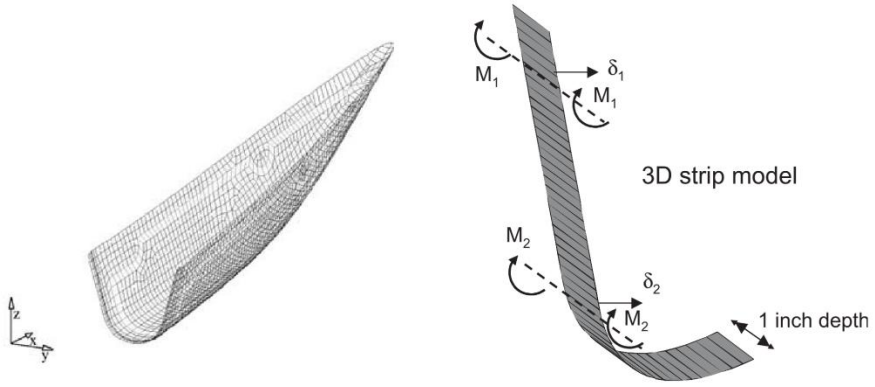

Figure 2.79 Full 3D model and 3D strip model of the 777 Aft Strut Trailing Edge Fairling. [55]

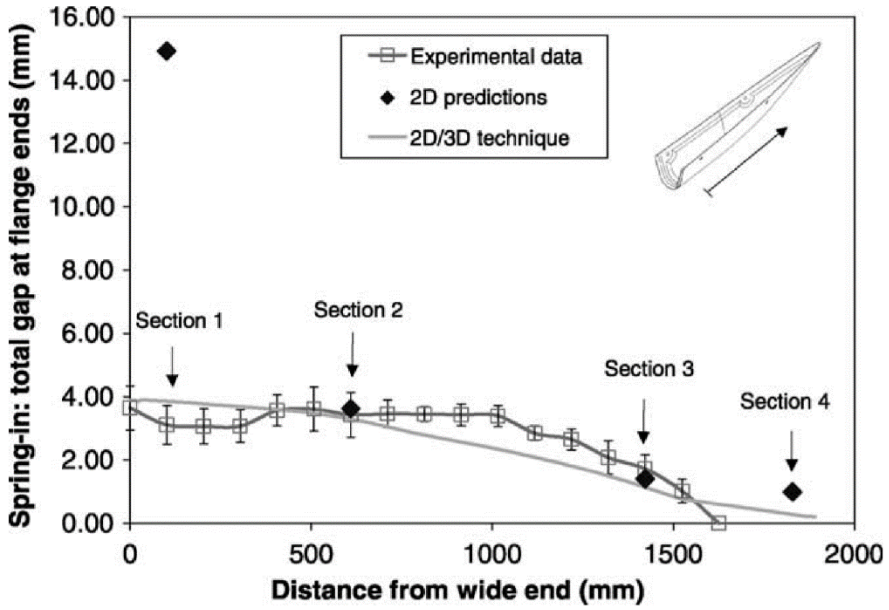

Figure 2.80 Comparison of experimental spring-in measurements and model predictions. [55]

Twigg et al. [106] performed numerical modelling for parametric study in another part of their investigation. In order to study the effect of shear layer and part properties, COMPRO software was used. The parameters were divided into four categories as shown in Table 2.14

Table 2.14 Design and results of COMPRO parametric study from Twigg et al. [106]

Shear layer modulus (6.9×10^x Pa)	Part resin modulus (4.1×10^x Pa)	Number of plies	Part warpage (mm)		
			300 mm Part length	600 mm Part length	1200 mm Part length
3	3	4	0.12	2.90	46.09
		8	0.03	0.83	13.61
		16	0.01	0.22	3.59
3	4	4	0.12	2.50	28.93
		8	0.03	0.78	11.19
		16	0.01	0.21	3.31
3	5	4	0.09	1.08	6.28
		8	0.03	0.53	4.70
		16	0.01	0.18	2.26
3	6	4	0.03	0.16	0.70
		8	0.02	0.15	0.71
		16	0.01	0.09	0.61
3	7	4	0.00	0.02	0.07
		8	0.00	0.02	0.07
		16	0.00	0.02	0.07
4	3	4	1.93	28.65	232.24
		8	0.55	8.23	98.00
		16	0.14	2.14	25.88
4	4	4	1.85	25.01	232.24
		8	0.54	7.80	90.31
		16	0.14	2.11	26.79
4	5	4	1.34	11.02	56.54
		8	0.47	5.52	43.15
		16	0.13	1.86	20.93
4	6	4	0.36	1.69	6.57
		8	0.24	1.52	6.87
		16	0.10	0.97	6.03
4	7	4	0.04	0.18	0.66
		8	0.04	0.18	0.72
		16	0.03	0.17	0.73

The results of numerical modelling for the effect of varying shear layer modulus and part resin modulus are illustrated in Figure 2.81. It could be summarized that part warpage is increased with higher shear layer modulus and lower part resin modulus, this is due to the reduction in interfacial shear stress. However, part thickness is seen to have an influence on part warpage when part resin modulus is low. Good agreement between COMPRO predictions and experimental results are from a shear layer modulus of 6.9 x 103 Pa and a part resin modulus of 4.1 x 104 Pa as shown in Figure 2.82, which four plies samples provided the best agreement.

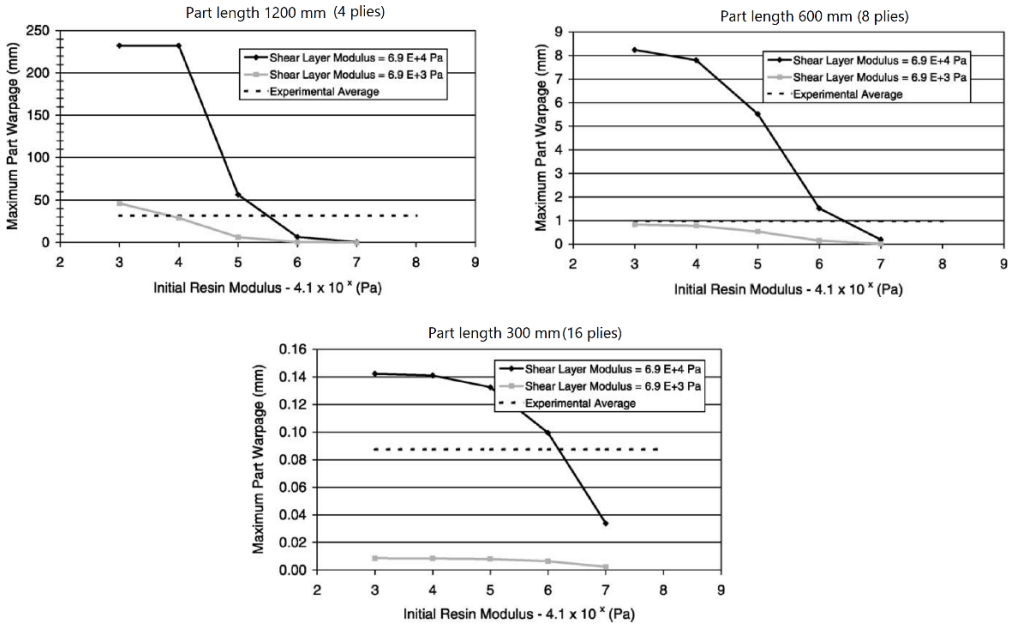

Figure 2.81 Effect of initial resin modulus and shear layer modulus on COMPRO warpage results. [106]

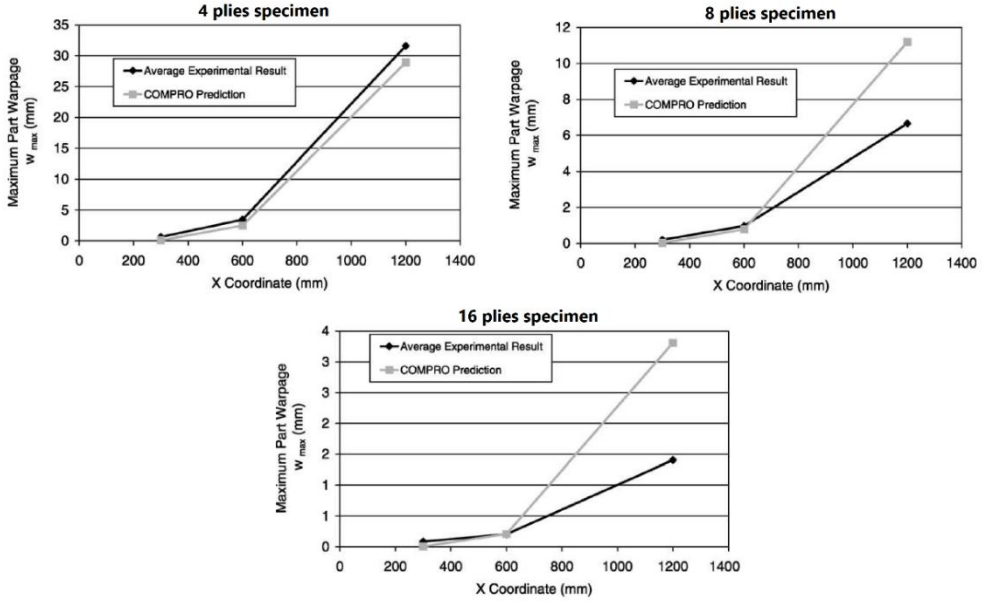

Figure 2.82 COMPRO prediction versus average experimental result for warpage. [106]

In addition, the effect of initial part resin modulus could be explained in more detail from the modelling of COMPRO in Figure 2.83. Each layer carries almost the same in-plane stress for high resin modulus of 4.1 x 10^7 while clearly different carrying was observed for lower resin modulus, which the stress was maximized at the location between tool surface and bottom ply, this can be seen Figure 2.84. Therefore, the difference in in-plane stress

gradient is generated between each ply due to low resin modulus and the bending moment can arise and lock in the part which can be calculated from equation 2-33.

$$M = \int \sigma(z) \cdot t_{element} \cdot c \cdot b \cdot dz \quad (2\text{-}33)$$

Where

σ = The in-plane stress

$t_{Element}$ = The element thickness

c = The distance between the element centroid and the neutral axis of the body

z = The height coordinate

b = The width of the body

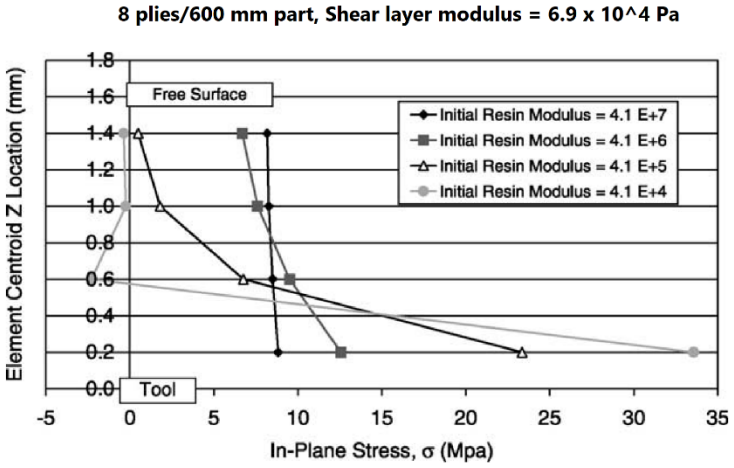

Figure 2.83 Effect of initial resin modulus on part in-plane stress distribution. [106]

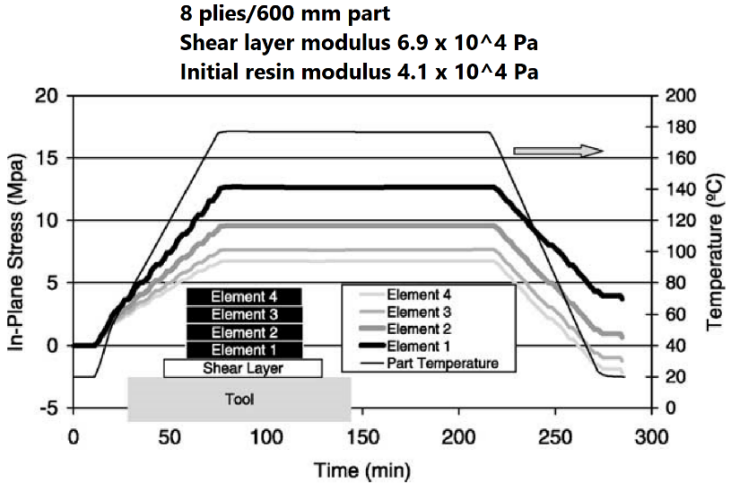

Figure 2.84 Development of part in-plane stress with respect to time. [106]

At the first stage of the cure cycle, the resin modulus is low during heat up and this can result in greater stress build up. After gelation, the resin modulus increases as indicated in Figure 2.85. In this conclusion, high initial resin modulus is more appropriate because the

bending moment generated during heat up can be reduced which can be seen in the comparison in Figure 2.86, the bending moment is greater for the lower initial modulus.

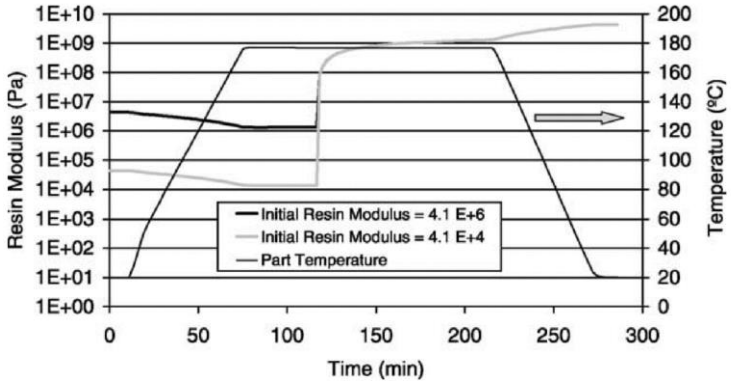

Figure 2.85 COMPRO prediction of resin modulus development with respect to time. [106]

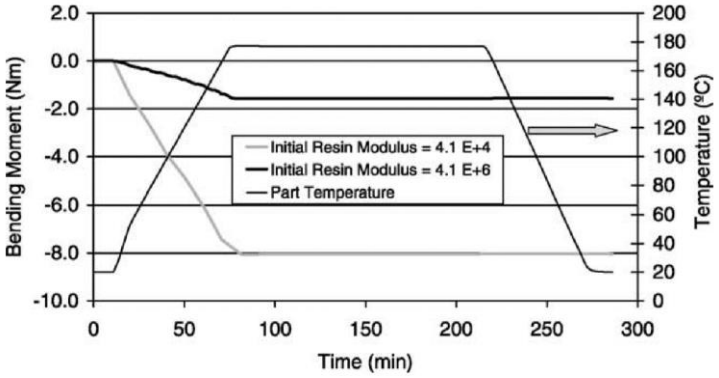

Figure 2.86 Development of bending moment with respect to time for models with different initial resin modulus. [106]

The parameters related to part and tool such as the layup, part geometry, and tool geometry were also numerically studied by Pooneh et al. [54], the characteristic of the models was referred to the experimental configuration discussed in section 2.2.1 (see Table 2.2 and more detailes in the reference). The 3D simulation was conducted by MSC Marc 2008 software. The objective of simulations was to estimate the maximum distortion of the flat panel as well as the warpage and spring-in of angle shape panel. Figure 2.87 shows an example of a 3D finite element model for L-shape panel and the tool, free surface of the panel and the tool are subjected to a temperature cycle while the autoclave pressure was applied only to the panel. Moreover, the effect of different radius and tool geometry were also investigated, tool shapes were divided into concave and convex shapes; the radius of 23 mm was designed only on convex tool while the radius of 5 mm was designed on both convex and concave tools.

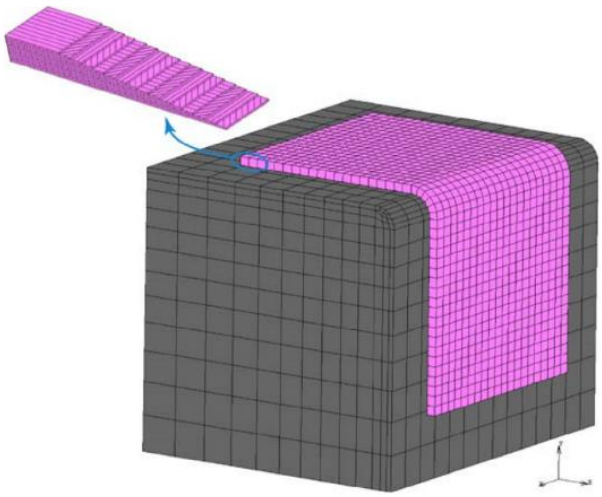

Figure 2.87 The 3D finite element mesh used for the L-shaped panel cured on an aluminium tool. [54]

The simulation results of flat panels were compared with experimental results in Table 2.15, a statistical T-test was analyzed to assess the accuracy of the model; there were no significant differences between experimental and simulation results. In conclusion, good agreement was observed for the maximum amount of distortion. For L-shape samples, simulation was performed only for asymmetric stacking sequence because it exhibited more distortion than the symmetric one. The comparison of simulation and experiment results is illustrated in Figure 2.88 including balanced and unbalanced conditions; good agreement was observed for both which asymmetric with balanced stacking showed better agreement than asymmetric with unbalanced stacking. With this reason, asymmetric and unbalanced stacking was selected to simulate the effect of curve radius and tool geometry as presented in Figure 2.89. Spring-in was larger for a larger radius which can be because of greater residual stress generated from geometry locking. Furthermore, concave tools exhibit 30% lower spring-in than convex tools. Unfortunately, the conclusion for this scenario was not provided in the literature.

Table 2.15 Comparison of Simulation and Experimental Results for Maximum Distortion of Flat Panels. [54]

			Maximum amount of distortion (mm)	
Panel no.	No. of plies	Panel type	Experiment	Simulation
1	16	Asymmetric, balanced	17.45 ± 2.12	17.70
2	16	Symmetric, balanced	1.08 ± 0.22	1.02
3	16	Symmetric, unbalanced	1.00 ± 0.12	1.02
4	16	Asymmetric, unbalanced	15.34 ± 1.5	13.46
5	8	Symmetric, balanced	3.20 ± 0.53	3.15
6	8	Asymmetric, balanced	43.25 ± 4.5	30.23

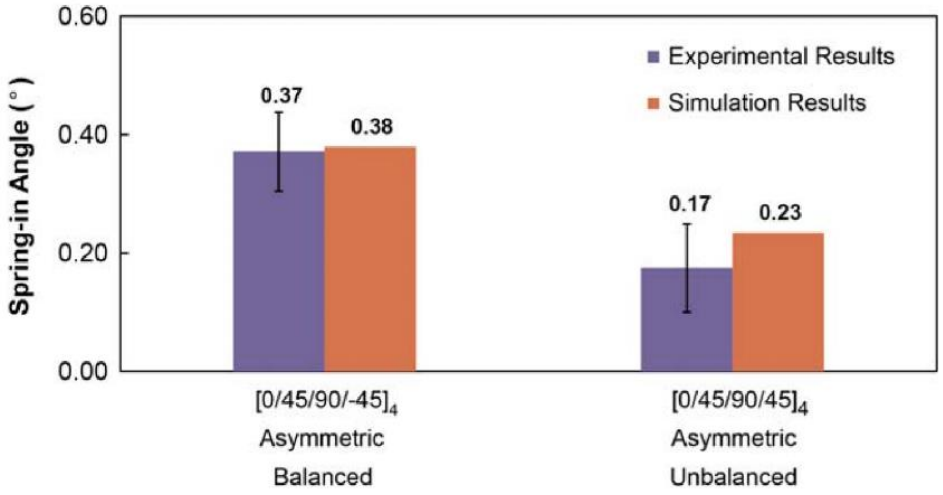

Figure 2.88 Comparison of simulation and experimental results for the L-shaped panels. [54]

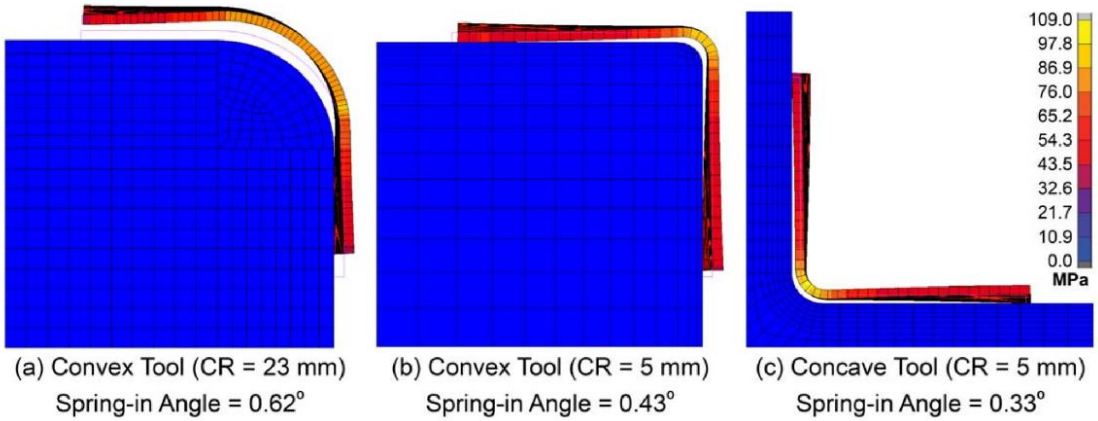

Figure 2.89 Effect of curve radius and tool geometry on spring-in angle of the L-shaped panel. [54]

2.5 Conclusion

First of all, let's summarize the intrinsic parameters. Only a few researchers focused on the effect of different raw materials because it can be assumed that the fibre/matrix system with high strength and stiffness will result in less deformation. In terms of part geometry, shape, size and thickness are the main factors to impose the characteristic of part deformation. Part section that is free standing without joint or support structure tends to show much warpage especially when a thin and large part is fabricated. Several researchers believed that a thick and small part generally provides less deformation. However, there are arguments against it and some researchers found that the part warpage is independent when critical size and thickness is reached. Secondly, the effect of part layup is predominant to final part deformation. However, stacking sequence effects are sensitive to various parameters. Therefore, other parameters, especially the part geometry must be identical. In

general, having the ply with fibre run along the length or the width of laminate is believed to enhance the in-plane and bending stiffness and reduce the deformation but there was some argument against it for some angle ply layup. The comparison of stacking effects throughout the research works from various researchers might be difficult because the condition of the experiment was usually different. It should be noted that the design of stacking sequence will determine the mechanical properties of the part after cured, the measurement of distortion should be carefully handled to avoid the effect of weak point especially for the measurement of curve composite part.

Finally, the extrinsic parameters from the fabrication process also play an important role in the distortion of laminated parts. Starting from tool or mould, three factors including mould materials, mould shape, and mould surface condition were generally considered. Metallic materials are normally selected to fabricate a mould due to their strength and stiffness with low forming cost but anyway their thermal expansion is high especially when aluminium is chosen. Several researchers certified that a tool with higher coefficient of thermal expansion can increase the deformation because the laminate part is forced to adhere with the tool during cure, it usually generates different stress gradients among each layer and is frozen after the part is removed. In terms of mould shape, mould angle and radius were investigated. Increasing in mould angle is believed to decrease warp angle due to the difference between in-plain and through-thickness thermal contraction and chemical shrinkage is reduced. In other words, some researchers concluded that the warp angle is induced only when tool angle is below 90˚ in particular for female mould. Mould radius was found to have little effect on final warp angle for part fabricated on male mould but small radius should be aware for female mould because it can induce a resin rich region at the corner which is the cause of low fibre volume fraction and fibre bridging behaviour. The last factor is tool surface conditions, in general, tool surfaces can be modified by mechanical polishing or by several release agents, including liquid and polymer film sheets. The main tool surface modification is to avoid the difficulty for part/mould removal. However, various conflicts in research works of tool surface condition were found to have and do not have the impact on part distortion and be unpredictable in some cases.

Curing cycle is another root cause of part distortion because the fabrication is operated at elevated temperature, thermal contraction and chemical shrinkage are generated to the resin matrix. Most research works indicated that low curing temperature can reduce part deformation due to the decrease in thermal contraction. However, composites always need to be fabricated at high temperature or manufacturing recommended cure cycle (MRCC) to achieve the degree of cure and strength of the final part. A few works focused on heating rate and Dwell time; slow heating rate and short Dwell

time were found to be able to reduce the distortion. The number of holds was also attentive from various researchers, some research works concluded that two holds has more influence on the deformation than one hold cure cycle while others did not obtain the effect from it. Regarding to cool down rate, it seems no effect to the deformation when the part is fully cured which has been mentioned from a few literatures, this can be assumed that there are no longer contraction or shrinkage during cool down stage while another study obtained the result that cooling rate only has an impact on non-post cure sample which slow cooling rate is a better choice. Post cure process is probably required to ensure the completion of curing but it usually increases part distortion because more thermal load is applied.

Chapter 3

Experimental study and numerical modelling of tool/part interaction in autoclave curing

This chapter is the start of the experiments made to study the effect of tool/part interaction. Firstly, the details of experiments, measurement methods and the explanations of thermomechanical model and model construction are provided. Finally, the comparison between experimental and numerical results are presented.

3.1 Objective and experimental plan

Out-of-plane deformation generally appears for laminate composite parts after autoclave processing due to unbalanced residual stress developed in the plies. This can lead to undesired shape and poor dimensional control in part manufactured. Several parameters including intrinsic and extrinsic sources have been studied to investigate their effect on the warpage (see Figure 1.10). This chapter presents a study on out-of-plane deflection of initially (prior to curing) flat laminate composites. The effect of stacking sequences and tool surface conditions (releasing agents) were analyzed. Firstly, the unidirectional prepreg M21EV/IMA was chosen as a raw material for ply layup. Aluminium 2024 was selected for the mould material in order to maximize the coefficient of thermal expansion of the mould and therefore the mould/part interaction. Freekote liquid release agent, ETFE release film and peel-ply were used to modify tool surface conditions. The reader can find more technical data about releasing agents in the annex A. Afterward, the four plies specimens with initial dimensions of in-plane 250x250 mm^2 and different layups (cross-ply $([0/90]_S)$ and angle-ply $([45/-45]_2$) were fabricated. Tool surface was classified into four conditions: 1) Freekote + one layer ETFE release film, 2) Freekote + one layer peel-ply, 3) Freekote + two layers ETFE release film, 4) Freekote + three layers ETFE release film. In addition, for a given stacking sequence, four specimens were manufactured for each configuration of tool surface for more replications. Thus, 16 specimens of cross-ply and angle-ply laminates were done for a total of 32 specimens. Other process parameters such as mould material, curing temperature profile and autoclave pressure remained unchanged for all this thesis work.

3.2 Experimental procedure

3.2.1 Preparation for raw material and mould

The unidirectional prepreg M21EV/IMA was selected as a raw material to form the layup of initially flat specimens. This prepreg was developed from a thermosetting matrix (polymer matrix) M21EV with 34% contents (in weight) and the reinforced fibre is the IMA (Intermediate Modulus carbon fibre). The M21EV is an epoxy resin embedded with thermoplastic nodules that improves the toughness of the composite, these nodules form thin layers between the ply stacking as shown in Figure 3.1. This material is produced by Hexcel composites. An aluminium mould was selected to be a support tool because it can provide higher coefficient of thermal expansion compared to other metallic materials such as steel or invar tool (CTE aluminium = 2.28 x 10^{-5} $°C^{-1}$, steel = 1.25 x 10^{-5} $°C^{-1}$, invar = 0.15 x 10^{-5} $°C^{-1}$) [44, 46, 48, 68]. Aluminium plate with an overall size 900 x 1400 x 10 mm^3 as shown in Figure 3.2 was used due to its availability and the size is limited by autoclave machine.

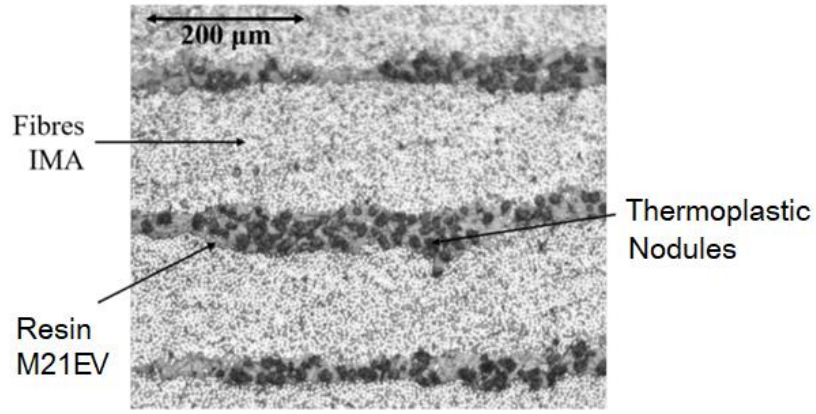

Figure 3.1 Microscopic structure through the thickness direction of an M21EV/IMA. [19, 100]

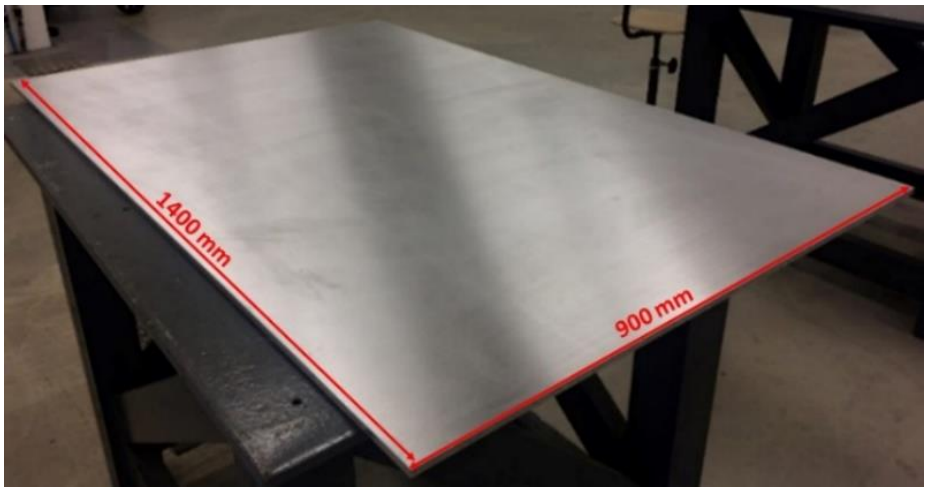

Figure 3.2 Aluminium plate used for the mould.

The experiment was designed to cure up to 16 specimens inside the autoclave together at the same time which needs to respect the suitable size of the specimens and also the replication for mould surface conditions. Therefore, the initial in-plane dimension of laminate specimens was decided to be 250x250 mm^2 so that eight laminated plates could be placed on the aluminium plate. Technically, 2 mould plates can be stacked to be two levels and the number of samples cured in one autoclave cycle becomes 16. The schematic of arrangement is shown in Figure 3.3 and Figure 3.4. The width of raw prepreg sheet is only 150 mm which is not enough to form a 250 x 250 mm^2 layer, thus, we decided to cut them in pieces and made a joining for each layer. The schematic of prepreg cutting for both cross-ply and angle-ply is illustrated in Figure 3.5.

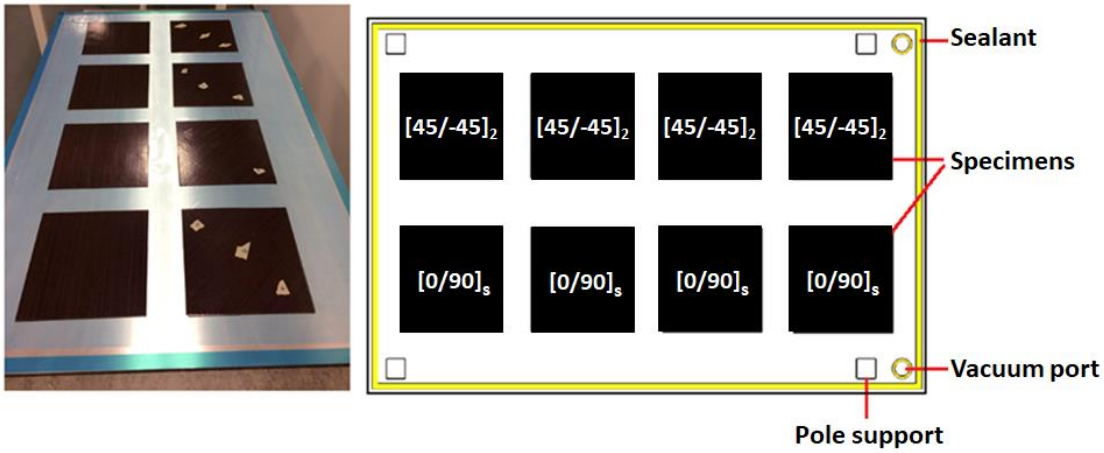

Figure 3.3 Arrangement of laminate specimens on a mould plate.

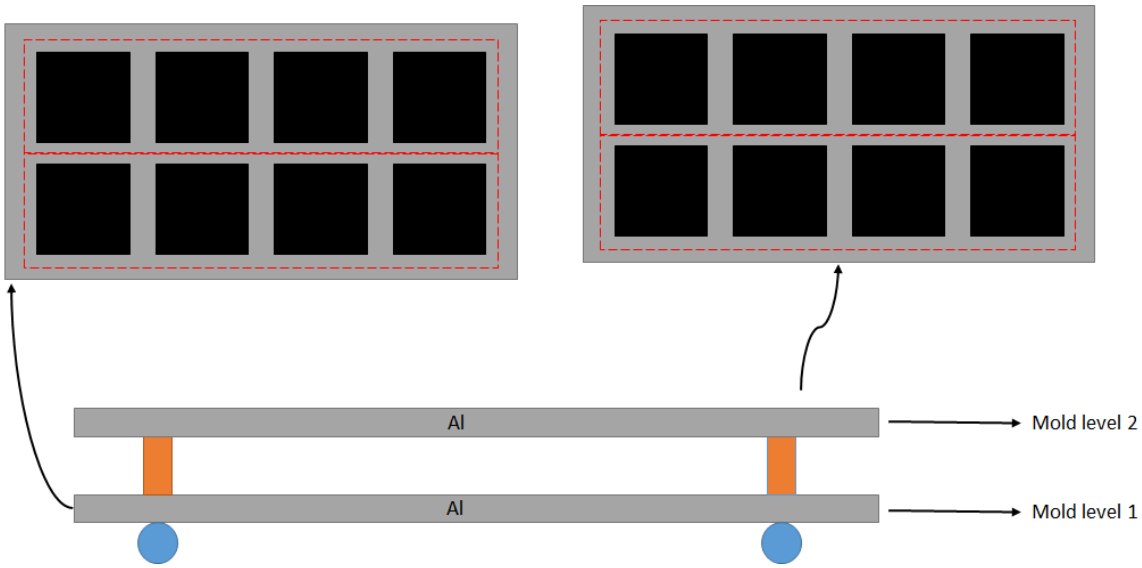

Figure 3.4 Schematic of 2 levels mould.

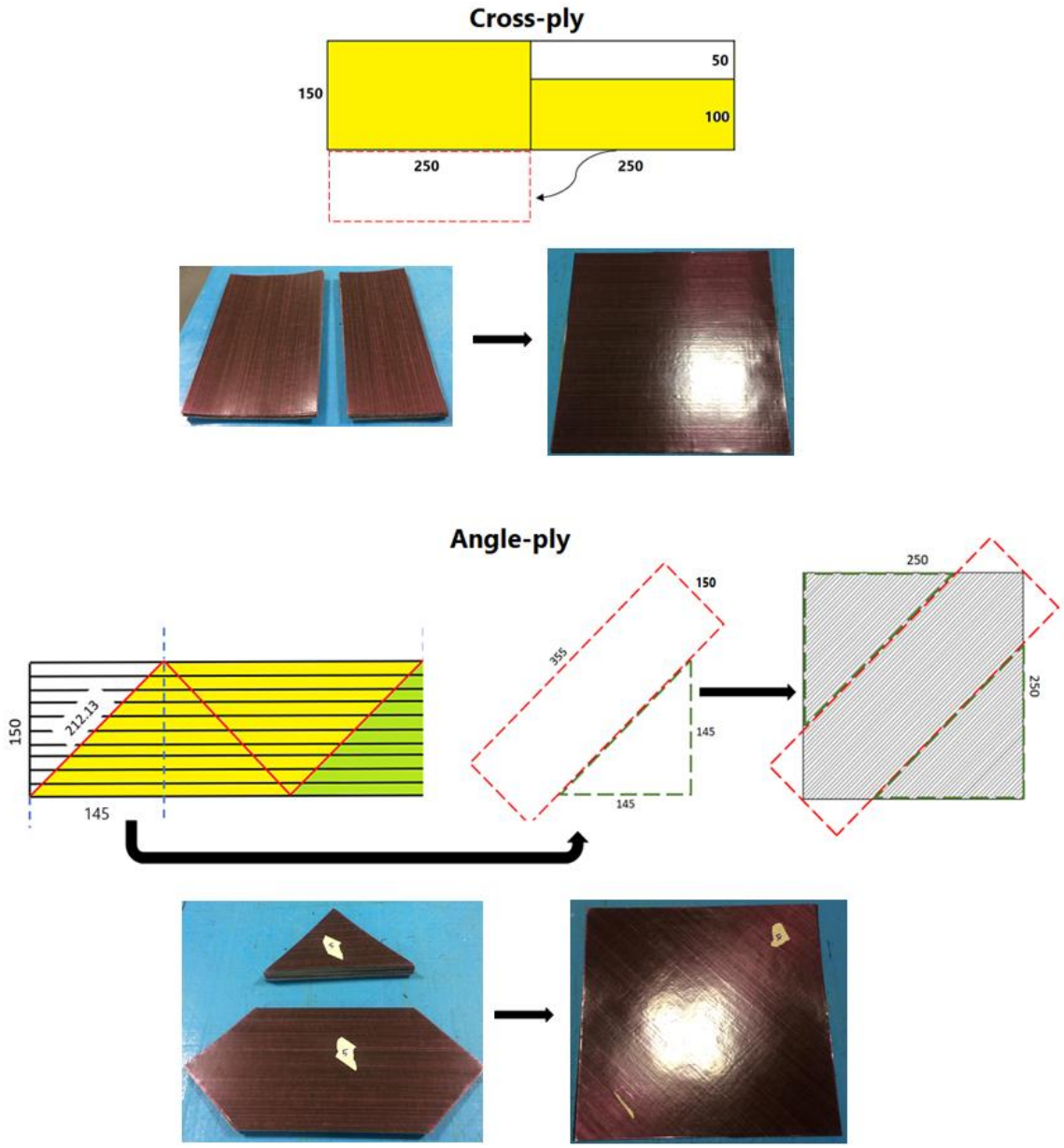

Figure 3.5 The schematic of prepreg cutting and joining for a layer of cross-ply and angle-ply laminates.

After completing the hand layup, vacuum compaction was done to all specimens for 20 minutes in order to remove air gap inside the plies and ensure bonding with to avoid the voids. All specimens were prepared in the laboratory clean room with controlled temperature (between 18 and 20 °C) and relative humidity (between 50 and 53%) in order to limit moisture absorption by the prepreg M21EV/IMA.

3.2.2 Preparation for tool surface conditions and bagging arrangement

Tool surface condition is not only one of important parameters regarding the deformation of laminate after autoclave curing, but also the one we wanted to focus our research on. Changing tool surface conditions can reduce or increase the effect of tool expansion to the laminate when subject to elevated temperatures. As already discussed in this study, tool surface conditions are classified into four conditions (see Figure 3.7) between the aluminium tool plate and the laminate:

1) Freekote + one layer of ETFE release film
2) Freekote + one layer of peel-ply
3) Freekote + two layers of ETFE release film
4) Freekote + three layers of ETFE release film.

Freekote and release film are usually employed as release agents but there is a lack of study on the effect of release fabric like peel-ply upon process-induced stress and deformations. First of all, aluminium mould plates were cleaned by using acetone to remove some dirt of handling stemming from previous curing. Freekote C-600 liquid release agent was applied on the aluminium mould surface. Four coats were done which each coat was applied perpendicular to each other and allowed 10 minutes to dry for each coating layer. ETFE release film and Peel-ply were chosen to modify the interaction between laminate and mould as indicated above; the arrangement of surface conditions and bagging product are illustrated in Figure 3.7.

As already said, due to the internal size of the autoclave, only 2 mould plates can be stacked as shown in Figure 3.6. By this reason, only 16 samples with 2 mould surface conditions could be operated in one autoclave cycle. Therefore, two autoclave cycles were required to complete all configurations. In conclusion, 32 specimens were fabricated with different layups and tool surface conditions, more details are presented in Table 3.1. The bagging products on the top of specimens remained identical, Peel-ply was placed adjacent to the top surface of laminate followed by perforated release film to transfer the excess resin to be absorbed by breather cloth. Two vacuum ports were installed for each mould plate to provide vacuum condition during the whole process and sealant was used to stick the vacuum bag with the mould plate. Three thermocouples (TCs) were installed on each mould plate in different locations to monitor the curing temperature (see Figure 3.6).

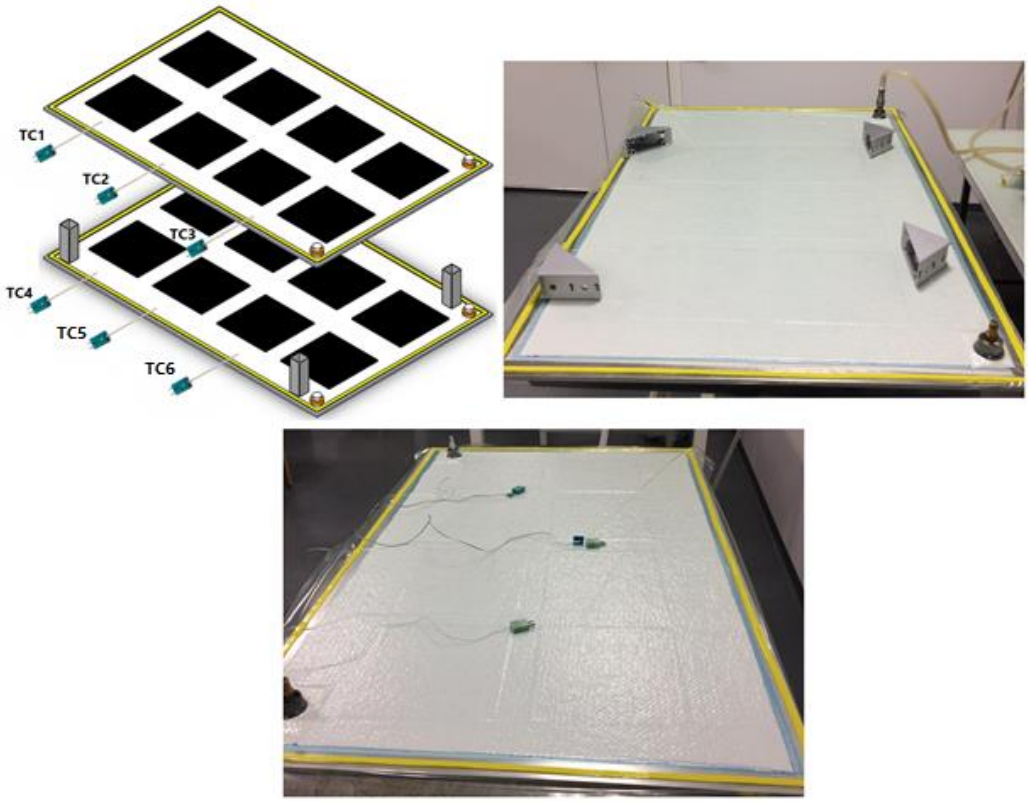

Figure 3.6 Mould arrangement.

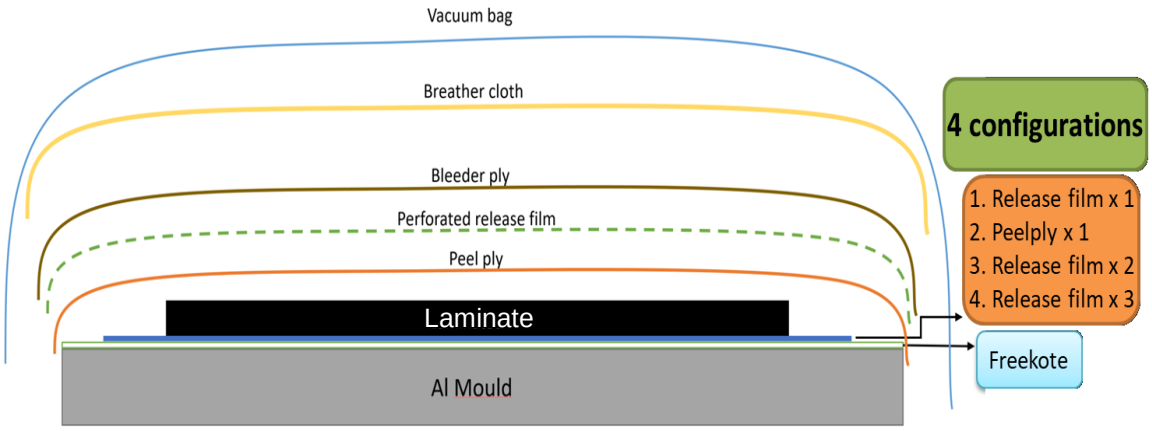

Figure 3.7 The arrangement of mould surface conditions and bagging products.

Table 3.1 Detail of experiments.

Experiment	Specimen no.	Layup	Tool surface
1	EX1-1 - EX1-4	[0/90]s	Freekote + 1 ETFE release film
1	EX1-5 - EX1-8	[0/90]s	Freekote + 1 Peel-ply
1	EX1-9 - EX1-12	$[45/-45]_2$	Freekote + 1 ETFE release film
1	EX1-13 - EX1-16	$[45/-45]_2$	Freekote + 1 Peel-ply
2	EX2-1 - EX2-4	[0/90]s	Freekote + 2 ETFE release films
2	EX2-5 - EX2-8	[0/90]s	Freekote + 3 ETFE release films
2	EX2-9 - EX2-12	$[45/-45]_2$	Freekote + 2 ETFE release films
2	EX2-13 - EX2-16	$[45/-45]_2$	Freekote + 3 ETFE release films

3.2.3 Curing temperature, pressure and vacuum conditions

The effect of curing conditions and pressure route applied during cure are not the main focus in this study. Therefore, they were kept identical for all experiments in order not to induce any changes in M21EV matrix degree of cure (α) and glass transition temperature (T_g) which would thermally induce stresses directly generated by temperature differences. Curing profiles regarding the work from Moretti et al. [19, 100] as illustrated in Figure 3.8 were employed. The curing starts by the first heating ramp of 1 °C/min and dwell at 150 °C for 1.5 hours followed by the second heating ramp of 1 °C/min and dwell at 180 °C for 2 hours and cooling down to room temperature at 1 °C/min, the autoclave pressure of 7 bars and full vacuum of 1 bar are applied throughout the curing.

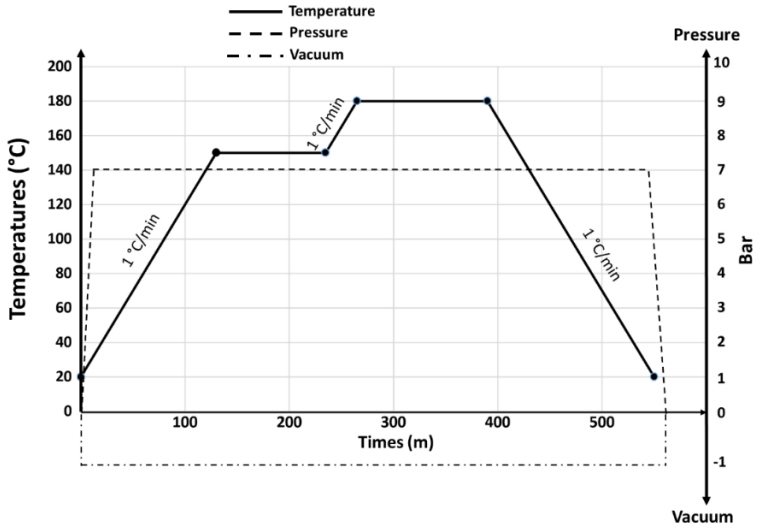

Figure 3.8 Curing profile, pressure and vacuum condition used in this study. [19, 100]

3.2.4 Samples observation after curing

After autoclave curing, mould pack was removed from the autoclave. The laminates inside vacuum bags were observed, the deformation of both cross-ply and angle-ply could be seen before demoulding as shown in Figure 3.9. However, the shape of distortion was similar due to the effect of vacuum. Moreover, the behaviour of resin flow was different between the use of release film and peel-ply. Resin flowed to the side of the laminates when using release film while it was forced to flow down to the bottom layer when using peel-ply, these are revealed in Figure 3.11.

Afterward, mould pack was disassembled in order to remove all bagging products and obtain the final shape of the specimens in a free standing state. Angle-ply laminates show much higher deformation than cross-ply laminates. Physically, bending shape along the 45° direction was observed for angle-ply laminates when both ETFE release film and Peel-ply were used while double curve and cylindrical shapes (see Figure 3.10) were observed for cross-ply laminates when using ETFE release film and peel-ply respectively. Figure 3.12 shows all laminates after demoulding. However, this section explains the observation for experiment 1 only because it was similar for experiment 2. Finally, appropriate measurements are required to measure the magnitude of deflection for all specimens.

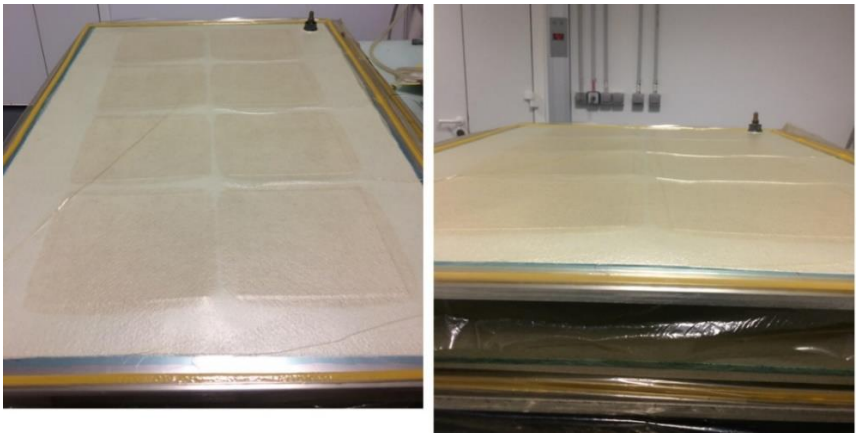

Figure 3.9 The deformation of laminates inside vacuum bag.

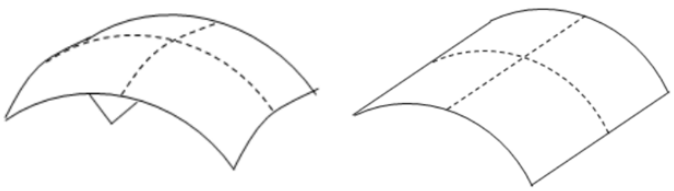

a) Double curve shaped **b) Cylindrical-shaped**

Figure 3.10 Illustration of deformed shapes observed from cross-ply laminates.

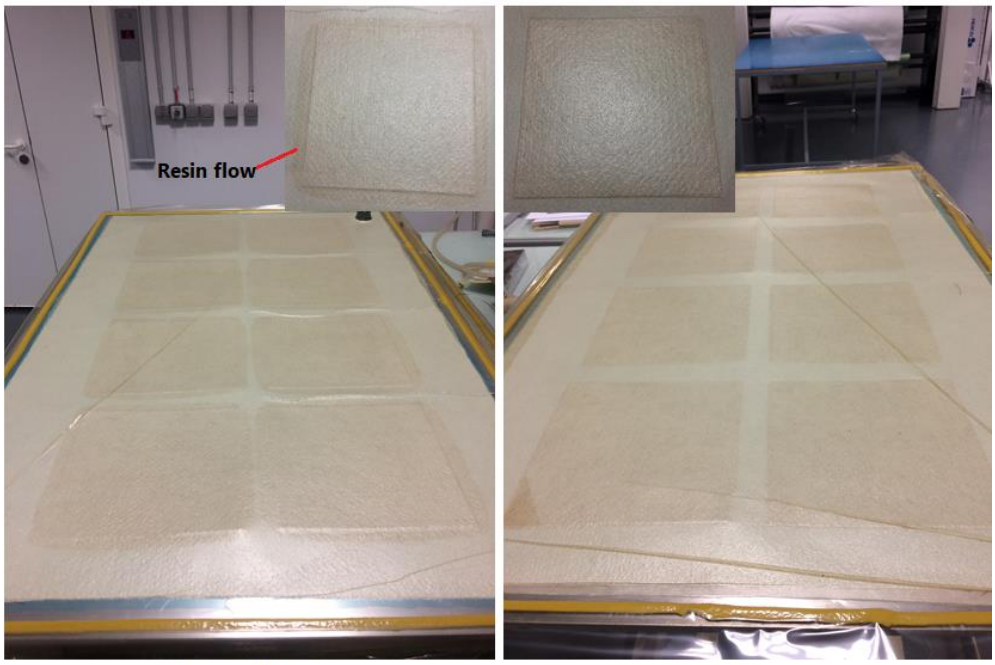

Figure 3.11 Different resin flow behaviour between using ETFE release film and peel-ply.

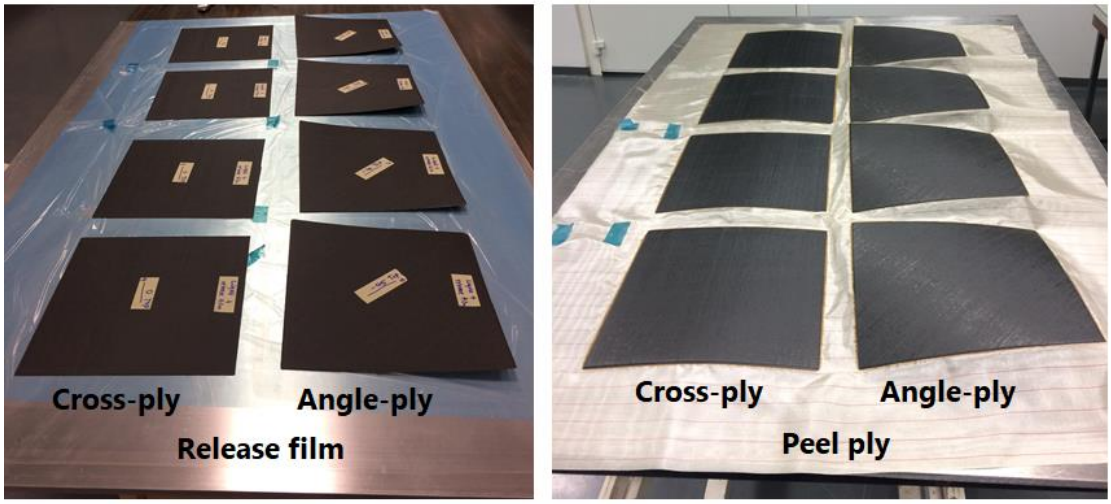

Figure 3.12 The samples after demoulding.

3.2.5 Laminate physical characteristic after curing

The difference of release agent combinations may possibly modify the physical characteristics of the laminates measured after curing. In order to proceed to a measurement to compare the results (deformed shape and magnitude) obtained with the types of tool/part configurations, we must ensure that the laminates have similar degree of cure (α) and glass

transition temperature (T_g). A TA Instruments differential scanning calorimeter (DSC) Q100 was employed to measure the heat flow released of cured samples. The heat flow measured was used to calculate the glass transition temperature (T_g) and degree of cure (α). The dynamic tests were run at 20 °C/min from -50 °C to 350 °C. The cured samples of M21EV/IMA were taken randomly from laminate plates cured on ETFE release film and peel-ply and were filled in sealed aluminium pans with 15 ± 0.5 mg which corresponded to about 5 ± 0.5 mg for 34% of resin. The calibration of DSC was done with indium samples. Each sample condition was repeatedly tested three time. The examples of the capture of entire exotherm of cured samples are presented in Figure 3.13. We can see a glass transition temperature (T_g) followed by a small exotherm which is related to any material in that epoxy had not fully cured. By knowing the amount of energy for the uncured portion and knowing the total enthalpy (from uncured exotherm), percentage or degree of cure can be calculated from equation 3-1. The total enthalpy of neat resin of uncured prepreg (ΔH_{TOT}) was not tested in this study but the values can be obtained from L. Moretti et al. [19, 100] which is 429.6 J/g. The average α and T_g are presented in Table 3.2. The significant differences are not observed for the physical characteristics of laminates (α, T_g) cured with ETFE release film and peel-ply.

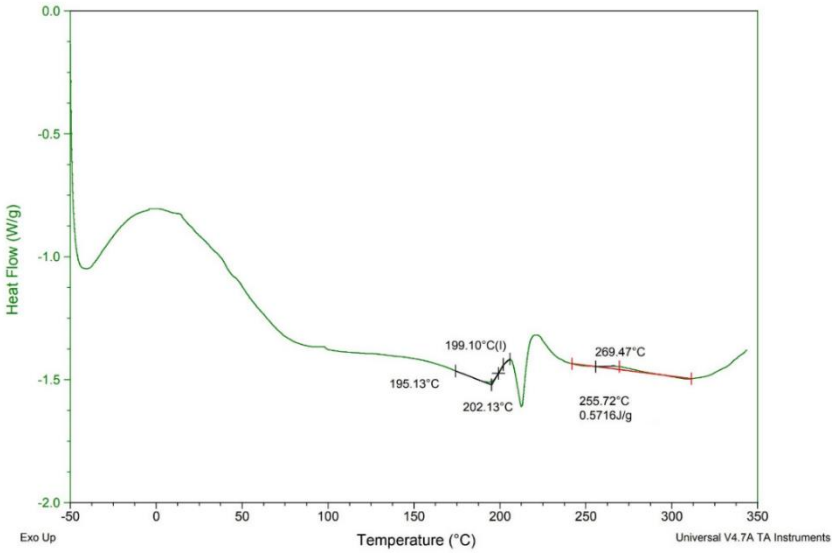

Figure 3.13 An example of exotherm of cured M21EV/IMA.

$$\%\ cure = \frac{\Delta H_{TOT} - \Delta H_{res}}{\Delta H_{TOT}} \text{ x } 100 \qquad (3\text{-}1)$$

Where

ΔH_{TOT} = Total enthalpy of neat resin of uncured prepreg (J/g)

ΔH_{res} = Residual enthalpy of neat resin of cured laminate (J/g)

Table 3.2 Control of the physical characteristics of laminates cured with ETFE release film and peel-ply.

Samples cured with	Degree of cure (α, %)	Glass transition temperature (T_g, °C)
ETFE release film	99.84	198.88
Peel-ply	99.75	199.45

3.2.6 Laminate fibre volume fraction after curing

Since we have previously mentioned that when the resin is in the liquid state, the laminate is subjected to the phenomenon of resin flow. Differences of resin flow behaviour were observed between the ETFE release film and peel-ply tool/part interfaces. It seems possible that changing the types of release agent (ETFE or peel-ply) could have an influence on the local fibre volume fraction (Vf%). Therefore, we carried out the fibre volume fraction (Vf%) on the cross-ply ([0°/90°]s) laminates cured either with an ETFE release film or with a peel-ply. To remind once again that all laminates manufactured in this study were pre-compacted under vacuum conditions. This procedure increased the preparation time but nevertheless made it possible to minimize the porosities inside the laminated plate. The samples of cross-ply ([0°/90°]s) laminates (see Figure 3.14) were randomly cut and embedded into the resin gel before polishing for image collection from microscope. The images collected from microscope are shown in Figure 3.15. The measurement of fibre volume fraction (Vf%) was carried out along the bottom ply because it is the ply adjacent to the release agent (ETFE and peel-ply) and mould. The average fibre volume fraction (Vf%) measured from various images along the bottom ply for the samples cured with the ETFE release film and peel-ply are 63.42 % and 61.56 % respectively. The difference between fibre volume fractions (Vf%) is about 3 % which is relatively low.

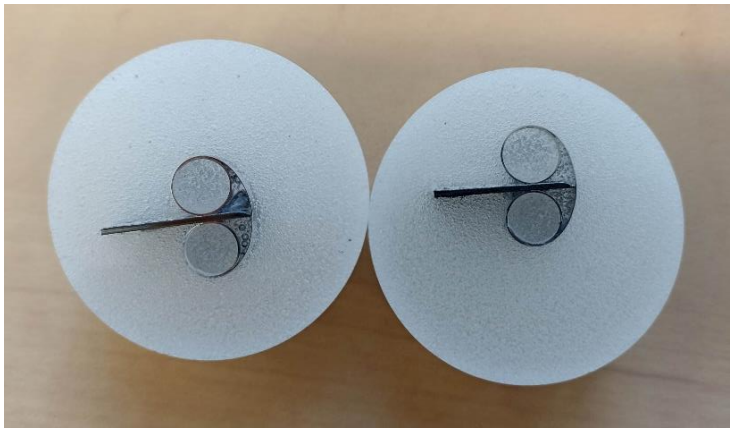

Figure 3.14 The samples for microscope.

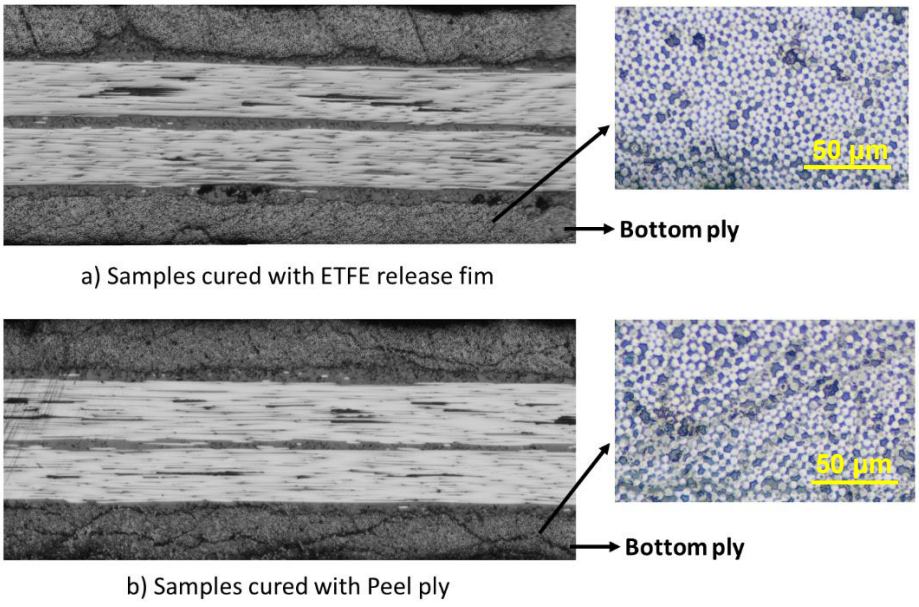

Figure 3.15 Microscopic images of the samples

3.3 Out of plane deformation measurement

Since we have shown that changing the types of release agents (ETFE or peel-ply) did not modify the physical characteristic (α, T_g) and fibre volume fraction (Vf%) of the laminates. Therefore, we can continue to carry out the out-of-plane deformation measurement. Digital image correlation (DIC) and laser displacement sensor (LDS) were employed to measure the out-of-plane deflection of all specimens in order to ensure the accuracy of measurement by comparison of both methods. Technically, the DIC can assist to examine the warpage shape of cured laminates and to indicate maximum and minimum values for magnitude of deformation, while laser displacement sensor is supportive to search for the maximum deformation point by measuring 17 points on each specimen.

3.3.1 Measurement by Digital Image Correlation (DIC)

Digital Image Correlation (DIC) is a contactless measurement technique which is usually used for strain and displacement determination during mechanical testing. The fundamental of DIC is the comparison of two images of the specimen before and after deformation. The image can be captured by one or more cameras and the analysis can be performed based on the intensity of speckle dot patterns applied on the surface of specimens. Since all the laminates are black, coating of white colour was required before producing a random black speckle pattern on a top surface. Two layers of white colour were sprayed on the top of the laminate surface as illustrated in Figure 3.16. The speckle kit from correlated solutions was utilised to produce the speckle pattern by the roller with 0.026'' dot

size. Two layers of speckle pattern were applied on the laminate surface in a perpendicular direction to each other. The example of laminates after rolling is presented in Figure 3.17.

Figure 3.16 Spray white colour on the top surface of laminate.

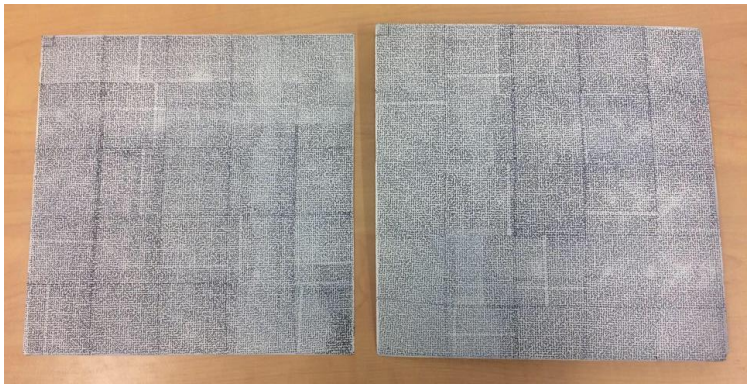

Figure 3.17 Laminate with speckle pattern.

In this study, two AVT cameras PIKE F-505B with the resolution 5 megapixels (image size 2452 (H) x 2054 (V)) were used to capture the images. Technically, two cameras were required in order to form and analyse the 3D shape. About 100 pictures of calibration plates were taken for calibration with different locations and angles adjustment of the calibration plate provided by VIC3D®. The laminates were placed on a flat table during the measurement. Images were taken from the top by two cameras which were mounted on a support structure together with light sources. The angle and the distance of both cameras were adjusted to be able to capture all the laminate areas. The measurement setup can be seen in Figure 3.18. Physically, cross-ply laminates could be simply placed on a table because it is approximately flat, but some supports were needed for two edges side of angle-ply laminates to prevent the movement of specimens during measurement. Two standard metallic blocks with total height 15.5 mm were used to support both bent up sides as illustrated in Figure 3.19.

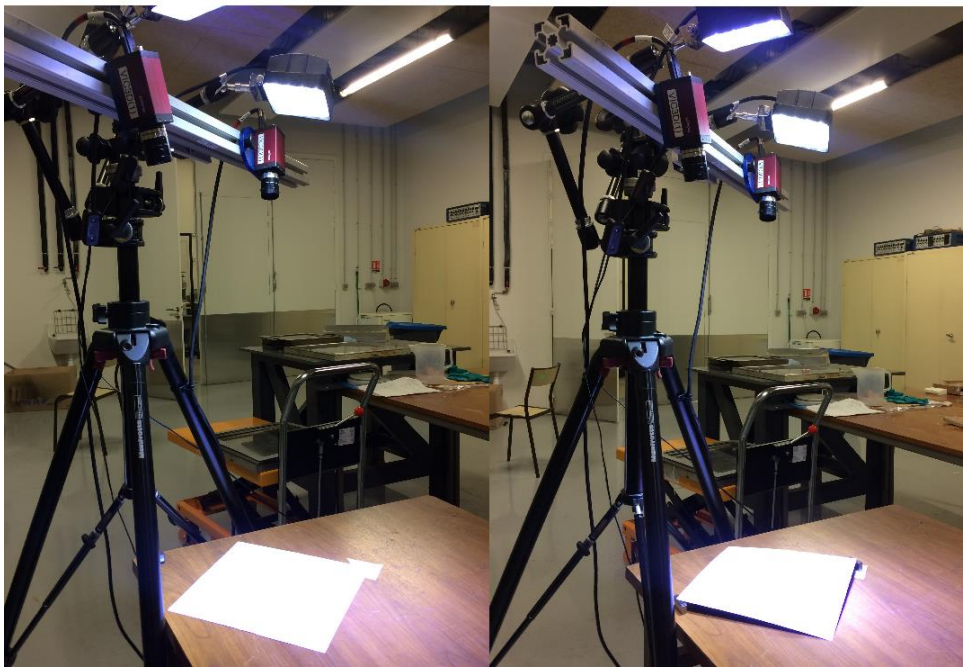

Figure 3.18 Measurement setup for DIC.

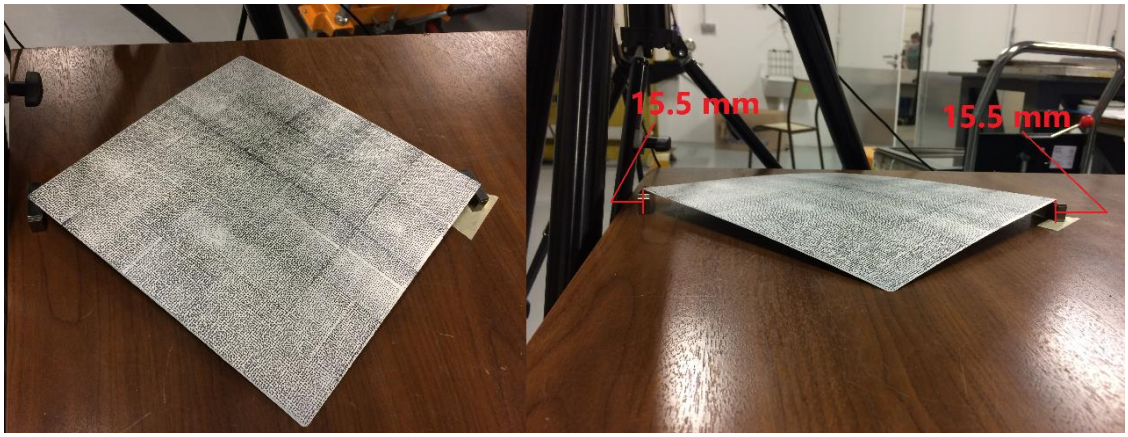

Figure 3.19 The setup of angle-ply laminate for DIC.

Both cameras were connected with a computer that contains VIC snap and VIC 3D software. VIC snap was employed to review the quality and capture for both calibration and specimen speckle images. It can also assist to adjust the aperture instead of adjusting from camera in order to obtain the suitable contrast between speckle dots and white surface. VIC 3D software was employed for analyzing deformations. Several calibration images were selected and analyzed for the reference before uploading a speckle image file into the software. The whole area of the speckle image has to be selected carefully as shown in Figure 3.20 to obtain the final shape. 2D and 3D images can be provided with maximum and minimum magnitudes of deflection which will be discussed in the section of result.

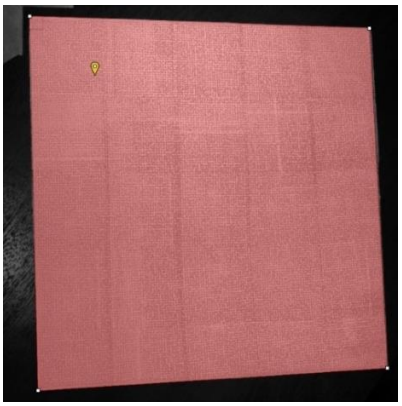

Figure 3.20 Area selection for analysis of shape deformation.

3.3.2 Measurement by laser displacement sensor (LDS)

Laser displacement sensor (LDS) was a second measurement method used to examine the distortion of both cross-ply and angle-ply laminates. 17 coordinated points (X, Y) were defined for measurement as shown in Figure 3.21. The first point (0,0) was located 5 mm away from the edges of specimen. A Keyence LK-G512 laser sensor head was used with Keyence LK-GD500 distance reader, measurement set up is illustrated in Figure 3.22. A laser head was mounted with the spindle of semi-automated milling machine. The surface of milling table was set as zero in Z direction and milling table can be moved in X and Y directions in order to change the location of measurement regarding to the coordinate points. The linearity accuracy of LK-G512 laser sensor is ±0.05% of F.S. (F.S. = Full scale = ±40 mm) [107]. So, the accuracy on the out-of-plane deflection is ±0.02 mm.

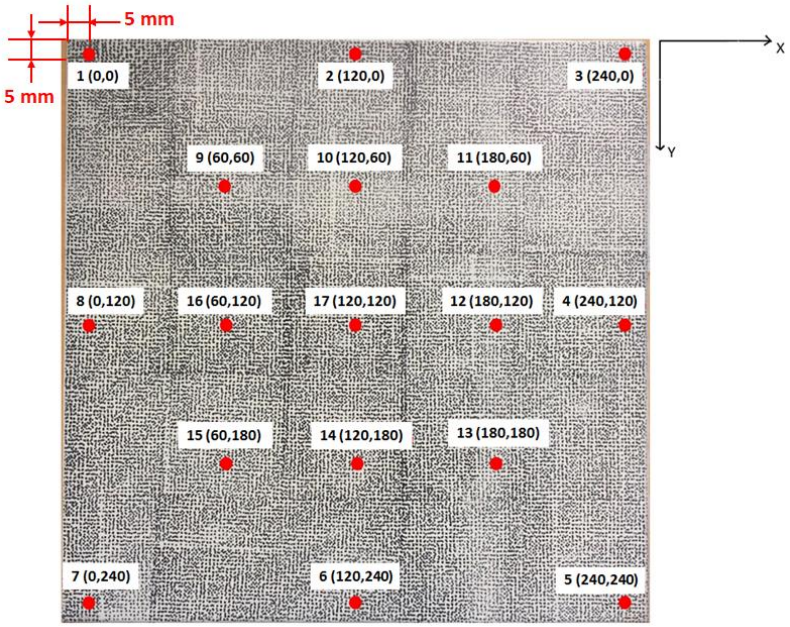

Figure 3.21 The 17 measurement points for laser displacement sensor.

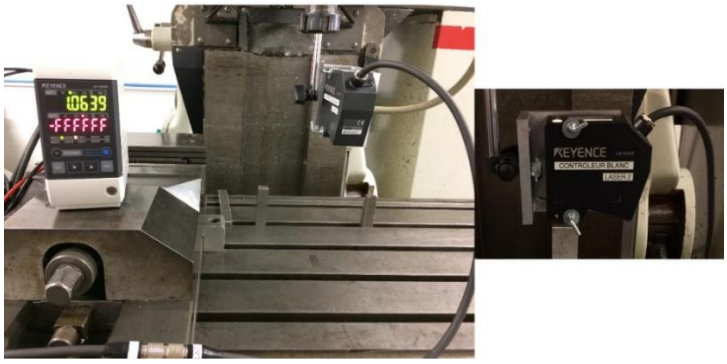

Figure 3.22 Measurement set up for laser displacement sensor.

In terms of specimen set up, it was the same as DIC in order to compare the results efficiently. The shape of cross-ply laminate could be simply placed on a milling table while metallic blocks were required to support 2 edges of angle-ply laminate as explained in the section of DIC measurement. The specimen setup is illustrated in Figure 3.23 and Figure 3.24 for cross-ply and angle-ply laminates respectively.

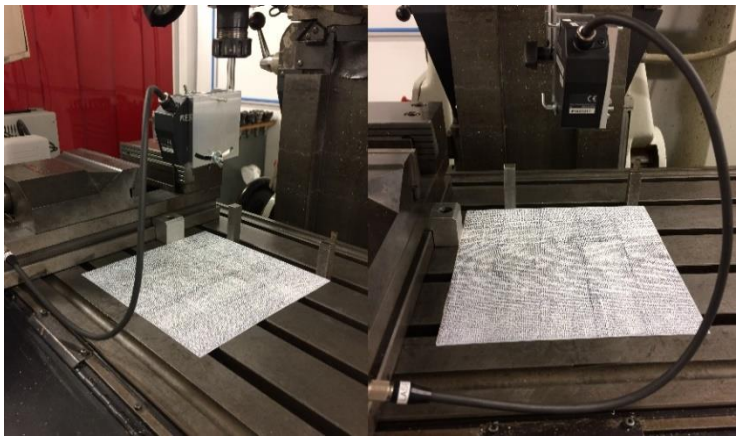

Figure 3.23 Specimen setup for cross-ply laminate.

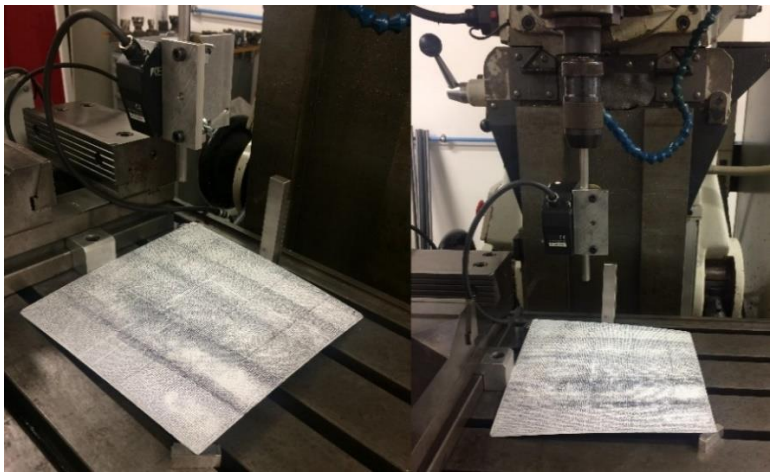

Figure 3.24 Specimen setup for angle-ply laminate.

3.4 Measurement results

3.4.1 Result from Digital Image Correlation (DIC)

All laminates were photographed by two cameras and analyzed by VIC3D software. 2D and 3D results could be obtained with the dispersion of colour to investigate the variation of deformation with respect to identical calibration images. The results for all specimens in 2D and 3D form are presented in Figure 3.26 to Figure 3.29. Moreover, maximum and minimum magnitudes of deformation for each specimen are provided in Table 3.3. All the values are given with respect to the mid-plane. The positive values refer to the maximum value above the mid-plane and the negative values refer to the maximum value below the mid-plane (see Figure 3.25).

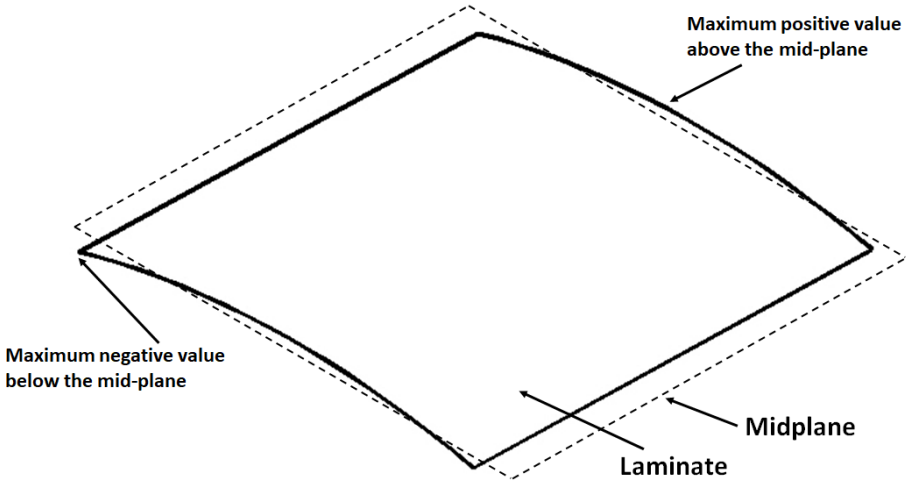

Figure 3.25 The illustration of out-of-plane deformation values obtained from DIC.

Table 3.3 Maximum and minimum magnitudes of deformation for each specimen

Experiment	Part no.	Layup	Tool surface	Max (mm)	Min (mm)
1	EX1-1	[0/90]s	Freekote+1 release film	0.567	-1.073
1	EX1-2	[0/90]s	Freekote+1 release film	0.552	-1.082
1	EX1-3	[0/90]s	Freekote+1 release film	0.511	-0.998
1	EX1-4	[0/90]s	Freekote+1 release film	0.621	-1.086
1	EX1-5	[0/90]s	Freekote+1 peel-ply	0.803	-1.624
1	EX1-6	[0/90]s	Freekote+1 peel-ply	0.888	-1.578
1	EX1-7	[0/90]s	Freekote+1 peel-ply	0.873	-1.565
1	EX1-8	[0/90]s	Freekote+1 peel-ply	0.785	-1.413
1	EX1-9	$[45/-45]_2$	Freekote+1 release film	4.369	-11.766
1	EX1-10	$[45/-45]_2$	Freekote+1 release film	4.189	-12
1	EX1-11	$[45/-45]_2$	Freekote+1 release film	4.201	-11.998
1	EX1-12	$[45/-45]_2$	Freekote+1 release film	4.133	-12.317
1	EX1-13	$[45/-45]_2$	Freekote+1 peel-ply	3.799	-12.314
1	EX1-14	$[45/-45]_2$	Freekote+1 peel-ply	3.671	-12.328
1	EX1-15	$[45/-45]_2$	Freekote+1 peel-ply	3.663	-12.31
1	EX1-16	$[45/-45]_2$	Freekote+1 peel-ply	3.858	-12.151
2	EX2-1	[0/90]s	Freekote+2 release films	0.609	-1.108
2	EX2-2	[0/90]s	Freekote+2 release films	0.562	-1.177
2	EX2-3	[0/90]s	Freekote+2 release films	0.603	-1.031
2	EX2-4	[0/90]s	Freekote+2 release films	0.621	-0.935
2	EX2-5	[0/90]s	Freekote+3 release films	0.554	-0.9901
2	EX2-6	[0/90]s	Freekote+3 release films	0.567	-1.035
2	EX2-7	[0/90]s	Freekote+3 release films	0.608	-1.095
2	EX2-8	[0/90]s	Freekote+3 release films	0.547	-0.987
2	EX2-9	$[45/-45]_2$	Freekote+2 release films	4.526	-11.404
2	EX2-10	$[45/-45]_2$	Freekote+2 release films	4.248	-12.117
2	EX2-11	$[45/-45]_2$	Freekote+2 release films	4.336	-11.501
2	EX2-12	$[45/-45]_2$	Freekote+2 release films	4.241	-11.734
2	EX2-13	$[45/-45]_2$	Freekote+3 release films	4.461	-11.856
2	EX2-14	$[45/-45]_2$	Freekote+3 release films	4.347	-11.867
2	EX2-15	$[45/-45]_2$	Freekote+3 release films	4.349	-11.557
2	EX2-16	$[45/-45]_2$	Freekote+3 release films	4.389	-11.657

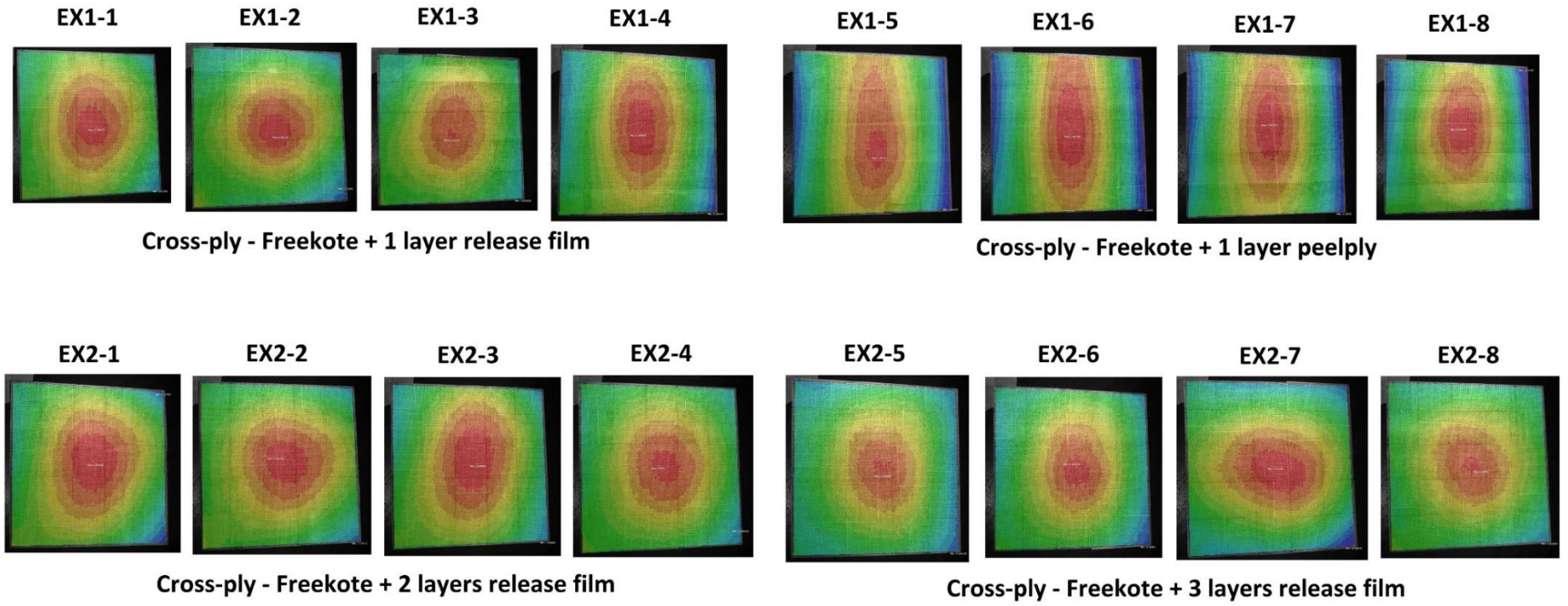

Figure 3.26 2D results for cross-ply laminate.

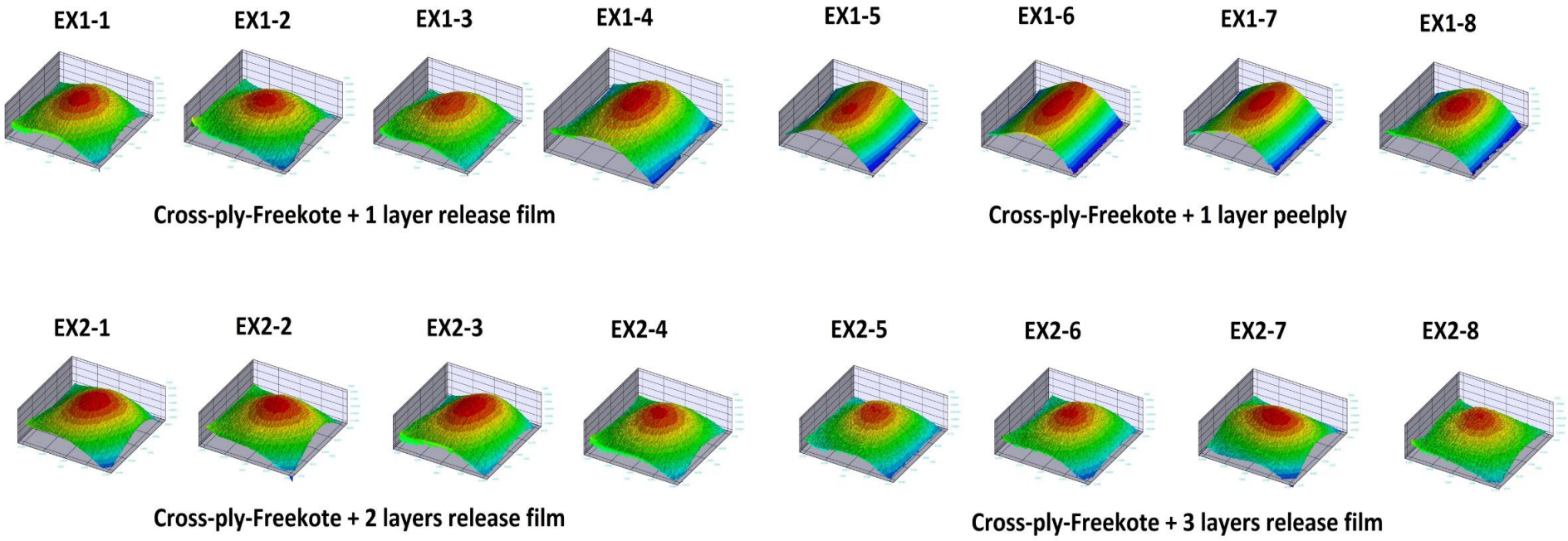

Figure 3.27 3D results for cross-ply laminate.

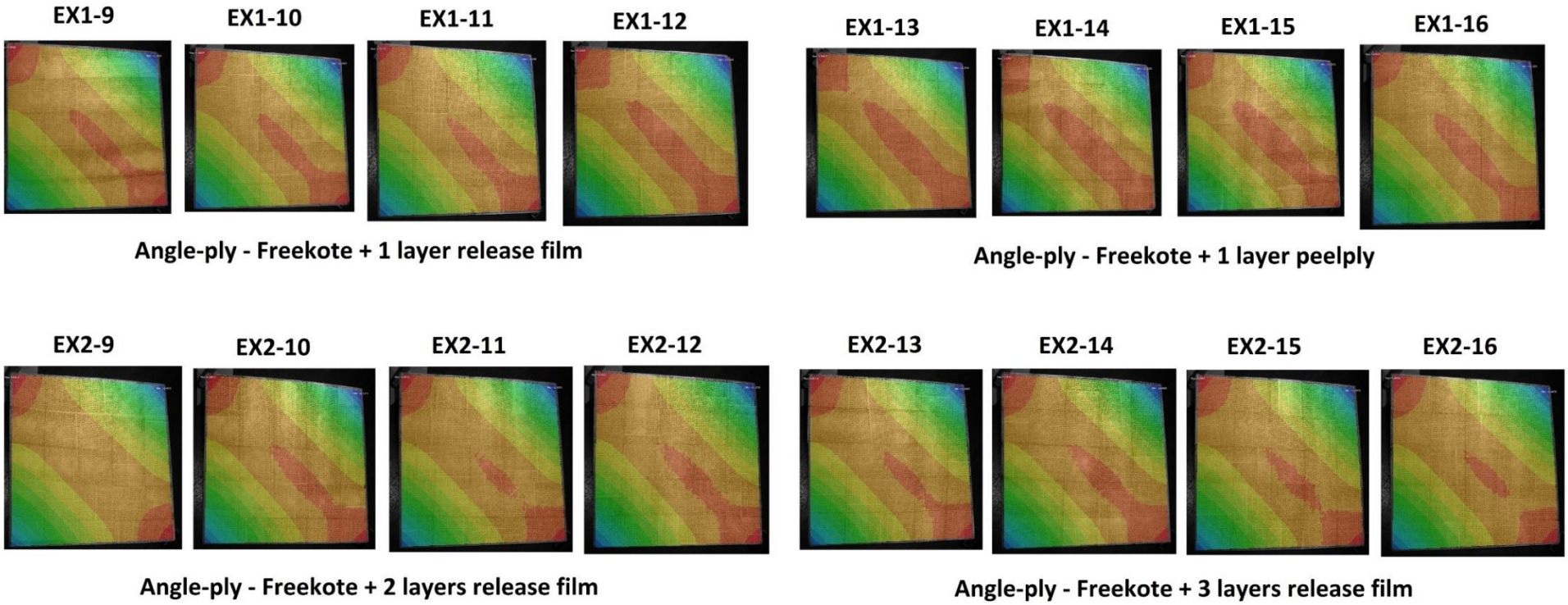

Figure 3.28 2D results for angle-ply laminate.

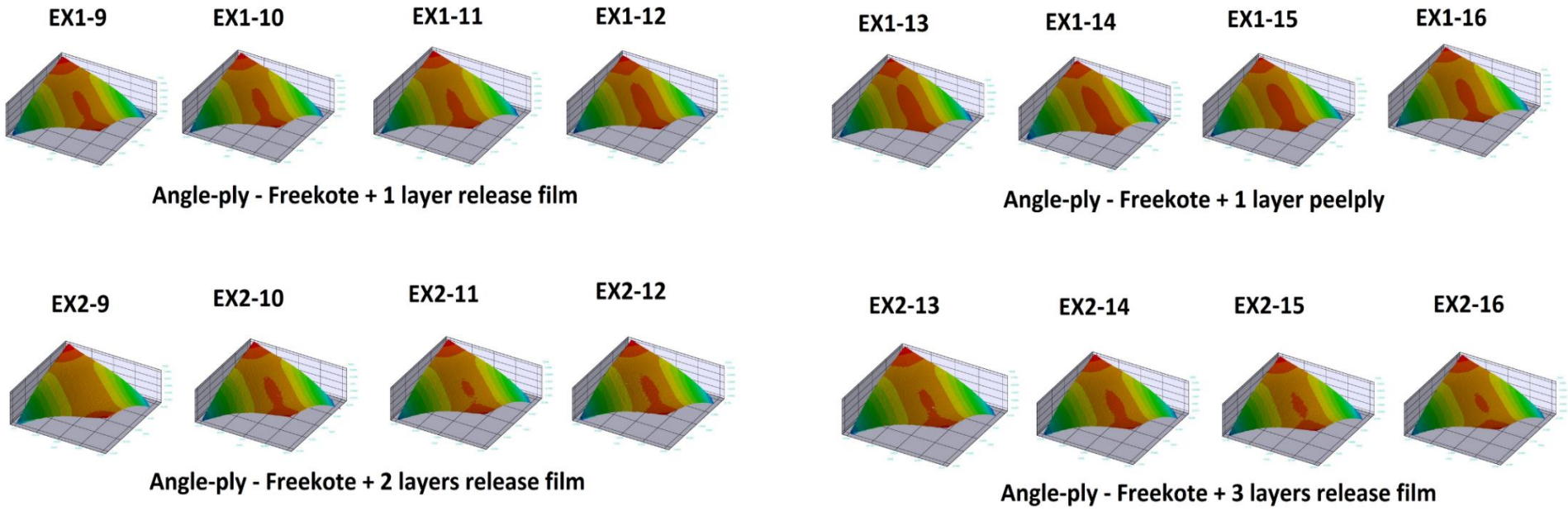

Figure 3.29 3D results for angle-ply laminate.

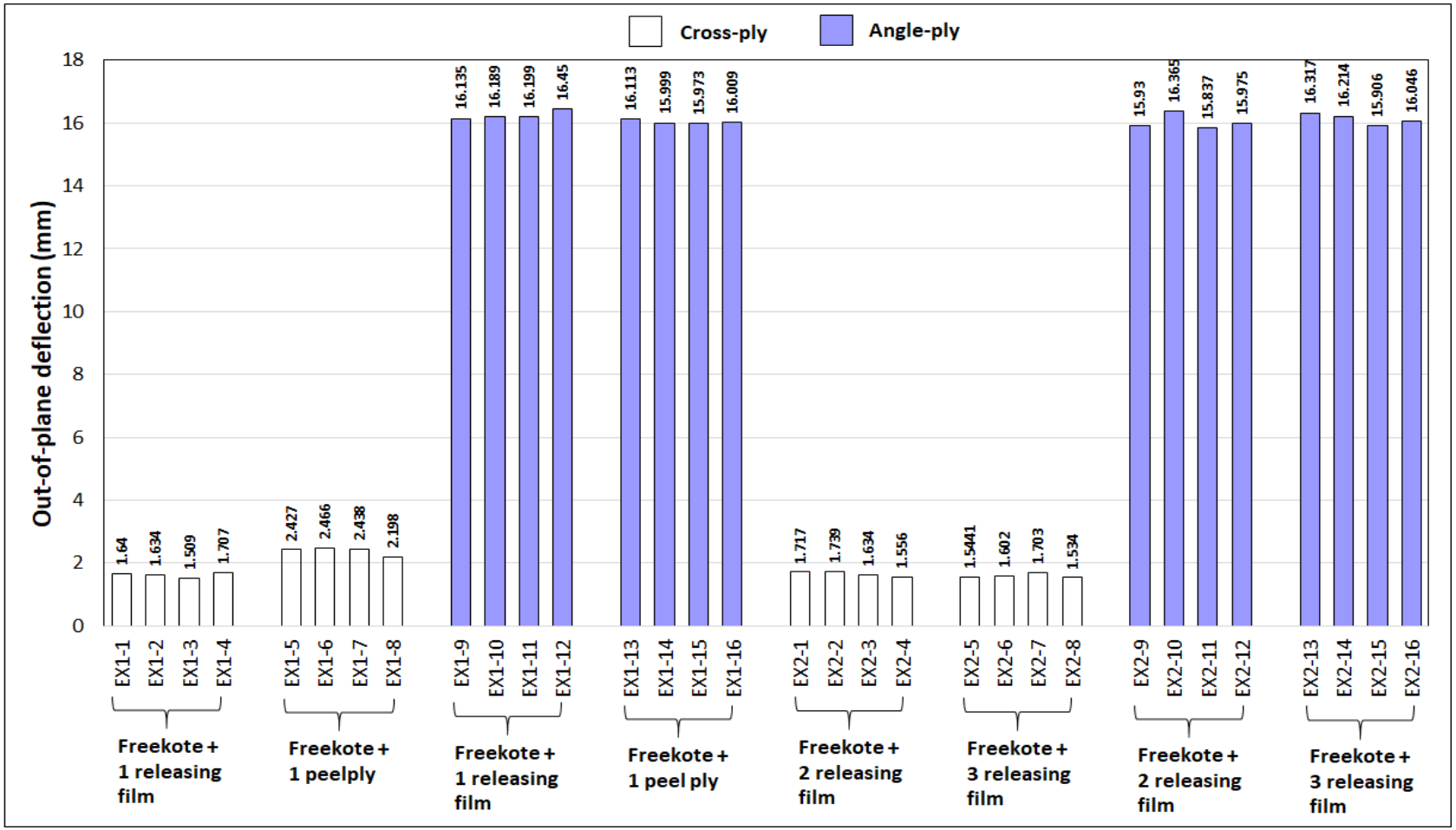

Figure 3.30 Summary of the total deformation values obtained from DIC.

The DIC measurement provided positive and negative values with respect to the mid-plane. Therefore, the total deformation can be determined by summation of both values without considering the sign. The maximum deformation values for all laminates are presented in Figure 3.30. In term of stacking effect, it is obviously seen that angle-ply laminates show extremely greater deflection than cross-ply laminate. Effectively, this large difference in maximum out-of-plane deflection values between cross-ply and angle-ply laminates could be expected to be linked to absence of symmetry for angle-ply laminates. Beyond the effects of the stacking sequence, let's look at those of the interfaces between the tool plate (or mould) and the laminates. At first sight, Figure 3.30 results do not show clearly the effect of releasing agent combinations for a given class of laminates (i.e. cross-ply and angle-ply), (see Table 3.1). Nevertheless, when considering cross-ply laminates ([0/90]s), it appears that the ones cured using peel-ply clothe (i.e. samples EX1-5 to EX1-8) always exhibit values of out-of-plane deflection higher than all the other laminates (i.e. those cured with 1,2 or 3 of ETFE release film layers). The same does not apply to angle-ply laminates ($[45/-45]_2$) for which the maximum out-of-plane deflection seems to be unsensitive to the combination of releasing agents. Always about cross-ply laminates ([0/90]s), Figure 3.26 and Figure 3.27 show that samples EX1-5 to EX1-8 those were cured using a peel-ply layer (see also Figure 3.7) exhibit deformed shapes that differ from those observed with all other cross-ply laminates (EX1-1 to EX1-4 and EX2-1 to EX2-8). Figure 3.27 shows the three-dimensional deformed shape of the 250 x 250 mm^2 cross-ply laminates once cured. It can be seen that laminates cured using a peel-ply layer have a cylindrical shape while all other [0/90]s samples exhibit two curvatures. This shows the effect of peel-ply. This confirms the specific role that Peel-ply cloth plays about the deformed shape of cross-ply laminates after curing and motivates a deeper analysis of the behaviour of this interface cloth during a cure cycle both from experimental (characterization) and from numerical (simulation) point of view.

3.4.2 Result from laser displacement sensor

A laser displacement sensor (LDS) was employed to measure the deformation of all laminated plates. The distance in Z direction of 17 points on the top surface of laminate was measured. The measurement data are presented in Table 3.4. Each value indicates the distance in vertical direction at each measurement point. The maximum deflection values of each specimen are plotted in Figure 3.31. The reader will be provided with a sub-section (3.4.3) dedicated to compare the results obtained from two measurement methods (DIC, LDS). Nevertheless, once again with LDS, the measurement of Figure 3.31 confirms that using a peel-ply cloth generates higher maximum out-of-plane deflection in cross-ply laminates ([0/90]s).

Table 3.4 Measurement data from laser displacement sensor.

Sample	Deformation at each one of the 17 measurement points (mm)																	
	1	2	3	4	5	6	7	8	9	10	11	12	13	14	15	16	17	Max
EX1-1	0.78	1.41	0.91	1.03	0.92	1.32	0.80	1.14	1.67	1.65	1.62	1.64	1.65	1.67	1.64	1.66	1.68	1.68
EX1-2	0.84	1.35	0.87	0.92	0.81	1.01	0.86	0.89	1.38	1.42	1.44	1.54	1.45	1.47	1.43	1.54	1.65	1.65
EX1-3	0.83	1.26	0.90	0.89	0.85	1.24	0.87	1.08	1.47	1.44	1.52	1.47	1.52	1.45	1.48	1.52	1.53	1.53
EX1-4	0.79	1.40	0.84	0.93	0.82	1.27	0.80	0.97	1.65	1.74	1.72	1.62	1.60	1.70	1.69	1.73	1.74	1.74
EX1-5	0.77	2.31	0.89	0.90	0.81	2.45	0.80	1.16	2.23	2.52	2.30	2.45	2.46	2.53	2.32	2.27	2.54	2.54
EX1-6	0.84	2.42	0.87	0.87	0.82	2.38	0.86	1.09	2.36	2.55	2.41	2.48	2.35	2.54	2.23	2.27	2.57	2.57
EX1-7	0.82	2.34	0.84	0.83	0.85	2.20	0.84	1.12	2.29	2.35	2.38	2.34	2.33	2.36	2.35	2.32	2.48	2.48
EX1-8	0.80	2.10	0.81	0.89	0.94	2.10	0.80	0.98	2.02	2.05	1.99	1.91	1.82	1.91	1.92	1.97	2.25	2.25
EX1-9	16.36	12.20	2.02	12.22	16.22	11.80	2.34	12.36	14.95	14.55	12.80	14.67	14.97	14.35	12.52	14.37	15.08	16.36
EX1-10	16.37	12.43	2.23	12.09	16.18	11.94	2.41	12.46	14.92	14.60	12.87	14.53	14.82	14.36	12.52	14.43	15.15	16.37
EX1-11	16.45	12.26	2.17	12.04	16.08	11.74	2.44	12.43	14.93	14.50	12.85	14.40	14.95	14.50	12.59	14.43	15.13	16.45
EX1-12	16.65	12.55	2.20	12.23	16.30	12.13	2.51	12.60	15.02	14.96	13.21	14.85	15.30	14.75	12.84	14.85	15.50	16.65
EX1-13	16.44	12.70	2.09	12.00	16.30	12.30	2.36	12.50	15.45	14.98	13.08	14.96	15.57	15.11	13.18	14.97	15.67	16.44
EX1-14	16.38	12.33	2.06	12.36	16.33	11.97	2.46	12.85	15.48	14.92	13.29	15.14	15.56	15.08	13.00	14.98	15.75	16.38
EX1-15	16.45	12.48	2.15	12.69	16.33	12.03	2.35	12.82	15.54	15.12	13.50	15.31	15.60	15.04	13.02	15.04	15.82	16.45
EX1-16	16.31	12.58	2.12	12.09	16.28	12.08	2.42	12.73	15.11	14.74	13.05	14.90	15.16	15.02	12.94	14.64	15.36	16.31

Table 3.3 Measurement data from laser displacement sensor (continue)

Sample	Deformation at each one of the 17 measurement points (mm)																	
	1	2	3	4	5	6	7	8	9	10	11	12	13	14	15	16	17	Max
EX2-1	0.79	1.66	1.04	1.05	0.90	1.65	0.82	1.18	1.72	1.72	1.73	1.75	1.70	1.74	1.72	1.74	1.75	1.75
EX2-2	0.85	1.57	0.80	1.02	0.81	1.59	0.87	0.92	1.78	1.75	1.74	1.78	1.76	1.75	1.77	1.77	1.78	1.78
EX2-3	0.98	1.69	1.06	0.95	0.87	1.63	1.04	1.03	1.55	1.65	1.62	1.64	1.67	1.58	1.63	1.65	1.69	1.69
EX2-4	0.93	1.32	0.86	0.93	0.86	1.57	0.91	0.93	1.56	1.57	1.54	1.52	1.54	1.55	1.55	1.57	1.58	1.58
EX2-5	0.83	1.22	0.87	1.01	0.96	1.35	0.85	1.25	1.35	1.40	1.37	1.30	1.32	1.35	1.40	1.42	1.53	1.53
EX2-6	0.81	1.25	0.84	0.90	0.94	1.38	0.80	0.92	1.32	1.38	1.40	1.31	1.34	1.36	1.30	1.46	1.62	1.62
EX2-7	0.82	1.18	0.82	1.15	0.90	1.48	0.82	1.22	1.40	1.44	1.47	1.38	1.42	1.42	1.51	1.62	1.74	1.74
EX2-8	0.94	1.14	0.92	1.09	0.80	1.30	0.92	1.08	1.42	1.42	1.38	1.27	1.30	1.33	1.40	1.47	1.56	1.56
EX2-9	16.57	12.18	2.19	12.00	16.26	11.64	2.27	12.50	14.44	14.07	12.58	14.07	14.37	14.12	12.36	14.05	14.55	16.57
EX2-10	16.58	12.70	2.17	12.07	16.24	11.96	2.35	12.22	15.04	14.73	13.11	14.80	15.01	14.48	12.42	14.38	15.21	16.58
EX2-11	16.64	12.32	2.23	12.06	16.30	11.78	2.23	12.57	14.82	14.51	12.83	14.58	14.92	14.40	12.41	14.39	15.10	16.64
EX2-12	16.61	12.20	2.05	12.18	16.27	11.64	2.27	12.55	14.86	14.51	12.90	14.58	14.91	14.41	12.39	14.23	15.03	16.61
EX2-13	16.43	12.20	2.00	11.79	16.11	11.58	2.25	12.35	14.68	14.48	12.61	14.32	14.71	14.12	12.28	14.08	14.89	16.43
EX2-14	16.56	12.60	2.16	12.32	16.22	11.62	2.28	12.38	14.74	14.51	12.55	14.35	14.65	14.15	12.30	14.12	14.92	16.56
EX2-15	16.42	12.48	2.08	12.15	16.17	11.74	2.30	12.42	14.59	14.46	12.44	14.40	14.68	14.20	12.25	14.20	14.95	16.42
EX2-16	16.65	12.45	2.11	12.17	16.25	11.52	2.21	12.29	14.65	14.57	12.63	14.38	14.57	14.23	12.35	14.05	15.12	16.65

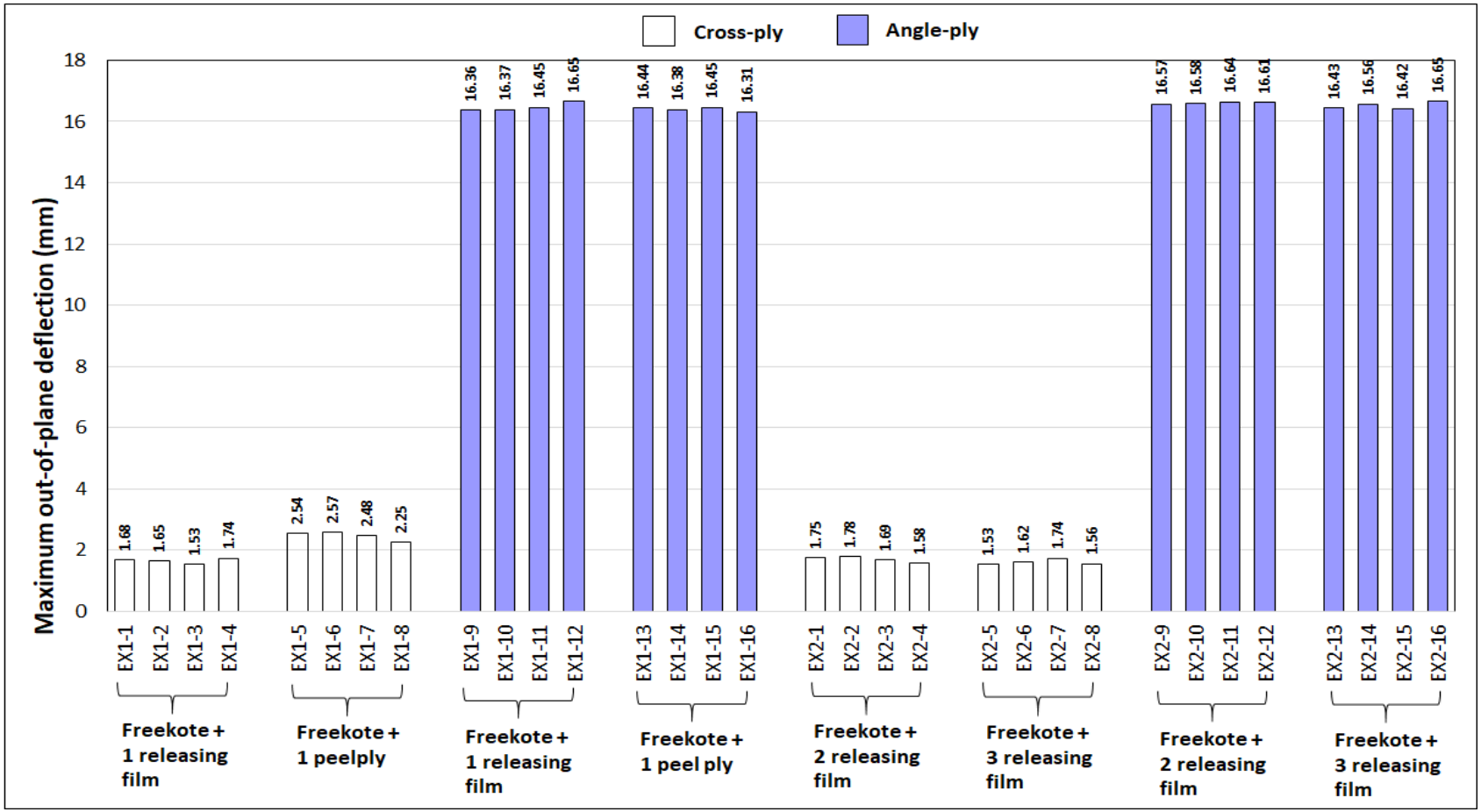

Figure 3.31 Maximum deformation result from laser displacement sensor.

3.4.3 Comparison of the results

The results from both measurements are compared. The comparison is between the total deformation from DIC (given by the difference between maximum and minimum values) and the maximum value from laser displacement sensor (choose the maximum value from 17 measurement points). This is presented in Figure 3.32 and Figure 3.33 for cross-ply and angle-ply laminates respectively.

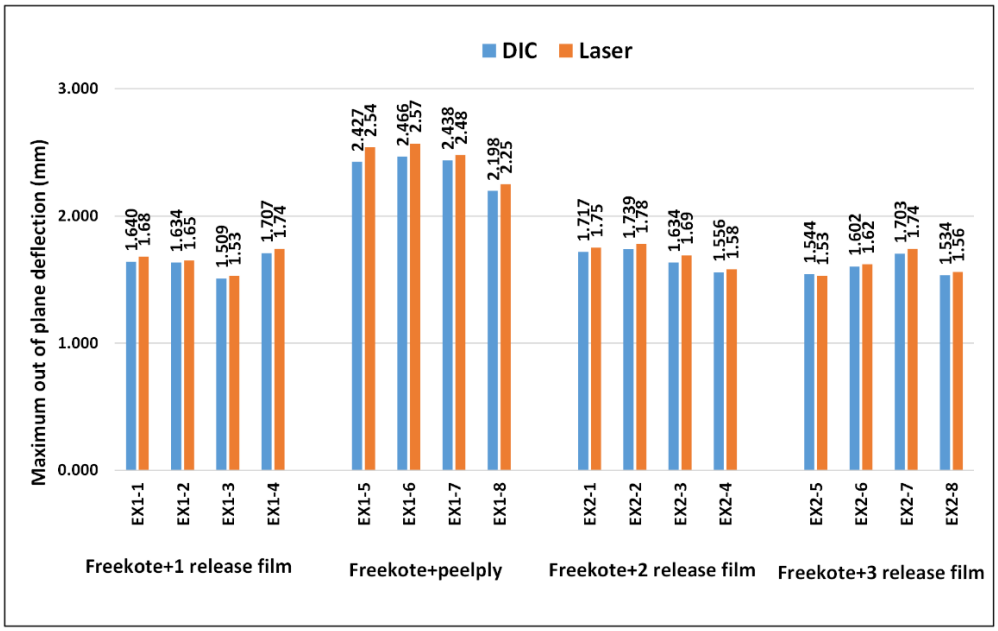

Figure 3.32 Comparison between the total deformation from DIC with the maximum value from laser displacement sensor for cross-ply laminate.

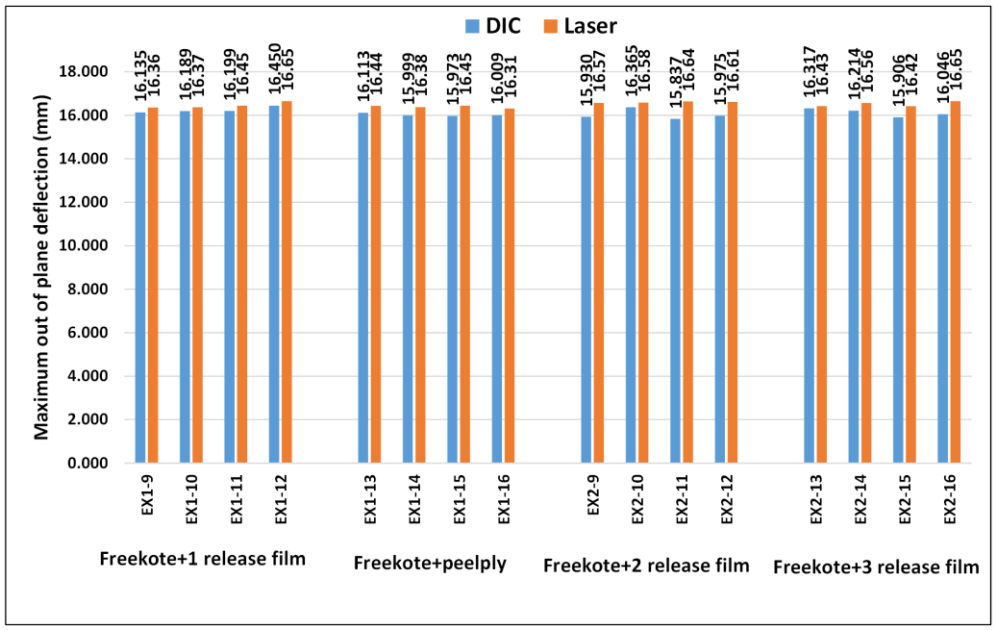

Figure 3.33 Comparison between the total deformation from DIC with the maximum value from laser displacement sensor for angle-ply laminate.

Both measurement methods give results in good agreement as shown in Figure 3.32 and Figure 3.33. It can be clearly seen that the effect of stacking layup plays an important role to the out of plane deflection in terms of shape and magnitude. Effectively, the level of maximum out-of-plane deflection after curing remains relatively low (between 1.5 and 2.6 mm) for cross-ply laminates ([0/90]s) while deflection values overcome 15 mm with angle-ply laminates ($[45/-45]_2$) for which the absence of symmetry generate coupling effect between bending and twisting.

In terms of tool surface effect, the difference of tool surface conditions has no significant effect for angle-ply laminates, while the use of Peel-ply provides a higher deflection for cross-ply laminates compared to the use of one, two and three layers release film. Moreover, the difference in deformation behaviour when using peel-ply and release film can be clearly observed for cross-ply laminates (Figure 3.26 and Figure 3.27).

3.4.4 Conclusion remark

- The preparation of the experiment took a long time especially for the prepreg cutting process that needs hand cutting and joining of the ply sheet before the layup. This might be the cause of small errors in the alignment of ply direction in each ply.

- The instability of ply cutting by hand was the cause of deviation of in-plane dimension of laminate plates.

- The vacuum compaction was not done ply by ply during hand layup but all together because the laminates are quite thin.

- The resin wall/dam was not placed around the laminate plates during cure to maintain the pressure effect on the edge of specimens because the laminates are quite thin and finally there is very small pressure effect observed on laminate edges.

- Mould surface was prepared prior to the use of releasing agents but the measurement of mould surface roughness was not done.

- The temperature, pressure and vacuum programmed by autoclave was considerably stable throughout the processing time.

3.5 Numerical simulation for prediction of warpage.

Numerical modelling is a method that is widely used to predict the deformation of composite parts. This method can be costly and time consuming in terms of computation but on the other hand it might be worth it to eliminate huge production costs. In this section, the numerical model using Abaqus will be presented. The model consists of the composite plate, interface and mould in order to simulate tool/part interaction and curing environment effect on the out of plane deformation of specimen. First of all, the behaviour of M21EV/IMA which

respects to the curing temperature will be briefly explained, the Characterization of this material was provided by Moretti et al. [100] in order to understand the thermo-kinetic, thermo-chemical, chemical shrinkage and thermomechanical behaviour. Afterwards, the construction of a finite element model in Abaqus will be explained. Finally, the comparison between numerical and experimental results are presented.

3.5.1 Characterization of M21EV/IMA

In this Ph.D thesis work we have used the development and the methodology settled by Moretti et al. [19, 100] to characterize the physical phenomena of M21EV/IMA during cure is illustrated in Figure 3.34. First, the general properties were identified. Then, the thermal and kinetic properties were studied and the thermo-kinetic behaviour of the material could be determined using the heat equation. The coupling of thermo-kinetic behaviour affects the transition of physical and chemical state of the material. Finally, the thermo-chemical and thermomechanical properties which correspond to crosslinking reactions of the resin were characterized. As mentioned earlier, the prepreg M21EV/IMA data (characteristics and behaviour laws) used in this thesis will be an input for a simulation. The general properties of this material are presented in Table 3.5 [19].

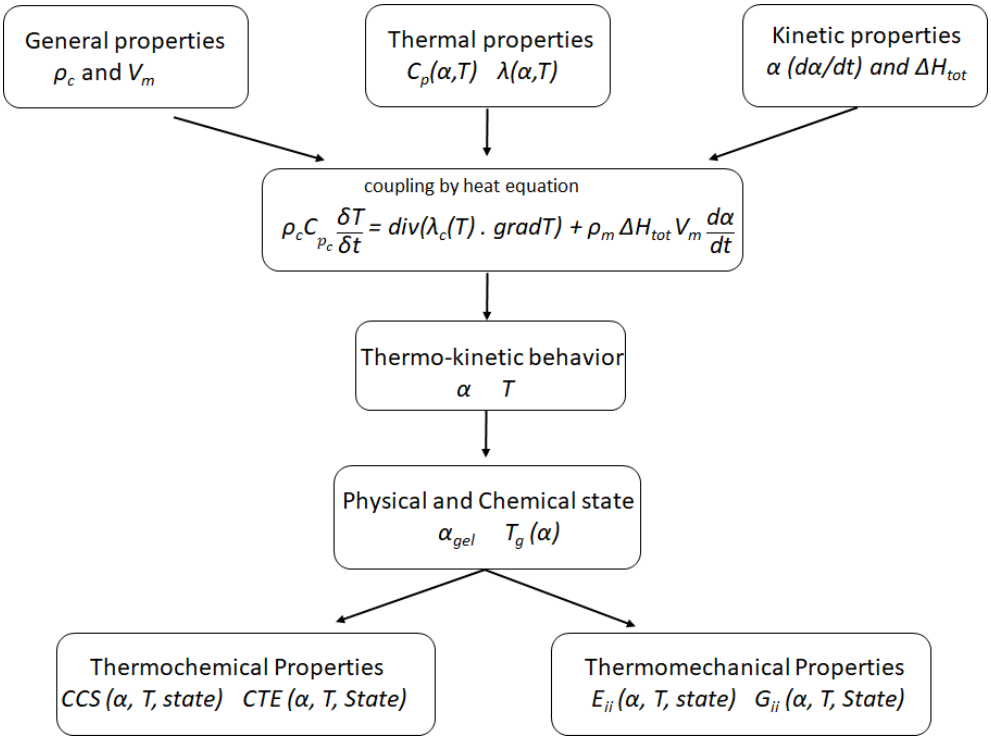

Figure 3.34 Methodology for behaviour characterization of M21EV/IMA during cure. [19, 100]

Table 3.5 General characteristics of prepreg M21EV/IMA. [19]

Properties	Unit	Value	Symbol
Density (cured)	g. cm^{-3}	1.575	ρ_c
Fibre Volume Fraction	%	56	V_f
Matrix Volume Fraction (cured)	%	44	V_m
Fibre Mass Fraction	%	66	M_f
Matrix mass Fraction (cured)	%	34	M_m
Ply thickness (cured)	µm	190	e

The Characterization of kinetic behaviour of the resin was operated by Differential Scanning Calorimeter (DSC) instrument which is a thermo-analytical technique that measures physical and chemical changes within a material in response to temperature. The equipment provides qualitative and quantitative information about endothermic and exothermic processes. The aim of this test was to identify the effect of time and temperature to the crosslink reaction of the resin. Various parameters could be obtained from DSC including the evolution of specific heat capacity (C_p) during cure, cure degree (α) behaviour, the evolution of glass transition temperature (T_g) and total enthalpy (ΔH_{tot}) of the complete cure reaction. The samples of M21EV/IMA were sliced to be about 23 ± 0.5 mg weight and contained in small sealed pans. The dynamic tests were run at different heat ramps from 1 to 20 °C/min and the temperature started from -50 up to 350 °C. The isothermal tests were carried out at 110 °C and 210 °C with heating ramp 10 °C/min. The repetition of each test was done for three times in order to ensure the validity of the results. The total enthalpy (ΔH_{tot}) of the resin was found to be 429.6 ± 7.0 J/g.

Laser Flash Analysis (LFA) was performed to determine the thermal diffusivity (a) and thermal conductivity (λ) of M21EV/IMA. The samples were tested with 2°C/min ramp rate and various isothermal dwells of 3 min with the increment of temperature gap 25 °C starting from 25 to 250 °C, 10 temperature cycles were defined. The thermal diffusivity was measured for both uncured and cured samples. Each temperature cycle was applied to the same sample twice, the first time providing the measurement of thermal diffusivity for the uncured sample and during cure while the second time allowed the measurement of thermal diffusivity for the cured sample. Afterward, the thermal conductivity as a function of cure degree (α) and temperature (T) can be calculated owing to equation 3-2 and the mixture law as shown in equation 3-3 was used to describe the evolution of thermal conductivity which the tests were operated at various thermal dwells.

$$\lambda(\alpha,T) = a(\alpha,T) \times C_p(\alpha,T) \times \rho(\alpha,T) \quad (3\text{-}2)$$

$$\lambda(\alpha,T) = \lambda_{cured}(T).(\alpha) + \lambda_{uncured}(T).(1-\alpha) \quad (3\text{-}3)$$

Where λ = Thermal conductivity a = Thermal diffusivity

C_p = Specific heat capacity ρ = Density of the material

After completing DSC and LFA test, the thermal and chemical state of the resin can be simulated owing to Fourier's law of heat equation (equation 3-4) in which an additional term stands for the heat of reaction of thermoset matrix. It can be seen that the properties of the resin can be predicted and strongly depends on the temperature and cure degree.

$$\rho_c C_{Pc} \frac{\delta T}{\delta t} = div(\lambda_C(T) . gradT) + \rho_m \Delta H_{tot} V_m \frac{d\alpha}{dt} \quad (3\text{-}4)$$

Where
- ρ_c = The density of the composite
- C_{pc} = The specific heat capacity of the composite
- λ_C = The thermal conductivity tensor of the composite
- T = Temperature
- ρ_m = The density of the resin
- ΔH_{tot} = The total enthalpy of the resin
- V_m = The resin volume fraction
- $d\alpha/dt$ = The reaction rate

The Kamal Sourour model as shown in equation 3-5 was widely used in many authors [108] [109] [110] [111] to describe the resin rate of reaction. In the thesis of Moretti et al [19, 100], the modified Kamal Sourour model (see equation 3-6) was chosen as a cure kinetic model to predict the reaction rate. The parameters k_1 and k_2 are the chemical reaction rate constants, m and n are the reaction order with respect to the reacting species.

$$\frac{d\alpha}{dt} = (k_1 + k_2(\alpha^m))(1-\alpha)^n \quad (3\text{-}5)$$

$$\frac{d\alpha}{dt} = (k_1 + k_2(\alpha^m))(\alpha_{max}-\alpha)^n \quad (3\text{-}6)$$

Where

- α = Cure degree
- α_{max} = Maximum cure degree
- k_1, k_2 = Chemical reaction rate constants such as $k_i = Ae^{\frac{-Ea}{RT}}$
- m, n = Reaction order
- A = The pre-exponential factor

E_a = The activation energy

R = The universal gas constant = 8.314 J/mol.K

T = The temperature in kelvins

The changes in specific heat capacity (C_p) during cure were studied by modulated DSC with heating ramp of 10 °C/min. The dynamic test ran for uncured and cured resin shown that the evolution of C_p can be described by a mixture law in equation 3-7. The two limits of C_p between which C_p values change during a cure cycle are denoted by $C_{p\text{-uncured}}$ (initial state C_p of prepreg) and $C_{p\text{-cured}}$ (C_p of fully cured material). The changes in $C_{p\text{-uncured}}$ and $C_{p\text{-cured}}$ are respectively given as a function of temperature by equation 3-9 and 3-8. The curing reaction and the corresponding state of resin can be followed during cure cycle not only owing to degree of cure (α) as we have seen, but also owing to the glass transition temperature (T_g). The changes in T_g can be described by equation 3-10 which was developed by Di Benedetto and modified by Pascault and William [112, 113, 114].

$$C_p(\alpha,T) = C_{p\text{-cured}}(T).\alpha + C_{p\text{-uncure}}(T).(1-\alpha) \quad (3\text{-}7)$$

$$C_{p\text{-cured}}\,(T(°C)) = 2.439T + 598.7 \quad (3\text{-}8)$$

$$C_{p\text{-uncure}}(T(°C)) = 1.990T + 725.0 \quad (3\text{-}9)$$

$$T_g = T_{g0} + \frac{(T_{g\infty} - T_{g0})b\alpha}{1-(1-b)\alpha} \quad (3\text{-}10)$$

Where

T_{g0} = The glass transition temperature of uncured resin

$T_{g\infty}$ = The glass transition temperature of cured resin

b = $\Delta C_{p1}/\Delta C_{p0}$

ΔC_{p0} = The difference in C_p between glassy and rubbery state of uncured resin

ΔC_{p1} = The difference in C_p between glassy and rubbery state of cured resin

In the next step, the thermal expansion (CTE) and the chemical shrinkage (CCS) behaviour of M21EV/IMA were characterized by thermal mechanical analysis (TMA). The strains were measured both in the in-plane directions (longitudinal and transverse directions) as well as in the through thickness direction. The 16 plies uncured quasi-isotropic pre-compacted laminate was prepared and the specimens of 3 x 10 x 10 mm^3 were cut to measure the strains in the thickness direction. Also, the $[0]_{40}$ laminate was prepared and the specimens of 6 x 8 x 8 mm^3 were cut to measure the thermo-chemical strains on both in-plane directions (longitudinal and transverse). All the samples were placed on the grips

covered by release film and subjected to a force of 1 mN to avoid bending during the test. To investigate the CCS, samples were heated from room temperature at 20 °C/min to 150 °C and maintained for 6 hours. The changes of CCS can be seen in Figure 3.35, a change in slope is observed when the curing stage reaches to the gel point. To investigate the CTE, the samples were heated at a very low ramp of 1 °C/min from room temperature to 300 °C and cooled down at the same rate. The thermo-chemical deformation was measured with the complete cure cycle. During the heat ramp, the resin changes the physical stage from viscous to rubbery and glassy states, the deformation is induced by the thermal strains (related to CTE). During the two isothermal dwells, the deformation is induced by chemical strains (related to CCS). The thermal strains are related to the coefficient of thermal expansion (CTE) during cure with the increment of temperature while the chemical strains will be described by the coefficient of chemical shrinkage (CCS) which depends on degree of cure (α). Both strains (thermal, $\mathcal{E}_{th}$ and chemical, $\mathcal{E}_{ch}$) are described by equation 3-11 and 3-12. The CTE and CCS vary in temperature and degree of cure respectively as presented in equation 3-13 and 3-14.

$$\Delta\mathcal{E}_{th} = CTE.\Delta T \tag{3-11}$$

$$\Delta\mathcal{E}_{ch} = CCS.\Delta\alpha \tag{3-12}$$

$$CTE_i = \begin{cases} CTE_i^{\inf Tg}, \ T < T_g(\alpha) \quad and\ i = 1,2,3 \\ CTE_i^{\sup Tg}, \ T \geq T_g(\alpha) \quad and\ i = 1,2,3 \end{cases} \tag{3-13}$$

$$CCS_i = \begin{cases} CCS_i^{bfgel}, \ \alpha < \alpha_{gel} \quad and\ i = 1,2,3 \\ CCS_i^{afgel}, \ \alpha \geq \alpha_{gel} \quad and\ i = 1,2,3 \end{cases} \tag{3-14}$$

Where T_g = The glass transition temperature

α_{gel} = The degree of cure at gelation point

i = Considered direction (1 = fibre direction, 2 = transverse direction, 3 = thickness direction)

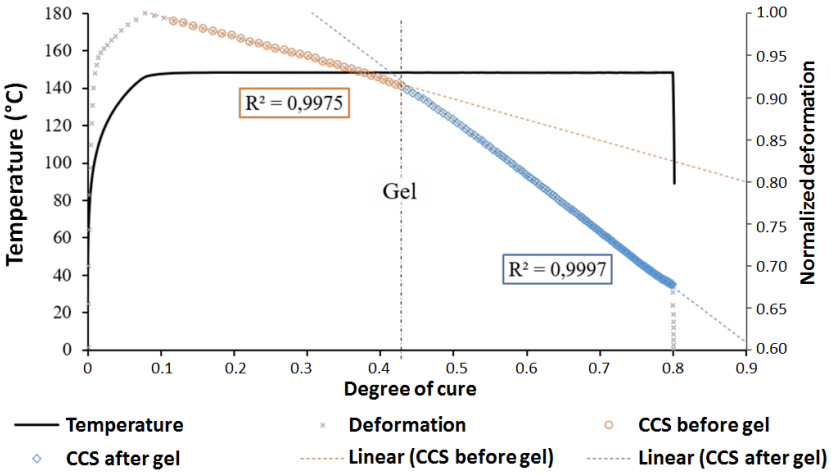

Figure 3.35 The CCS measured by TMA during an isotherm of 150 °C in the thickness of an M21EV/IMA specimen. [19]

The measurement was also performed with the cured specimens which were cut from a cured UD laminated plate to measure the CTE after cured. The specimens were subjected to a heat ramp of 2 °C/min from room temperature to 300 °C and cooled down at the same rate. Figure 3.36 shows that the CTE in the fibre direction (CTE11) is considerably stable and close to 0 while the CTEs in the transverse and through thickness directions (CTE22 and CTE33) are almost linear to the temperature

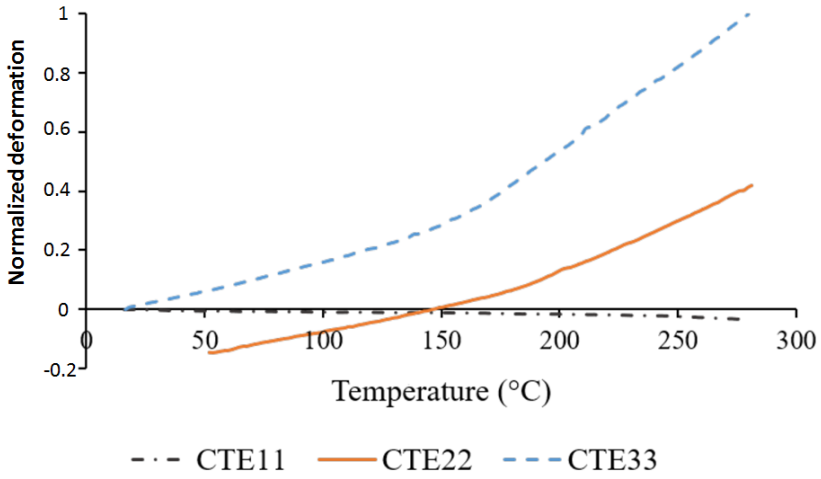

Figure 3.36 Measurement of thermal expansion on a cured specimen of M21EV/IMA according to each material direction. [19]

The last step of characterization was the dynamic mechanical analysis (DMA). This method was employed to measure the evolution of Young modulus (E) of M21EV/IMA during cure. A lot of published researches have made the choice to model the mechanical behaviour of a composite material during its curing according to the CHILE model. While CHILE stands for Cure Hardening Instantaneous Linear Elastic, this modelling was developed by Bogetti

and Gilespie [98] and modified by Johnston et al. [51] in 1999. In this modelling, as shown by equation 3-15, the changes in a thermoset matrix modulus during a cure cycle are described by the functions which have their own temperature domain of definition. In equation 3-15, the reader will understand that the thermoset matrix modulus remains constant between ambient and T_{C1}^{*}, linearly increase when the temperature is laying between T_{C1}^{*} and T_{C2}^{*} and stay constant once again when temperature overcomes T_{C2}^{*}. All this process is described on Figure 3.37 where T_{C1}^{*} and T_{C2}^{*} are given schematically. E_1 is the un-relax modulus during the cure state before the beginning of vitrification or when the resin temperature is below T_g while E_2 is the relax modulus during the cure state after end of vitrification or when the resin temperature is over T_g. T^* is the difference between resin temperature and T_g. T_{C1}^{*} and T_{C2}^{*} are the critical temperatures of T^* at the beginning and at the end of vitrification respectively.

$$E = \begin{cases} E_1 & , \quad T^* < T_{C1}^{*} \\ E_1 + \frac{T^* - T_{C1}^{*}}{T_{C2}^{*} - T_{C1}^{*}}(E_2 - E_1) & , \quad T_{C1}^{*} \le T^* < T_{C2}^{*} \\ E_2 & , \quad T^* > T_{C2}^{*} \end{cases} \tag{3-15}$$

With the aim to get closer to thermoset matrix thermomechanical behaviour during a cure cycle, Khoun [99] proposed an enhancement of Johnton CHILE modelling by discretizing the temperature range into subdomains as shown by equation 3-16 and see also Figure 3.38 [19].

$$E = \begin{cases} E_1 & , \quad T^* < T_{C1}^{*} \\ E_1 + \frac{T^* - T_{C1}^{*}}{T_{C2}^{*} - T_{C1}^{*}}(E_2 - E_1) & , \quad T_{C1}^{*} \le T^* < T_{C2}^{*} \\ E_2 + \frac{T^* - T_{C2}^{*}}{T_{C3}^{*} - T_{C2}^{*}}(E_3 - E_2) & , \quad T_{C2}^{*} \le T^* < T_{C3}^{*} \\ A \,.\exp(-KT^*) & , \quad T_{C3}^{*} \le T^* < T_{C4}^{*} \\ E_4 & , \quad T^* > T_{C4}^{*} \end{cases} \tag{3-16}$$

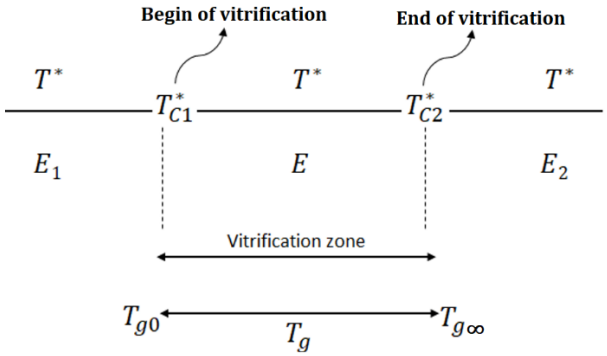

Figure 3.37 Parameter chart for CHILE model.

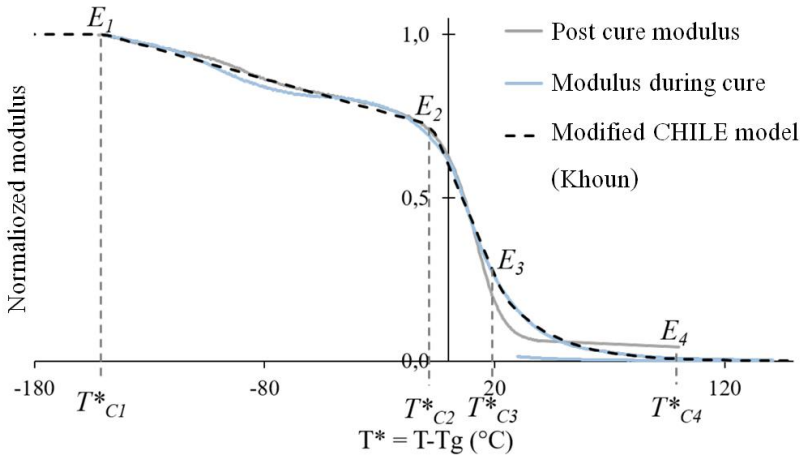

Figure 3.38 Modified CHILE model of Khoun. [19, 100]

Because all these modelling (original CHILE, enhanced versions by Johnton or by Khoun) were obtained by analyzing in DMA fully cured resin or composite samples submitted to heating ramps, it has been decided at Institute Clement Ader (Toulouse) to work on a CHILE modelling with a different new approach. This has been performed within the frame of Laure Moretti Ph.D work. Effectively analyzing already cured samples by taking them back to their curing temperature does not enable to catch what is going on during the early stage of a cure cycle in terms of increase in uncured resin modulus. This is why we have performed DMA experiments simulating the temperature path of M21EV/IMA cure cycle. These DMA tests were performed on $[90°]_4$ initially uncured samples submitted to a low tensile force at a frequency of 0.1 Hz. Obtained results are plotted in Figure 3.39. They show the changes in transverse modulus (E_t) as a function of T^* knowing that T^* represents the temperature difference between current temperature and T_g.

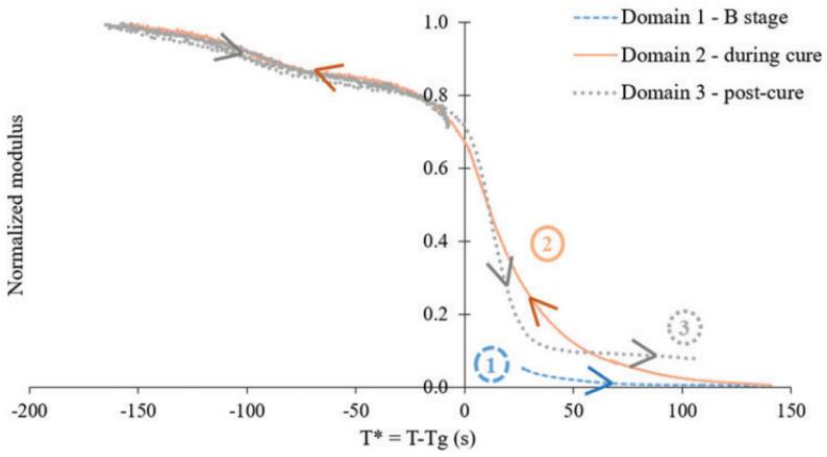

Figure 3.39 The three domains of the CHILE model developed. [19, 100]

In the modelling of the thermomechanical behaviour of an unidirectional ply while the transverse in-plane modulus was described as shown by Figure 3.39, the longitudinal modulus (in the fibre direction) was considered as independent of the degree of cure (α) and kept constant. Lastly, given the specific microstructure of M21EV/IMA composite (see Figure 3.15), it has been decided to measure the changes in transverse and through-thickness moduli just as made for E_t by DMA, Table 3.6 [19] summarizes the tests carried out and the identification of the mechanical properties. In that case it has been assumed that the through-thickness (i.e. perpendicular to lamination plane) modulus E_z of an U.D are the same in traction and in compression. This because the changes in E_z during a cure cycle were studied by DMA in compression mode.

Table 3.6 Tests program of thermomechanical properties of the M21EV/IMA. [19]

Properties	Test program (cured samples)	Test program (uncured samples)	Model used
E_{11}	Static tests DMA $[0]_8$	-	Constant
E_{22}	Static tests DMA $[90]_8$	Static tests DMA [+45/-45/+45]	CHILE 3 domains
E_{33}	Static tests DMA compression	Static tests DMA compression	CHILE 3 domains
G_{12}	Static tests DMA [+45/-45/+45]	Static tests DMA [+45/-45/+45]	CHILE 3 domains
G_{13}	Static tests DMA [+45/-45/+45]	Static tests DMA [+45/-45/+45]	CHILE 3 domains
G_{23}	Static tests DMA [+45/-45/+45]	Static tests DMA [+45/-45/+45]	CHILE 3 domains
ν_{12}	Static tests	-	Constant
ν_{13}	Static tests	-	Constant
ν_{23}	Static tests	-	Constant

Finally, Moretti et al. [19, 100] developed FORTRAN subroutines to implement all characterizations in Abaqus. The instruction of subroutines is presented in Figure 3.40. The finite element model was implemented in Abaqus using various user subroutines. The structure of subroutines was divided into two main modules, thermo-kinetics and stress/strain modules. The thermo-kinetics module contains three main subroutines, HETVAL, FSOUROUR and DVERK. The HETVAL subroutine performs the resolution of thermo-kinetic behaviours, the FSOUROUR subroutine defines the differential equation of modified Kamal Sourour model and the DVERK subroutine solves equation using Runge Kutta method. The USDFLD defines the degree of cure (α) with respect to temperature field, these values also determine the update of the conductivity (λ) and specific heat capacity (C_p) of composite. The SDVINI subroutine defines the initial value of the state variables and initial conditions assigned to the model. The UEXPAN subroutine is used to calculate the thermal ($\mathcal{E}_{th}$) and chemical ($\mathcal{E}_{ch}$) deformations, while the UMAT subroutine enables updating the mechanical properties of the resin and stiffness tensor of the composite. The FORTRAN subroutines can be used for finite element simulation for both 2D and 3D geometries. Full detail explanation can be found in [19, 100].The units of the model are presented in table Table 3.7.

Table 3.7 Units of the model. [19]

Parameter	**Unit**
Length	mm
Temperature	° C
Time	Second (s)
Mass	Ton (t)
Pressure	MPa

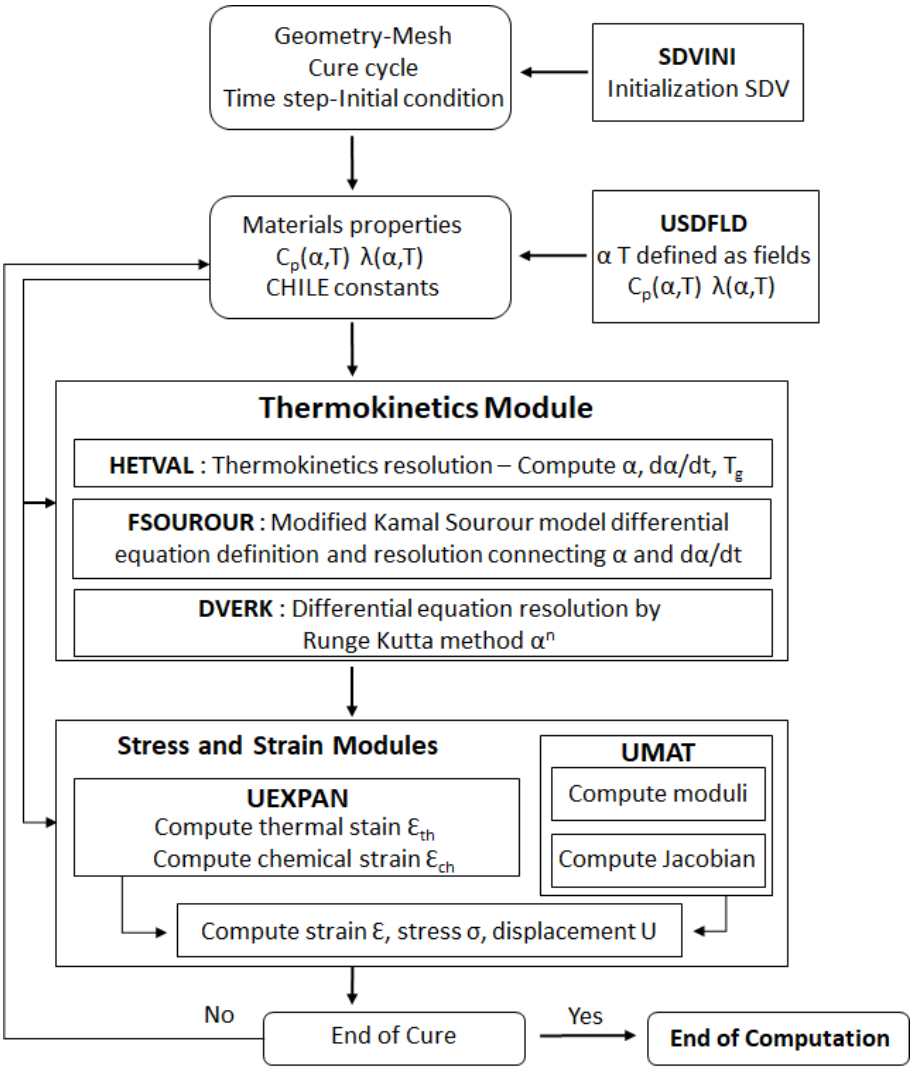

Figure 3.40 The instruction of FORTRAN subroutines of the FEA model. [19, 100]

3.5.2 Model construction with tool/part interface

As mentioned earlier, this thesis focuses on the influence of tool/part interaction on the process induced deformation in laminate composite. The effect of a curing environment consisting of a tool and interface are integrated with the model developed by Moretti et al [19, 100]. The 3D model was built up in Abaqus to be concordance with the experiment explained in section 3.2. Finally, the simulation results for the out of plane deflection will be compared with experimental results on both shape and magnitude of deformation.

The components of the model contain three main parts which are composite plate, mould plate and release materials (release film or peel-ply). In order to simulate the actual condition of the experiment, the symmetrical condition is ignored and a full model is chosen although the simulation time will be increased. In other words, this means that none symmetrical was considered in the FEA problem in order to avoid any numerical artefact

stemming from the computational process. Each ply of the laminate was splitted by the partition assigned to the thickness and orientation was assigned to each layer with respect to the fibre direction. In this case, the bonds between each lamina are assumed to be perfect and no delamination was allowed. The model construction can be simply shown in Figure 3.41 and the properties of aluminium mould and release materials are presented in Table 3.8. The properties in Table 3.8 was not experimentally tested but was taken from other sources. The properties of aluminium mould were selected from aluminium 2024 [115] which is the same grade used for experiment. The properties of ETFE release film were taken from [116, 117, 118] while the properties of peel-ply were mainly taken from AEROVAC® [119] and nylon 66 [120]. Unfortunately, the properties of M21EV/IMA provided by Moretti et al. [19, 100] must remain confidential since our laboratory and its industrial partner are still by contract until 2025. Therefore, they cannot be presented here.

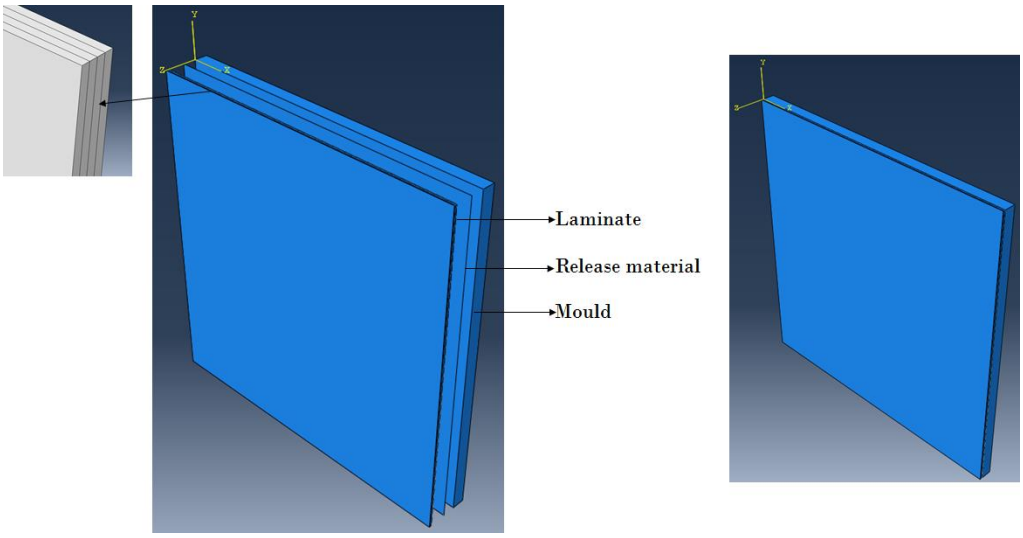

Figure 3.41 Abaqus model construction

Table 3.8 The properties of aluminium mould and release materials used for simulation

	Density (t/ mm^3)	Thermal conductivity (T.mm/s^3 ° C)	Young modulus(E) (MPa)	Poisson ratio	CTE (1/°C)	Specific heat (C_p) (mm^2/ s^2° C)
Aluminium	2.78x10^{-9}	190	70600	0.345	2.28x10^{-5}	875x10^6
ETFE release film	1.7x10^{-9}	0.238	800	0.45	9x10^{-5}	1900x10^6
Peel-ply	5.5x10^{-10}	1.08	3620	0.40	9.5x10^{-5}	1720x10^6

The simulation was divided into three steps, initial step, curing step and demoulding step. Initial step is a step before curing start where the temperature was set to 20 °C as a predefined field and bottom of the mould surface was constrained as a boundary condition in Z direction (U3). Effectively since the mould thickness is much smaller than its in-plane dimensions, only in-plane expansions were considered. This boundary condition was also propagated to the curing step. The curing step contains many designations, first was the pressure load 0.7 MPa was applied on all surfaces of the model as the autoclave pressure except the bottom surface of the mould, curing temperature path was also applied in this step. The demoulding step is the step in which all boundary conditions and pressure are inactive, mould and release material are deactivated in order to allow the laminate to freely deform.

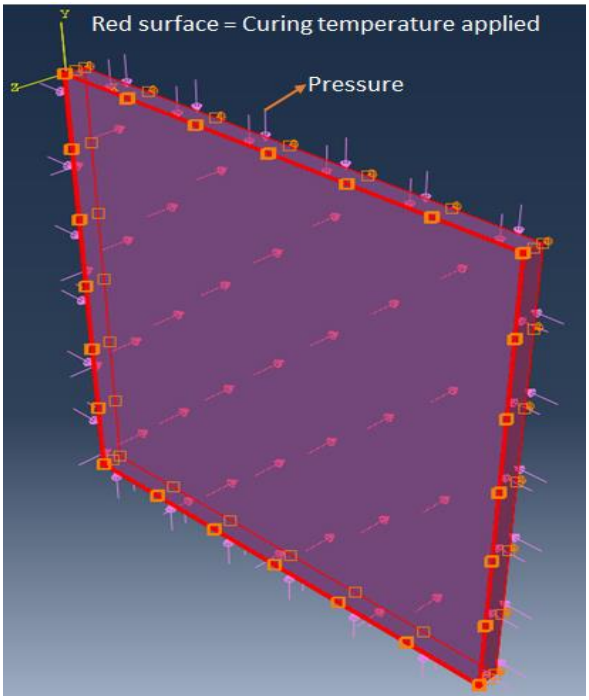

Figure 3.42 Curing temperature and pressure applied to the model.

The contact modelling was chosen to set up for two surfaces interactions (see figure Figure 3.43), the first interaction occurred between the surfaces of mould and release material, the second interaction occurred between the surfaces of release material and laminate. In case of release film, surface to surface contact with tangential behaviour was set for both surface interactions (1 and 2 see Figure 3.43). When using a peel-ply cloth located between the laminate bottom ply and the mould surface, some resin flows occur during the curing filling through the peel-ply cloth because of its own permeability to liquid resin. Figure 3.44 taken immediately after a cure cycle clearly shows the resin flow through the peel-ply cloth. This is why in that case it has been decided in first consumption and the

next chapter will focus upon peel-ply behaviour in order to set up a new modelling strategy to use a tie constraint between the two surfaces of interaction. In order to maximize the numerical effect of interaction and to see if the modelling manages to get close from experimental results, it has been decided to set the friction coefficient value to one. Lastly, it should be underlined that in the first numerical simulation campaign the behaviour of the ETFE release film as well as the peel-ply cloth were assumed to be isotropic.

All three parts were meshed with 20 x 20 elements in the main plane. The thicknesses of laminate and release material were meshed with one element per ply, while the thickness of mould was meshed with three elements. The element type is set to C3D20T standard quadratic with Coupled Temperature-Displacement family. The FORTRAN subroutine explained earlier was integrated into the model by existing Microsoft Visual Studio 2010 and Intel Parallel XE 2011.The model was run in Abaqus 2016 installed in Antec with CPU 4 cores and 8 threads, it takes about 5 hours to simulate one cycle with such equipment.

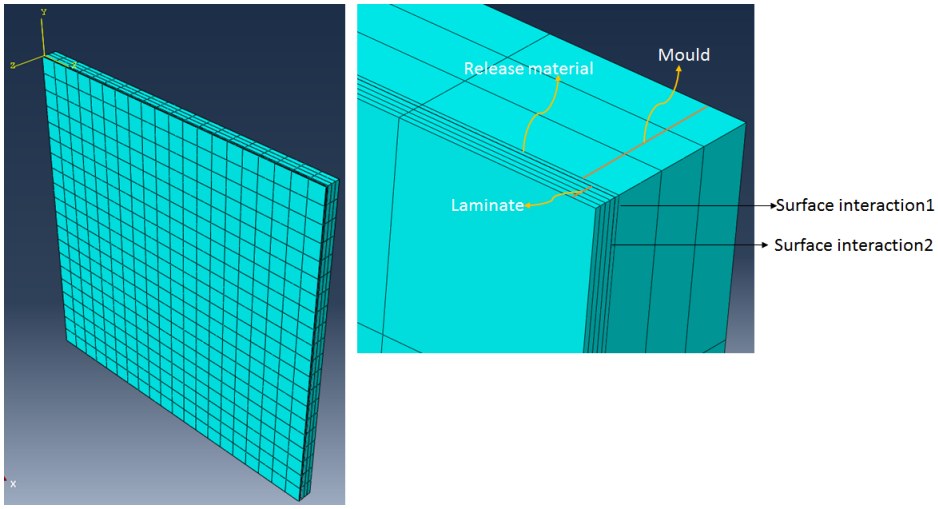

Figure 3.43 Surface interactions of the model and mesh.

Figure 3.44 Permeability of peel-ply to liquid resin.

3.5.3 Results from numerical simulation

The results from numerical simulation were compared with experimental results from DIC measurements for both cross-ply and angle-ply laminates and also for the use of release film and peel-ply. Both shape and magnitude of out of plane deflections were compared. The comparison of cross-ply with the use of ETFE release film is presented in Figure 3.45. The concordance of both shape and magnitude of deformation could be observed for almost all laminated plates. This means that the input properties of release film and curing environment applied to the model is able to work simultaneously with its own modified CHILE model and produce numerical results simulating correctly the cured shape of the cross-ply ([0/90]s) laminates with a rather good accuracy. Since we have seen with the experimental work presented in the first part of this chapter that there was no influence from the number of layers of ETFE release film, only a model with one layer of ETFE release film was simulated to reduce computational time. The comparison of cross-ply with the use of peel-ply is presented in Figure 3.46. The conflict between experimental and simulation results was observed both for shape and magnitude of deformation. This means that the properties of peel-ply assigned to the model might be incorrect. This will be the first priority to investigate because the curing environment are identical to those used in the model with the ETFE release film. It can be noted that the point exhibiting maximum deflection is always in the middle of the plate for symmetrical cross-ply ([0/90]s) laminates. As we have seen in Figure 3.26 in the experimental section and as reminded here in Figure 3.46, the deformed cured shape of cross-ply ([0/90]s) laminates produced using the peel-ply is cylindrical while one predicted by our numerical simulation is different and symmetrical with respected to the two in-plane axes X and Y as shown in Figure 3.46. In addition, Figure 3.46 shows that the maximum out-of-plane deflection predicted over estimates the deformation. Effectively, the maximum out-of-plane deflection predicted is of 3.263 mm while the average maximum out-of-plane deflection recorded on samples EX1-5 to EX1-8 is only of 2.382 mm. This represents about 37% error in maximum out-of-plane deformation while the error is about 6.2 % in the case of laminates cured with ETFE release film. These results not only clearly show the influence of peel-ply upon the process-induced shape of thin laminates but also that peel-ply is going to be more complex to model than what it could be firstly thought. In fact, we have supposed that peel-ply behaves as an isotropic material for these ABAQUS simulations but the facts show that this is not the case since experimental results are not correctly predicted by our modelling. In addition, the interface condition used about the interaction between peel-ply and laminate may be wrong when considering what the laminates really experience during their curing (with peel-ply). Therefore, it needs to pay

more attention to this cloth made of nylon fibres which is called peel-ply as frequently used in the process of parts manufacturing.

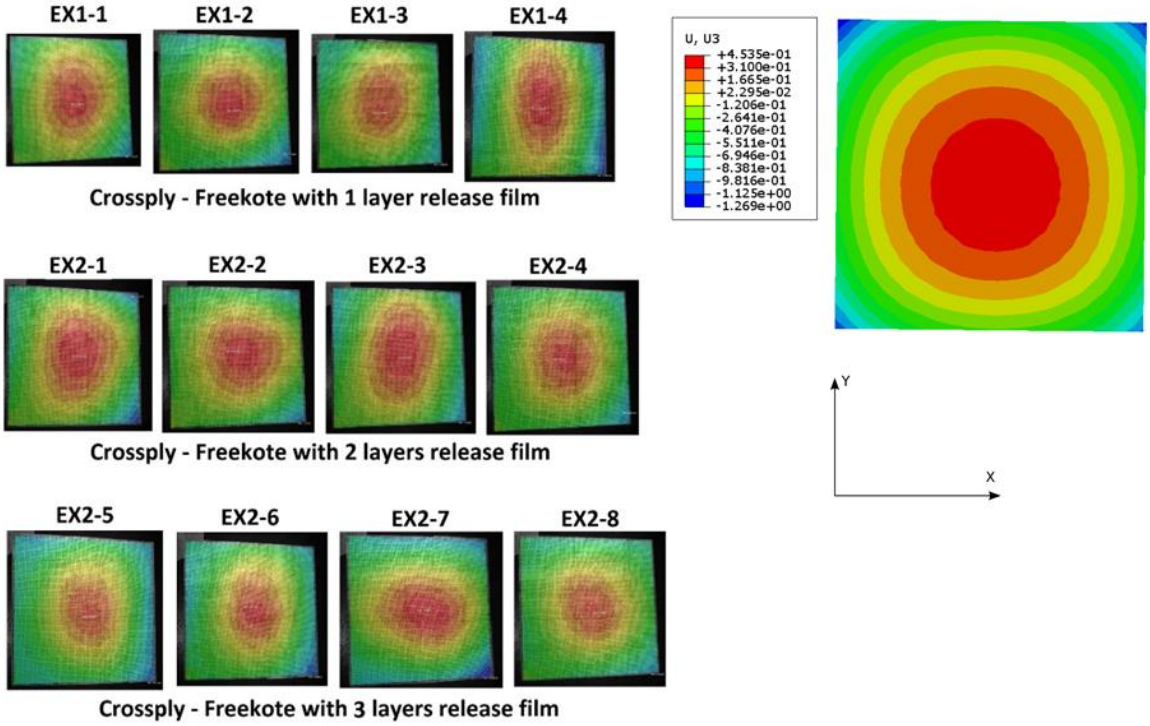

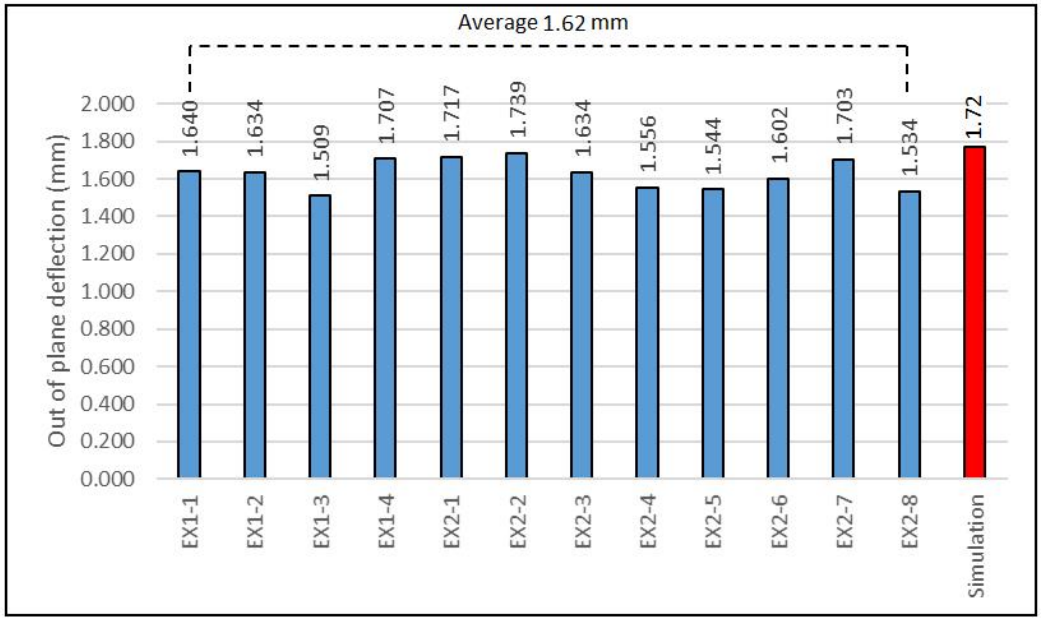

Figure 3.45 Experimental and numerical comparison for cross-ply laminates with the use of ETFE release film.

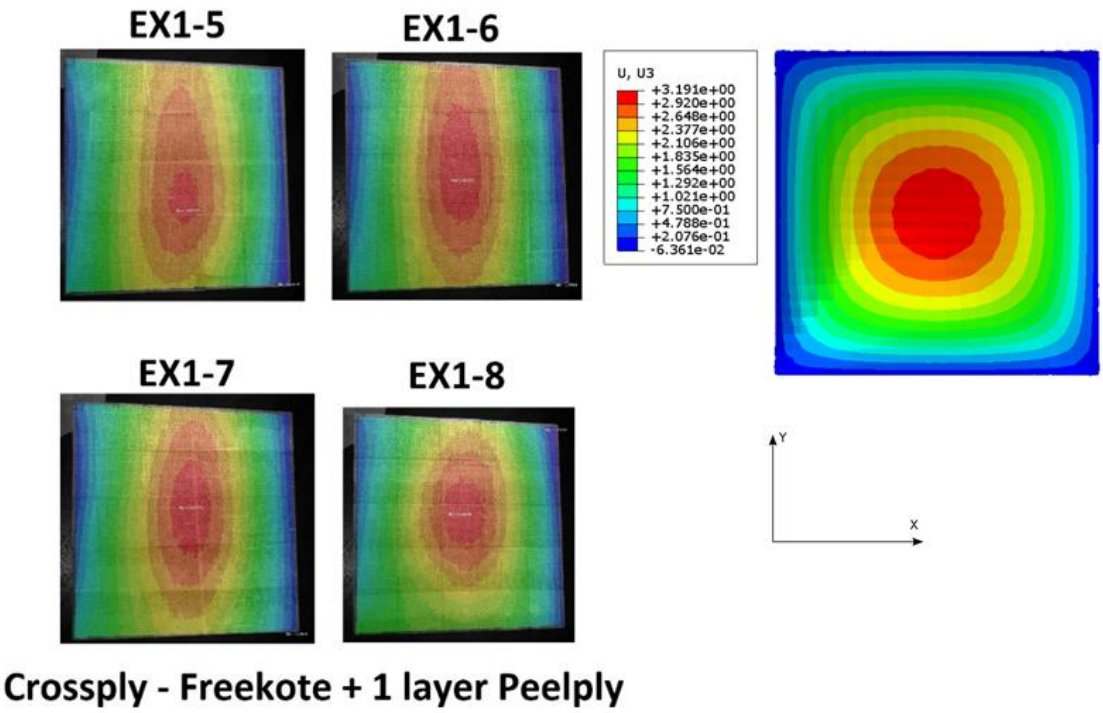

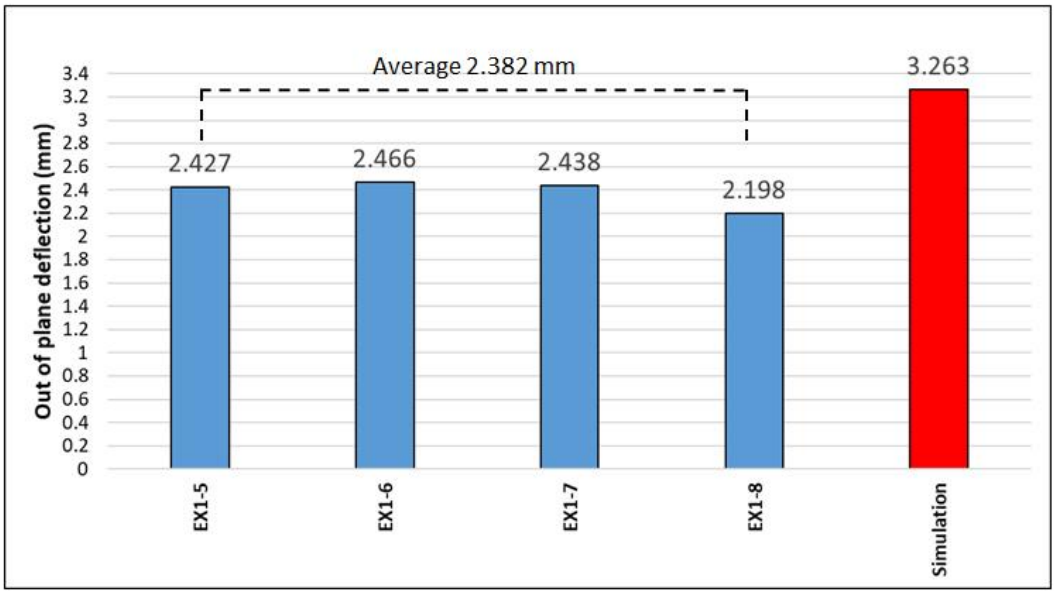

Figure 3.46 Experimental and numerical comparison for cross-ply laminates with the use of peel-ply.

The comparison between experimental and numerical model of angle-ply laminate with the use of ETFE release film and peel-ply are presented in Figure 3.47 and Figure 3.48 respectively. The concordance of both shape and magnitude of deformation is observed for all configurations. This can be mentioned that there is no influence of interface for process induced distortion of angle-ply laminate.

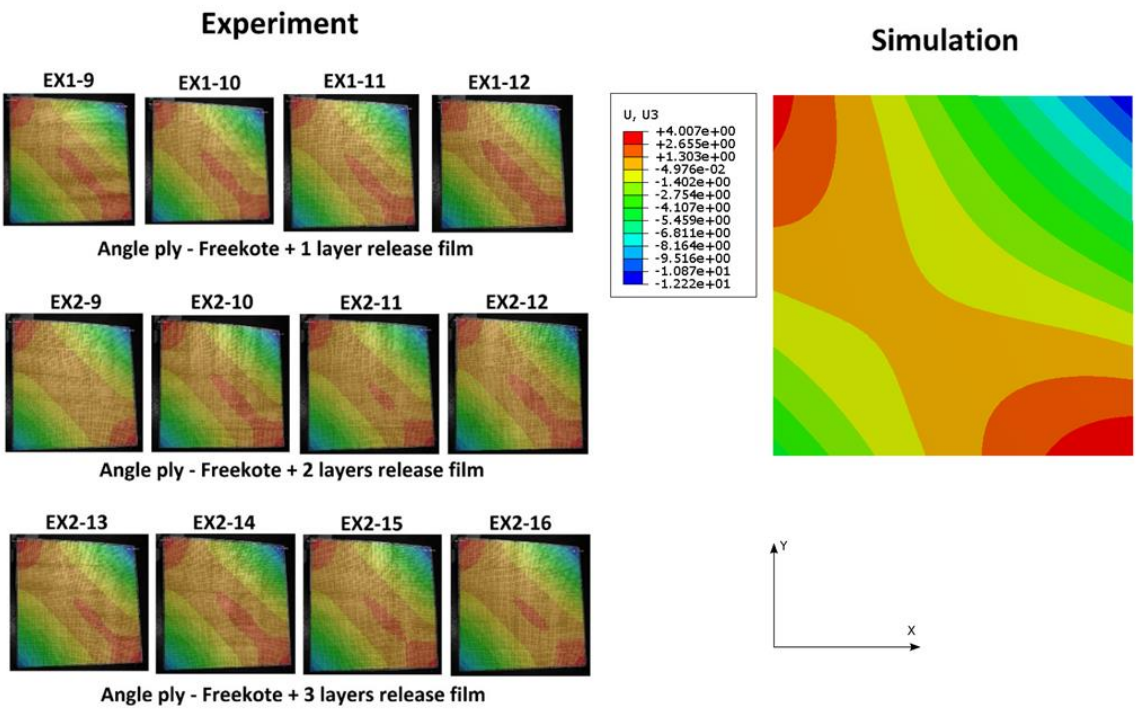

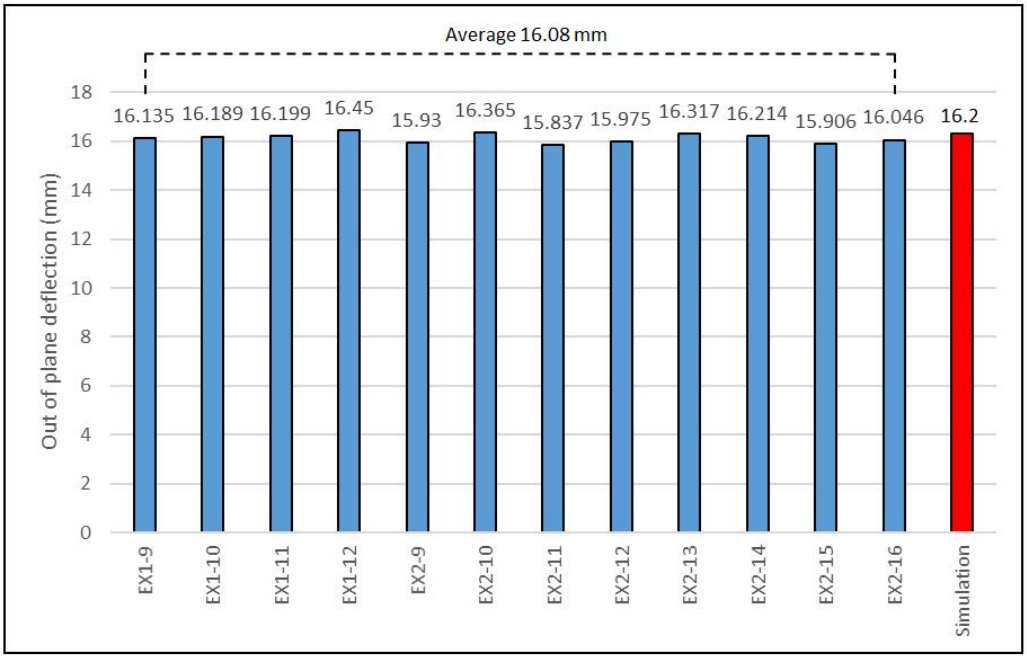

Figure 3.47 Experimental and numerical comparison for angle-ply laminates with the used of ETFE release film.

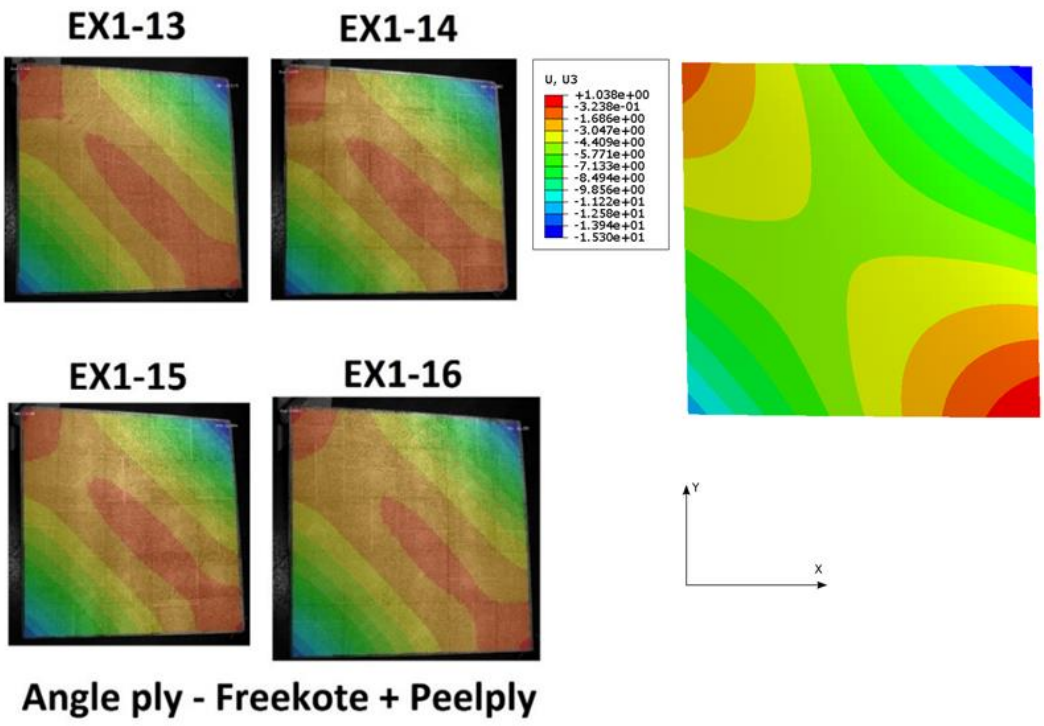

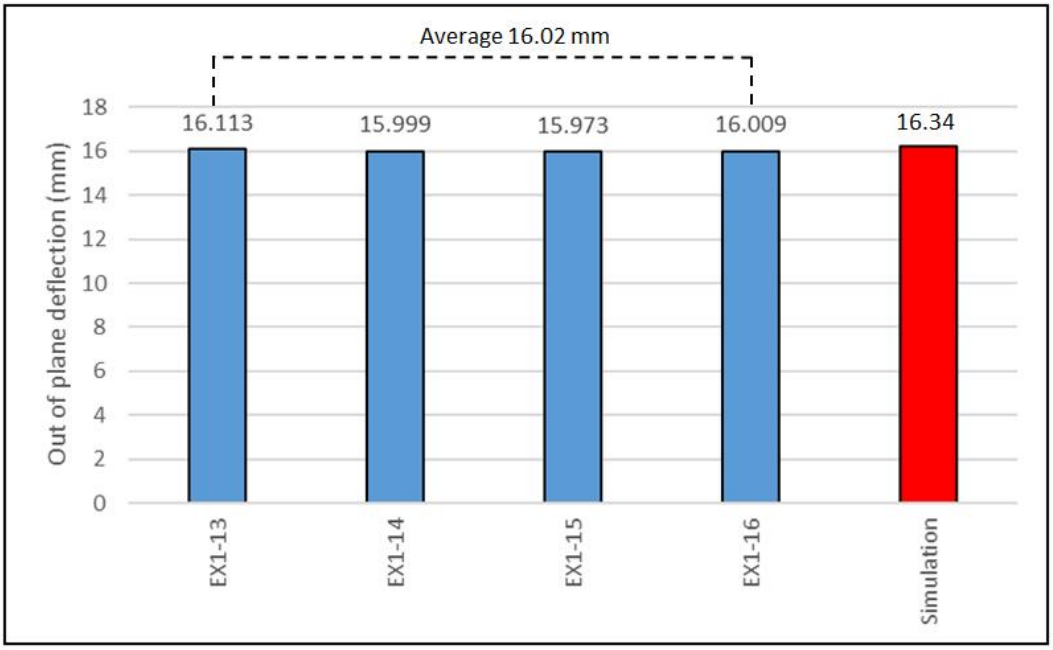

Figure 3.48 Experimental and numerical comparison for angle-ply laminates with the used of peel-ply.

3.6 Conclusion

The experiment was developed to study the influence of stacking sequence (angle-ply and cross-ply laminates) and tool/part interaction to the out-of-plane deflection of flat laminate specimens manufactured through the autoclave process. The manufacturing of all specimens was in good replication and exhibited a similar outcome. The results revealed that the stacking sequence plays a key role to the shape and magnitude of deformation. Angle-ply laminates exhibit extremely greater deflection than cross-ply laminate because of a lack of symmetrical stacking. The laminate plate is symmetrical in size and of course the ply tends to bend around the fibre direction for unidirectional ply due to the fibre dominance effect. This is the reason that the geometrical distortion of cross-ply laminate generated at the center of the plate due to balancing in-plane behaviour while angle-ply laminate bends around 45° (or -45°) direction.

Another factor in this study is the effect of tool/part interface. Referring to the results obtained from DIC, cross-ply laminates are sensitive to the presence of peel-ply compared to the use of other configurations of ETFE releasing film where the distortion area at the center is enlarged to the edge of the specimen. Moreover, the magnitude of deformation of cross-ply laminates significantly increases when peel-ply is used as an interface confirmed by both measurements (DIC and LDS). Since the peel-ply is a textile material that contains weft and warp yarns, it might have an impact on the thermal behaviour when subjected to temperature variation in which further experiment is required and will develop in the next chapter. On the other hand, the number of ETFE release film layers has no significant effect on the shape and magnitude of distortion for both cross-ply and angle-ply laminates. It can conclude that only one layer is sufficient or it might not reach the critical number of layers to have an impact yet. On the other hand, different tool/part interfaces did not show noticeable impact to the shape and magnitude of deformation for angle-ply laminate. The conclusion for this phenomenon is complicated but one can imagine that the effect of the interface is hidden by large distortion of angle-ply laminates.

In the numerical simulation developed, the existing thermomechanical model operates well with the tool/part interface assigned to the model, the geometrical distortion predicted was validated and in accordance with the experiment. However, some improvements are required for the properties of the interface, this issue is taken into consideration for more investigation.

Chapter 4

Characterization of interface behaviour and mould compensation strategy

The experimental results show that cross-ply ([0°/90°]s) laminates are sensitive to presence of peel-ply layer, while the deflection of angle-ply ($[45°/-45°]_2$) ones does not exhibit any sensitivity to peel-ply presence. In order to understand the origins of these differences, thermal behaviours of ETFE releasing film and peel-ply (balance plain weave made of polyamide yarns) will be studied by ThermoMechanical Analyzer (TMA) simulating the cure cycle temperature path. Obtained results will be implemented in our FEA simulation. Finally, the mould compensation strategy is firstly focused on the warpage shape of angle-ply laminate in order to modify the mould shape to minimize or eliminate the distortion.

4.1 Characterization of thermal behaviour of interface release materials

4.1.1 Sample preparation

As mentioned earlier, the out of plane deformation of cross-ply laminates is sensitive to the presence of the peel-ply layer of the interface between the Freekoted mould and the laminate. The thermal behaviour of peel-ply might have an influence on the shape deformation of laminated plates. Since peel-ply is a textile fabric that contains warp and weft yarns drawn perpendicular to each other, it can be considered as a non-isotropic material. Therefore, the thermal behaviour of peel-ply in weft and warp directions was firstly characterized by a Netzsch TMA 402 F3 Hyperion apparatus to identify the thermal expansion or contraction. Cured resin impregnated peel-ply was reused from the experiment. The samples with a size of 8 x 25 mm^2 (see Figure 4.1) were cut from used peel-ply sheets in both weft and warp directions and clamped with alumina clamping jaws and placed inside the TMA. Moreover, to obtain the properties of all release materials used in this study, ETFE release film was also cut with the same size for this characterization. All samples were subjected to a 1 mN axial force to avoid bending of the sample during the test. A complete cure cycle as explained in section 3.2.3 was set up, three samples of each configuration (peel-ply sample in weft direction, peel-ply sample in warp direction and release film sample) were tested in order to check the scatter of the results.

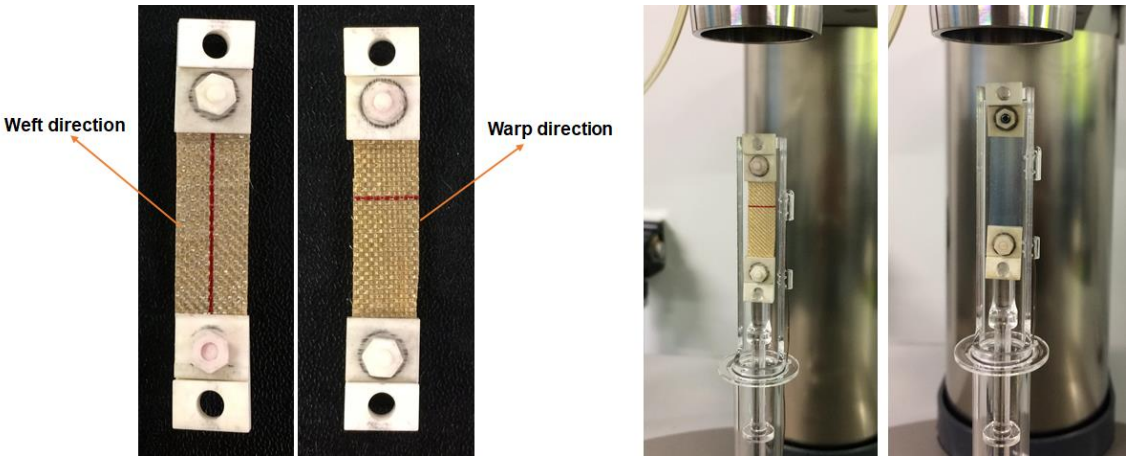

Figure 4.1 Samples for TMA.

4.1.2 Experimental result from TMA

The results for peel-ply samples from the TMA NETZSCH Proteus Thermal Analysis software are presented in Figure 4.2, the time (X-axis) is plotted versus the strain and temperature (Y-axis), each line on the chart represents one sample. Another chart is plotted

separately to monitor the strain as a function of temperature presented in Figure 4.3. Both expansion and contraction are observed. It can be seen that the thermal behaviour is dramatically different between weft and warp directions, numerous contractions are noticed for the samples in weft direction represented by three bottom curves (Figure 4.2). The curve line response to temperature of both weft and warp samples looks similar but the strain magnitude is dissimilar. The resin shrinkage might have an influence on this phenomenon since the contraction is still observed during the isothermal dwell. Moreover, the contraction is larger during the second heat ramp. The analysis of peel-ply thermal behaviour is difficult to find in the published literature because mostly it focused mainly on the effect of peel-ply on the bonding and surface quality of composite parts.

The peel-ply is made from nylon. The nylon itself has a positive CTE as it can be found in many datasheets. The shrinkage behaviour observed here (Figure 4.3) was identified in the research work of A. Ribnick [121] who studied the thermal behaviour of oriented nylon-66 yarns. He found that the thermal shrinkage of nylon-66 is increased when subjected to temperature up to 180 °C. The shrinkage of nylon yarn was also investigated and endorsed by Gupta et al [122]. and Simal et al [123]. These authors found that the shrinkage of Nylon-6 and nylon-66 increases almost linearly with the increase in temperature.

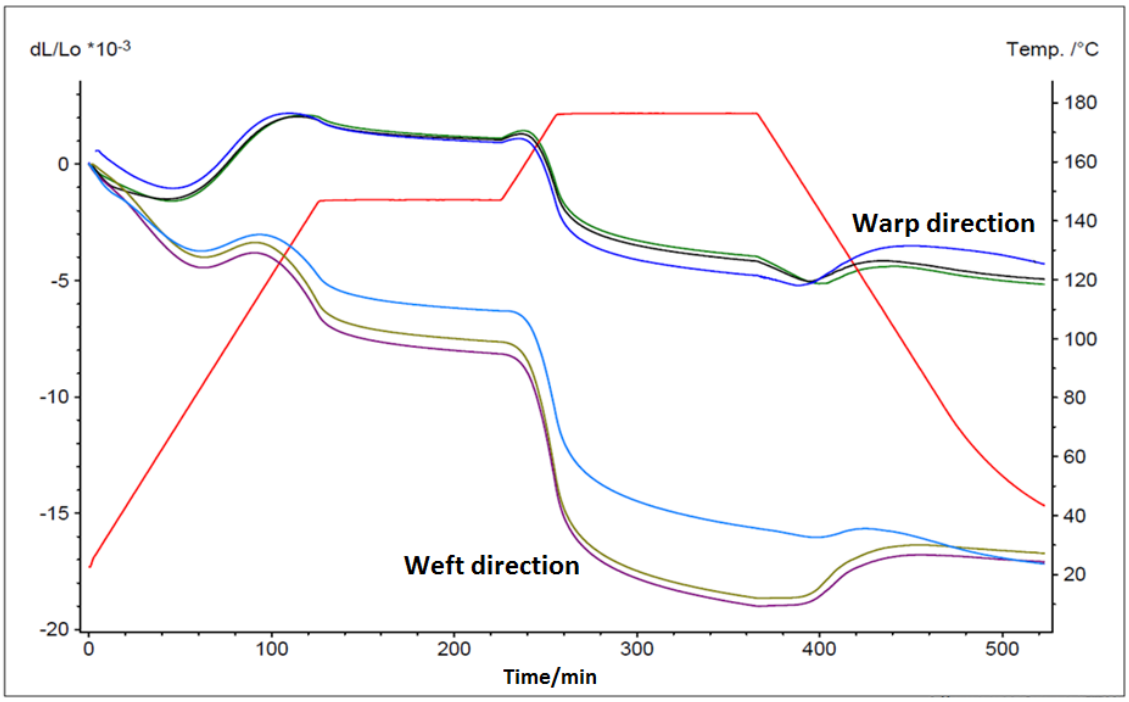

Figure 4.2 Strain and temperature vs time for cured resin impregnated peel-ply samples from TMA tests.

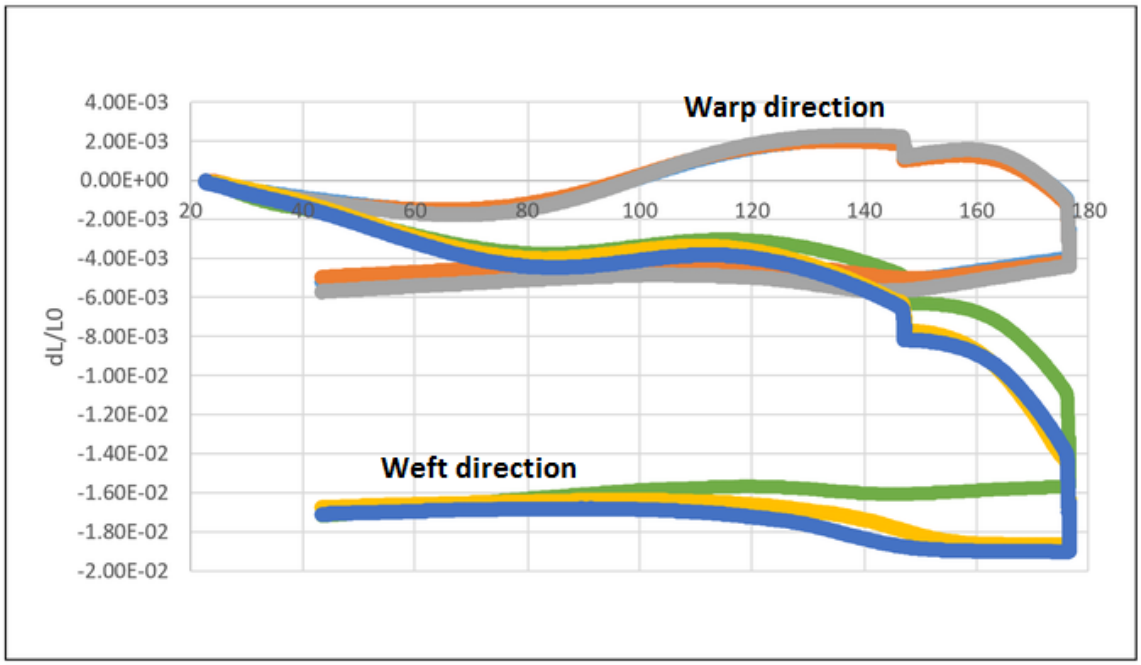

Figure 4.3 Strain as a function of temperature for cured resin impregnated peel-ply samples.

The peel-ply is a plain weave structure made of nylon yarns. Therefore, the dimensional changes of the peel-ply also depend on the peel-ply textile structure and the behaviour of nylon yarns according to temperature. A. Ribnick [121] has shown that nylon-66 underwent a large shrinkage under various constant temperatures as it can be seen in Figure 4.4. The percent thermal shrinkage was almost linearly with respect to time increment. It can be noticed that at 180 °C which is the maximum of our curing temperature dwell, the percent thermal shrinkage reached to about 9 % after 1,000 seconds while the shrinkage is about 8 % after 1,000 seconds for 154 °C which is close to 150 °C for the first curing dwell. The shrinkage of nylon yarns when subjected to temperature seems to be due to loosen hydrogen bonds in crystalline structure [123]. It is this shrinkage that was recorded at 150 and 180 °C during first and second dwells of our own experiment by TMA plotted in Figure 4.2. In Figure 4.2, the shrinkage continues up to the end of the 180°C plateau and the thermal relaxation was observed during cool down.

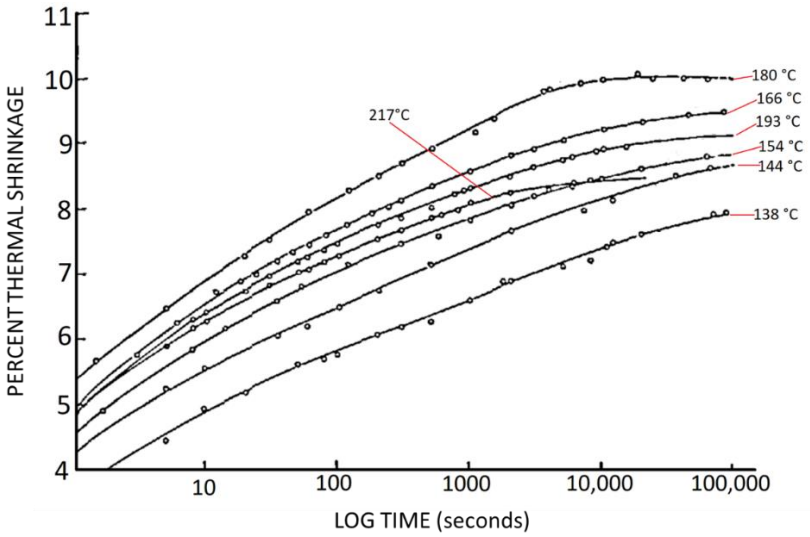

Figure 4.4 Percent thermal shrinkage of nylon 66 yarns at various constant temperatures as a function of time. [121]

The factors and causes of textile fabric shrinkage were discussed in Pariss Textile [124]. The percentage of shrinkage mainly depends on the raw material of fibres, the arrangement of textile structure, the density of the textile and the production process. Normally, the fibres are subjected to external tension force during the fabric manufacturing process. The fibres are stretched out and the tension force is freezing inside the textile structure. When the fibres are soaking with the liquid (in this case is the resin), the fibre's diameter will be enlarged and the tension force is overcome so that the internal stress is released which results in shortening the textile length. In the same way, applying heat will result in fibres expansion that forces each other to get closer, reducing the space and releasing the tension force, inducing the textile sheet to shrink to its original state. The mechanism of fabric shrinkage can be graphically illustrated in Figure 4.5 [125].

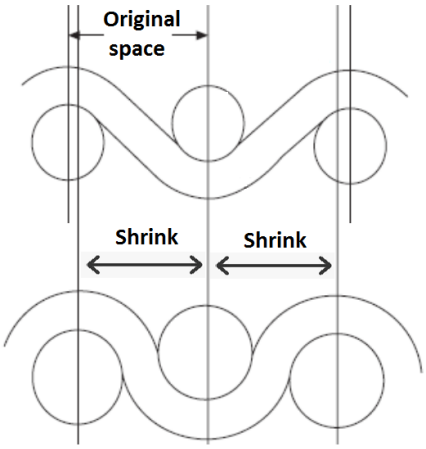

Figure 4.5 Shrinkage mechanism of textile fabric. [125]

In addition, the shrinkage behaviour between weft and warp directions of fabric was also investigated by some research works. Islam et al. [126, 127] studied the effect of temperature on the percentage of shrinkage between weft and warp directions of six types of cotton spandex woven fabrics. In their studies, the temperature ranged from 160 °C to 200 °C. The weft direction was found to shrink more than the warp direction in all cases. The difference in percentage of shrinkage between both directions is about 30-50% based on the type of cotton spandex woven fabric and the magnitude of temperature applied. These results are in accordance with those of Kumpikaite et al. [128] who investigated the shrinkage of blankets and woolen fabric with various weaves including diamond twills, derived baskets, derived twills and honeycombs. All samples were treated to washing temperature 40 °C. The results are presented in Figure 4.6. The shrinkage in the weft direction is clearly higher than the warp direction for all samples. The physical behaviour for this difference is that the weft direction contains less tension force in the fabric structure compared to the warp direction, this can increase the possibility of tension force to be overcome by the expansion of fibres as explained earlier.

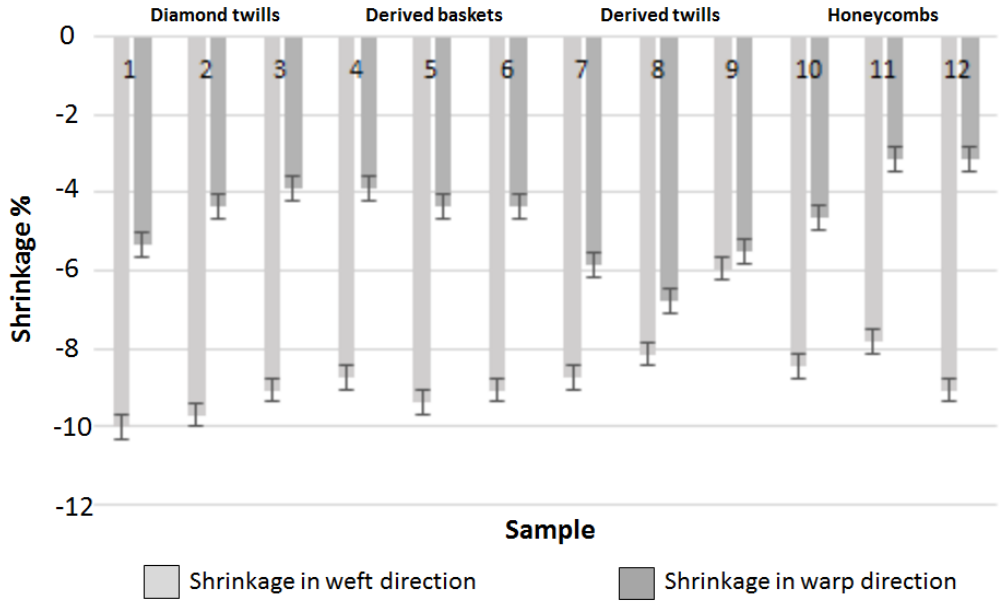

Figure 4.6 Shrinkage in weft and warp directions for different weave samples from the study of Kumpikaite et al. [128]

The results of ETFE release film are presented in Figure 4.7 and Figure 4.8. ETFE release film is a homogeneous and isotropic material, so the direction is not concerned for the sample preparation. The thermal behaviour follows the temperature profile, therefore the expansion increases with the increment of temperature. The contraction is observed during the cool down state but it did not return to its original length as in Figure 4.9, probably because of the wrinkles.

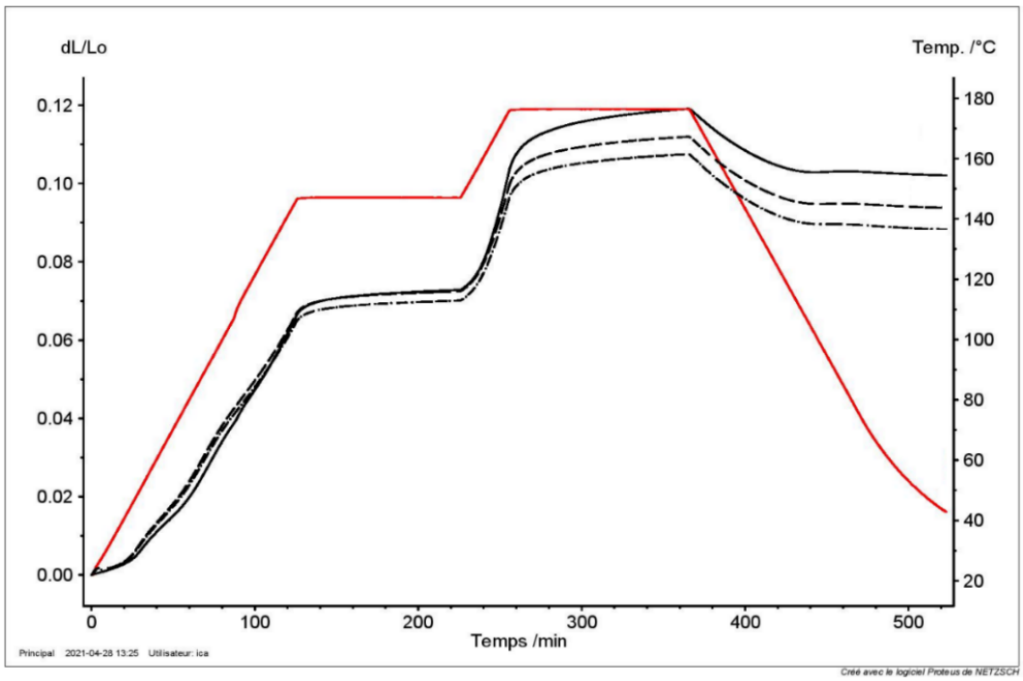

Figure 4.7 Dimensional changes in ETFE samples during a cure cycle obtained by TMA.

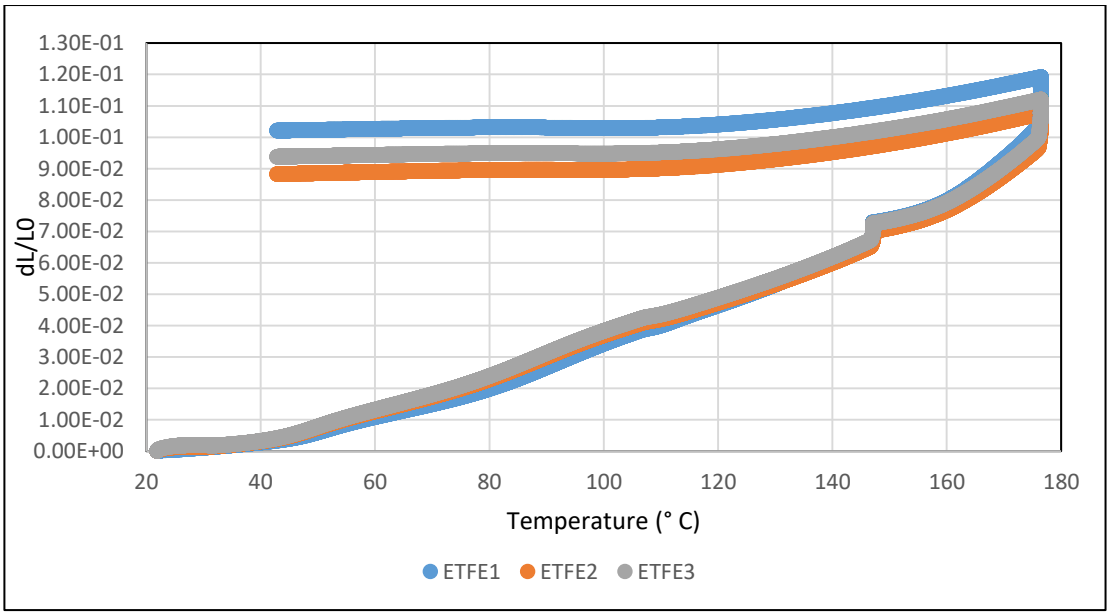

Figure 4.8 Changes in strains of ETFE samples as a function of temperature during a cure cycle.

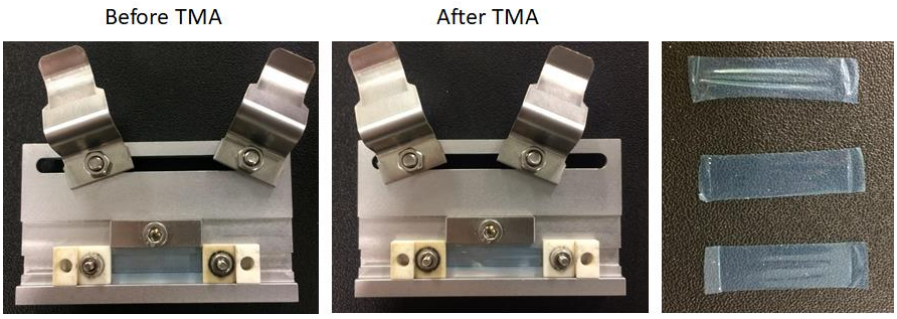

Figure 4.9 ETFE release film samples before and after TMA testing.

4.1.3 Experimental identification of the CTE for the release materials.

The coefficient of thermal expansion (CTE) of release materials (peel-ply and ETFE release film) can be determined from previous experimental data. Normally, the CTE can be calculated as a linear function recommended by Netzsch [129] as presented in Figure 4.10 and equation 4-1. The coefficient of linear thermal expansion (CLTE) is the ratio of change in length of a material when the temperature is changed. The average value of CLTE is determined as the slope of expansion curve as a relation between length change and temperature.

$$\bar{\alpha}(T_0,T) = \frac{\Delta L}{L_0 \Delta T} \tag{4-1}$$

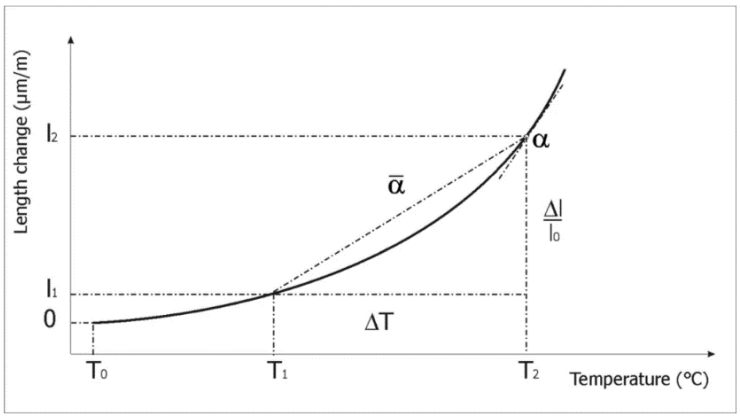

Figure 4.10 The coefficient of linear thermal expansion (CLTE). [129]

However, from the results obtained between thermal strain and temperature for ETFE release film and peel-ply, the evolution of CTE is non-linear and not constant throughout the cure cycle. In order to simplify the problem, we firstly decided to use $\bar{\alpha}$ to be the CTE of the release material for each curing section. Therefore, we separately plotted the relation between thermal strain and temperature divided by the range of temperature. The range of temperature was based on the thermal strain behaviour. We tried to separate each section

that enabled to fit the curve properly by a linear function and the slope of the linear function is the CTE.

Starting from peel-ply, we selected one data set for each sample (one from weft direction and one from warp direction) to re-plot separately. Due to the complexity of the curve, 10 sections are needed for peel-ply based on temperature range including 6 sections for first heating ramp, 1 section for first dwell, 1 section for second heating ramp, 1 section for second dwell and 1 section for cool down. It should be noted that the temperature path defined by TMA as an average temperature with a tolerance of ±5 °C. This is why there are some variations of temperature observed in the following curves especially for the dwell periods that the temperature is not actually constant at 150 and 180 °C. All these explanations are presented in Figure 4.11 to Figure 4.20 with the marks of sample types and linear functions.

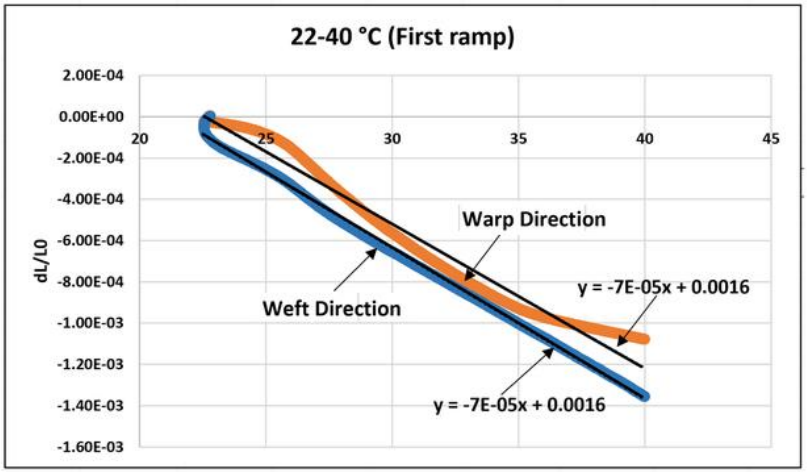

Figure 4.11 Changes in the strains of cured resin impregnated peel-ply as a function of temperature between 22-40 °C.

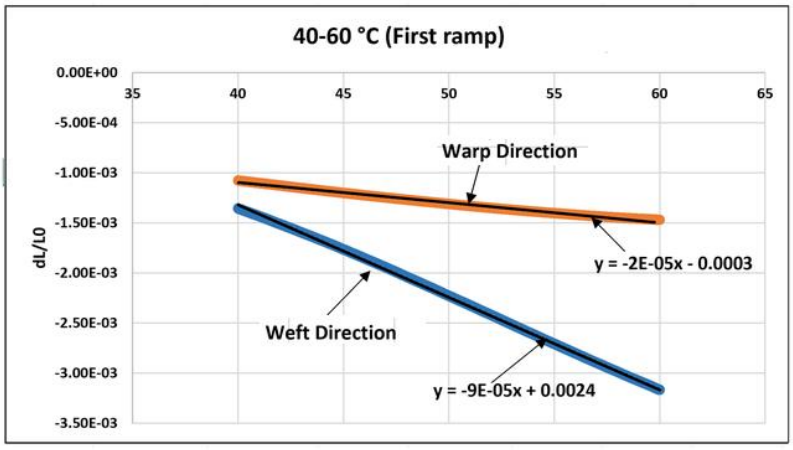

Figure 4.12 Changes in the strains of cured resin impregnated peel-ply as a function of temperature between 40-60 °C.

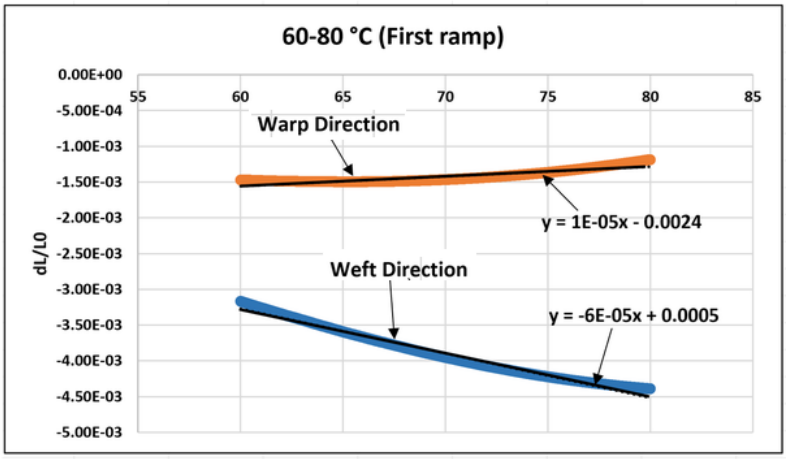

Figure 4.13 Changes in the strains of cured resin impregnated peel-ply as a function of temperature between 60-80 °C.

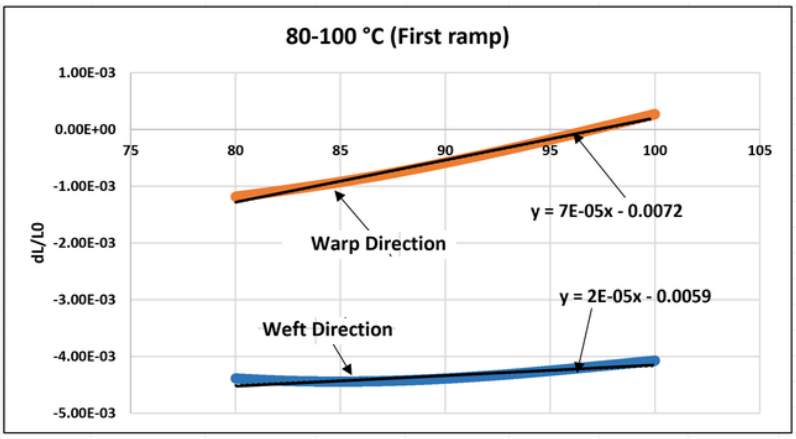

Figure 4.14 Changes in the strains of cured resin impregnated peel-ply as a function of temperature between 80-100 °C.

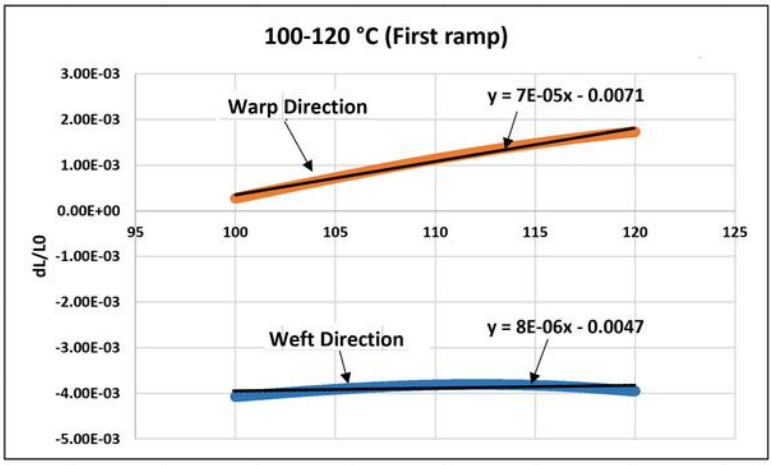

Figure 4.15 Changes in the strains of cured resin impregnated peel-ply as a function of temperature between 100-120 °C.

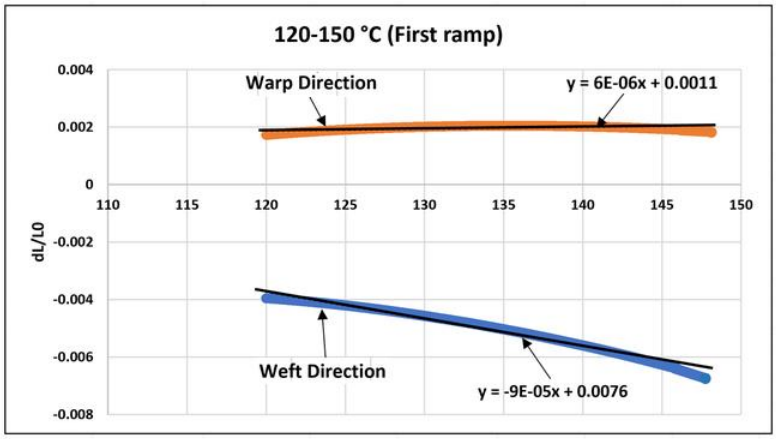

Figure 4.16 Changes in the strains of cured resin impregnated peel-ply as a function of temperature between 120-150 °C.

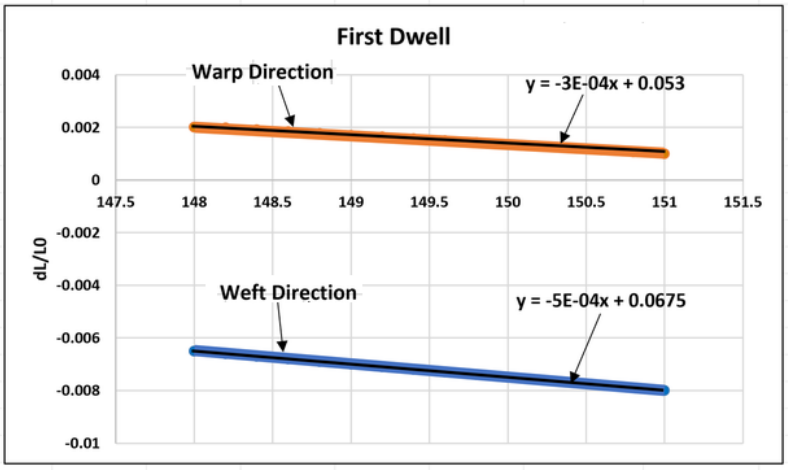

Figure 4.17 Changes in the strains of cured resin impregnated peel-ply as a function of temperature during first dwell.

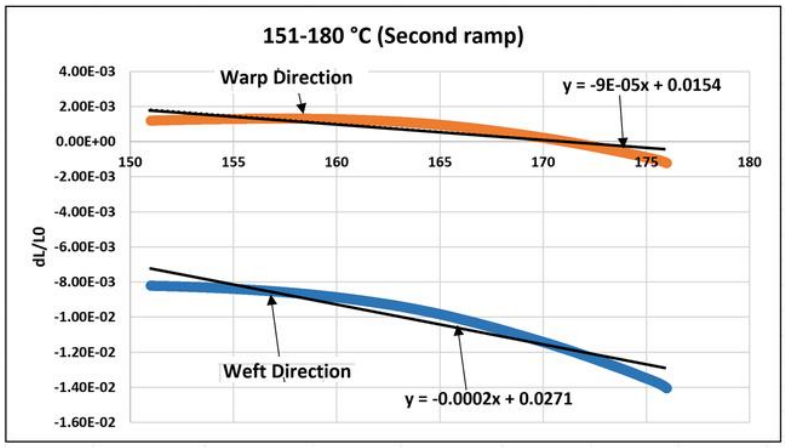

Figure 4.18 Changes in the strains of cured resin impregnated peel-ply as a function of temperature during second heat ramp.

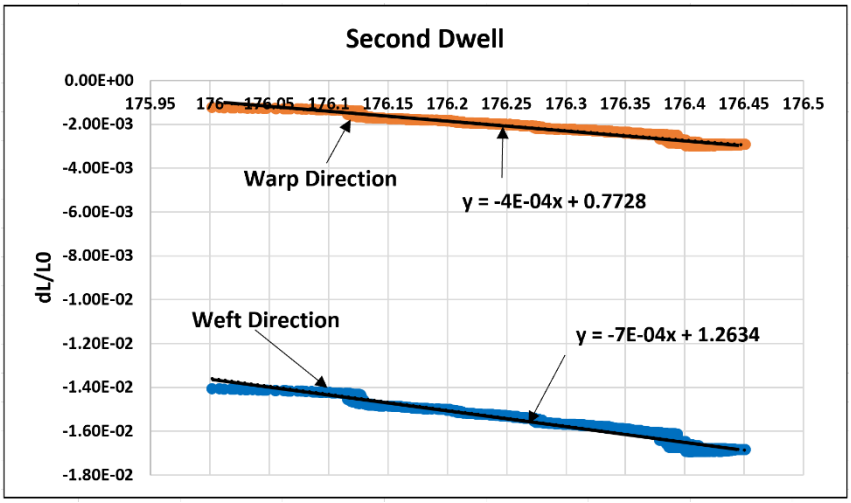

Figure 4.19 Changes in the strains of cured resin impregnated peel-ply as a function of temperature during second dwell.

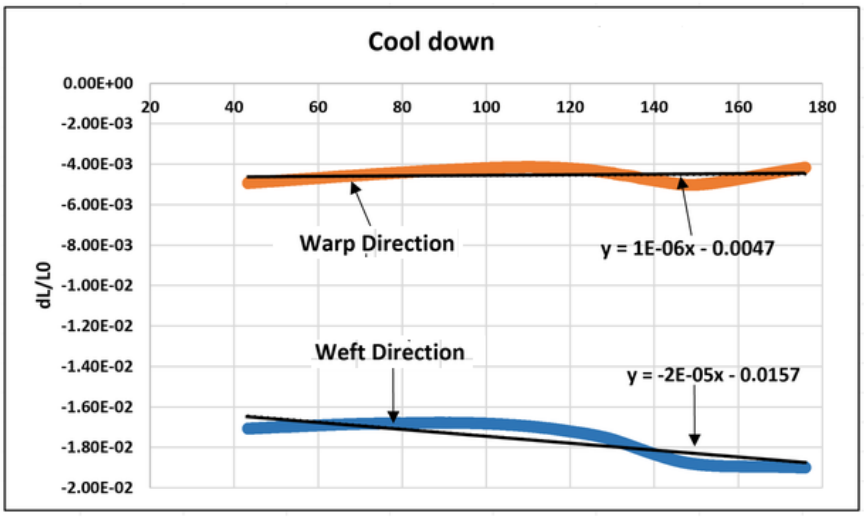

Figure 4.20 Changes in the strains of cured resin impregnated peel-ply as a function of temperature during cool down to 40 °C.

Same idea was also used for ETFE release film but the complexity of the curve is much lower than the one of peel-ply so that the whole temperature path of the cure cycle can be divided into 5 sections including first ramp, first dwell, second ramp, second dwell and cool down stage. These 5 sections are presented in Figure 4.21 to Figure 4.25.

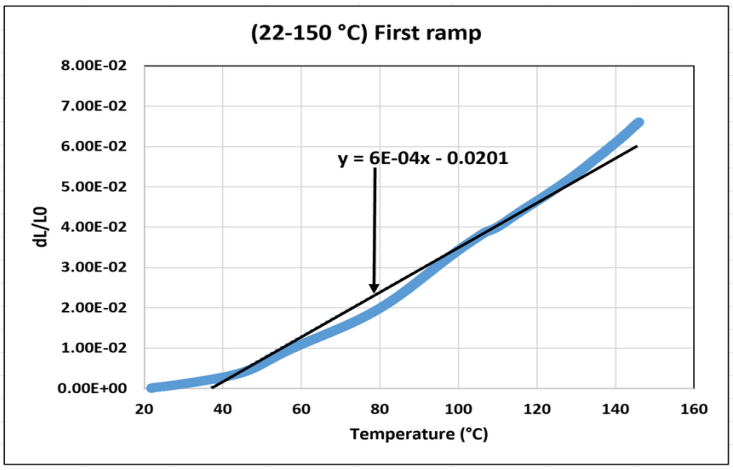

Figure 4.21 Changes in the strains of ETFE release film as a function of temperature during first ramp.

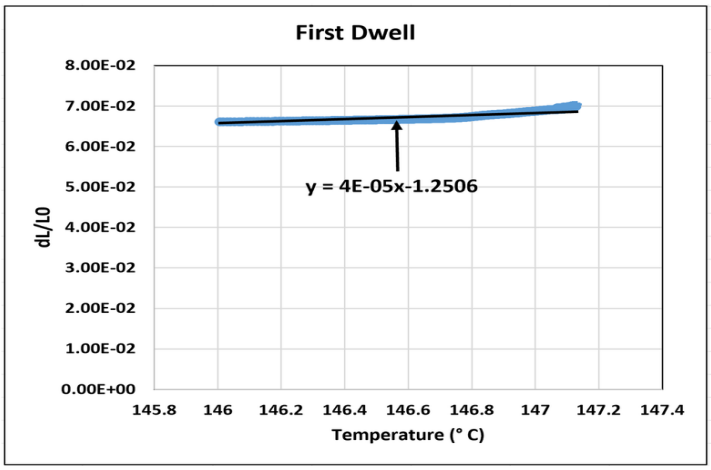

Figure 4.22 Changes in the strains of ETFE release film as a function of temperature during first dwell.

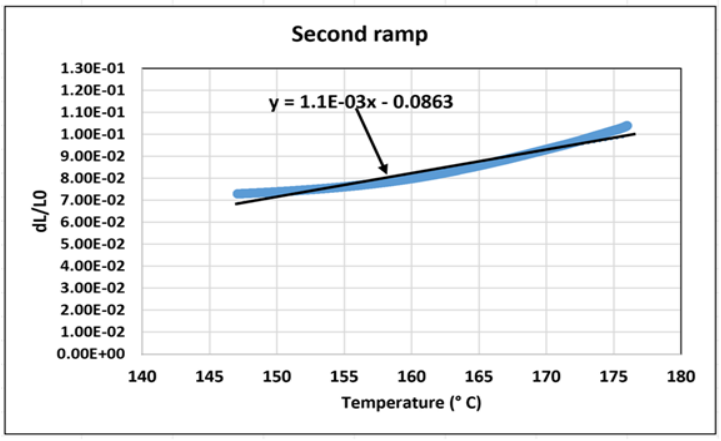

Figure 4.23 Changes in the strains of ETFE release film as a function of temperature during second heat ramp.

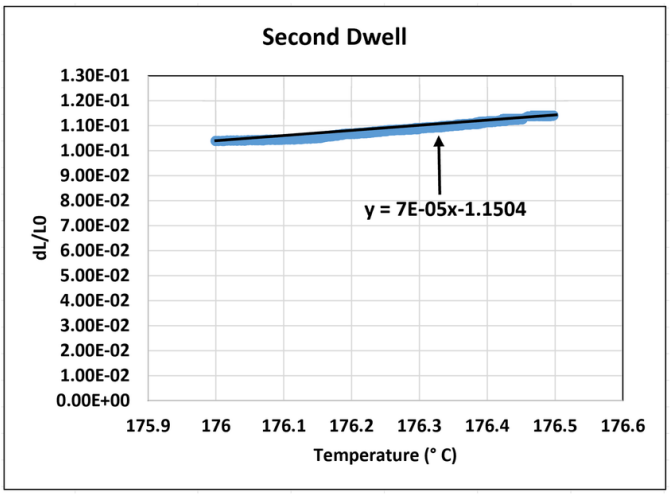

Figure 4.24 Changes in the strains of ETFE release film as a function of temperature during second dwell.

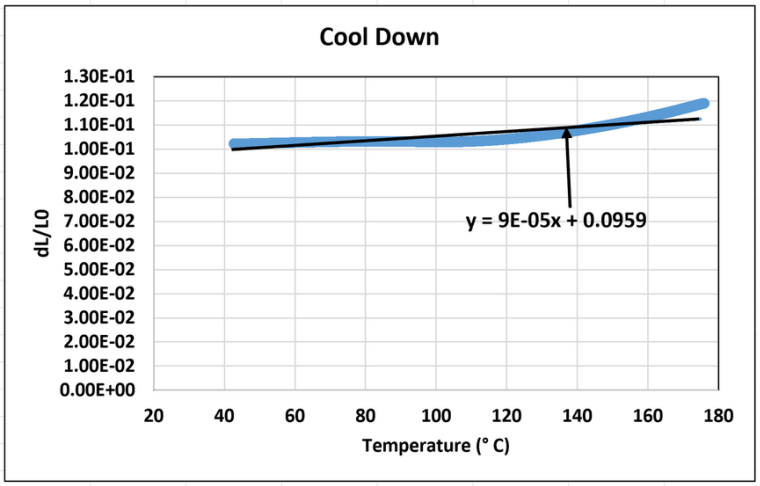

Figure 4.25 Changes in the strains of ETFE release film as a function of temperature during cool down to 40 °C.

The CTE values of peel-ply and ETFE release film obtained from linear slope at each range of temperature are summarized in Table 4.1 and Table 4.2 respectively, the negative sign of the CTEs represents the contraction (shrinkage). Figure 4.26 shows the difference of CTE values of peel-ply between weft and warp directions throughout the cure cycle. As explained before, this curve represents the thermal answer of the complex structure of the peel-ply during the curing cycle and must not be seen as a simple material response.

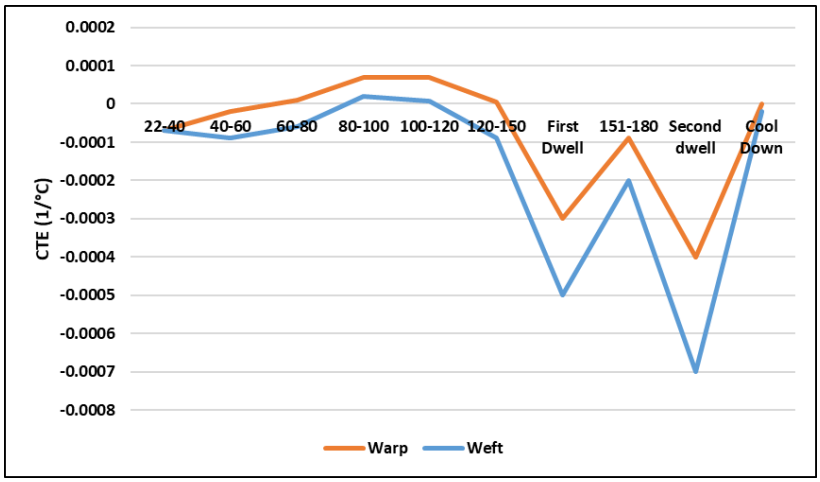

Figure 4.26 The difference of CTEs of Peel-ply between weft and warp direction throughout the cure cycle.

Table 4.1 The CTE values of peel-ply for weft and warp directions at different temperature ranges.

Temperature range (°C)	CTEs in warp direction ($°C^{-1}$)	CTEs in weft direction ($°C^{-1}$)
22-40	-7×10^{-5}	-7×10^{-5}
40-60	-2×10^{-5}	-9×10^{-5}
60-80	1×10^{-5}	-6×10^{-5}
80-100	7×10^{-5}	2×10^{-5}
100-120	7×10^{-5}	8×10^{-6}
120-150	6×10^{-6}	-9×10^{-5}
First Dwell (150 °C)	-3×10^{-4}	-5×10^{-4}
150-180	-9×10^{-5}	-2×10^{-4}
Second dwell (180 °C)	-4×10^{-4}	-7×10^{-4}
Cool Down	1×10^{-6}	-2×10^{-5}

Table 4.2 The CTE values of ETFE release film at different temperature ranges.

Temperature range (°C)	CTEs of release film ($°C^{-1}$)
22-150	6×10^{-4}
First Dwell (150 °C)	4×10^{-5}
150-180	1×10^{-3}
Second Dwell (180 °C)	7×10^{-5}
Cool down	9×10^{-5}

4.2 Implementation and FE simulation

The thermal behaviour for the interfaces characterized from the previous section has to be implemented into numerical simulation. In this case, the thermal behaviour of ETFE release film and peel-ply is non-linear in response to the cure cycle and this provides various CTE values depending on the range of temperature (Table 4.1 and Table 4.2). However, the idea of simulation is to test the effect of CTE of the interface materials especially for the peel-ply since the CTE of the mould was not tested and assumed to be constant. The CTEs of release film and peel-ply were assigned into the numerical modelling instead of the values previously used in Table 3.8 by the use of temperature-dependent data available in the property module. An isotropic CTE can be used in the case of the ETFE release film. On the other hand, two orientations need to be assigned to the peel-ply part and the orthotropic CTE was selected in the property module to be able to implement the CTEs in weft and warp directions. Once again, the CTEs of peel-ply are the CTE of the textile structure and not the CTE of the material. Nevertheless, in the finite element model the CTEs of peel-ply are considered to be the CTE of homogeneous material in order to simplify the model construction.

The simulation results for cross-ply ([0/90]s) laminate with ETFE release film and peel-ply are presented in Figure 4.27 and Figure 4.28 respectively. No change is observed for the simulation model with ETFE release film (Figure 4.27) while the simulation overestimates about 13 % compared to experimental result (average value 1.62 mm in Figure 3.45). The shape conformity is achieved for the model with peel-ply (Figure 4.28) with about 15 % overestimation of experimental result (average value 2.382 mm in Figure 3.46). It should be noted that the CTE of interface materials was usually assumed to be constant through the cure cycle and this can prove that the thermal behaviour of the interface plays an important role to the shape of deformation of cross-ply thin laminate. Moreover, peel-ply that contains weft and warp directions with several and different CTEs enables to clearly catch the experimental shape of cross-ply ([0/90]s) laminate after curing. That was not the case in chapter 3 (Figure 3.46) results in which the shape is different from the experimental one. Beyond the fact of the effect of peel-ply with cross-ply laminate, we have numerically studied the influence of peel-ply layer orientation by modifying the direction of peel-ply to 45° instead of 0°. Figure 4.29 shows that peel-ply orientation has little effect on the dispersion of deformation but totally still keeps similar warpage pattern. Therefore, we did not consider performing more experiments.

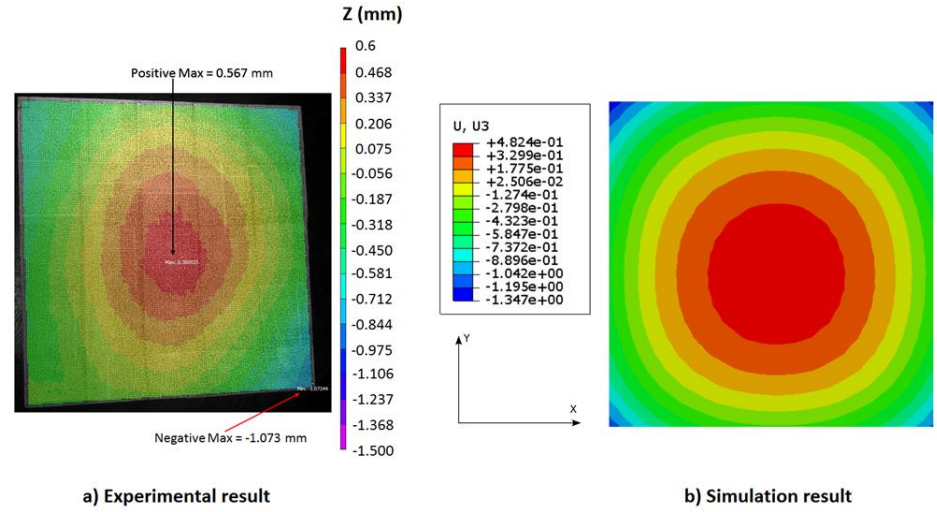

Figure 4.27 Comparison between experimental and simulation results for cross-ply laminate with ETFE release film after characterization of CTEs.

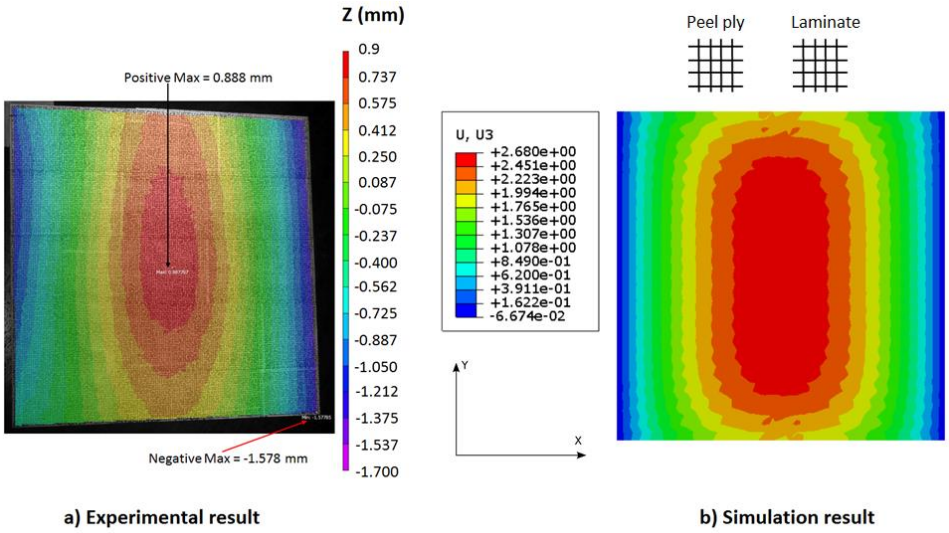

Figure 4.28 Comparison between experimental and simulation results for cross-ply laminate with peel-ply after characterization of CTEs.

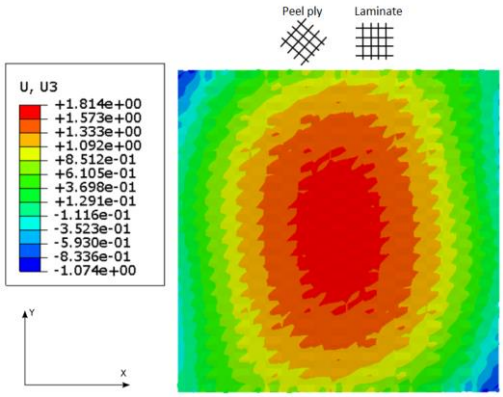

Figure 4.29 The simulation of cross-ply laminate with a peel-ply oriented at 45 °.

The simulation results for angle-ply (±45) laminate with ETFE release film and peel-ply are presented in Figure 4.30 and Figure 4.31 respectively. Similar shape and magnitude of deformation are observed in both cases and the agreement between experimental and numerical results is still achieved. It seems that the change in release material types as well as the change in the CTE law have little influence on the shape and magnitude of deformation of angle-ply laminates. The explanation for this observation is quite complex and it might be too early to reach a conclusion now since angle-ply laminates exhibit a considerably larger distortion compared to cross-ply laminates. We remind that cross-ply laminates have a symmetrical stacking sequence, while angle-ply ones do not and this induces coupling effects. The effect of peel-ply might be dissimulated by the huge level of deformation stemming from coupling effects for angle-ply laminates. In our opinion, it might have the different in-plane strain in the ply level of laminate during cure when ETFE release film and peel-ply are used as an interface which required more experiments to monitor these phenomena. It is obvious that in order to face such complexities, using optical fibres such as FBG (Fibre Bragg Grating) would enable to bring new elements of comprehension as made in [130].

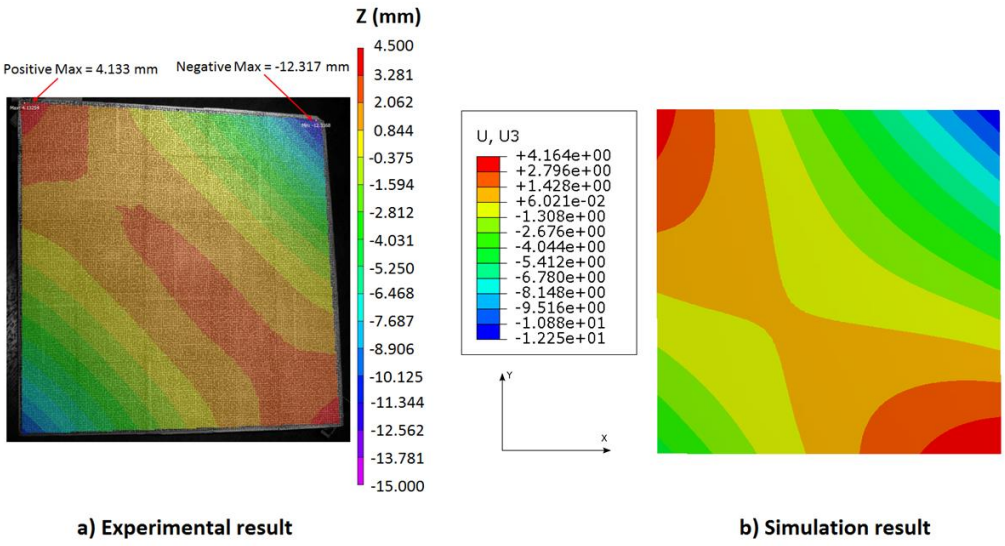

Figure 4.30 Comparison between experimental and simulation results for angle-ply laminate with ETFE release film after characterization of CTEs.

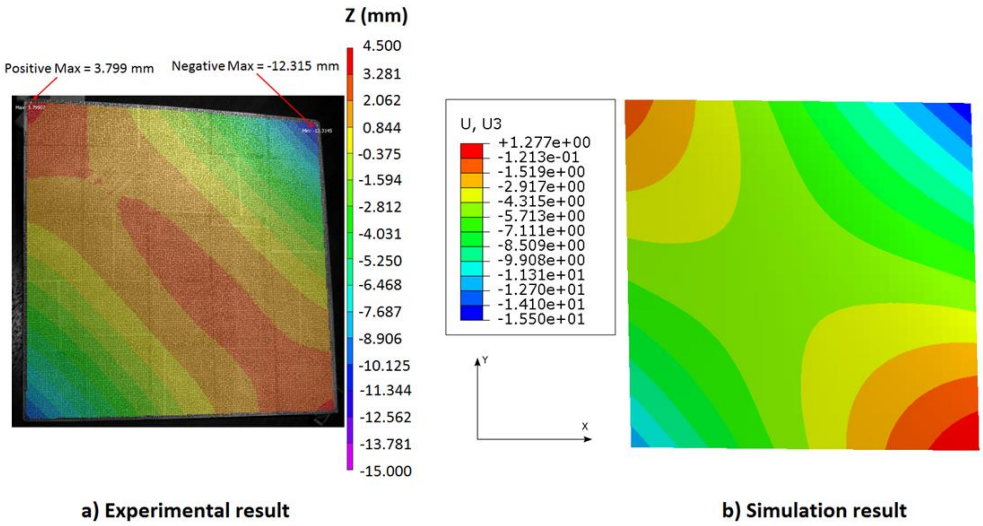

Figure 4.31 Comparison between experimental and simulation results for angle-ply laminate with peel-ply after characterization of CTEs.

4.3 Feasibility study of mould compensation for angle-ply laminate

The compensation of mould geometry is a common way to eliminate or reduce the distortion of composite parts. This method is usually used for the angle or curve shape composite part. However, the distortion mode must be known prior to starting the process for designing compensation. From a literature survey, a considerable number of research works performed both experiment and simulation on tool geometrical modification. E. Kappel [131] conducted the simulation-based tool compensation and validated experiment on the spring-in angles on the side area of composite rectangular box structure [132]. W. K. Jung et al. [17] directly modified the mould shape based on software prediction to compensate spring-forward of C and U shape hybrid composite shell and also the out of plane deflection of flat hybrid composite beam [65]. E. Kappel et al. [61] used the simulation result to modify concave tool geometry in order to compensate the convex warpage of very long unidirectional flat laminate. This way these authors could also reduce the spring-in of U shape specimens validated by experimental results [49].

In our study, the compensation for a final flat shape is investigated. We are going to face a new challenge since we work with unsymmetrical laminate (angle-ply) and that coupling effects are very pronounced. We firstly focus on the angle-ply laminate which has a huge deformation level in diagonal direction. The objective of this study is to simulate the feasibility of a compensated mould to eliminate or reduce the deformed shape of angle-ply laminate. The idea is to seek for the optimal mould shape to be able to obtain a zero deform shape or by default the lowest out of plane deflection of angle-ply laminate. Based on

experimental and numerical results, all angle-ply specimens distorted away from flat mould surface then the female mould (concave shape) should be initially considered but anyway we also decided to test numerically the male mould (convex shape).

4.3.1 Model construction

The shapes of mould, interface and laminate are redesigned regarding to the shape and magnitude of deformation obtained from our numerical modelling strategy of angle-ply laminate. We start with the direct method to form a mirror mould shape which has usually been done in general research works on compensated shape moulds. First step, the numerical deformed shape (from Figure 3.48) was imported into ABAQUS as a new part and then the function of “geometry edit” was used to delete the mesh and fill the solid into the shape (see Figure 4.32). Second step, the deformed part was exported from ABAQUS to CAD software in order to measure the distance between maximum and minimum point of the deformation to be the reference for mould shape.

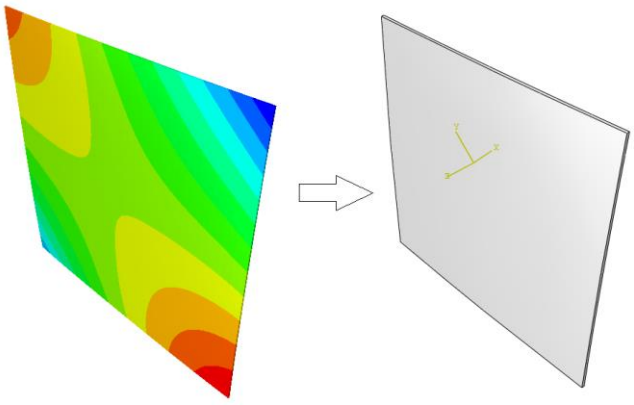

Figure 4.32 The exported deformed part of angle-ply laminate.

The female and male moulds were created as shown in Figure 4.33. The upper surface of female mould is considered to be a mirror shape of angle-ply laminate deformed shape, while the upper surface of male mould is the same as a deformed shape of angle-ply laminate. The Z dimension is the distance between maximum and minimum points of the upper mould surface which is defined to be 16 mm (the magnitude of deformation of angle-ply laminate) or we can say that Z is the depth and the height of the mould curve for female and male moulds respectively. The parts of the interface and laminate were formed based on the shape of the upper mould surface. Moreover, the alignment of the fibre of the laminate for each ply was also modified by using the discrete definition for material orientation in the property module to conform with the initial curvature of the laminate (see Figure 4.34). This is to form a bend shape of fibre along with mould curve prior to curing simulation.

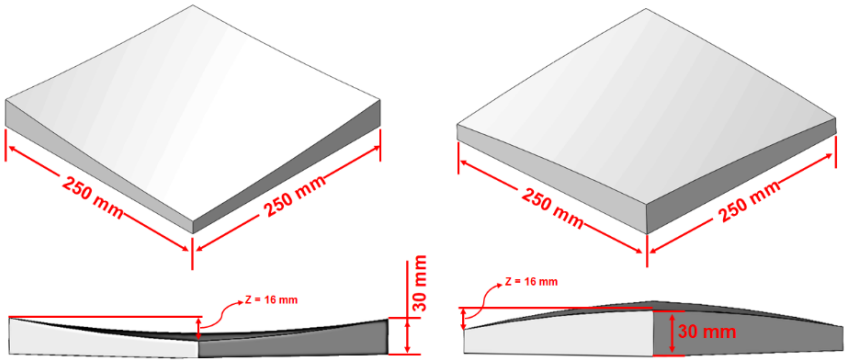

a) Female mould b) Male mould

Figure 4.33 Female and male moulds.

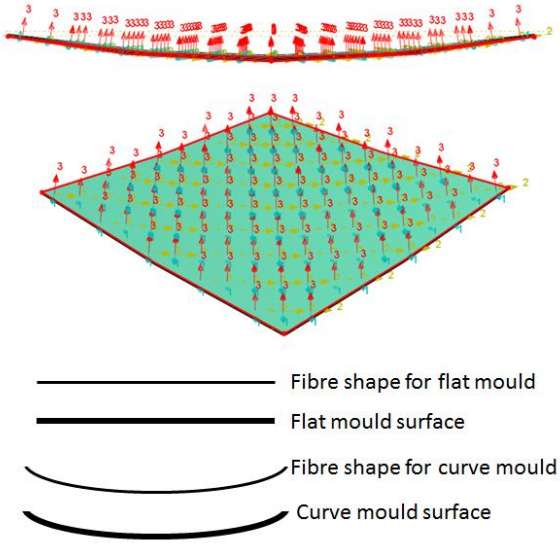

Figure 4.34 The conformity between initial laminate curvature and fibre alignment.

The whole Abaqus model contains 3 parts including mould, interface, and laminate with the shape conformity. The parameters, as well as curing environments including curing temperature and pressure condition assigned to the model are identical to those explained in chapter3 (section 3.5.2). The thickness of female and male compensated mould is larger than the flat mould and it is assumed to gain more weight, the boundary condition ENCASTRE was set to the bottom of moulds to prevent the displacement and rotation of the mould during simulation. To simplify the model and later the manufacturing, only the properties of the ETFE release film were assigned to the interface part. The model contains three steps including initial, curing and demoulding. The initial step defines a predefined field of initial room temperature (25 °C) and boundary condition, the curing step defines the cure cycle temperature and pressure, the demoulding step is the end of simulation to remove interface and mould.

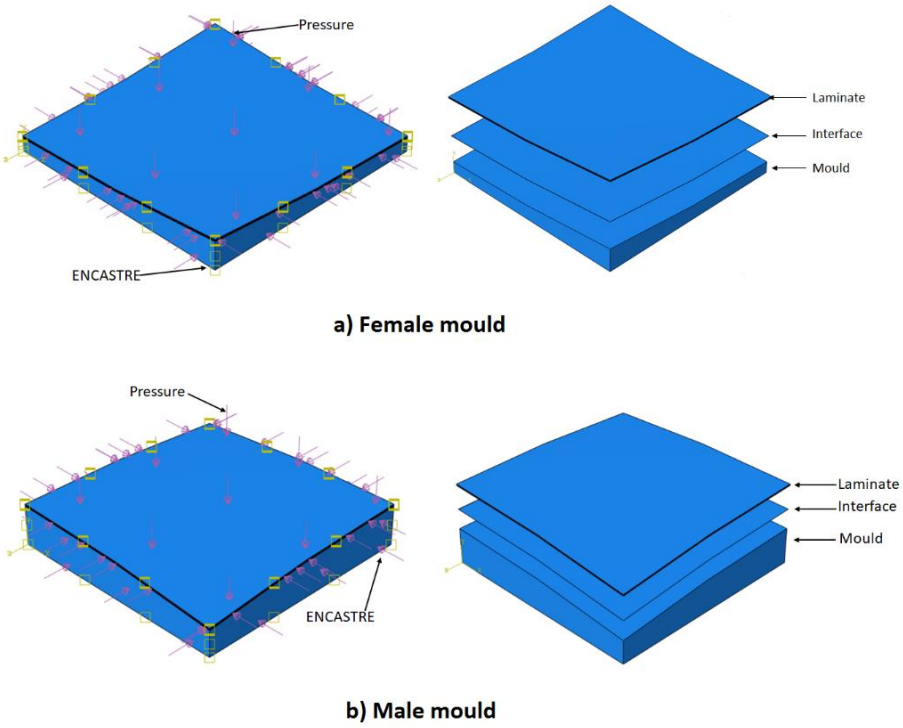

Figure 4.35 Model construction of female and male moulds.

4.3.2 Simulation results for mould compensation

The simulation results of angle-ply laminate cured on mirror compensated female and male moulds are shown in Figure 4.36. Flat shape could not be achieved from both moulds and the warpage pattern of angle-ply laminate (when simulated on flat mould) is obtained. The compensated female mould can only reduce the magnitude of warpage about 33% (compared to the magnitude of 16 mm) while the magnitude of warpage is increased about 29% with the use of compensated male mould. It is reasonable for a male mould to enlarge the deformation because the angle-ply laminate is warping away from flat mould after curing, the convex curve of male mould can induce more warpage. For the female mould, it is surprising that the warpage could not be eliminated and a very low percentage of reduction is obtained. In this case, the warpage of angle-ply laminate is large (up to 16 mm out of plane deflection) compared to cross-ply laminate in this study (lower than 3 mm) and other research works about mould compensation such as the deformation of hybrid composite beam (maximum 2.5 mm), the spring-back of C and U shape laminates (0.24° to 2.86°) from W. K. Jung et al. [17, 65]. The mirror mould (female mould) is unable to compensate for the shape because the depth of the mould surface is large. The compensated mould is functioning like a curved mould to cure a curved laminate plate. The laminate is forced with the deep mould surface and there is insufficient elasticity for laminated plates to spring-back to flat shape after demoulding.

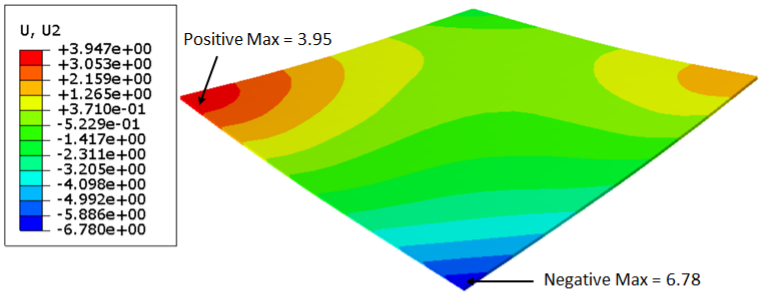

a) Cured shape of Angle-ply laminate from compensate female mould

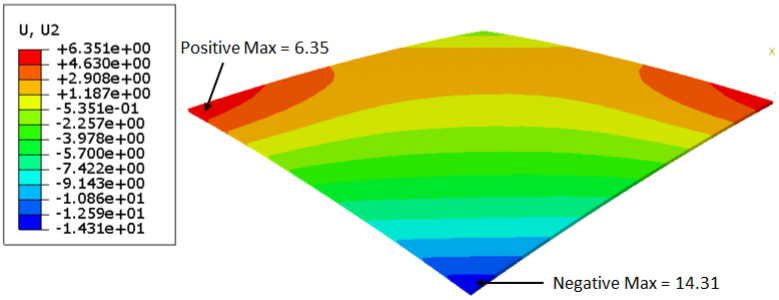

b) Cured shape of Angle-ply laminate from compensate male mould

Figure 4.36 Cured shape of angle-ply laminate from compensate female and male moulds.

4.3.3 Experimental identification for mould compensation

However, we decided to perform an experiment to verify the first stage of simulation. We choose to fabricate only a female mould because it requires a very thick aluminium sheet to fabricate a male mould and there is no availability in the laboratory. The compensated female mould was made of 2024 aluminium sheet. In order to prevent the folding of one or more laminate edges due to vacuum condition, the compensated mould was scaled up to be a little bit bigger than the laminate plate. The 3D file of compensated mould was imported into CATIA V5 to perform virtual simulation of the milling machine. The aluminium sheet was cut with an overall size about 260 x 260 mm prior to the milling process. The upper mould surface was machined by Ball End Mill with diameter 10 mm to be able to obtain a curved surface, the fabrication was operated by DMU 85 monoBLOCK-5 Axis Milling machine. The finished compensated female mould is shown in Figure 4.37. Mould surface in contact with laminate was cleaned by acetone and coated by Freekote liquid release agent. Then, the mould pack was prepared (see Figure 4.38), ETFE release film was chosen to be a release agent interface between mould and laminate to avoid the difficulty of part/mould removal.

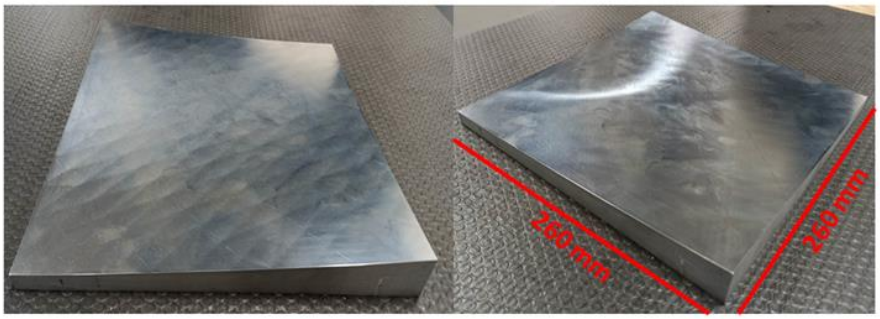

Figure 4.37 Compensated female mould.

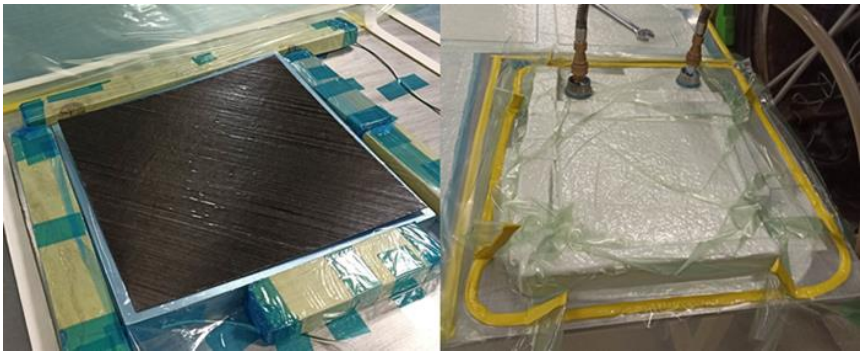

Figure 4.38 Preparation of compensated mould pack for autoclave curing.

The result of angle-ply laminate cured on compensated female mould after demoulding is presented in Figure 4.39, we were unable to experimentally obtain a flat shape from mirror female mould shape which is in agreement with numerical simulation. The distortion shape and magnitude were measured by Digital Image Correlation (DIC) as shown in Figure 4.40. The simulation result underestimates the experimental one by about 17 % (compare between Figure 4.36a) and Figure 4.40).

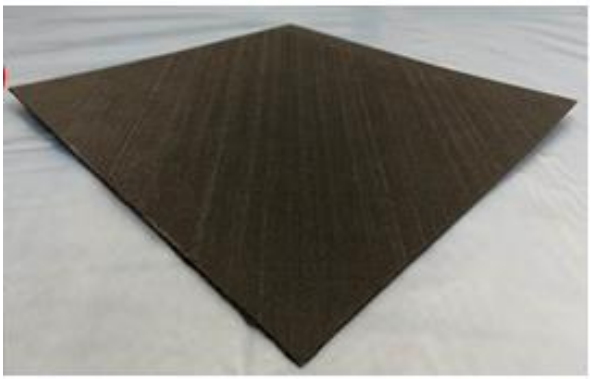

Figure 4.39 The result of deformed shape of angle-ply laminate cured on compensated female mould.

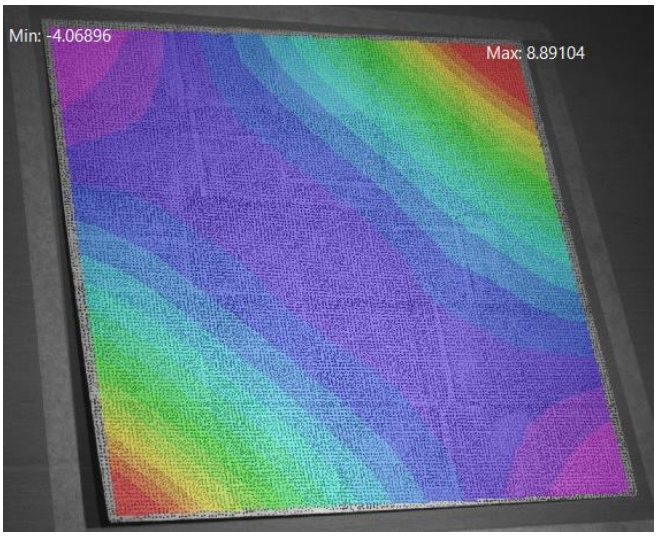

Figure 4.40 Distortion shape and magnitude of angle-ply laminate cured on compensated female mould.

However, there was one problem found during cure that was the irregular temperature program of the autoclave which can be seen in Figure 4.41. Focusing on blue line which is the temperature program ordered from the autoclave, the first dwell appears in the series of steps instead of stable line at 150 °C and the second dwell only reaches to about 165 °C instead of 180 °C. Moreover, the temperature cycle is uncommon since the cycle starts to go up and down at the beginning of the first dwell measured by autoclave and four thermocouples, this phenomenon remains last until the end of curing. The cool down stage does not appear and the second dwell was held drastically longer than usual so that the autoclave was manually stopped to terminate the cure cycle. In total, the laminate was cured inside the autoclave for about 16 hours. Finally, we decided to validate this experiment by using the Differential Scanning Calorimetry (DSC) to examine the glass transition temperature (T_g) and degree of cure (α) of the resin from this autoclave curing. The measurement was prepared in the same way as described in section 3.2.5. The average α and T_g of angle-ply laminate cured on compensated female mould are 89.5% and 190.5 °C respectively. The α and T_g are lower than the ones obtained by ETFE release film in Table 3.2 about 11% and 4.4 % respectively which is not really different. This means that we are probably able to validate the simulation by this experiment.

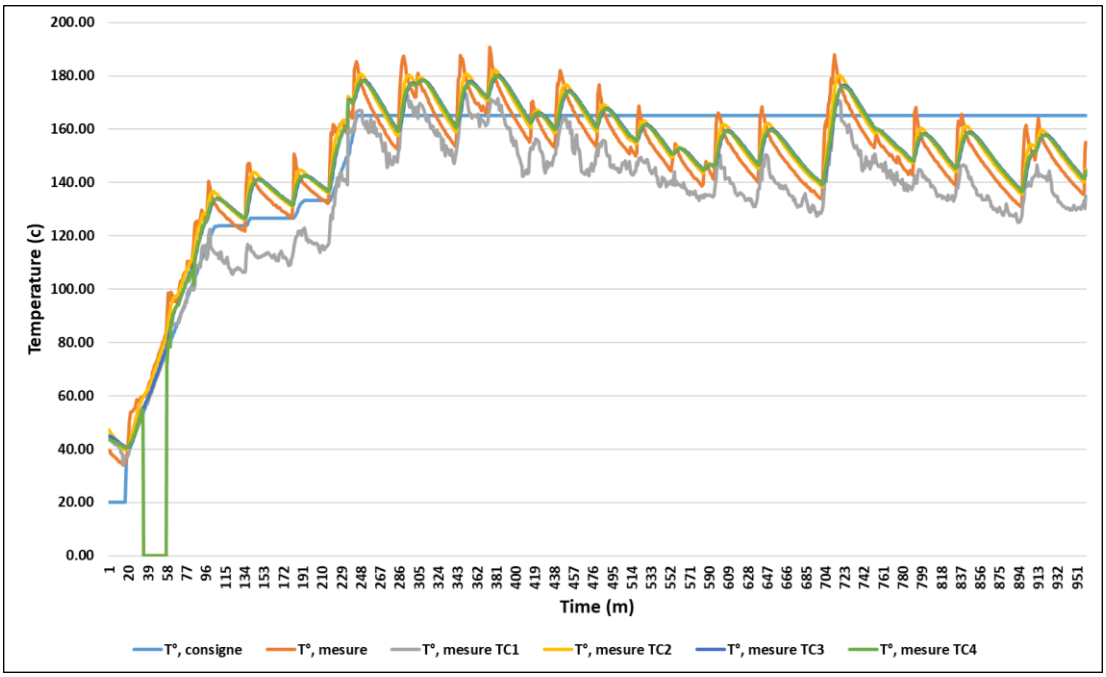

Figure 4.41 Irregular temperature program of the autoclave.

4.3.4 Extended numerical simulation for mould compensation

However, we continued to perform more simulations to compensate or minimize the warpage of angle-ply laminate. We firstly focus on the female mould because there is a possibility to achieve what we expect. We got some guideline from the research works of W. K. Jung et al. [65] who played with the depth of the compensated mould (ΔZm, see Figure 4.42) to minimize the spring-back of hybrid composite beam. Moreover, the work from the same research group [17] confirmed that the mirror mould shape is not always able to compensate the deformation. Their study was performed with glass/carbon prepreg hybrid composite shell specimens C and U shapes (see Figure 4.43). The spring-back of C and U shapes were specified by θ_{PC} and θ_{PU} which are 0.24° and 2.86° respectively. The bending angle of aluminium mould (θ_M) was diversely modified. Figure 4.44 shows that the spring-back of C and U shaped composite parts could be compensated at the bending angle about -1.43° and -1.91° respectively.

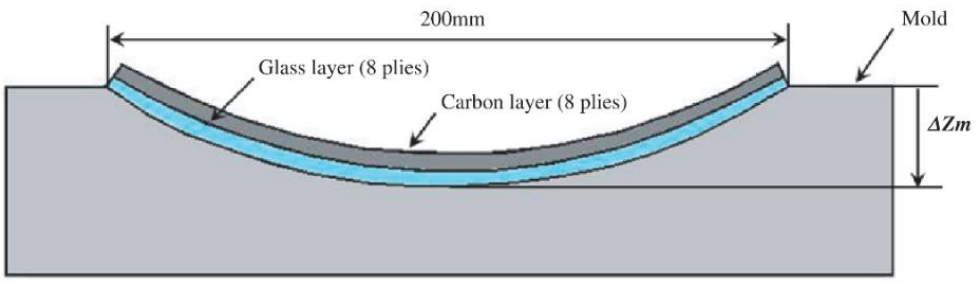

Figure 4.42 Compensated mould for hybrid composite beam. [65]

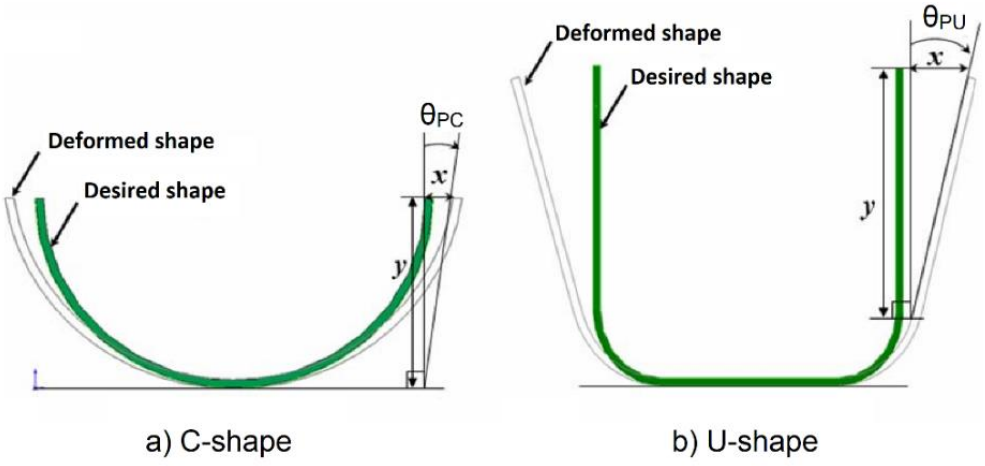

Figure 4.43 Curve hybrid composite beam. [17]

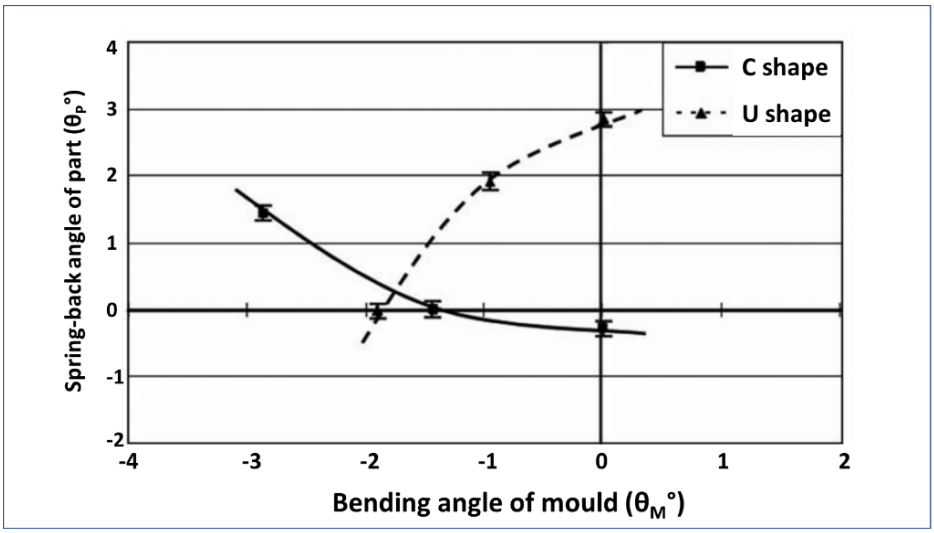

Figure 4.44 Results of spring-back compensation for C and U shape parts from W. K. Jung et al. [17]

In order to determine the optimum mould shape, we decided to modify a compensated female mould shape by reducing the depth of the mould surface (Z in Figure 4.33 a)). The Z dimension was sequentially reduced 3 mm starting from 16 mm to 4 mm, the shape of interface and laminate plate was also modified regarding the mould shape. The idea is to evaluate the depth of the mould surface that allows the elasticity of angle-ply laminate to spring-back closest to zero deform shape. The results of laminate cure simulation with varying female mould depths are shown in Figure 4.45. The warpage pattern of angle-ply deformation is observed and the warpage is decreased with the reduction of mould depth to 7 mm that gives the magnitude of distortion closest to zero. The mould depth of 4 mm which is very shallow tends to give the rise in deformation again because the mould depth is close to zero (flat mould). However, the effect of male mould curve was also investigated. We modified two more male mould heights (Z in Figure 4.33 b)), the Z dimension was reduced to 10 mm and 4 mm only to see the trend of deformation. The results are presented in Figure 4.46, all mould heights provide a similar trend (warpage pattern) of out of plane deflection and smaller magnitude of deformation is obtained from lower mould heights but they are still larger compare to female mould.

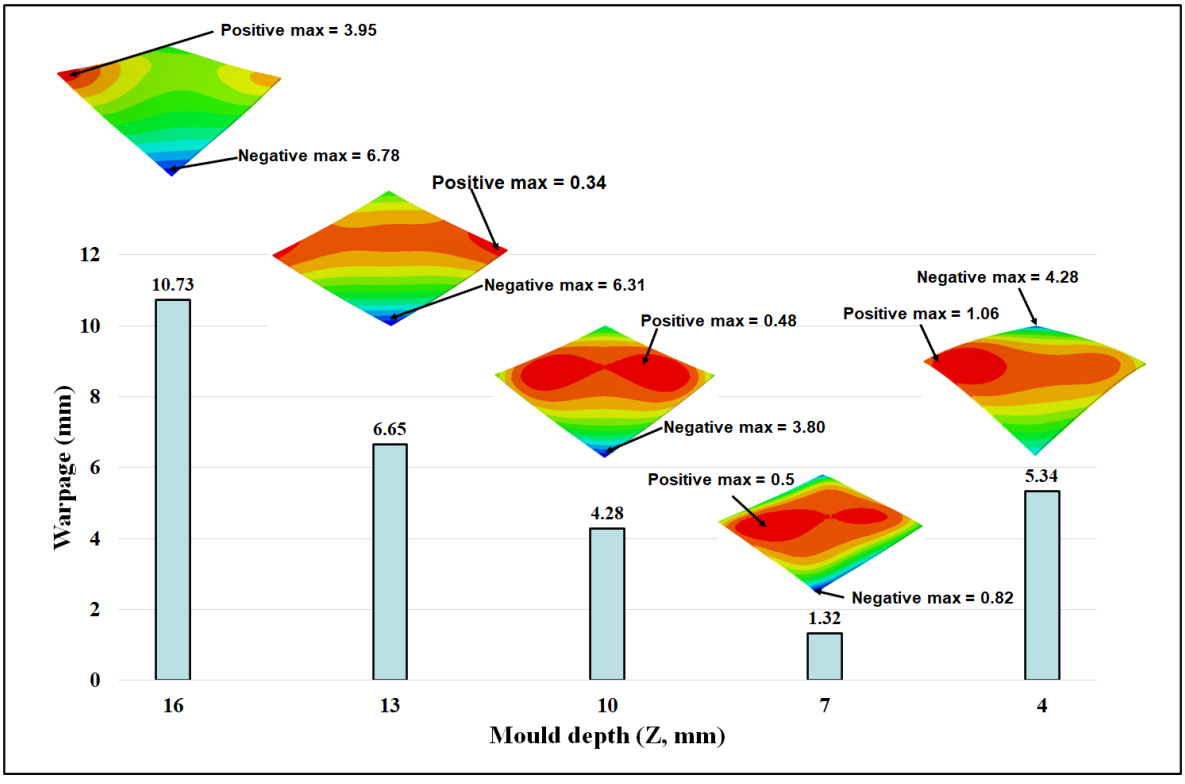

Figure 4.45 Warpage results from varying female mould depths.

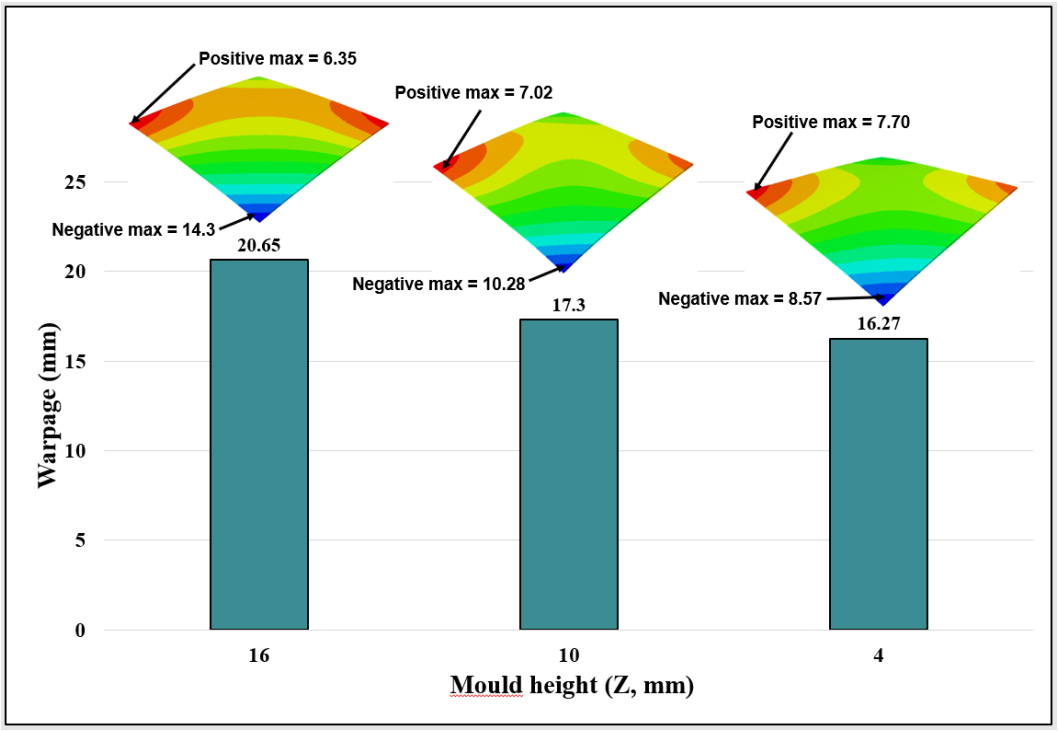

Figure 4.46 Warpage results from modified male mould heights.

It is important to note that the deformed shapes and magnitudes obtained here are based on computer simulation. In this case, we propose a shallower mould shape as shown in Figure 4.47. However, the feasibility of this mould to minimize the out of plane deflection of angle-ply laminate needs to be verified experimentally. We intend to cure the angle-ply laminate in autoclave with a compensated female mould but it was unfortunately that we found a problem of new program setup of the autoclave and required long time to repair. We cannot avoid the resumption of autoclave temperature program but we believe that the experiment result will provide more insight for future improvement.

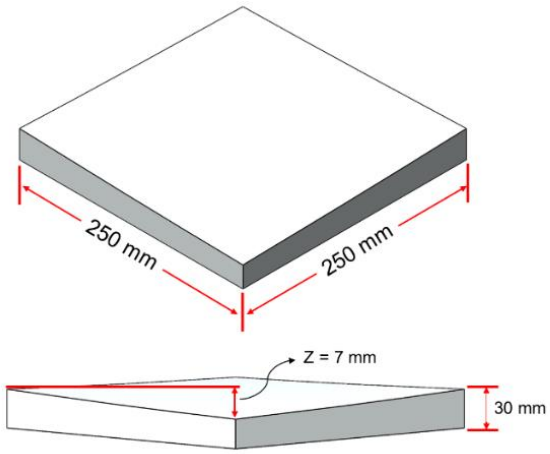

Figure 4.47 Proposed female mould shape and dimension.

4.4 Conclusion

This chapter extends the study on the characterization of interface materials. The thermal behaviour was firstly characterized by TMA in terms of the coefficient of thermal expansion. The results revealed that peel-ply provides different thermal behaviours (expansion and contraction) between weft and warp directions throughout the cure cycle while release film exhibits only expansion following the cure cycle. The coefficient of thermal expansion of both interfaces was determined separately for each curing section by the slope of linear curve fitting and finally implemented into the numerical model to simulate the cured shape of cross-ply and angle-ply laminate. The simulation result is satisfactory in terms of shape and magnitude of distortion and captures the sensitivity of peel-ply to the cured shape of cross-ply laminate. This can be noted that the property on interface between mould and laminate part cannot be ignored.

The last part of this chapter pays attention to the feasibility study of mould compensation to obtain flat shape for angle-ply laminate. It started from the simulation of mirror mould compensation for female and male moulds. The first results from simulation revealed that both female and male moulds designed with a simple mirror symmetry were unable to compensate the warpage of plain angle-ply laminate. It was shown numerically that a female mould would be able to minimize the warpage. By lack of time, the experimental verification was not possible but is still considered for future work.

General conclusion and perspective

The thesis work presented in this manuscript devoted the study of tool/part interaction for process-induced deformation in thermoset matrix composite laminate parts manufactured through the autoclave process. The objectives were to collect data based on deformation of composite specimens in different fibre directions and tool surface conditions, expand more investigations on the effect of tool/part interface by measurement and simulation of the deformed parts after curing and finally provide a modified mould shape to compensate or reduce part deformation. The material used for this study was determined by previous PhD work of Laure Moretti, it is therefore the M21EV/IMA prepreg.

The bibliographical study carried out in chapter 2 provided more insights on the parameters related to process induced distortion which can be classified into intrinsic (referring to characteristic of composite part) and extrinsic (related to fabrication process) sources. Several past research works were studied in order to see the overview for what has been done in the literature. This makes it possible to notice that the effect of tool/part interaction plays an important role in curing distortion of composite laminated parts. The effects of part characteristic are from the effect of materials (fibre/matrix system), part geometry (shape and dimension) and stacking sequences. The effects of mould are from the effect of mould materials, mould shapes and mould surface conditions. It is quite clear that part shape and dimension have strong effect on the final deformation after cure but these parameters are usually not allowed to be modified in terms of design, it is better to focus on stacking sequence. Several researchers mentioned that higher coefficients of thermal expansion of mould material increase part distortion while there were some arguments about the effect of release agent between mould and part. Also, the past researches usually played with the effect of release agent for liquid and polymer film sheet, the influence of the textile release fabric remained less studied.

Therefore, the start of the experiments for this Ph.D thesis focused on the tool/part interaction in terms of the effect of stacking sequences and tool surface conditions. The thin (four plies) cross-ply and angle-ply laminates were chosen to fabricate on aluminium flat mould with varying tool surface conditions between the use of ETFE release film and peel-ply textile release fabric. All the specimens were autoclave cured with the same cure cycle, pressure and vacuum conditions. The physical characteristics of specimens were measured and remain unchanged regarding different tool/part interfaces. Finally, the measurements were performed to examine the shape and magnitude of deformation, thanks to the availability of Digital Image Correlation (DIC) and Laser Displacement Sensor (LDS) to confirm the accuracy of the results. In terms of stacking effect, the measurement results

revealed that angle-ply laminates exhibited considerably larger out-of-plane deflection than cross-ply laminates as expected due to the absence of symmetry. In term of tool surface effect, cross-ply laminates are sensitive to the presence of peel-ply, even if the distortion is relatively small but it provides different shapes and magnitudes of deformation compared to those cured on ETFE release film, whereas the effect of peel-ply does not have any influence with the angle-ply laminates.

The numerical simulation of tool/part interaction was carried out in ABAQUS in order to compare the results with the experimental ones. The behaviour of prepreg M21EV/IMA was characterized in the Ph.D work of Laure Moretti and implemented with the Cure Hardening Instantaneous Linear Elastic (CHILE) model, thanks to the available FORTRAN subroutines as the input for the part of composite plate. The properties of mould and interface materials were not tested at the beginning but were gained from various sources. The simulation results were in good agreement with the experiment except for the cross-ply laminate cured with peel-ply. The assumption was emphasized to the thermal behaviour of peel-ply that might interact differently from the ETFE release film.

The thermal behaviour in terms of thermal expansion of the ETFE release film and peel-ply was experimentally tested by Thermomechanical analysis (TMA). The samples of both release agents were prepared and submitted to the cure cycle. The thermal expansion follows the cure cycle for the ETFE release film whereas the contraction was observed for peel-ply and also the range of contraction is different between weft and warp direction. Several works related to the contraction of textile structures were reviewed to support this finding with reasonable explanations. The coefficient of thermal expansions of the ETFE release film and peel-ply were characterized and implemented into numerical modelling. Good agreement between experimental study and numerical simulation in shape and magnitude of distortion can be obtained. This is to confirm that the effect of the tool/part interface cannot be ignored in the process induced deformation in composite parts.

The last part of this thesis is devoted to the modification of metallic mould shape to compensate the out-of-plane deformation of laminated plates. The idea is to study the feasibility of mould compensation strategy. The first consideration emphasized the compensation of angle-ply laminate. It is very challenging because the angle-ply laminate exhibited very large out-of-plane distortion. The study started from the numerical modelling of mirror modified mould shape for female and male moulds. The simulation results showed that both female and male moulds were unable to eliminate the warpage of angle-ply laminate. Male mould enlarged more deformation as expected because angle-ply laminate usually warps away from flat mould while female mould could slightly reduce the warpage due to the mould curve being too deep and there is not enough elasticity for laminate to

springback to flat shape. However, there was a possibility to reduce the distortion for female mould.

The perspectives are quite numerous. Starting from the tool/part interaction scheme, it is very interesting to investigate the sensitivity of other properties of the interfaces as well as the effect of other types of textile release fabrics available on the market on curing distortion of thin laminate. So, it would be possible to determine which one has the least impact on cure deformation. The unbalances CTE of peel-ply might have an impact only on thin cross-ply laminate, a comparison could also be made with thicker laminates (8 plies or 16 plies for instant) as well as the other stacking sequences (symmetrical and unsymmetrical). Since aluminium provides higher CTE than steel and Invar, the effect of interface should also be experimentally studied for other metallic mould materials. Due to lack of time, our work has performed the tool/part interaction only with flat laminates, it is very attractive to verify these interactions with more complex shapes.

Finally, it is reasonable to devote more time to studying the mould compensation strategy of flat laminated plates because most research works usually pay attention to the curve or strip laminates. In this Ph.D thesis, the experimental validation should be performed for the proposed female mould shape in order to examine whether it is actually able to compensate for large deformation of unsymmetrical flat laminate or not. In our opinion, the mould compensation method is a very specific job and has to be analyzed case by case because the distortion pattern of laminate parts must be known and of course laminates deform differently based on several factors. In this case, it is difficult to judge and draw some conclusions from just a few studies and it will be better to have more insights and guidelines for future development.

References

[1] A. Quilter, "Composites in Aerospace Applications," IHS Corporate Headquarters, USA.

[2] L. Zhang, X. Wang, J. Pei and Y. Zhou, "Review of automated fibre placement and its prospects for advanced composites," *Journal of Materials Science,* vol. 55, pp. 7121-7155, 2020.

[3] W.D. Callister, Materials Science and Engineering An Introduction, Utah: 7th, 2007.

[4] K.S. Shankar, C. Harish, B. Praharshini, Amulya and Rahul, "Fabrication of Fiber Reinforced Composite," *International Journal of Innovative Research in Science, Engineering and Technology,* vol. 5, no. 7, pp. 12927-12928, 2016.

[5] S. Prashanth , K. Subbaya, K. Nithin and S. Sachhidananda, "Fiber Reinforced Composites - A Review," *Journal of Material Sciences & Engineering,* vol. 6, no. 3, pp. 1-6, 2017.

[6] Q. E. Incorporated, "Composites 101," Quartus Engineering Incorporated, [Online]. Available: https://www.quartus.com/resources/composites-101/. [Accessed 22 May 2019].

[7] F. Basim, "Effect of Plies Stacking Sequence and Tube Geometry on the Crush Behavior of Tube under Low Velocity Impact –Numerical Study," *International Journal of Mechanics and Applications,* vol. 3, no. 2, p. 46, 2013.

[8] F.C. Campbell, Structureal Composite Materials, Ohio, 2010.

[9] N. Nayak, "Composite Materials in Aerospace Applications," *International Journal of Scientific and Research Publications,* vol. 4, no. 9, pp. 1-10, 2014.

[10] R. Antil, Amit, Garvit and Ritesh, "Applications of composite materials in aerospace," *International Journal of Science Technology and Management,* vol. 4, no. 11, pp. 246-252, 2015.

[11] L. Serrano, "Systèmes époxyde : cuisson hors autoclave et basse température," Toulouse, 2018.

[12] Hexcel Composites, *Product Data Sheet HexPly M21,* Stamford, 2022.

[13] P.P. Parlevliet, H.E.N. Bersee and A. Beukers, "Residual stresses in thermoplastic composites—A study of the literature—Part I: Formation of residual stresses," *Composites: Part A,* vol. 37, p. 1847–1857, 2006.

[14] P. Olivier, Handbook on residual stress: Polymer Matrix Composites, Bethel: 2, 2005.

[15] P.A. Olivier, "A note upon the development of residual curing strains in carbon/epoxy laminates. Study by thermomechanical analysis," *Composites Part A: Applied Science and Manufacturing,* vol. 37, no. 4, pp. 602-616, 2006.

[16] S. Rapp, "Shape Memory Polymers in Fiber Composite Structures for Shape Adjustment," Technische Universitat Munchen , Munchen, 2011.

[17] W.K. Jung, B. Kim, M. S. Won and S. H. Ahn, "Fabrication of radar absorbing structure (RAS) using GFR-nano composite and spring-back compensation of hybrid composite RAS shells," *Composite Structures,* vol. 75, p. 571–576, 2006.

[18] R. K. Singh and M. L. Rinawa, "An Analytical Study of Composite Laminate Lay-up Using Search Algorithms for Maximization of Flexural Stiffness and Minimization of Springback Angle," in *Advances in Mechanical Design, Materials and Manufacture*, Maharashtra, India, 2018.

[19] L. Moretti, "Simulation of cure distortions of composite parts co-bonded in autoclave," Université de toulouse, Ecole nationale supérieure des mines d'albi-carmaux, Toulouse, France, 2019.

[20] J.P. Pascault, H. Sautereau, J. Verdu and R.J.J. Williams, Thermosetting polymers, New York: Marcel Dekker, Inc, 2002.

[21] University Federico II of Naples, Italy and European Chemistry Thematic Network, "Epoxy resins," European Chemistry Thematic Network;, [Online]. Available: http://www.whatischemistry.unina.it/en/maglepoxy.html. [Accessed 15 May 2019].

[22] P. S. L. Center, "Epoxy Resins," Polymer Science Learning Center, 2003. [Online]. Available: https://pslc.ws/macrog/epoxy.htm. [Accessed 15 May 2019].

[23] T. Garstka, N. Ersoy , K.D. Potter and M.R. Wisnom, "In situ measurements of through-the-thickness strains during processing of AS4/8552 composite," *Composites: Part A,* vol. 38, p. 2517–2526, 2007.

[24] G. Jeff, "Thermoset Characterization Part 4: Introduction to Gelation," Polymer Innovation Blog, 5 May 2014. [Online]. Available: https://polymerinnovationblog.com/thermoset-characterization-part-4-introduction-gelation/. [Accessed 18 May 2019].

[25] C. Paris, P.A. Olivier and G. Bernhart, "Modelling the thermokinetic behaviour and the phase transitions of a carbon/polymeric composite unpublished to high heating ramps," *International Journal of Material Forming,* vol. 3, pp. 639-642, 2010.

[26] I.E. Sawi, P.A. Olivier, P. Demont and H. Bougherara, "Investigation of the Effect of Double-Walled Carbon Nanotubes on the Curing Reaction Kinetics and Shear Flow of an Epoxy Resin," *Journal of Applied Polymer Science,* vol. 126, no. 1, pp. 358-366, 2012.

[27] C. Paris, "Étude et modélisation de la polymérisation dynamique de composites à matrice thermodurcissable," Toulouse, 2011.

[28] M. S. Madhukar, M. S. Genidy and J. D. Russell, "A New Method to Reduce Cure-Induced Stresses in Thermoset Polymer Composites, Part I: Test Method," *Journal of Composite Materials,* vol. 34, no. 22, pp. 1882-1904, 2000.

[29] W. Li and L. J. Lee, "Shrinkage control of low-profile unsaturated polyester resins cured at low temperature," *Polymer,* vol. 39, no. 23, pp. 5677-5687, 1998.

[30] J. D. Russell, "Cure shrinkage of thermoset composites," *SAMPEQ,* vol. 24, no. 2, pp. 28-33, 1993.

[31] P. Olivier, M. Cavarero and J. P. Cottu, "Study of the development of residual curing stresses during the manufacturing of composite laminates by TMA," in *Proceedings of the fifth international conference on residual stresses (ICRS5), 16-18 June*, Sweden: Linkoping, 1997.

[32] L.S. Penn, R.C.T. Chou, W.K. Binienda and A.S.D. Wang, "The Effect of Matrix Shrinkage on Damage Accumulation in Composites," *Journal of Composite Materials,* vol. 23, no. 6, pp. 570-586, 1989.

[33] Y. A. Chekanov, V. Korotkov, B. Rozenberg, E. A. Dhzavadyan and L. Bogdanova, "Cure shrinkage defects in epoxy resins," *Polymer,* vol. 36, no. 10, pp. 2013-2017, 1995.

[34] P. He and Z. Zhou , "Epoxy resin copolymer with zero shrinkage," *Journal of Materials Science,* vol. 26, p. pages3792–3796, 1991.

[35] P. W. K. Lam and M. R. Piggott , "The durability of controlled matrix shrinkage composites," *Journal of Materials Science,* vol. 24, p. 4068–4075, 1989.

[36] Y. A. Msallem, F. Jacquemin, N. Boyard, A. Poitou, D. Delaunay and S. Chatel, "Material characterization and residual stresses simulation during the manufacturing process of epoxy matrix composites," *Composites Part A: Applied Science and Manufacturing,* vol. 41, no. 1, pp. 108-115, 2010.

[37] J. Enns and J. Gillham, "Time–temperature–transformation (TTT) cure diagram: Modeling the cure behavior of thermosets," *Journal of Applied Polymer Science,* vol. 28, no. 8, pp. 2567-2591, 1983.

[38] Y. Larberg and M. Akermo, "In-plane deformation of multi-layered unidirectional thermoset prepreg – Modelling and experimental verification," *Composites: Part A,* vol. 56, pp. 203-212, 2014.

[39] M.N.M. Nasir, M.A. Seman, L. Mezeix, Y. Aminanda, A. Rivai and K.M. Ali, "Effect of Stacking Layup on Spring-back Deformation of Symmetrical Flat Laminate Composites Manufactured through Autoclave Processing," in *International Conference on Mechanical, Automotive and Aerospace Engineering*, Kuala Lumpur, Malaysia, 25–27 July 2016.

[40] M.N.M Nasir, Y. Aminanda, L. Mezeix, A. Seman, A. Rival and K.M. Ali, "Spring-back simulation of flat symmetrical laminates with angles plies manufactured through autoclave processing," in *AERITECH VI-Innovation in Aerospace Engineering and Technology*, Kuala Lumpur, Malaysia, 2016.

[41] L. Mezeix, A. Seman, M.N.M. Nasir, Y. Aminanda, A. Rivai, B. Castanié, P. Olivier and K.M. Ali, "Spring-back simulation of unidirectional carbon/epoxy flat laminate composite manufactured through autoclave process," *Composite Structures,* vol. 124, pp. 196-205, 2015.

[42] L. Sun, J. Wang, A. Ni, S. Li and A. Ding, "Modelling and experiment of process-induced distortionin unsymmetrical laminate plates," *Composite Structures,* vol. 182, pp. 524-532, 2017.

[43] G. Fernlund, N. Rahman, R. Courdji, M. Bresslauer, A. Poursartip, K. Willden and K. Nelson, "Experimental and Numerical study of the effect of cure cycle, tool surface, geometry, and lay-upon the dimensional fidelity of autoclave-processed composite parts," *Composite: Part A,* vol. 33, pp. 341-351, 2002.

[44] C. Albert and G. Fernlund, "Spring-in and warpage of angled composite laminates," *Composites Science and Technology,* vol. 62, p. 1895–1912, 2002.

[45] D.W. Radford and T.S. Rennick, "Separating source of manufacturing distortion in lamunate composite," *Journal of Reinforced Plastics and Composites,* vol. 19, no. 8, pp. 621-641, 2000.

[46] E. Kappel, "Forced-interaction and spring-in – Relevant initiators of process-induced distortions in composite manufacturing," *Composite Structures,* vol. 140, p. 217–229, 2016.

[47] N. Ersoy, K. Potter, M.R. Wisnom and M.J. Clegg, "An experimental method to study the frictional processes during composites manufacturing," *Composites: Part A,* vol. 36, p. 1536–1544, 2005.

[48] E. Kappel, D. Stefaniak and C. Hühne, "Process distortions in prepreg manufacturing – An experimental study on CFRP L-profiles," *Composite Structures,* vol. 106, p. 615–625, 2013.

[49] E. Kappel, D. Stefaniak and C. Hühne, "Semi-analytical spring-in analysis to counteract CFRP manufacturing deformations by tool compensation," in *International Congress of the Aeronautical Sciences*, Brisbane, Australia, 2012.

[50] C. Bellini, L. Sorrentino, W. Polini and A. Corrado, "Spring-in analysis of CFRP thin laminates: numerical and experimental results," *Composite Structures,* vol. 173, p. 17–24, 2017.

[51] A. Johnston, R. Vaziri and A. Poursartip, "A Plane Strain Model for Process-Induced Deformation of Laminated Composite Structures," *Journal of Composite Materials,* vol. 35, no. 16, pp. 1435-1469, 2001.

[52] L.K. Jane, B.G. Lutton, Y.W. Mai and R. Paton, "Stresses and Deformations Induced during Manufacturing. Part II: Astudy of the Spring-in Phenomenon," *Journal of Composite Materials,* vol. 31, no. 7, pp. 696-719, 1997.

[53] C. Bellini and L. Sorrentino, "Analysis of cure induced deformation of CFRP U-shaped laminates," *Composite Structures,* vol. 197, pp. 1-9, 2018.

[54] P. Roozbehjavan, B. Tavakol, A. Ahmed, H. Koushyar, R. Das, R. Joven and B. Minaie, "Experimental and Numerical Study of Distortion in Flat, L-shaped, and U-shaped Carbon Fiber–Epoxy Composite Parts," *Journal of Applied Polymer Science,* pp. 1-8, 2014.

[55] G. Fernlund, A. Osooly, A. Poursartip, R. Vaziri, R. Courdji, K. Nelson, P. George , L. Hendrickson and J. Griffith, "Finite element based prediction of process-induced deformation of autoclaved composite structures using 2D process analysis and 3D structural analysis," *Composite Structures,* vol. 62, p. 223–234, 2003.

[56] G. Twigg, A. Poursartip and G. Fernlund, "Tool–part interaction in composites processing. Part I: experimental investigation and analytical model," *Composites: Part A,* vol. 35, p. 121–133, 2004.

[57] K. E. Tarsha Kurdi and P. Olivier, Contraintes résiduelles de cuisson dans les stratifiés composites à finalité aéronautique : Intégration du procédé de mise en œuvre et étude de leur influence sur les caractéristiques mécaniques, Toulouse: PhD thesis, 2003.

[58] K. E. Tarsha-Kurdi and P. Olivier, "Thermoviscoelastic analysis of residual curing stresses and the influence of autoclave pressure on these stresses in carbon/epoxy laminates," *Composites Science and Technology,* vol. 62, no. 4, pp. 559-565, 2002.

[59] T. Gajjar, D.B. Shah, S.J. Joshi and K.M. Patel , "Prediction of Spring-back Deformation for CFRP Reflectors Manufactured using Various Processes," *International Journal of Applied Engineering Research,* vol. 136, pp. 144-148, 2018.

[60] D. Stefaniak, E. Kappel, T. Spröwitz and C. Hühne, "Experimental identification of process parameters inducing warpage of autoclave-processed CFRP parts," *Composites: Part A,* vol. 43, p. 1081–1091, 2012.

[61] E. Kappel , D. Stefaniak, T. Spröwitz and C. Hühne, "A semi-analytical simulation strategy and its application to warpage of autoclave-processed CFRP parts," *Composites: Part A,* vol. 42, p. 1985–1994, 2011.

[62] M. Zakaria, M.S. Dawood, Y. Aminanda, S.A. Rashidi and M.A. Mat Sah, "Spring-back of thick curved uni-directional carbon fibre reinforced composite laminate for aircraft structure application," *International Journal of Recent Technology and Engineering (IJRTE),* vol. 7, no. 65, pp. 224-228, 2019.

[63] M. zakaria, Y. Aminanda, S. Rashidi and M. Sah, "Spring-back of Thick Uni-Directional Carbon Fibre Reinforced Composite Laminate for Aircraft Structure Application," in *5th International Seminar of Aerospace Science and Technology* , Medan, 2018.

[64] S.K. Bapanapalli and L.V. Smith, "A linear finite element model to predict processing-induced distortion in FRP laminates," *Composites: Part A,* vol. 36, p. 1666–1674, 2005.

[65] W.K. Jung, W.S. Chu and S.H. Ahn, "Measurement and Compensation of Spring-back of a Hybrid Composite Beam," *Journal of Composite Materials,* vol. 41, no. 7, pp. 851-864, 2007.

[66] K.J. Yoon and J.S. Kim, "Effect of Thermal Deformation and Chemical Shrinkage on the Process Induced Distortion of Carbon/Epoxy Curved Laminates," *Journal of Composite Materials,* vol. 35, no. 3, pp. 253-263, 2001.

[67] M.R. Wisnom, M. Gigliotti, N. Ersoy, M. Campbell and K.D. Potter, "Mechanisms generating residual stresses and distortion during manufacture of polymer–matrix composite structures," *Composites: Part A,* vol. 37, p. 522–529, 2006.

[68] R. de Oliveira, S. Lavanchy, R. Chatton, D. Costantini, V. Michaud, R. Salathé and J.-A.E. Månson, "Experimental investigation of the effect of the mould thermal expansion on the development of internal stresses during carbon fibre composite processing," *Composites: Part A,* vol. 39, p. 1083–1090, 2008.

[69] Y. Lu, Y. Li, N. Li and X. Wu, "Reduction of composite deformation based on tool-part thermal expansion matching and stress-free temperature theory," *The International Journal of Advanced Manufacturing Technology,* vol. 88, p. 1703–1710, 2017.

[70] C. K. Huang and S. Y. Yang, "Warping in advanced composite tools with varying angles and radii," *Composites Part A ,* vol. 28, pp. 891-893 , 1997.

[71] C. Sonnenfeld, R. Agogué, P. Beauchêne, Y. Nawab, A. Saouab, E. Anfray and B. Desjoyeaux, "Characterization and modelling of spring-in effect on Z-shape composite part," in *17th European Conference on Composite Materials (ECCM17)*, Munich, 2016.

[72] M.N.M. Nasir, M.A. Seman, L. Mezeix, Y. Aminanda, A. Rivai and K.M. Ali, "Effect of the corner angle on spring-back deformation for unidirectional L-shaped laminate composites manufactured through autoclave processing," *ARPN Journal of Engineering and Applied Sciences,* vol. 11, no. 1, pp. 315-318, 2016.

[73] I. Baran, K. Cinar, N. Ersoy, R. Akkerman and J.H. Hattel, "A Review on the Mechanical Modeling of Composite Manufacturing Processes," *Archives of Computational Methods in Engineering,* vol. 24, p. 365–395, 2017.

[74] Y. Mujahid, N. Sallih, M. Mustapha, M. Z. Abdullah and F. Mustapha, "Effects of Processing Parameters for Vacuum-Bagging-Only Method on Shape Conformation of Laminated Composites," *Process,* vol. 8, no. 1147, pp. 2-16, 2020.

[75] N. jared, "Mold release update," CompositesWorld, 1 February 2005. [Online]. Available: https://www.compositesworld.com/articles/mold-release-update. [Accessed 29 June 2019].

[76] Y. Mosaferi, B. Crawford, J. Torres and A. Milani, "On static and dynamic friction characterization of tool-fiber interaction: effect of mould type and processing conditions," *MOJ Polymer Science,* vol. 1, no. 2, pp. 87-92, 2017.

[77] K. Godber, "Release Agents," NetComposites, 24 JANUARY 2019. [Online]. Available: https://netcomposites.com/guide/resin-systems/release-agents/. [Accessed 1 July 2019].

[78] R. Joven, B. Tavakol, A. Rodriguez, M. Guzman and B. Minaie, "Characterization of Shear Stress at the Tool-Part Interface During Autoclave Processing of Prepreg Composites," *Journal of Applied Polymer Science,* vol. 129, no. 4, pp. 2017-2028, 2013.

[79] K.E. Tarsha-Kurdi and Ph. Olivier, "Influence of process-induced stresses on mode I delamination behavior of carbon/epoxy laminates: study of 0°/0° and ±45° interfaces.," in *11th European Conference for Composite Materials (ECCM-11)*, Rhodes – Greece, 2004.

[80] J.M. Svanberg and J.A. Holmberg, "An experimental investigation on mechanisms for manufacturing induced shape distortions in homogeneous and balanced laminates," *Composites: Part A,* vol. 32, pp. 827-838, 2001.

[81] N. Kumbhare, R. Moheimani and H. Dalir, "Analysis of Composite Structures in Curing Process for Shape Deformations and Shear Stress: Basis for Advanced Optimization," *Journal of Composites Science,* vol. 5, no. 63, pp. 1-19, 2021.

[82] O. Sicot, X.L. Gong, A. Cherouat and J. Lu, "Determination of Residual Stress in Composite Laminates Using the Incremental Hole-drilling Method," *Journal of Composite Materials,* vol. 37, no. 9, pp. 831-844, 2003.

[83] S.R. White and H.T. Hahn, "Cure Cycle Optimization for the Reduction of Processing-Induced Residual Stresses in Composite Materials," *Journal of Composite Materials,* vol. 27, no. 14, pp. 1352-1378, 1993.

[84] H.S. Kim, S.H. Yoo and S.H. Chang, "In situ monitoring of the strain evolution and curing reaction of composite laminates to reduce the thermal residual stress using FBG sensor and dielectrometry," *Composites: Part B,* vol. 44, p. 446–452, 2013.

[85] O.G. Kravchenko, S.G. Kravchenko and R.B. Pipes, "Cure history dependence of residual deformation in a thermosetting laminate," *Composites: Part A,* vol. 99, p. 186–197, 2017.

[86] C.M. Warnock and T.M. Briggs, "Cure Cycle Development and Qualification for Thick-Section Composites," in *SAMPE 2016* , California, May 23-26, 2016.

[87] C.C. Chamis, "Mechanics of load transfer at the interface," in *Interfaces in polymer matrix composites, Chapter2*, Plueddemann Academic Press London, 1974, pp. 31-37.

[88] H.T. Hahn and N.J. Pagano, "Curing stresses in composite laminates," *Journal of Composite Materials,* vol. 9, pp. 91-106, 1975.

[89] Y. Weitsman, "Residual thermal stresses due to cool-down of epoxyresin composites," *Journal of Applied Mechanics,* vol. 46, pp. 563-567, 1979.

[90] S.R. White and Y.K. Kim, "Effects of staged curing on mechanical properties of thermosetting matrix composites," in *Proceedings of American Society for Composite Materials 7th Technical Conference*, University Park, PA, USA, 1992.

[91] S.R. White and Y.K. Kim, "Process-induced residual stress analysis of AS4/3501-6 composite material," *Mechanics of Composite aterials and Structures,* vol. 5, pp. 153-186, 1998.

[92] H.T. Hahn and R.Y. Kim, "Swelling of composite laminates," in *Proceedings of Conference on Advanced composite materials – Environmental effects-ASTM STP 658*, J. R. Vinson editor, P. 98-120, 1978.

[93] G. Jeronimidis and A.T. Parkyn, "Residual stresses in carbon fibre-thermoplastic matrix laminates," *Journal of Composite Materials,* vol. 22, pp. 401-415, 1988.

[94] T.J. Chapman and J. Gillespies, "Prediction of process-induced residual stresses in thermoplastic composites," *Journal of Composite Materials,* vol. 24, no. 24, pp. 616-643, 1990.

[95] T.M. Wang, I.M. Daniel and J.T. Gotro, "Thermoviscoelastic analysis of residual stresses and warpage in composite laminates," *Journal of Composite Materials,* vol. 26, no. 6, pp. 883-899, 1992.

[96] Y.K. Kim and S.R. White, "Viscoelastic analysis of processing-induced residual stresses in thick composite laminates," *Mechanics of composite materials and structures,* vol. 4, pp. 361-387, 1997.

[97] J.T. Zhang, M. Zhang, S.X. Li, M.J. Pavier and D.J. Smith, "Residual stresses created during curing of a polymer matrix composite using a viscoelastic model," *Composites Science and Technology,* vol. 130, pp. 20-27, 2016.

[98] T. Bogetti and J. Gillespie, "Process-induced stress and deformation in thick-section thermoset composite laminates," *Journal of composite materials,* vol. 26, pp. 626-660, 1992.

[99] L. Khoun, "Process-induced stresses and deformations in woven composites manufactured by resin transfer moulding," PhD Thesis-Mechanical Engimeering, McGill University, Canada, 2009.

[100] L. Moretti, B. Castanié, G. Bernhart and P. Olivier, "Characterization and modelling of cure-dependent properties and strain during composite manufacturing," *Journal of Composite Materials,* vol. 54, no. 22, pp. 3109-3124, 2020.

[101] D.W. Radford, "Volume fraction gradient induced warpage in curved composite plates," *Composites Engineering,* vol. 5, no. 7, pp. 923-934, 1995.

[102] J.M. O'Neill, T.G. Rogers and A.J.M. Spencer , "Thermally Induced Distortions in the Molding Laminated Channel Section," *Mathematical Engineering in Industry,* vol. 1, pp. 65-72, 1988.

[103] M. Fiorina, A. Seman, B. Castanie, K.M. Ali, C. Schwob and L. Mezeix, "Spring-in prediction for carbon/epoxy aerospace composite structure," *Composite Structures,* vol. 168, pp. 739-745, 2017.

[104] P. Hubert, R. Vaziri and A. Poursartip, "A two-dimensional flow model for the process simulation of complex shape composite laminates," *International Journal for Numerical Methods in Engineering,* vol. 44, pp. 1-26, 1999.

[105] A. Johnston, P. Hubert, G. Fernlund, R. Vaziri and A. Poursartip , "Process Modeling of Composite Structures Employing a Virtual Autoclave Concept," *Science and Engineering of Composite Materials,* vol. 5, no. 3-4, pp. 235-252, 1996.

[106] G. Twigg, A. Poursartip and G. Fernlund, "Tool–part interaction in composites processing. Part II: numerical modelling," *Composites: Part A,* vol. 35, p. 135–141, 2004.

[107] Keyence Corporation of America, "Sensor Head: Long Distance, Small spot LK-G152," Illinois, 2022.

[108] N.C.R. Zapata, T.A. Osswald, U. Madison and J.P. Hernández-Ortiz, "Modeling and analysis of cure kinetics of aliphatic epoxy resin with and without diffusion," in *ANTEC 2012 Plastics: Annual Technical Conference Proceedings*, Orlando, Florida USA, 2012.

[109] E. Franieck, M. Fleischmann, O. Hölck, L. Kutuzova and A. Kandelbauer, "Cure Kinetics Modeling of a High Glass Transition Temperature Epoxy Molding Compound (EMC) Based on Inline Dielectric Analysis," *Polymers,* vol. 13, no. 1734, pp. 1-19, 2021.

[110] A. Bernath, F. Groh, W. Exner, C. Hühne and F. Henning, "Experimental and numerical study of the spring-in of angled brackets manufactured using different resins and fiber textiles," *Journal of Composite Materials,* vol. 53, no. 28-30, pp. 4173-4188, 2019.

[111] A. Hosseinpour, H. Nazockdast, T. Behzad and H.R. SalimiJazi, "Investigation of the cure kinetics of an epoxy resin by advanced isoconversional and model-fitting methods," in *The 31st International Conference of the Polymer Processing Society*, Jeju Island, Korea, 2016.

[112] A.T. DiBenedetto, "Prediction of the glass transition temperature of polymers: A model based on the principle of corresponding states," *Journal of Polymer Science: Part B: Polymer Physics,* vol. 25, no. 9, pp. 1949-1969, 1987.

[113] J.P. Pascault and R.J.J. Williams , "Relationships between glass transition temperature and conversion," *Polymer Bulletin,* vol. 24, pp. 115-121, 1990.

[114] J.P. Pascault and R.J.J. Williams, "Glass transition temperature versus conversion relationships for thermosetting polymers," *Journal of Polymer Science: Part B: Polymer Physics,* vol. 28, no. 1, pp. 85-95, 1990.

[115] P. Poolperm and W. Nakkiew, "Effect of Porosity on Residual Stress of 2024-Aluminum GTAW Specimen," *Materials Science Forum,* vol. 872, pp. 28-32, 2016.

[116] Fluorotherm™, "Materials Overview: ETFE Properties," Fluorotherm™, 2021. [Online]. Available: https://www.fluorotherm.com/technical-information/materials-overview/etfe-properties/. [Accessed 15 January 2021].

[117] Omnexus, "The material selection platform," [Online]. Available: https://omnexus.specialchem.com/polymer-properties/properties/young-modulus. [Accessed 15 January 2021].

[118] fabrix360, "What is ETFE?," fabrix360, [Online]. Available: https://www.fabrix360.com/what-is-etfe. [Accessed 15 January 2021].

[119] Aerovac System LTD, *Aerovac Product Catalogue,* Bradford Borough, United Kingdom.

[120] MatWeb, "Overview of materials for Nylon 66, Unreinforced," MatWeb Material property data, [Online]. Available: http://www.matweb.com/search/datasheettext.aspx?matguid=a2e79a3451984d58a8a442c37a226107. [Accessed 15 January 2021].

[121] R. Arthur, "Thermal Shrinkage of Oriented Nylon 66 Yarns as a Function of Time, Temperature, and Stress," *Textile Research Journal,* vol. 39, no. 5, pp. 428-434, 1969.

[122] V.B. Gupta, K. Hemant and S.R. Huilgol, "Shrinkage characteristics of poly(ethylene terephthalate), nylon-6 and polypropylene yarns," *Indian Journal of Fibre & Textile Research,* vol. 21, pp. 101-108, 1996.

[123] S.A. Lisbao and M.A. Regina, "Structure of heat-treated Nylon 6 and 6.6 fibers. I. The shrinkage mechanism," *Journal of Applied Polymer Science,* vol. 68, no. 3, pp. 441-452, 1998.

[124] Pariss textile, "Fabric Shrinkage, How and Why?," 11 June 2021. [Online]. Available: https://www.parisstextile.com/fabric-shrinkage-how-and-why/. [Accessed 20 December 2022].

[125] Textileblog, "What is Fabric Shrinkage/Mechanism of Fabric Shrinkage," Dhaka, Bangladesh, 2022.

[126] S. Islam, S. Md, M. Alam and S. Akter, "The Consequences of Temperature on the Shrinkage Properties of Cotton Spandex Woven Fabric," *Journal of Textiles and Polymers,* vol. 7, no. 1, pp. 25-29, 2019.

[127] S. Alam, S. Islam and S. Akter, "Achieving Optimal Shrinkage of Cotton Spandex Woven Fabrics by Apposite Heat Setting Temperature," *Advance Research in Textile Engineering,* vol. 5, no. 2, pp. 1-8, 2020.

[128] E. Kumpikaite, G. Laureckiene, D. Milasiene and S. Petraitene, "Investigation of the Shrinkage and Air Permeability of Woolen Blankets and Blankets Made with Regenerated Wool," *materials,* vol. 15, no. 10, pp. 1-17, 2022.

[129] NETZSCH, "Coefficient of Linear Thermal Expansion (CLTE/CTE)," NETZSCH-Gerätebau GmbH, [Online]. Available: https://www.netzsch-thermal-analysis.com/en/contract-testing/glossary/coefficient-of-linear-thermal-expansion-clte/. [Accessed 3 June 2021].

[130] L. Moretti, P. Olivier, B. Castanié and G. Bernhart, "Experimental study and in-situ FBG monitoring of process-induced strains during autoclave co-curing, co-bonding and secondary bonding of composite laminates," *Composites Part A: Applied Science and Manufacturing,* vol. 142, p. 106224, 2021.

[131] E. Kappel, "Compensating process-induced distortions of composite structures: A short communication," *Composite Structures,* vol. 192, pp. 67-71, 2018.

[132] E. Kappel, D. Stefaniak, D. Holzhüter, C. Hühne and M. Sinapius, "Manufacturing distortions of a CFRP box-structure – A semi-numerical prediction approach," *Composites: Part A,* vol. 51, pp. 89-98, 2013.

Annex

Annex 1: Bagging products

A6000 Fluoropolymer Release Film (ETFE release film)

- High temperature, tough, fluoropolymer ETFE release film exhibiting excellent release characteristics, combined with high elongation.

- Suitable for use with all commonly used resin systems.

- Opaque blue for ease if identification on the cured laminate.

Physical properties

Maximum use temperature	Up to 260 °C
Colour	Blue
Tensile strength at break	(7000 psi)/48 MPa
Elongation at Break	> 350%
Density	1.75 g/cm^3
Melting point	275-285 °C

Availability and Packaging

Thickness	0.12, 0.15 and 0.2 mm
Yield	28.5, 38.0 and 47.5 sq. m per kg
Roll size	150 x 1.3 m wide

Available in a range of perforations

Storage & Handling

Store in original packaging

No handling problems experienced

A100PS Nylon Release Fabric (peel-ply)

- A100PS is a porous nylon release fabric.

- Heat set and scoured – can be used directly against laminates or bond line.

- Identical to release fabric A100 (general white colour) apart from the addition of a red tracer yarn spaced every 30 mm along the warp direction of the fabric for ease of identification on the cured laminated. This is particularly useful when working with very large mouldings which a typically found in the marine industry where secondary bonding could be compromised should any release fabric be inadvertently left behind on the laminate.

- Will release from most commercial resin systems

- A comprehensive selection of slit widths is available

Physical properties

Maximum cure temperature	180 °C
Fabric thickness	0.145 mm
Fabric weight	80 g/m^2
Colour	Natural (white) with red tracer yarn

Availability & Packaging

Roll size	100 x 1.52 m wide

Slit widths available

Storage & handling

No special storage conditions required

Airbleed 20 Polyester Bleeder/Breather fabric

- An ultra heavyweight polyester breather fabric
- Useful for very high pressure curing of flat or single curvature laminates
- Also available in fire retardant
- Has no release characteristics and should be separated from the laminate by a suitable release film or fabric.

Physical properties

Maximum cure temperature	205 °C
Fibre	100% Polyester
Weight	650 g/m^2
Thickness	4 mm

Availability & Packaging

Standard roll size	50 x 1.52 m wide up to 3 m wide available
Cut shape/Slit widths	Available to order.
Packaging	Heavy gauge polyethylene
	Would on 76 mm diameter cores

Storage & Handling

No special storage conditions required

No skin irritation problems experienced

SM5144 Vacuum bag sealant tape

- An industry standard tape for autoclave bonding, composite fabrication and vacuum processing for cure temperature of up to 191 °C.
- Achieves rapid positive vacuum sealing with all tool surfaces and bagging materials and allows easy fabrication of pleats, pressure intensifiers and resin dams.

- Strips cleanly and quickly from the mould surface on cooling below 66 °C.

Physical properties

Maximum use temperature	191 °C
Colour	Yellow
Solids	100 %
Flammability	Will not support combustion

Availability & Packaging

Roll size	9.14 m x 12 mm x 3 mm
Standard box contents	32 rolls

Storage & Handling

SM5144 is non-toxic, non-irritant, non-injurious to skin

Material should be used within 6 months of date of manufacture

Material must be stored flat

Cartons should not be stacked more than 5 high

Capran 518 heat stabilized nylon 6 blown tubular film (Vacuum bag)

- A green heat stabilized, blown nylon 6 film.
- It has excellent elongation and heat ageing characteristics having been successfully used at pressure of 7 bar (100 psi) and temperature of up to 200 °C for several hours.
- A Caprolactam level of less than 1% makes it an ideal choice for most vacuum bagging applications
- It is available both as lay flat or slit tube and in sheet form.

Physical properties

Maximum use temperature	199 °C
Colour	Green
Tensile strength	112 MPa
Yield strength	28 MPa
Elongation	375%
Shrinkage	<2% (0.5 hr @ 149 °C)
Tear strength	130 g/layer (ASTM D1922)
Flammability	Self-extinguishing melts
Crystalline melt point	218-220 °C

Availability & Packaging

Pack weight	45 kg
Yield	17.4 sq.m per kg

Standard widths

A wide range of widths in tube and sheet are available from stock.

Storage & Handling

All nylon film absorbs water. The higher the moisture content the more flexible they become, conversely at low moisture levels flexibility is reduced. Capran 518 is dispatched with an optimum moisture content to provide maximum performance and handleability. To preserve these characteristics during storage the roll should be wrapped in polyethylene and stored at around 65% RH (humidity) and 20 °C.

Annex 2 : Unit transformation

Aluminium

Density = 2.78 g/cm^3
= 2.78 x 10^{-6} t/cm^3
= 2.78 x 10^{-9} t/mm^3

Thermal conductivity = 190 W/m. °C
= 190 $\frac{\frac{kg.m^2}{s^3}}{m.°C}$
= 190 kg.m/ s^3.°C
= 190 t.mm/ s^3.°C

Young's modulus (E) = 70600 MPa
Poisson's ratio (v) = 0.345
CTE (α) = 2.28 x 10^{-5} °C^{-1}

Specific heat capacity (C_p) = 875 J/kg. °C
= 875 $\frac{\frac{kg.m^2}{s^2}}{kg.°C}$
= 875 m^2/ s^2.°C
= 875 x 10^6 mm^2/ s^2.°C

ETFE

Density = 1.7 g/cm^3

= 1.7 x 10^{-6} t/cm^3

= 1.7 x 10^{-9} t/mm^3

Thermal conductivity = 0.238 W/m. °C

$$= 0.238 \frac{\frac{kg.m^2}{s^3}}{m.°C}$$

= 0.238 kg.m/ s^3.°C

= 0.238 t.mm/ s^3.°C

Young's modulus (E) = 0.8 GPa

= 800 MPa

Poisson's ratio (v) = 0.45

CTE (α) = 9 x 10^{-5} °C^{-1}

Specific heat capacity (C_p) = 1.9 kJ/kg. °C

= 1.9 x 10^3 J/kg. °C

$$= 1.9 \times 10^3 \frac{\frac{kg.m^2}{s^2}}{kg.°C}$$

= 1.9 x 10^3 m^2/ s^2.°C

= 1900 x 10^6 mm^2/ s^2.°C

Peel ply

Density = 80 g/m^2 (thickness = 0.145 mm)

= 80 x 10^{-6} t/m^2

$= \frac{80\ x\ 10^{-6}}{1\ x\ 1\ x\ 0.145\ x\ 10^{-3}} \quad \frac{t}{m^3}$

= 551.7 x 10^{-3} $\frac{t}{m^3}$

$= \frac{551.7\ x\ 10^{-3}}{1\ x\ 10^{9}} \quad \frac{t}{mm^3}$

= 551.7 x 10^{-12} $\frac{t}{mm^3}$

= 5.5 x 10^{-10} $\frac{t}{mm^3}$

Thermal conductivity = 1.08 W/m. °C

$= 1.08\ \frac{\frac{kg.m^2}{s^3}}{m.°C}$

= 1.08 kg.m/ s^3.°C

= 1.08 t.mm/ s^3.°C

Young's modulus (E) = 3.62 GPa

= 3620 MPa

Poisson's ratio (v) = 0.4

CTE (α) = 9.5 x 10^{-5} °C^{-1}

Specific heat capacity (C_p) = 1.72 J/g. °C

$= 1.72\ \frac{\frac{kg.m^2}{s^2}}{g.°C}$

= 1.72 x 10^3 m^2/ s^2.°C

= 1720 x 10^6 mm^2/ s^2.°C

Résumé de la thèse en français

MOTS-CLÉS : Matériaux composites, cuisson autoclave, interaction outil/pièce, compensation de moule, simulation numérique, éléments finis.

En raison de leur rapport rigidité/poids et résistance/poids exceptionnels, les plaques stratifiées en matériaux composites renforcés de fibres de carbone sont largement utilisées dans plusieurs secteurs industriels, dont les pièces d'avion de hautes performances. Les plaques composites stratifiées doivent être traitées à une température de durcissement élevée, ce qui induit des contraintes résiduelles et entraîne une déformation des pièces après la fabrication. Cette thèse se concentre sur l'effet de l'interaction outil/pièce sur la distorsion lors de la fabrication, dans la continuité de travaux antérieurs récemment achevés sur la caractérisation du comportement thermomécanique du pré-imprégné M21EV/IMA et l'étude (à la fois expérimentale et numérique) des déformations et des contraintes induites par le processus de cuisson.

Objectifs de la thèse

Dans le travail précédent de la thèse de doctorat de L. Moretti, la simulation numérique des contraintes, des déformations et des tensions induites par le processus d'élaboration a été réalisée au moyen d'Abaqus® avec une loi spécifique de comportement du matériau carbone-époxy pendant sa cuisson. Des effets de modélisation ont été intégrés pour simuler la fabrication de panneaux auto-raidis co-cured ("cuis ensemble") ou co-bonded ("liés ensemble"). Par conséquent, les travaux de la thèse ont manqué de temps pour se concentrer sur l'interaction entre la pièce stratifiée et le moule. C'est pourquoi il a été décidé, dans le cadre de la thèse actuelle, d'étudier l'interaction outil/pièce et de mettre en place une modélisation s'appuyant sur des développements antérieurs afin de prédire les formes singulières des pièces stratifiées déformées après cuisson. Un intérêt particulier est accordé à l'influence de l'agencement des plis avec des conditions de surface d'outil variables sur le gauchissement des stratifiée cuis en autoclave.

Les objectifs de la thèse peuvent être résumés comme suit :

1) Recueillir une base de données sur la déformation d'échantillons composites avec différentes directions de fibres et dans différents états de surface de l'outil.

2) Étudier l'effet de l'interaction outil/pièce en mesurant puis simulant les formes modifiées et déformées des pièces stratifiées après cuisson.

3) Prévoir le gauchissement à l'aide de la simulation par éléments finis.

4) Proposer une simulation robuste par méthode des éléments finis prouvée expérimentalement ainsi qu'une méthode pour modifier la forme du moule métallique afin de compenser ou de réduire la déformation de la pièce.

Structure de la thèse

Cette thèse est divisée en 4 chapitres qui couvrent l'effet de l'interaction outil/pièce sur la distorsion du stratifié lors de fabrication et la stratégie de compensation du moule :

Le chapitre 1 contient une introduction générale qui présente les caractéristiques du procédé et le contexte de la méthode de fabrication et la déformation des pièces stratifiées.

Le chapitre 2 porte sur la revue bibliographique des travaux de recherche antérieurs, relatifs aux paramètres influençant la déformation des pièces stratifiées durant leur fabrication.

Le chapitre 3 est consacré à l'identification expérimentale de l'interaction outil/pièce sur la distorsion des plaques stratifiées et à la simulation numérique.

Le chapitre 4 présente la caractérisation du comportement thermique de l'interface des matériaux de démoulage et la stratégie de compensation des pièces déformées.

Etat des lieux de la distorsion induite par le processus de cuisson dans la fabrication des composites

Au cours de la fabrication, des contraintes résiduelles se forment en raison de plusieurs paramètres. La première considération à l'échelle micromécanique doit se concentrer sur la disparité des coefficients de dilatation thermique entre les fibres et la matrice, suivie à l'échelle mésoscopique par la disparité des coefficients de dilatation thermique entre la pièce et le moule. Les paramètres influençant la déformation des pièces stratifiées après leur fabrication peuvent être classés en sources intrinsèques et extrinsèques. L'aspect intrinsèque est lié aux caractéristiques de la pièce elle-même, tandis que l'aspect extrinsèque est lié au processus de fabrication. En ce qui concerne les paramètres intrinsèques, seuls quelques travaux se sont concentrés sur l'effet des différentes matières premières, car il était supposé que le système fibre/matrice ayant une résistance et une rigidité élevées celui-ci entraînerait une déformation moindre. En ce qui concerne la géométrie des pièces, la forme, la taille et l'épaisseur sont les principaux facteurs qui influent les caractéristiques de la déformation des pièces. La stratification choisie pour la réalisation des pièces est le critère le plus prédominant sur la déformation finale des pièces car la conception de cette séquence d'empilage détermine l'effet de couplage des pièces stratifiées. Pour les paramètres extrinsèques, à partir de l'outil ou du moule, trois facteurs principaux, les matériaux du moule, la forme du moule et l'état de la surface du moule, sont généralement mentionnés et pris en compte. Pour les paramètres extrinsèques, à partir de

l'outil ou du moule, trois facteurs principaux sont généralement mentionnés et pris en compte : les matériaux du moule, la forme du moule et l'état de la surface du moule. Plusieurs études ont certifié qu'un outil ayant un coefficient de dilatation thermique plus élevé peut fortement augmenter la déformation de la pièce réalisée parce que la pièce stratifiée est contrainte d'adhérer à l'outil pendant la cuisson, ce qui génère généralement un gradient de contraintes différent entre chaque couche et ce gradient est figé après le démoulage. En ce qui concerne la forme du moule, l'angle et le rayon ont été étudiés. Toujours d'après nombres d'études, il est présumé que l'augmentation de l'angle de moulage diminue l'angle de gauchissement de la pièce stratifiée en raison de la différence de contraction thermique dans le plan et à travers l'épaisseur mais aussi du rétrécissement chimique. Le dernier facteur est l'état de la surface de l'outil. En général, la surface de l'outil peut être modifiée par polissage mécanique ou par plusieurs agents de démoulage, y compris des liquides ou des films polymères. L'objectif principal de la modification de la surface de l'outil est d'éviter les difficultés liées au démoulage des pièces. Cependant, diverses oppositions dans les travaux de recherche sur l'état de la surface de l'outil ont été relevés : dans certains cas l'état de la surface s'est avéré avoir un impact sur la distorsion de la pièce et dans d'autres cas non ; de plus les résultats semblent être imprévisibles dans certains cas. Le cycle de polymérisation est une autre cause fondamentale de distorsion des pièces stratifiées, car la fabrication est effectuée à une température élevée, ce qui entraîne une contraction thermique et un rétrécissement chimique de la matrice en résine. La plupart des travaux de recherche indiquent qu'une température de cuisson basse peut réduire la déformation des pièces en raison de la diminution de la contraction thermique. Quelques travaux se sont concentrés sur la vitesse de chauffe et la durée de maintien de la température. Il a été constaté qu'une vitesse de chauffe lente et une durée de maintien en température courte permettaient de réduire la distorsion. Certains travaux de recherche ont conclu que deux températures de maintien ont plus d'influence sur la déformation qu'une seule température de maintien, tandis que d'autres travaux de recherche n'ont pas obtenu d'effet à ce sujet. En ce qui concerne le taux de refroidissement, ce dernier ne semble pas avoir d'effet sur la déformation lorsque la pièce est complètement durcie, ce qui a été mentionné dans quelques travaux de recherche. Ceci peut laisser supposer qu'il n'y a plus de contraction ou de rétrécissement pendant la phase de refroidissement.

Étude expérimentale et modélisation numérique de l'interaction outil/pièce lors de la polymérisation en autoclave

L'aspect expérimental a été développé et conduit de manière à étudier l'influence de la séquence d'empilage et de l'interaction outil/pièce sur la déformation hors plan des spécimens de stratifiés plats fabriqués en autoclave. Il y a eu une bonne reproductibilité de la fabrication de tous les spécimens et ils ont donné des résultats similaires en test expérimental. Les résultats ont montré que la séquence d'empilement joue un rôle clé dans la forme finale de la pièce et sur l'ampleur de la déformation. Les stratifiés à plis angulaires présentent une déflexion extrêmement plus importante que les stratifiés à plis croisés en raison de l'absence d'empilement symétrique. Un autre facteur pris en compte dans cette étude est l'effet de l'interface outil/pièce. D'après les résultats des mesures, les stratifiés à plis croisés sont plus sensibles à la présence d'un tissu d'arrachage que les autres configurations de séparateur type ETFE non perforé, où la zone de distorsion au centre est élargie jusqu'au bord de stratifié. L'ampleur de la déformation des laminés à plis croisés augmente considérablement lorsque le tissu d'arrachage est utilisé comme interface. Étant donné que le tissu d'arrachage est un matériau textile qui contient des fils de trame et de chaîne, le processus de cuisson peut avoir un impact sur le comportement thermique de ce tissu lorsqu'il est soumis à des (fortes) variations de température, ce qui nécessite d'autres essais pour évaluer son comportement. D'autre part, le nombre de couches de film séparateur ETFE non perforé n'a pas d'effet significatif sur la forme et l'ampleur de la distorsion pour les stratifiés à plis croisés et à plis angulaires. On peut en conclure qu'une seule couche suffit ou que le nombre de couches n'est pas encore suffisant pour avoir un impact sur la forme finale. D'autre part, les différentes interfaces outil/pièce n'ont pas eu d'impact notable sur la forme et l'ampleur de la déformation pour le stratifié à plis angulaires. La conclusion de ce phénomène est compliquée, mais on peut imaginer que l'effet de l'interface est dissimulé par une grande distorsion des stratifiés à plis angulaires. Dans la simulation numérique développée, le modèle thermomécanique existant fonctionne bien avec l'interface outil/pièce assignée au modèle et la distorsion géométrique prédite a été validée, étant conforme à l'expérimentation. Cependant, certaines améliorations sont nécessaires pour les propriétés de l'interface, et cette question est prise en considération pour une étude plus approfondie.

Caractérisation du comportement de l'interface et stratégie de compensation du moule

Cette partie prolonge l'étude sur la caractérisation des matériaux d'interface. Le comportement thermique a d'abord été caractérisé par TMA (Thermo Mechanical Analyzer) en termes de coefficient de dilatation thermique. Les résultats ont révélé que le tissu d'arrachage présente des comportements thermiques différents (expansion et contraction) entre les directions de la trame et de la chaîne tout au long du cycle de polymérisation, tandis que le séparateur ETFE non perforé ne présente qu'une seule expansion après le cycle de polymérisation. Le coefficient de dilatation thermique des deux interfaces a été déterminé séparément pour chaque section de cuisson par la pente de l'ajustement linéaire de la courbe et a finalement été intégré dans le modèle numérique pour simuler la forme durcie du stratifié à plis croisés et à plis angulaires. Le résultat de la simulation est satisfaisant et garantit la sensibilité du tissu d'arrachage à la déformation du stratifié à plis croisés. On peut noter que les propriétés de l'interface entre le moule et la pièce stratifiée ne peuvent pas être ignorées. La dernière partie est consacrée à l'étude de faisabilité de la compensation des moules afin d'obtenir une forme plate pour le stratifié à plis angulaires. Le problème a été abordé par la simulation numérique de la compensation des moules à miroir pour les moules mâles et femelles. Les premiers résultats de la simulation ont révélé que les moules femelles et mâles conçus avec une simple symétrie miroir n'étaient pas en mesure de compenser le gauchissement du stratifié à plis angulaires. Il a été démontré numériquement qu'un moule femelle serait capable de minimiser le gauchissement. Par manque de temps, la vérification expérimentale n'a pas été possible, mais elle est toujours envisagée.